University of Nevada, Reno

Analytical studies of a large-scale laminar soil-box for experiments in soil-structure-interaction

A thesis submitted in partial fulfillment of the
requirements for the degree of Master of Science in
Civil and Environmental Engineering

by

Anastasia Bitsani

Dr. Ian G. Buckle/Thesis Advisor

Dr. Ramin Motamed/Thesis Co-advisor

August, 2017

THE GRADUATE SCHOOL

We recommend that the thesis
prepared under our supervision by

ANASTASIA BITSANI

Entitled

Analytical Studies Of A Large-Scale Laminar Soil-Box For Experiments In Soil-Structure-Interaction

be accepted in partial fulfillment of the
requirements for the degree of

MASTER OF SCIENCE

Ian G. Buckle, Ph.D., Advisor

Ramin Motamed, Ph.D, Committee Member

John Anderson, Ph.D., Graduate School Representative

David W. Zeh, Ph.D., Dean, Graduate School

August, 2017

Abstract

Nuclear facilities frequently have deep massive foundations, which are large enough to affect the response of neighboring soil and the nature of ground shaking these facilities have to withstand. Despite this well-recognized phenomenon, the ramifications of soil-structure interaction (SSI) are not completely understood due to the complexity of the mechanics involved. As a consequence, only simplified elastic models are currently used to study SSI for these and other facilities. To address this situation, the U.S. Department of Energy (DOE) has funded a multi-institutional project to investigate SSI effects in nuclear facilities. To this end, the research team at University of Nevada Reno (UNR) is fabricating a 400-ton, laminar, biaxial soil box and corresponding shake table, which will be used to (a) explore SSI phenomena at a scale not currently possible in the U.S., and (b) validate the ESSI nonlinear computational framework, developed by UC Davis.

This thesis presents some of the numerical analyses that have been conducted in order to inform the design of the soil-box and shake-table, and to understand the (a) dynamic behavior of the soil-box, (b) the role of soil nonlinearity, (c) the fundamental interaction of the soil with the walls of the box, and (d) the effect of friction and gapping at the soil-wall interface. The preliminary design phase included the modelling of a 1D soil-column in DEEPSOIL and compared results from linear, equivalent linear and nonlinear analyses, for a suite of eight recorded ground motions obtained from the PEER database, and different scale factors, with scaled PGAs between 0.25g and 1.0g. Simulation of the nonlinear hysteretic soil-behavior was achieved via the use of the Pressure-

Dependent Modified Kodner Zelesko model and the new General Quadratic Hyperbolic model. The effect of several parameters, such as the hysteretic soil material, the reference curve, the time-step and the time-scaling of the input motion, on the results of the nonlinear dynamic analyses was also evaluated. Furthermore, finite element modeling and nonlinear dynamic analyses of a 1D soil column and a more realistic 2D slice of the soil including the box walls were conducted in LS-DYNA using a nested surface plasticity model. Different mesh sizes, wall configurations, and contact conditions at the soil-wall interface, ranging from frictionless contact to perfect contact, were examined in order to decipher the role of sliding, friction and gapping on the behavior of the box. Wall configurations with and without vertical constraints, with linear axial springs, and with compression-only springs were investigated. The boundary effect close to the walls was also examined and the area of uniform soil stresses was identified for different design alternatives.

The nonlinear dynamic analyses were used to quantify the base shear, overturning moment, pressures below the box, response spectra at different locations of the soil, forces in the walls, and the accelerations, displacements, strains and stresses of the soil and the box. The advanced numerical analyses presented in this thesis give an insight into the seismic behavior of the soil-box and are expected to be useful to other research teams designing their own soil-box. The numerical work demonstrated that:

- Equivalent linear site response analyses give similar results with nonlinear analyses for small to moderate levels of shaking (PGA=0.5g), but they over-predict the base shear forces and under-predict the shear strains for higher levels of shaking.

- The soil nonlinearity limits the increase of the base shear, offsets the fundamental period of the soil (from 0.13sec to about 0.5-0.6sec for input motions with PGA=1.04g), increases significantly the soil-strains (1-7% for aforementioned motions), and results in de-amplification of the input motion towards the surface.
- It is important to use soil materials models (GQ/H) that can properly simulate the soil behavior at large-strains by reaching the correct shear strength especially at high levels of shaking, because such models can give a significantly different response of the soil column and reduce the base shear by 15% and increase the maximum shear strains by a factor of 2.
- Laminar walls that are flexible in every direction (lateral and vertical) are witnessing vertical soil displacements in regions close to the walls, indicating that the soil is not in pure shear. For this case the stresses are not uniform along the whole length of a layer, with soil regions closer to the walls witnessing different stresses than the ones close to the center of the box, demonstrating the existence of a significant boundary effect caused by the walls.
- Large overturning moment is generated at the bottom of the soil-box during strong lateral shaking, and this moment can introduce significant uplift in the walls, meaning that they should be designed not only for shear but also for tension.
- To ensure that the soil-box will behave as realistically as possible, it is necessary to have walls with small lateral shear stiffness but very high axial and bending stiffness, together with a high-coefficient of friction at the soil-wall interface, which will transfer the complementary shear of the soils to the walls and minimize the boundary effect.

Acknowledgements

This thesis has been sponsored by the Department of Energy, as part of a multi-institutional collaborative research project between University of Nevada, Reno, University of California Davis, Lawrence Berkeley National Laboratory, and the Lawrence Livermore National Laboratory. The title of the project is "A Modern Computational Framework for the Nonlinear Seismic Analysis of Nuclear Facilities and Systems" and the DOE/LBNL Subcontract number is 7236255.

Foremost, I would like to express my sincere gratitude to my advisors Dr. Ian Buckle and Dr. Ramin Motamed for their guidance, support and encouragement throughout my research work. I would also like to thank Dr. John Anderson for being part of the examining committee and for providing valuable feedback.

Moreover, special thanks go to Dr. Patrick Laplace, Dr. Raj Siddharthan, Dr. Sherif Elfass and Dr. Denis Istrati, who have been part of the UNR soil-box research team and have provided useful input for this thesis over the last two years. I would also like to recognize and thank Dr. David McCallen, Dr. Boris Jeremic, Dr. Jenna Wang, Dr. Floriana Petrone and Dr. Frank McKenna for the pleasant collaboration and the exchange of ideas during the review meetings. This thesis has given me the opportunity to evolve intellectually by interacting with all the experts mentioned above, and I am grateful to all of them.

Last but not the least, I would like to thank my family, whose value to me only grows with age.

Table of Contents

List of Tables

List of Figures

Chapter 1: Introduction

1.1 Motivation and objectives

Nuclear power plants play a significant role in energy production in the U.S. These massive structures are designed to withstand environmental hazards, including earthquakes, to ensure public safety and continuity of function. However, it has been observed that large embedded structures, can affect the response of the soil around them and the nature of the ground shaking they have to withstand. Despite this known phenomenon, the effects of soil-structure interaction (SSI) are not yet well understood due to the complexity of the mechanics involved. In an attempt to improve this situation, the U.S. Department of Energy (DOE) has funded a multi-institutional research project to investigate SSI effects for nuclear facilities. Principal investigators are David McCallen from Lawrence Berkeley National Lab, Boris Jeremic from the University of California, Davis and Ian Buckle from the University of Nevada, Reno. The research team at UNR is responsible for designing and building a soil-box and a dedicated shake table (Figure 1-1) as well as for conducting SSI experiments under strong earthquakes using the new equipment.

The main objectives of the UNR research team are as follows:

- Design and construction of a large-scale biaxial soil box and a dedicated shake table

- Conduct soil-structure interaction (SSI) experiments at the largest possible scale to (a) gain direct physical insight into SSI phenomena for nonlinear soils and structures during strong earthquakes, (b) validate the ESSI nonlinear computational framework, developed by UC Davis

The main objectives of this particular thesis was to conduct extensive numerical analyses and generate information that can be used in order to:

- Understand the dynamic behavior of a simplified soil column and a complex soil-box system, the role of soil nonlinearity, the interaction of the walls with the neighboring soil columns, the effect of friction and gapping at the soil-wall interface, and the expected capabilities of the soil-box for SSI experiments (e.g. what accelerations can be achieved at the surface of the box, what soil-strains)

- Determine the most appropriate material properties for the walls of the box and provide data for the design of the whole soil-box shake table system. Examples of parameters of interest include shear and axial forces for the design of the walls, base shear and demands on stroke and velocity for the design of the actuators, overturning moment and pressures at the bottom of the box for the design of the platen and bearings of shake table.

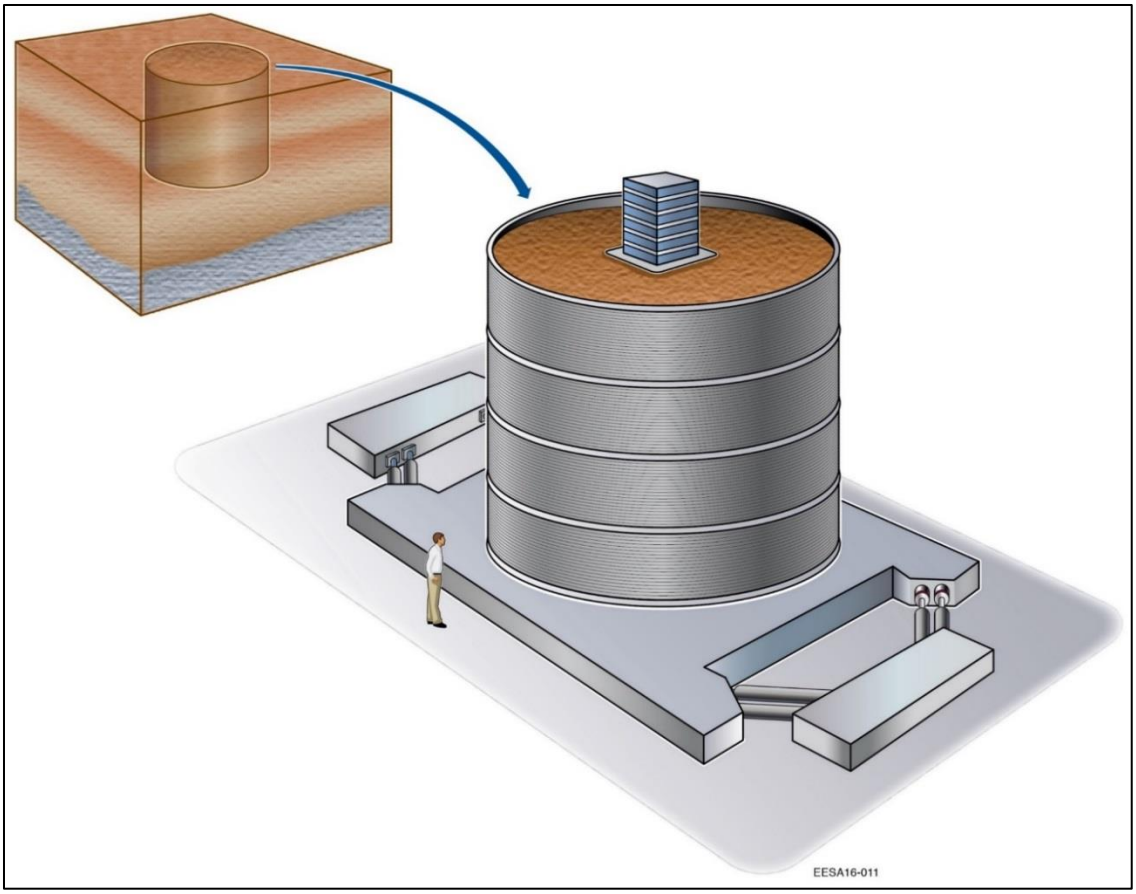

Figure 1-1: 3D conceptual drawing of the new shake table and the soil box (credit: Lawrence Berkeley National Lab)

1.2 Literature Review

When the ground is subjected to seismic loading the soil can move freely in the lateral direction as it was an infinite domain. All the vertical soil columns behave in pure shear and have the same response if the soil is in free-field and the waves propagate in the vertical direction (no oblique angle). Therefore, in order to study the seismic behavior of the soil in such cases it is sufficient to study the behavior of one vertical soil column via site response analyses. Various methods and tools have been developed and are currently

available for site response analyses, including both frequency domain (e.g. SHAKE) and time-domain approaches (e.g. DEEPSOIL). Linear and equivalent linear analyses are commonly used because they are simple and can be conducted in the frequency domain, eliminating the sensitivity to certain numerical parameters (e.g. time-step) that characterize the time-domain analyses as discussed Phillips et al (2012). Although equivalent linear analyses are robust and give results very similar to nonlinear analyses for a wide range of strains, for large strains and high frequencies they deviate from nonlinear analyses (Bolisetti et al, 2014).

Nonlinear analyses can simulate more accurately the soil response however they are not as commonly used as the equivalent linear analyses due to their complexity, lack of guidance and validation with actual recorded data during strong shaking with large strains. Kwok et al (2007) and Stewart and Kwok (2008) have provided recommendations on the proper user of several numerical codes for conducting nonlinear analyses. The aforementioned studies suggested that in addition to the hysteretic damping automatically calculated by the hysteretic material, viscous damping should also be assigned using a Rayleigh damping with at least two specified frequencies that will match the small-strain damping. Moreover, the authors presented three alternative approaches on how to develop the backbone curves, by either matching the soil-behavior at small-strains, or large-strains, or a hybrid approach. The author also discussed the possibility of optimally fitting both the backbone and damping curves.

Using full Rayleigh damping with two frequencies gave better results than using the simple Rayleigh damping in the two aforementioned studies. The complexity in this approach is

on selecting the second frequency for the Rayleigh damping. Despite the increased accuracy of full Rayleigh Damping, which is frequency dependent, it can result in over-damping at high frequencies (Stewart and Kwok, 2008, Phillips and Hashash, 2009). To solve this issue, Phillips and Hashash (2009) developed a frequency-independent viscous damping formulation for use in DEEPSOIL. Using this type of damping is more realistic, since the small-strain damping has been seen to be frequency independent for small-strains and the usual frequency content of earthquakes (Lai&Rix, 1998).

In recent years, several studies have focused on comparison of nonlinear analyses with recorded data from vertical arrays (Kwok et al 2008, Stewart and Yee 2012, Yee et al 2013 and Motamed et al 2015, 2016). The most recent studies have demonstrated the importance of properly simulating the soil behavior at large strains especially for large magnitude shaking, and have suggested different approaches on how to achieve that. Yee et al (2013) and Motamed et al (2016) used modified backbone curves with existing nonlinear soil materials in order to match both the soil stiffness at small-strains and the shear strength at large strains, improving the over-all accuracy of the analyses. Moreover, Groholski et al (2015) presented a new soil material model, called the General Quadratic Hyperbolic model, which was implemented in DEEPSOIL. This model is very promising and user friendly because it can automatically match both the small-strain behavior and the user defined shear-strength, eliminating the need for manual development of the strength-adjusted backbone curves by the user. Additional, interesting information about advances in nonlinear site-response analyses can be found in Hashash et al (2010).

Although site response analyses are a very useful tool they can be used only for free-field motions, which are motions that are not affected by the presence of a structure, and only for certain field conditions/topographies where the wave propagation is totally vertical. To study the dynamic soil behavior for areas where soil-structure interaction is significant and the soil behavior is affected by the structure (e.g. a massive or embedded structures), more advanced numerical and experimental methods are required. On the numerical side, two-dimensional and three-dimensional finite element analyses are required in order to capture properly the soil-structure interaction. On the experimental side, two common approaches include centrifuge testing or 1g-shake table testing. The advantage of centrifuge tests is that the gravitational acceleration can be modified in order to properly simulate the vertical effective stresses of the soil, however they are usually small-scale experiments, which limit the capability of accurately simulating the dynamic properties of a structure in SSI experiments. On the other hand, 1-g shake table tests are usually conducted at larger-scale than centrifuge tests allowing for more detailed representation of the structure, however they cannot simulate properly the vertical effective stresses. Therefore, for 1-g shake table tests it is important to conduct the experiments at the largest possible scale.

Several soil-boxes with different dimensions and wall configurations have been developed in the last few decades. Jafarzadeh (2004) presented the design of a square laminar shear box with 1m x 1m x 1m dimensions. The box consisted of 24 aluminum layers sitting one on top of each other and having 12 ball bearings in between two layers, which acted as rollers with minimized friction and allowed for shaking in both directions.

Ueng et al (2005) described a biaxial shake table with a more complex design that consisted of 15 layer of sliding frames with two nested frames for each layer, and an outside rigid frame. The dimensions of the box were 1.88m x 1.88x 1.52m. In the experimental tests of the box filled with soil the aforementioned authors observed that the accelerations at the center of the box and close to the walls were very similar for a sinusoidal shaking with PGA=0.05g and no liquefaction, but they were very different when liquefaction occurred at PGA=0.075g. In the latter case, the soil accelerations at the center of the box were significantly reduced after the occurrence of the liquefaction while the accelerations on the walls increased substantially and presented many spikes.

Chunxia et al (2008) presented the design and evaluation of the performance of a large-scale uniaxial laminar shear box with dimensions of 3m x 1.5m x 1.8m (height). The box consisted of 15 rigid frames, each of which was connected to an external frame via bearings in order to transfer the weight of the box off the shake-table. A similar approach of reducing the applied weight and the base shear on the shake-table via the use of an external frame was implemented in Turan et al (2009), with the external frame however being totally different than the one used in the previous study. The box in this case consisted of 24 aluminum layers supported by linear bearings and steel guide rods supported on the external frame. Last but not least, Dihoru et al (2010) investigated the dynamic behavior of two uniaxial laminar shear boxes with the larger one having dimensions 5m x 1.2 m x 1.2m. Both soil-boxes had low stiffness and mass in order for the soil to drive the response. In the high amplitude tests with 0.5g input motion horizontal flow was observed from the center of the box towards the walls at the surface. Moreover,

the tests demonstrated significant wall end effects for large magnitude shaking, which led to circulation of the soil close to the walls and deviation from 1D pure shear behavior, highlighting the significance of the soil-wall interaction. Their study revealed that the dynamic behavior of the laminar box with soil can differ substantially from an idealized 1D soil behavior, especially close to the walls, and that it is important to understand the behavior of the box itself in order to properly interpret the experimental results. Other large-scale soil-box have been used in several studies such as the ones conducted by Tokimatsu et al (2005), Suzuki et al (2008), Kawamata et al (2012), Motamed et al (2013), Wilson and Elgamal (2015), Antonellis et al (2015).

1.3 Organization of the thesis

For the design of the soil-box a wide range of numerical models were developed by the UNR research team, including 1D models of a soil-column, 2D model of a soil slice, 2D models of a slice of the soil-box and 3D models of the whole box, as shown in Figures 1-2 and 1-3. The main contribution of the author of the thesis was on the 1D and 2D modelling, which will be described in the following chapters.

The second and third chapter of this thesis present results from numerical analyses conducted in DEEPSOIL. The first part focuses on the comparison of a 1D soil column response in DEEPSOIL with recorded data at a free-field vertical array near the Kashiwazaki-Kariwa Nuclear Power Plant in Japan during the Niigataken Chuetsu-oki earthquake. This comparison was done in an attempt to increase the confidence on the modelling skills of the user and the capabilities of the software tool. The second part of the chapter presents detailed results from 1D site response analyses of a soil-column with a height equal to the expected height of the soil-box, which were conducted during the preliminary design phase. Linear, equivalent linear and nonlinear analyses are presented for a suite of recorded ground motions with scaled PGAs between 0.25g and 1.0g. The effect of soil nonlinearity of the surface response spectra is also evaluated. Moreover, the sensitivity of the nonlinear dynamic analyses results to several parameters such as, the hysteretic soil material (MKZ vs GQ/H), time-step, frequency removal and time-scaling is investigated.

Chapters 4, 5 and 6 present the finite element models and results from nonlinear dynamic analyses that were conducted in LS-DYNA. Chapter 4 discusses the equivalent

1D soil model that was developed in LS-DYNA, using 3D solid elements and a nested surface plasticity model with direct input of shear stress-strain curves for each soil layer, as was also done in Motamed et al (2016). This model is compared with results obtained form DEEPSOIL for both linear and nonlinear analyses. The rest of the chapters present several 2D models of the soil-box with gradually increasing complexity. Different contact conditions at the soil-wall interface, ranging from a perfect contact to frictionless contact were examined in order to decipher the role of sliding, friction and gapping on the behavior of the box. The boundary effect close to the walls was also examined and the area of uniform soil stresses was identified for different design alternatives. The effect of the mesh size, ground motion magnitude and properties of the walls was also examined.

Parameters of interest in the numerical analyses included the base shear, the overturning moment, the pressures below the box, the response spectra at the surface, the forces in the walls and the accelerations, displacements, strains and stresses of the soil and the box. The advanced numerical analyses and iterations presented in this thesis give an insight into the seismic behavior of the soil-box and are expected to be useful to other research teams designing their own soil-box.

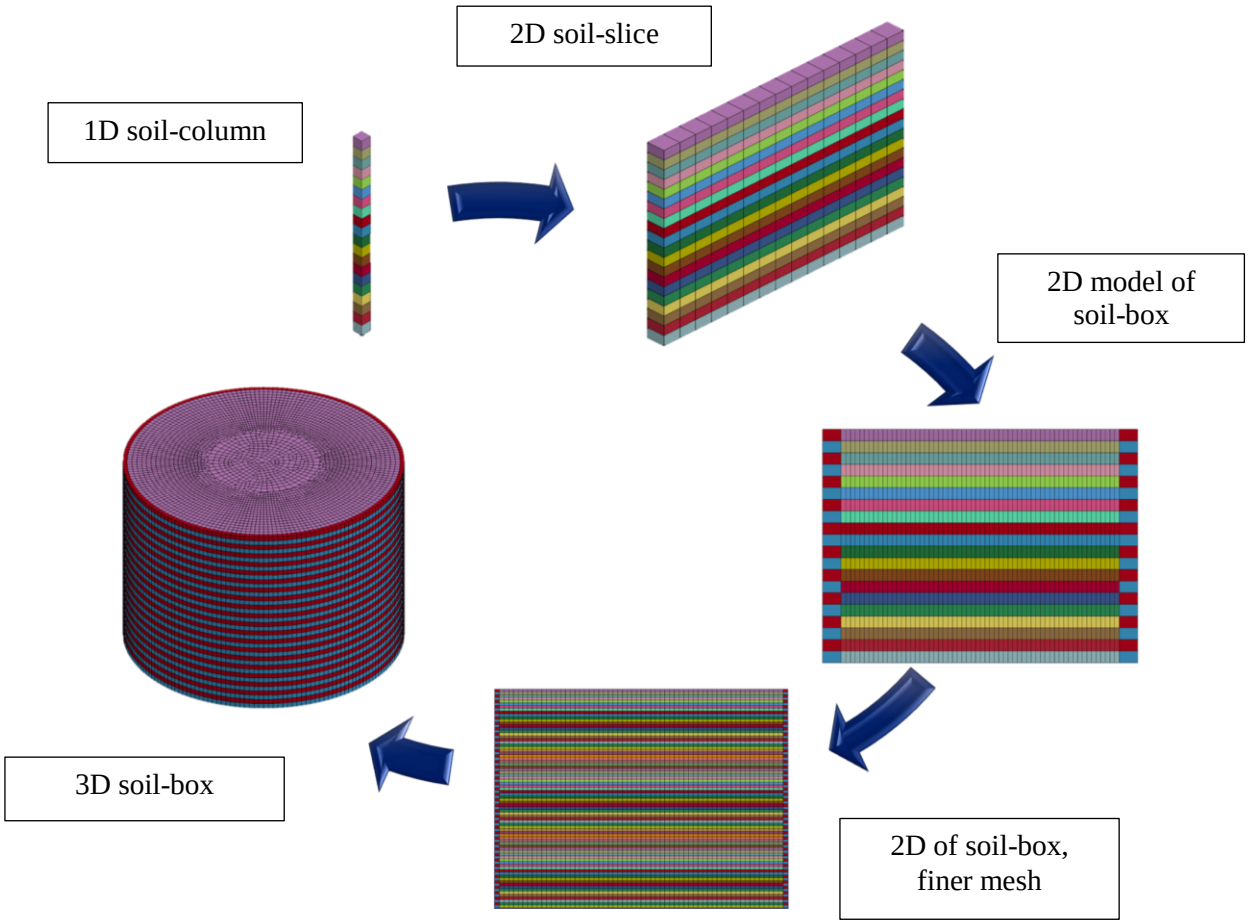

Figure 1-2: Overview of numerical models of the soil-box, developed in LS-DYNA by the UNR research team

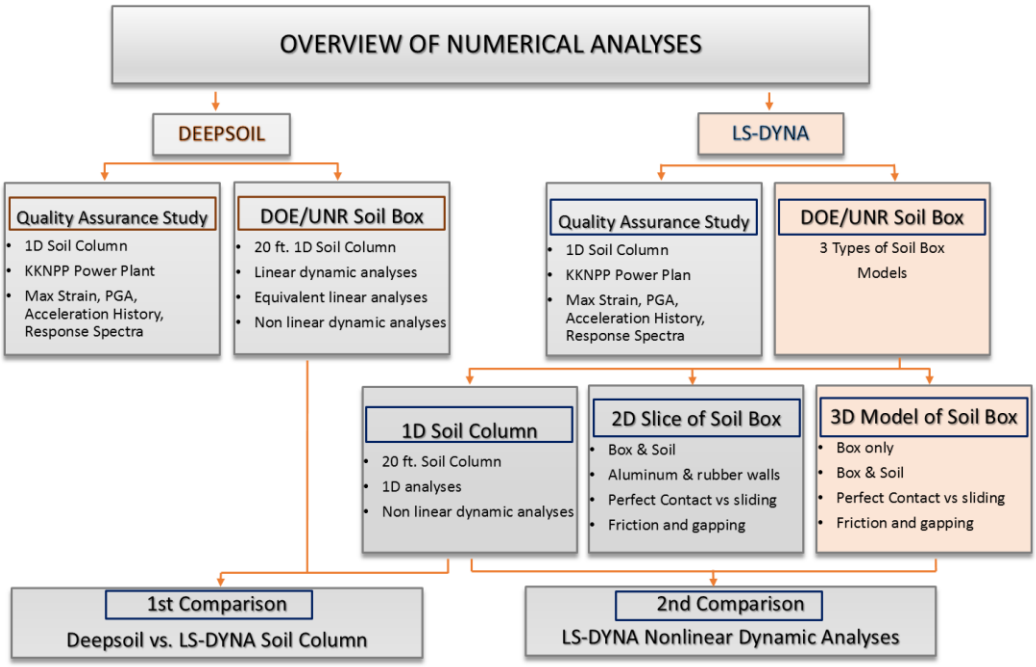

Figure 1-3: Diagram showing the numerical conducted in DEEPSOIL and LS-DYNA by the UNR research team

Chapter 2: Site Response Analysis in DEEPSOIL

2.1 Quality Assurance Study

One of the main objectives of the DOE SSI project is to study the seismic behavior of nuclear power plants under strong earthquake motions, where high soil nonlinearity is expected to occur. Therefore, it is essential for the design of the UNR-DOE soil-box to study the behavior of the soil at large shear strains, using existing numerical tools. The first step is to investigate the behavior of a 1D soil column via site response analyses and then move to more complex models of the soil-box. In this study, DEEPSOIL (Hashash et al 2001 and 2015) has been selected as the software program for conducting site response analyses due to its capability to conduct different type of analyses (linear, equivalent linear and nonlinear) and the availability of different soil materials (Modified Kodner Zelesko model, General Quadratic/Hyperbolic model). To ensure the proper use of the software by the author and increase the confidence in the capabilities of the software tool it was decided to conduct a quality assurance study. In this study a vertical array with recorded response was selected and used for comparison with numerical results from DEEPSOIL.

2.1.1 Description of vertical array

Although in the literature different vertical arrays with recorded earthquake data have been used for comparison with numerical analyses, most of the data correspond to low or moderate seismic motions. One of the fee-field vertical arrays with data recorded for a high seismic motion is the Service Hall Array at the Kashiwazaki-Kariwa Nuclear Power Plant (KKNPP), which was strongly shaken during 2007 Niigata-ken Chuetsu-oki Earthquake. This vertical array was recently used in other studies such as Stewart and Yee (2012), Yee et al (2013), Motamed et al (2016). Figures 2-1 and 2-2, which have been obtained from Yee et al (2012), show that the site conditions consist of about 70 m of medium-dense sands over clayey bedrock, with groundwater located at 45 m. The three-component accelerations were measured at depths of 2.4 m, 50.8 m, 99.4 m and 250 m, and the accelerations at the two deepest locations (99.4 and 250m) were seen to be similar. Interestingly the recorded PGAs were 0.52g at the bedrock and 0.4g at the surface indicating nonlinear soil behavior. A more detailed description about the vertical array can be found in Yee et al (2013).

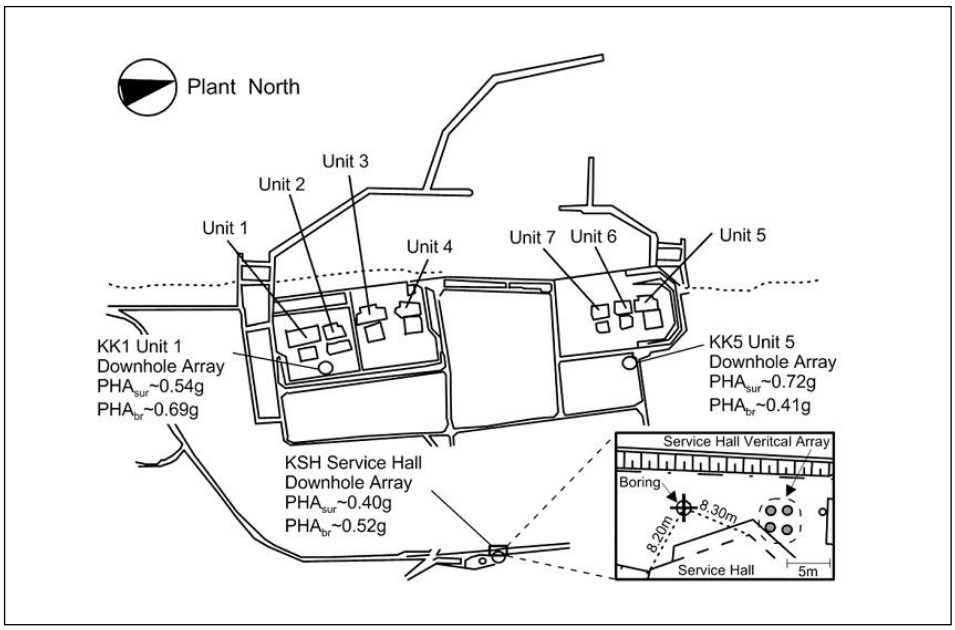

Figure 2-1: Map of KKNPP showing locations of downhole arrays and geometric mean peak accelerations from 2007 Niigata-ken Chuetsu-oki earthquake (source: Stewart and Yee, 2012)

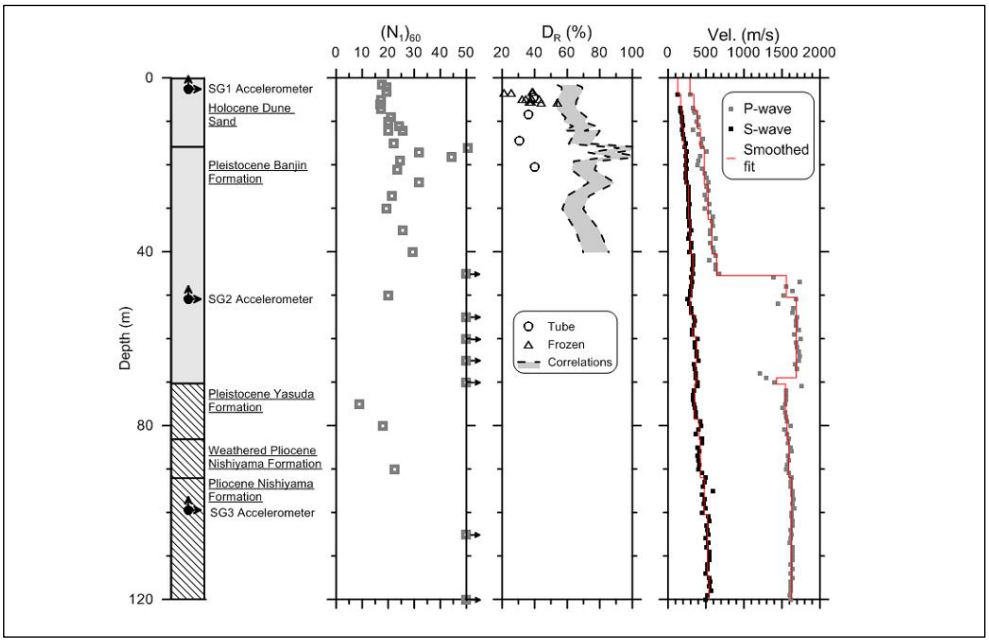

Figure 2-2: Geologic log at SHA site and results of penetration and suspension logging geophysical testing (source: Stewart and Yee, 2012)

2.1.2 Description of DEEPSOIL model

The aforementioned studies conducted by Stewart and Yee (2012) used a nonlinear soil material with strength-adjusted backbone curves. In order determine the properties of the soil, the researchers of the previous study conducted laboratory tests (resonant column and torsional shear tests). Based on these tests the modulus reduction and damping curves were determined, however they were expected to be valid up to moderate shear strains ($\leq$0.5%). To extend these curves to large strains the authors presented a procedure according to which the backbone curves asymptotically approached the shear strength. As shown in Figure 2-3. Using this approach in nonlinear dynamic analyses conducted in DEEPSOIL the authors were able to achieve a reasonable agreement with the recorded data at the Service Hall Array. Based on this approach, Motamed et al (2016) presented a modified method that gives the user the capability of adjusting the shape of the curve beyond the transition strain, allowing for better fitting of the backbone curve. This approach was implemented in LS-DYNA using a model of stacked 3D solid elements, for both uniaxial and biaxial shaking and a good agreement with the measured response at the Service Hall Array was again achieved. For the quality assurance study presented in this thesis, the same two-stage backbone curves used in Motamed et al (2016) are implemented in DEEPSOIL as user defined curves. One of the main differences between DEEPSOIL and LS-DYNA is that the first one uses a lumped mass approach as shown in Figure 2-4, while the second one uses finite elements.

Since the recorded motions at the SHA during the 2007 Niigata-ken Chuetsu-oki Earthquake was the same at z=250m and z=99.4m the soil column model in DEEPSOIL

was developed with a height of 99.4m. The recorded accelerations at z=99.4m (Figure 2-5) was used as an input motion in the numerical model. Both equivalent linear and nonlinear analyses were conducted using the MKZ model with extended Masing rules. Detailed information about the material model in DEEPSOIL can be found in Hashash et al (2015). Acceleration histories and response spectra, PGAs profiles and peak strain profiles were output from DEEPSOIL and used for comparison with recorded data and the numerical results published by Stewart and Yee (2012), as will be shown in the next section.

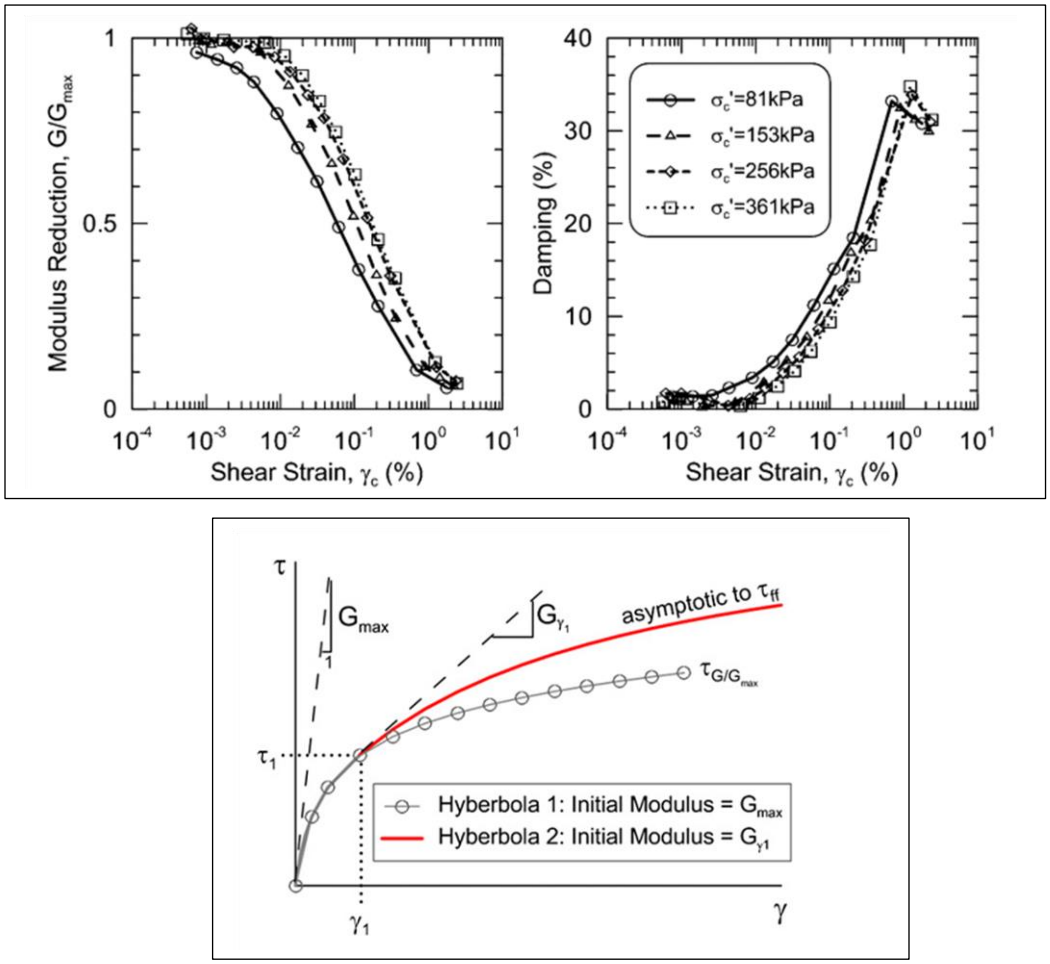

Figure 2-3: Modulus reduction and damping curves from resonant column and torsional shear tests (top) and graph of shear strength–adjusted modulus reduction curves (bottom), from Stewart and Yee, 2012

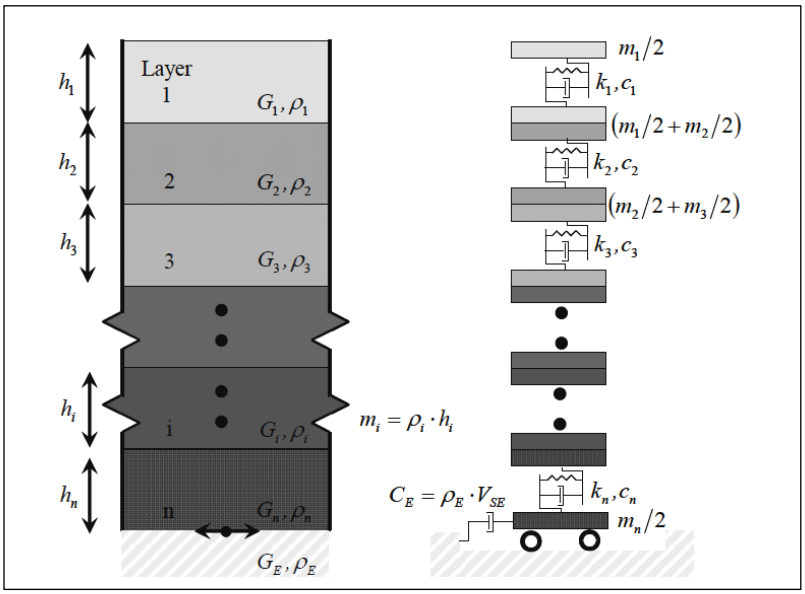

Figure 2-4: The lumped-mass models for site-response analysis (source: Hashash et al. (2010))

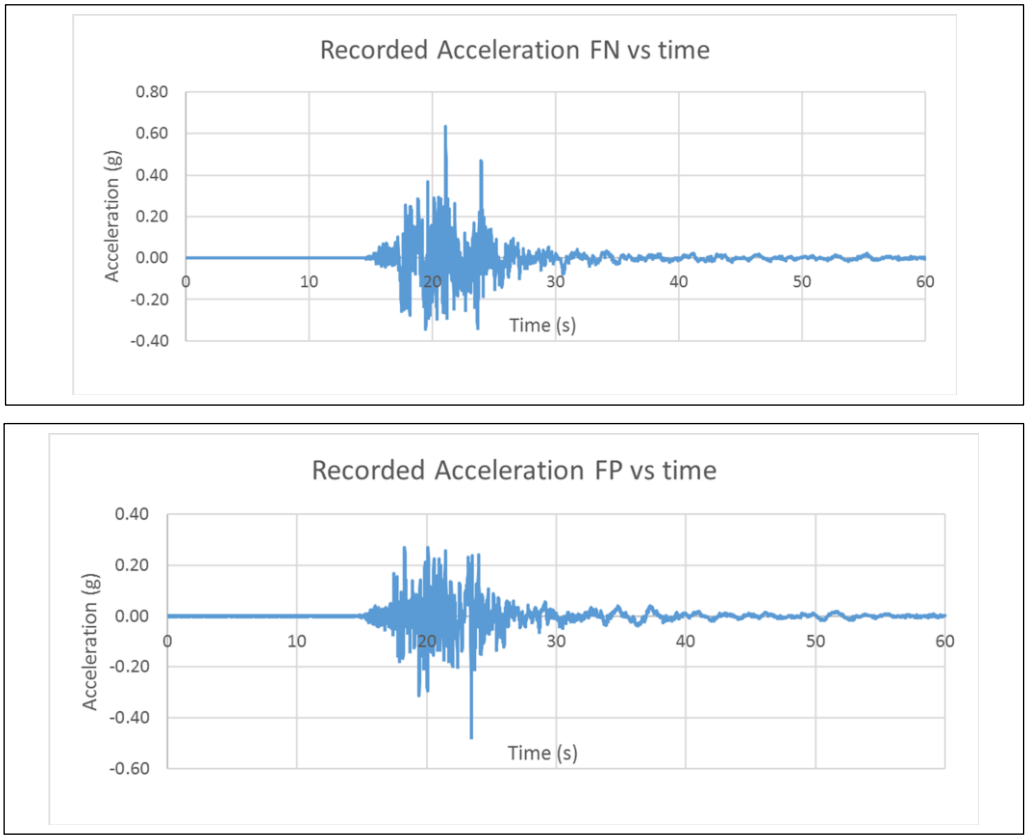

Figure 2-5: Input motion for DEEPSOIL model

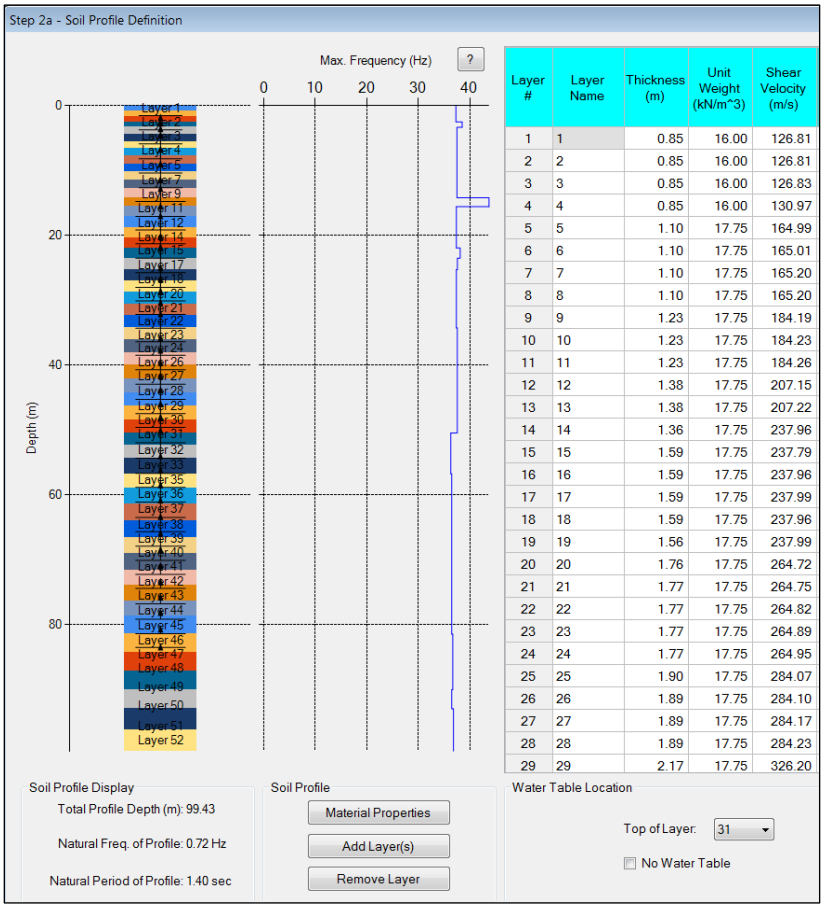

Layer #	Layer Name	Thickness (m)	Unit Weight (kN/m^3)	Shear Velocity (m/s)
1	1	0.85	16.00	126.81
2	2	0.85	16.00	126.81
3	3	0.85	16.00	126.83
4	4	0.85	16.00	130.97
5	5	1.10	17.75	164.99
6	6	1.10	17.75	165.01
7	7	1.10	17.75	165.20
8	8	1.10	17.75	165.20
9	9	1.23	17.75	184.19
10	10	1.23	17.75	184.23
11	11	1.23	17.75	184.26
12	12	1.38	17.75	207.15
13	13	1.38	17.75	207.22
14	14	1.36	17.75	237.96
15	15	1.59	17.75	237.79
16	16	1.59	17.75	237.96
17	17	1.59	17.75	237.99
18	18	1.59	17.75	237.96
19	19	1.56	17.75	237.99
20	20	1.76	17.75	264.72
21	21	1.77	17.75	264.75
22	22	1.77	17.75	264.82
23	23	1.77	17.75	264.89
24	24	1.77	17.75	264.95
25	25	1.90	17.75	284.07
26	26	1.89	17.75	284.10
27	27	1.89	17.75	284.17
28	28	1.89	17.75	284.23
29	29	2.17	17.75	326.20

Figure 2-6: DEEPSOIL model

Table 2-1: DEEPSOIL model

Layer #	Layer Name	Thickness (m)	Unit Weight (kN/m^3)	Shear Velocity (m/s)
1	1	0.85	16.00	126.81
2	2	0.85	16.00	126.81
3	3	0.85	16.00	126.83
4	4	0.85	16.00	130.97
5	5	1.10	17.75	164.99
6	6	1.10	17.75	165.01
7	7	1.10	17.75	165.20
8	8	1.10	17.75	165.20
9	9	1.23	17.75	184.19
10	10	1.23	17.75	184.23
11	11	1.23	17.75	184.26
12	12	1.38	17.75	207.15
13	13	1.38	17.75	207.22
14	14	1.36	17.75	237.96
15	15	1.59	17.75	237.79
16	16	1.59	17.75	237.96
17	17	1.59	17.75	237.99
18	18	1.59	17.75	237.96
19	19	1.56	17.75	237.99
20	20	1.76	17.75	264.72
21	21	1.77	17.75	264.75
22	22	1.77	17.75	264.82
23	23	1.77	17.75	264.89
24	24	1.77	17.75	264.95
25	25	1.90	17.75	284.07
26	26	1.89	17.75	284.10
27	27	1.89	17.75	284.17
28	28	1.89	17.75	284.23
29	29	2.17	17.75	326.2

2.1.3 Recorded data vs Numerical analyses in DEEPSOIL

Figures 2-7 and 2-8 show the acceleration histories in fault normal direction at z=2.4m and z=50.8m calculated from nonlinear analyses and equivalent linear analyses respectively. The nonlinear analyses seem to give results that match quite well with the recorded histories, however they seem to have some higher frequencies, especially at z=50.8m which are not observed in the recorded data. This higher frequency content had

been observed also in the analyses conducted by Stewart and Yee (2012). The equivalent linear analyses also give reasonable results, with a very good matching of the accelerations at z=50.8m and a noticeable overestimation at z=2.4m. Another characteristic of the results from equivalent linear analyses is that they do not have the artificial high frequencies that were observed in the nonlinear analyses, indicating that those frequencies are probably related to the nonlinear material. Similar observations can made also for the accelerations in fault parallel direction, shown in Figures 2-9 and 2-10, with the difference that the equivalent linear analyses do not show a clear over-estimation at z=2.4m, as was the case with the fault normal direction.

Figure 2-11 shows the PGAs profile and the acceleration response spectra at z=2.4m and z=50.8m in the fault normal direction. As was noticed in the acceleration histories and is verified by the response spectra, the nonlinear numerical analyses conducted in the current study and by Stewart and Yee (2012) overestimate the response in the high-frequency region. Moreover, the numerical PGAs match quite well the PGAs recorded at the two aforementioned depths, with the equivalent linear analyses matching better the PGA at z=50.8m and the nonlinear analyses at z=2.4m. The good agreement of PGAs and over-estimation of PSA in the high-frequency region is also observed in the fault parallel direction shown in Figure 2-12.

Since the shear strains were not recorded at SHA, but were output by Stewart and Yee (2012), Figure 2-13 shows a comparison of the shear-strain profiles produced by the aforementioned researchers and the one produced by the current study. Generally, similar trends are observed, with the nonlinear analyses giving consistently larger strains than the

equivalent linear ones in both studies, and the current study giving larger values in the fault parallel direction than the previous study.

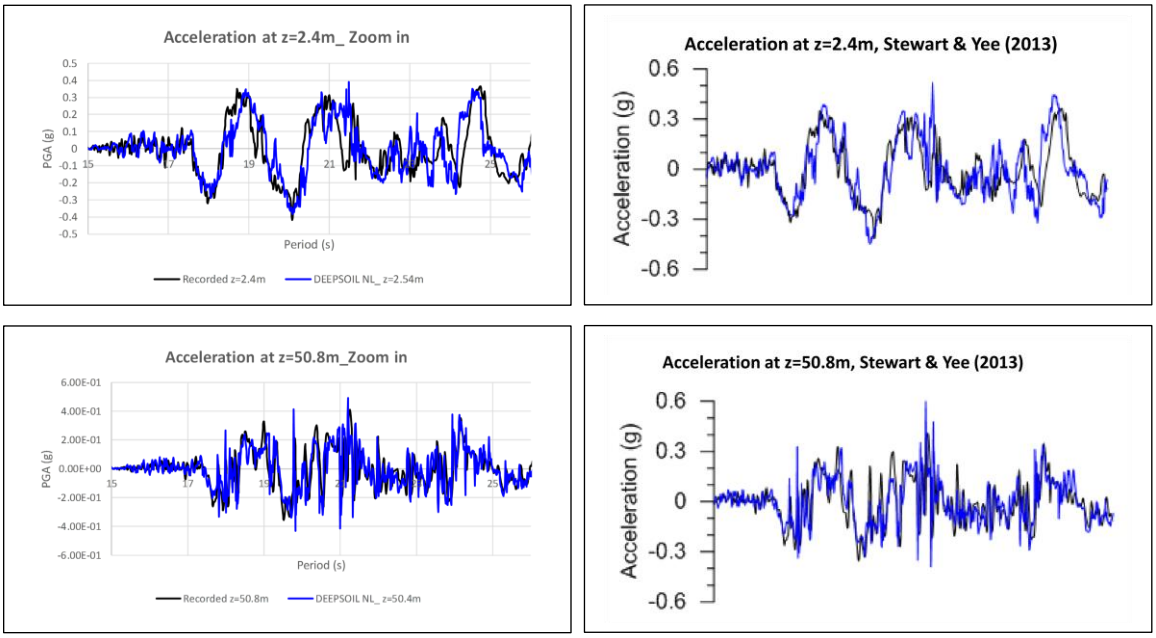

Figure 2-7: Fault Normal, Nonlinear Acceleration Histories from (a) current study (left) and (b) Stewart and Yee, 2012 (right)

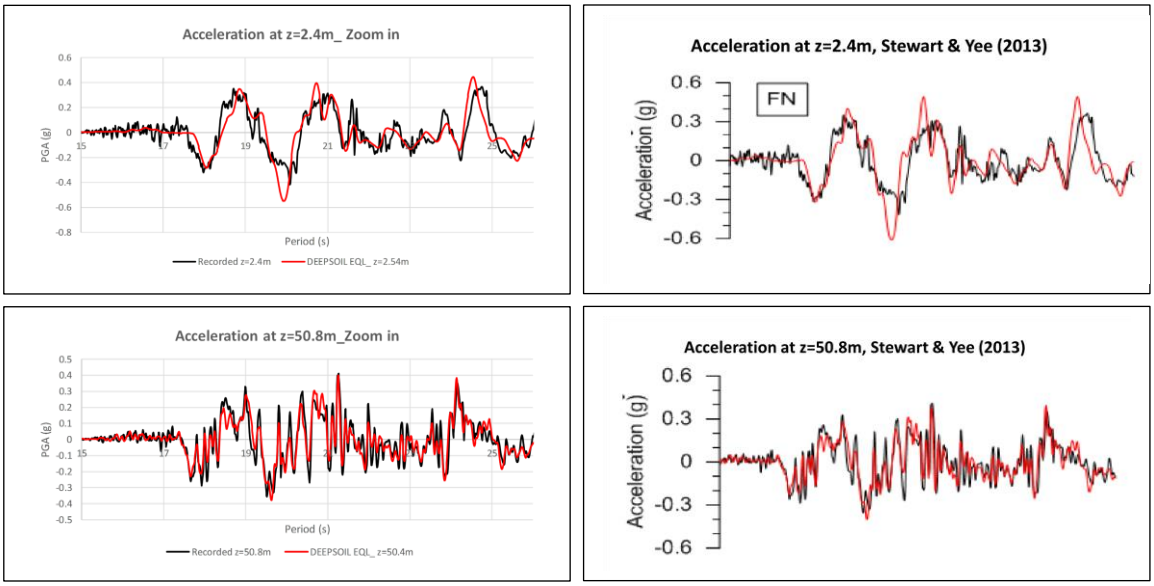

Figure 2-8: Fault Normal, Equivalent Linear Acceleration Histories from (a) current study (left) and (b) Stewart and Yee, 2012 (right)

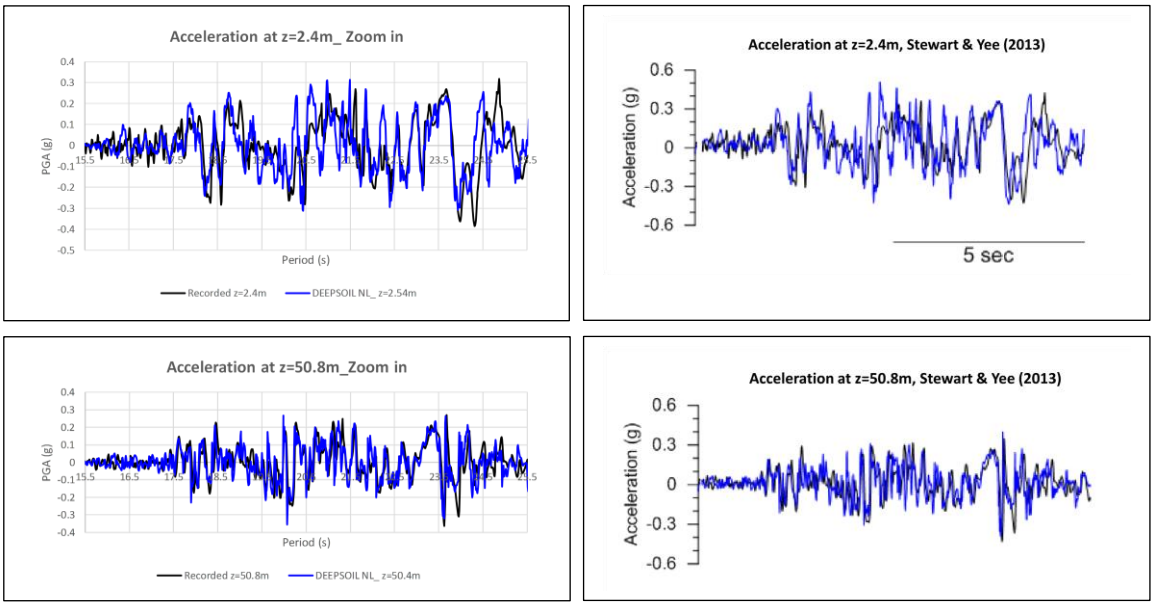

Figure 2-9: Fault Parallel, Nonlinear Acceleration Histories from a) current study (left) and b) Stewart and Yee, 2012 (right)

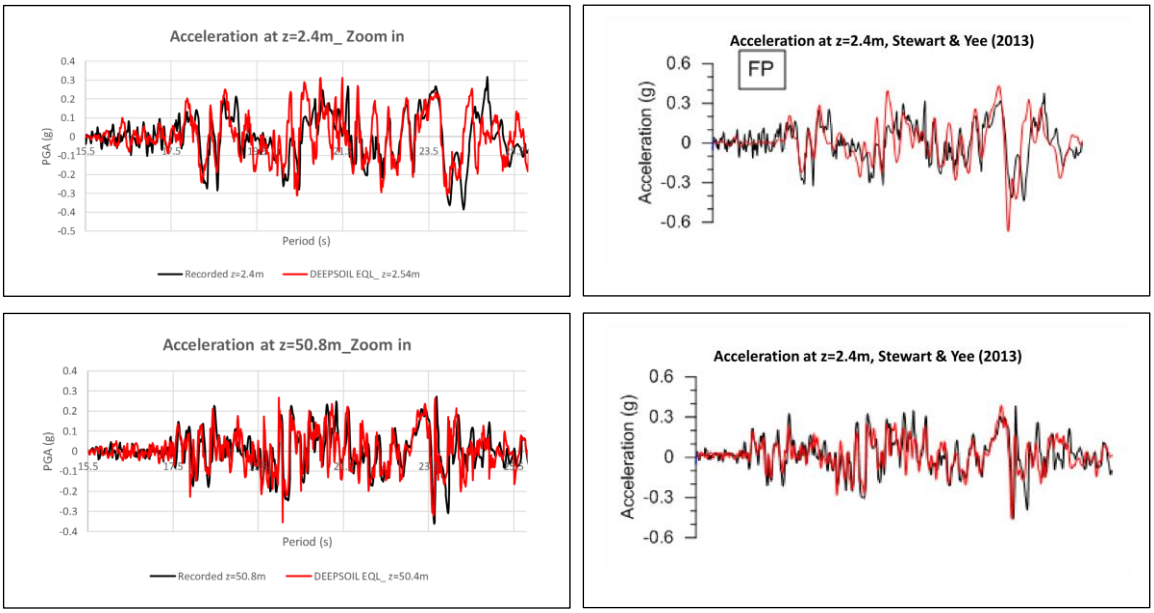

Figure 2-10: Fault Parallel, Equivalent Linear Acceleration Histories from (a) current study (left) and (b) Stewart and Yee, 2012 (right)

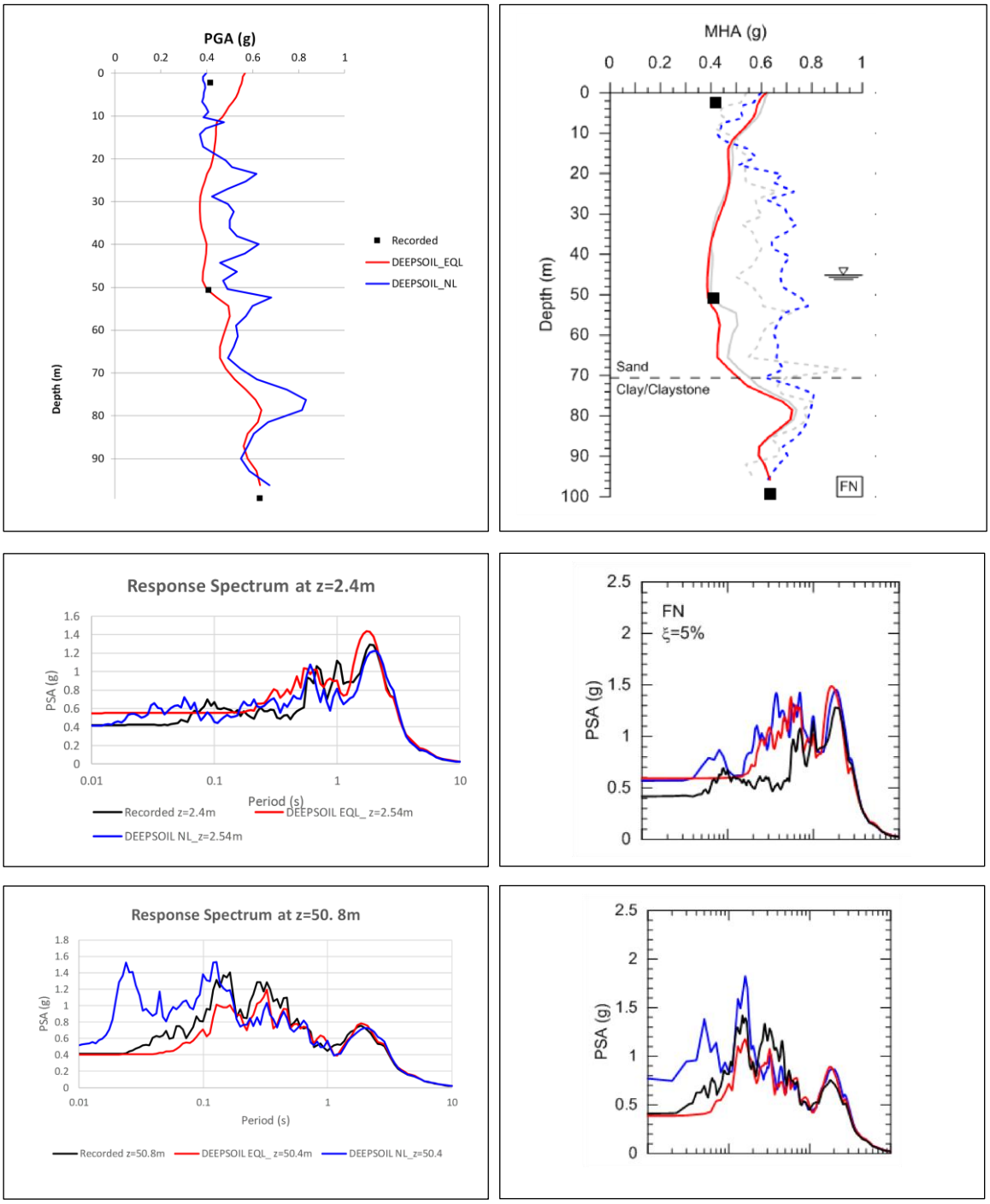

Figure 2-11: Fault Normal Soil Profiles and Response Spectra from (a) current study (left) and (b) Stewart and Yee, 2012 (right)

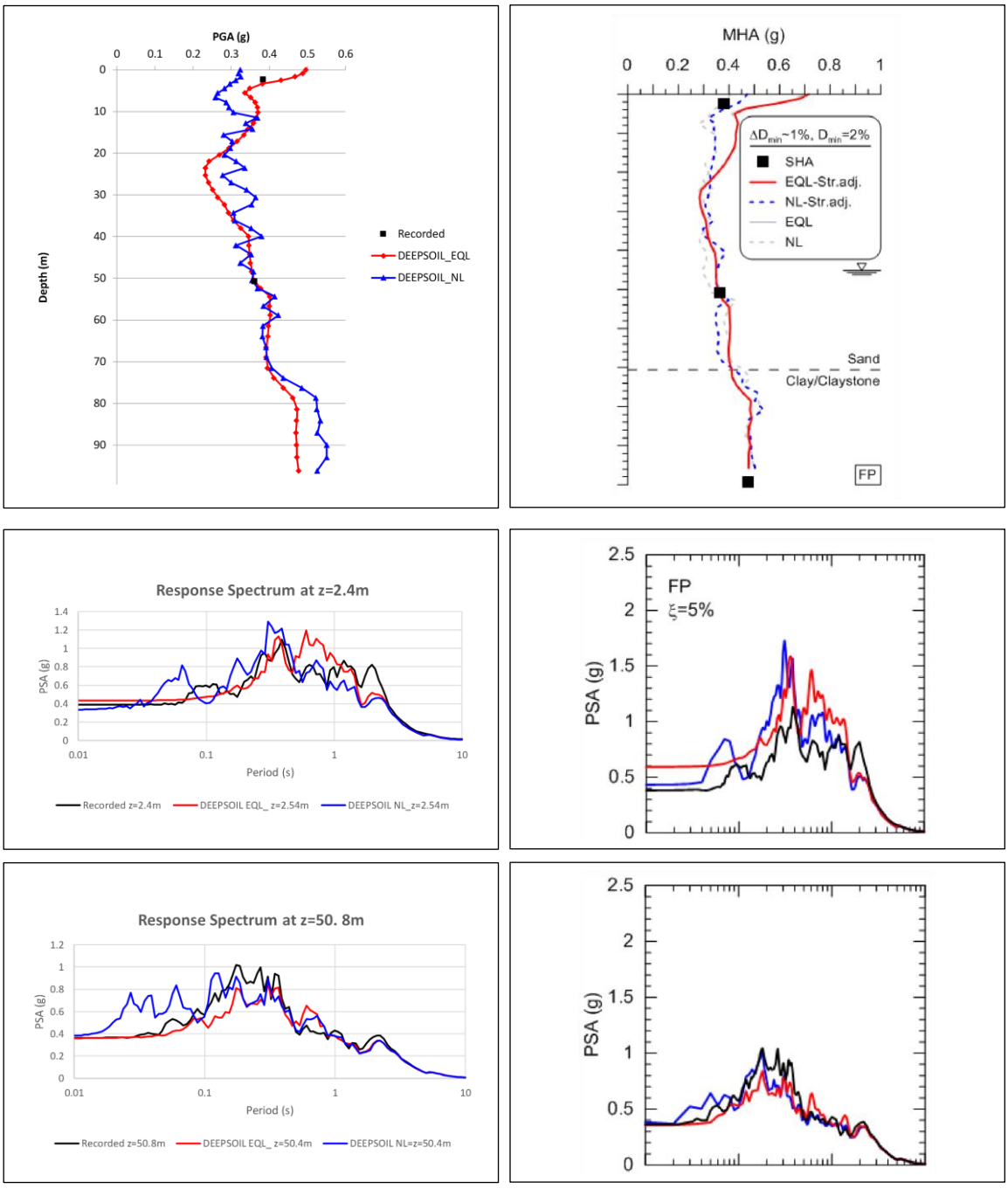

Figure 2-12: Fault Parallel Soil Profiles and Response Spectra from (a) current study (left) and (b) Stewart and Yee, 2012 (right)

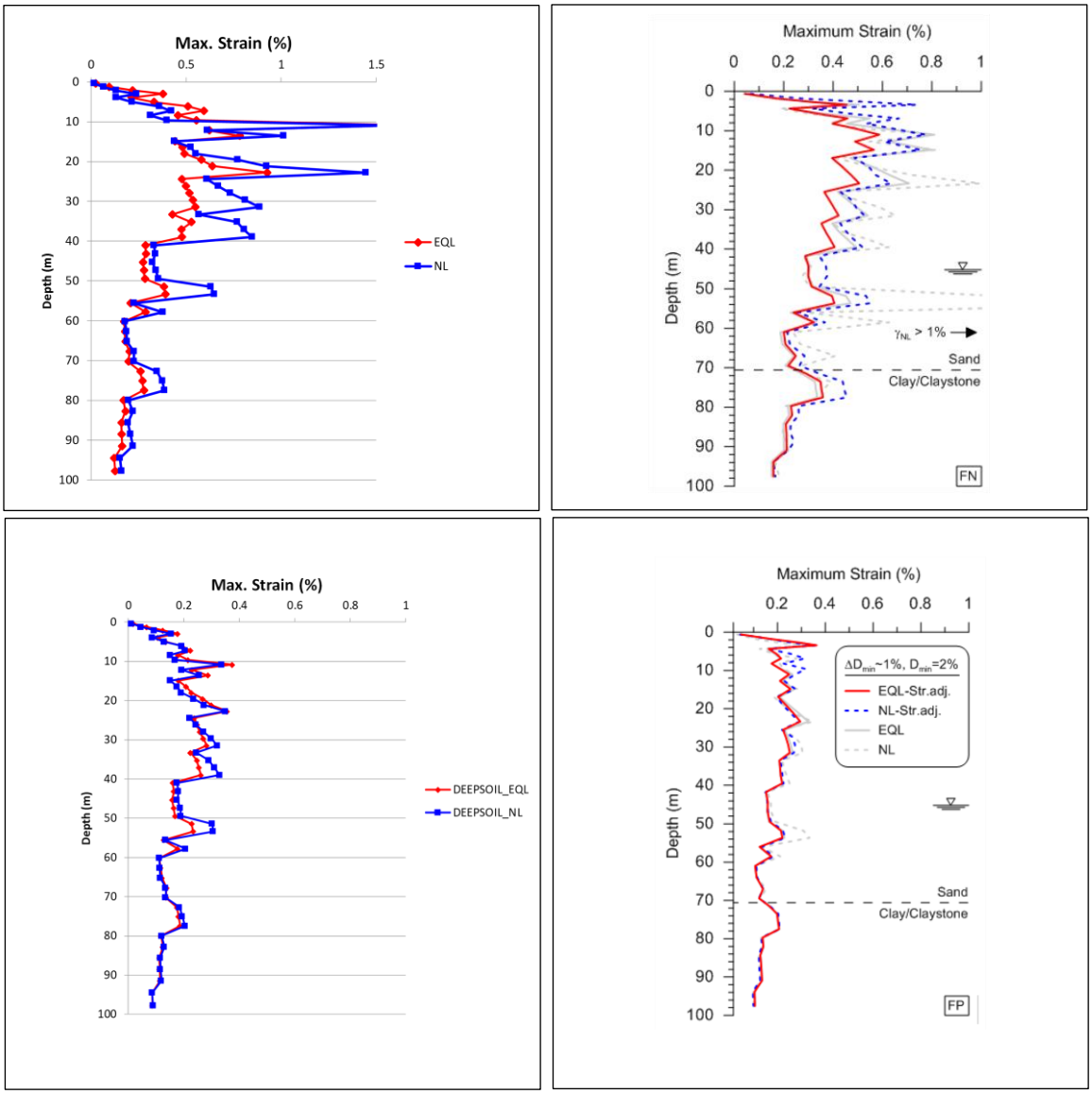

Figure 2-13: FN (top) and FP (bottom), Peak strain profiles from (a) current study (left) and (b) Stewart and Yee, 2012 (right)

2.2 One-Dimensional Analyses of 20ft soil-column

2.2.1 Ground motions

The good agreement of the 1D nonlinear analyses with the recorded data and the past work done by Stewart and Yee (2012) gives confidence in the modelling skills of the user and the capabilities of the software to simulate reasonably the soil response at large strains. The next step was to develop a model that would resemble the behavior of the soil-box, and would be used for providing data for the design of the box. To this end a suite of eight, two-component ground motions were selected and taken from the PEER database, for sites with similar seismogenic and geotechnic features as found at the sites of different nuclear facilities (competent soil). The selected motions with the corresponding site conditions are shown in Table 2-2. These ground motions were initially scaled (linearly) to have the same PGA (0.26g) and then different scaling factors were used in order to achieve strong shaking of up to 1.04g, as shown in Table 2-3.

Table 2-4 shows the PGAs, PGVs and PGDs of the scaled motions, while Figure 2-14 shows the acceleration response spectra of the seed motions. Clearly the ground motions cover a wide range of frequencies, with Landers having a higher frequency content than the rest of the motions, and some motions having a near-fault pulse, such as Erzincan and Nishi-Akashi.

Table 2-2: Selected Ground motions

No.	Earthquake	Station	M	Site Vs30 (m/s)	Site Class
1	1940 Imperial Valley-02	El Centro Array #9	6.95	213	D
2	1989 Loma Prieta	Gilroy Array #1	6.9	1428	B
3	1995 Kobe	Nishi-Akashi	6.9	609	C
4	1999 Hector Mine	Hector	7.1	726	C
5	1979 Imperial Valley	Cerro Prieto	6.5	472	C
6	2002 Denali, Alaska	Carlo (temp)	7.9	399	C
7	1992 Landers	Lucerne	7.3	1369	B
8	1992 Erzincan	Erzincan	6.7	352	D

Table 2-3: PGAs corresponding to each scale factor

Scale Factor	1.0	2.0	3.0	4.0
PGA	0.26g	0.52 g	0.78 g	1.04 g

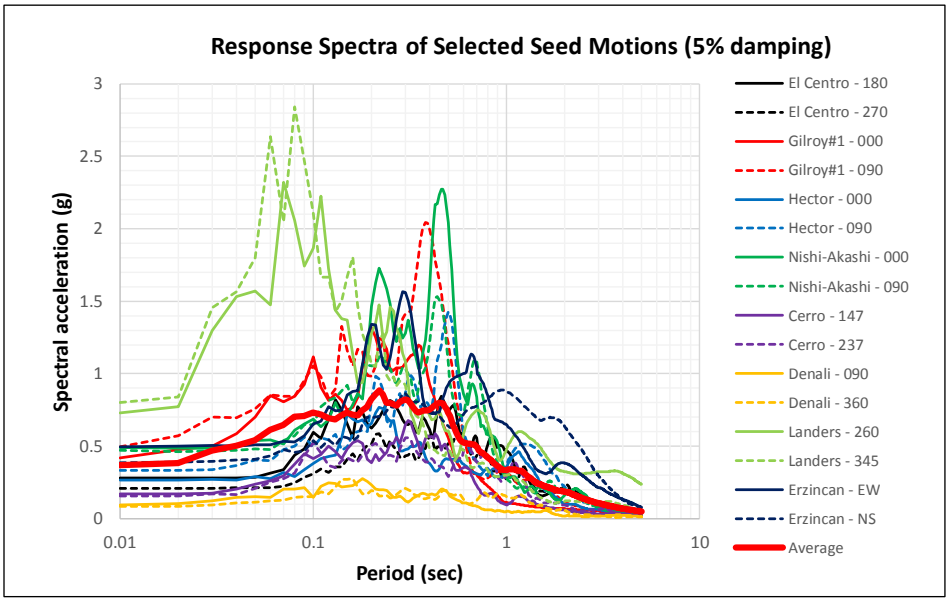

Figure 2-14: Response spectra of selected seed motions (credit: Dr. Motamed)

Table 2-4: PGAs, PGVs, PGDs for selected ground motions

Ground Motions	PGA (g)	PGV (cm/s)	PGD (cm)
Nishi-Akashi 090	0.26	21.67	6.84
Nishi-Akashi 000	0.26	25.48	4.57
Landers 345	0.26	9.37	8.514
Landers 260	0.26	48.38	41.31
Hector 090	0.26	35.88	8.56
Hector 000	0.26	25.77	19.57
Gilroy 090	0.26	17.61	8.49
Gilroy 000	0.26	21.3	5.08
Erzincan ns	0.26	72.87	21.76
Erzincan ew	0.26	41.42	14.86
El Centro 270	0.26	39.09	30.15
El Centro 180	0.26	28.98	8.11
Denali 360	0.26	34.18	26.7
Denali 090	0.26	19.15	11
Cerro 237	0.26	32.28	13.14
Cerro 147	0.26	18.06	8.2

2.2.2 Description of model

During the preliminary design phase the height of the soil-box was estimated to be 20ft, therefore the soil column model in DEEPSOIL had the same height. The model was discretized using 1ft deep soil layers, meaning that there were 20 soil layers in total. For the analyses two soil types were initially considered, a dense one with γ= 120pcf and Dr= 75%, and a loose one γ= 90pcf and Dr= 30%. The fundamental periods were 0.13sec and 0.16sec for the two previous soil types respectively. Since the software has the capability of conducting different types of analyses, the author conducted linear analyses (in time-domain and frequency domain) as well as equivalent linear and nonlinear analyses.

In the analyses the MKZ model was used with Non-Masing unloading-reloading rules in order to capture the hysteretic soil behavior. The Seed&Idriss backbone curves (mean) was used as a reference curve in the initial analyses, and then the sensitivity of the results to the backbone curve was examined via comparison with Darendeli's curves. The numerical analyses were conducted for scale factors of 0.5, 1.0, 1.5, 2.0, 3.0, and 4.0. Figures 2-15 and 2-16 show information regarding the numerical model and the G/Gmax and Damping Curves in DEEPSOIL.

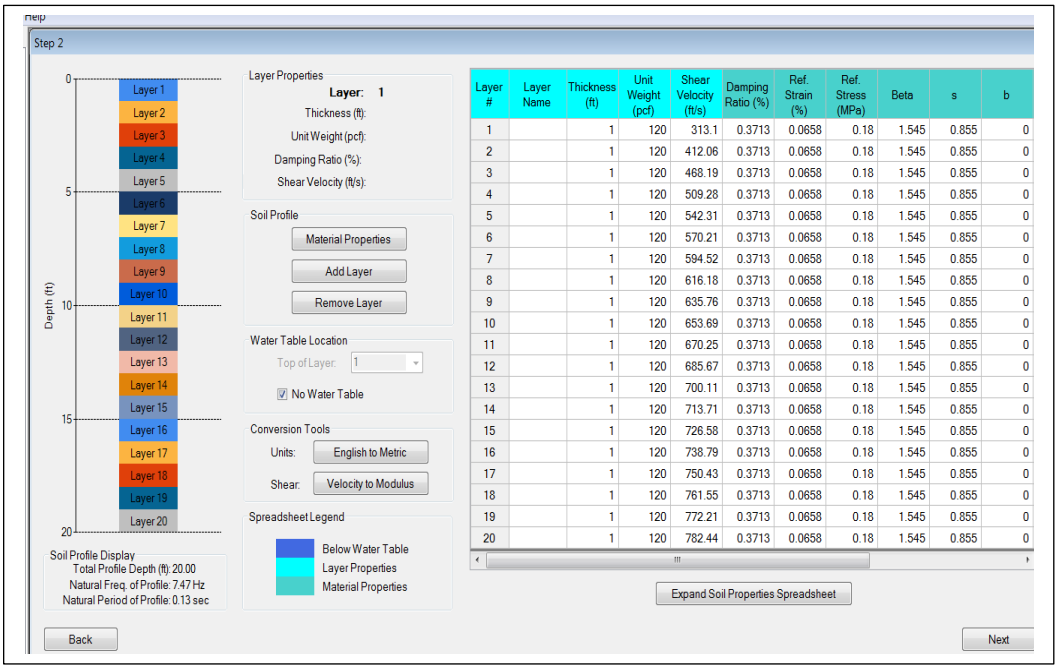

Layer #	Layer Name	Thickness (ft)	Unit Weight (pcf)	Shear Velocity (ft/s)	Damping Ratio (%)	Ref. Strain (%)	Ref. Stress (MPa)	Beta	s	b
1		1	120	313.1	0.3713	0.0658	0.18	1.545	0.855	0
2		1	120	412.06	0.3713	0.0658	0.18	1.545	0.855	0
3		1	120	468.19	0.3713	0.0658	0.18	1.545	0.855	0
4		1	120	509.28	0.3713	0.0658	0.18	1.545	0.855	0
5		1	120	542.31	0.3713	0.0658	0.18	1.545	0.855	0
6		1	120	570.21	0.3713	0.0658	0.18	1.545	0.855	0
7		1	120	594.52	0.3713	0.0658	0.18	1.545	0.855	0
8		1	120	616.18	0.3713	0.0658	0.18	1.545	0.855	0
9		1	120	635.76	0.3713	0.0658	0.18	1.545	0.855	0
10		1	120	653.69	0.3713	0.0658	0.18	1.545	0.855	0
11		1	120	670.25	0.3713	0.0658	0.18	1.545	0.855	0
12		1	120	685.67	0.3713	0.0658	0.18	1.545	0.855	0
13		1	120	700.11	0.3713	0.0658	0.18	1.545	0.855	0
14		1	120	713.71	0.3713	0.0658	0.18	1.545	0.855	0
15		1	120	726.58	0.3713	0.0658	0.18	1.545	0.855	0
16		1	120	738.79	0.3713	0.0658	0.18	1.545	0.855	0
17		1	120	750.43	0.3713	0.0658	0.18	1.545	0.855	0
18		1	120	761.55	0.3713	0.0658	0.18	1.545	0.855	0
19		1	120	772.21	0.3713	0.0658	0.18	1.545	0.855	0
20		1	120	782.44	0.3713	0.0658	0.18	1.545	0.855	0

Figure 2-15: DEEPSOIL model of 20ft column

Table 2-5: DEEPSOIL model of 20ft column

Layer #	Layer Name	Thickness (ft)	Unit Weight (pcf)	Shear Velocity (ft/s)	Damping Ratio (%)	Ref. Strain (%)	Ref. Stress (Mpa)	Beta	s	b
1		1	120	313.10	0.3713	0.658	0.18	1.545	0.855	0
2		1	120	412.06	0.3713	0.658	0.18	1.545	0.855	0
3		1	120	468.19	0.3713	0.658	0.18	1.545	0.855	0
4		1	120	509.28	0.3713	0.658	0.18	1.545	0.855	0
5		1	120	542.31	0.3713	0.658	0.18	1.545	0.855	0
6		1	120	570.21	0.3713	0.658	0.18	1.545	0.855	0
7		1	120	594.52	0.3713	0.658	0.18	1.545	0.855	0
8		1	120	616.18	0.3713	0.658	0.18	1.545	0.855	0
9		1	120	635.76	0.3713	0.658	0.18	1.545	0.855	0
10		1	120	653.69	0.3713	0.658	0.18	1.545	0.855	0
11		1	120	670.25	0.3713	0.658	0.18	1.545	0.855	0
12		1	120	685.67	0.3713	0.658	0.18	1.545	0.855	0
13		1	120	700.11	0.3713	0.658	0.18	1.545	0.855	0
14		1	120	713.71	0.3713	0.658	0.18	1.545	0.855	0
15		1	120	726.58	0.3713	0.658	0.18	1.545	0.855	0
16		1	120	738.79	0.3713	0.658	0.18	1.545	0.855	0
17		1	120	750.43	0.3713	0.658	0.18	1.545	0.855	0
18		1	120	761.55	0.3713	0.658	0.18	1.545	0.855	0
19		1	120	772.21	0.3713	0.658	0.18	1.545	0.855	0
20		1	120	782.44	0.3713	0.658	0.18	1.545	0.855	0

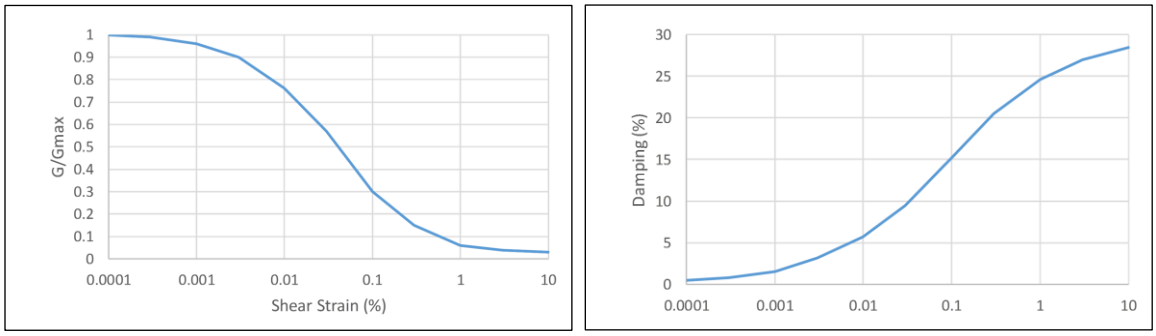

Figure 2-16: Example of G/Gmax and Damping curves used in the DEEPSOIL model (layer 10)

2.2.3 Selected results

This section will present results from nonlinear dynamic analyses for two selected ground motions, namely Hector 090 and El Centro 180, and a scale factor equal to 2.0 (PGA=0.50g). Before proceeding to the comparison of the two motions, Figure 2-17 is showing the base shear histories calculated with two different approaches. In the first approach the acceleration of each soil layer is output and then it is multiplied with its corresponding mass (for the assumed dimensions of the soil-box), and then once the inertia forces of each soil layer is calculated then all the forces are summed in order to calculate the total inertia force. An alternative approach was to calculate the base shear by assuming that it is equal to the shear force that the bottom soil layer is transferring to the ground, which would be τ*A. The latter method is more convenient because only the the shear stresses of the bottom layer are required as an input, however, as shown in Figure 2-17 this method can slightly underestimate the base shear. This can be explained by the fact that the total inertia forces generated along the height of the soil column is transferred to the support via the shear force (spring) and the damping force (dashpot). Therefore, the most accurate way for calculating the total lateral force that the actuators of the shake table must be able to apply, is to consider the total inertia forces of the soil column.

Figure 2-18 shows the accelerations at the top of layer 20 and layer 1 (surface) for the two aforementioned ground motions. Both motions seem to undergo significant amplification as they propagate vertically towards the surface of the column reaching a PGA of approximately 0.74g and 0.93g at the surface for El Centro and Hector respectively, although both input motions had a PGA of 0.50g (note that ground motion is

input at the bottom of layer 20). This amplification is verified in Figure 2-19 that shows the PGAs for all soil layers, and the acceleration response spectra at the surface and the top of layer 20. Interestingly, although the magnification of the PGAs is common for both ground motions, the response spectra reveals that the peaks of the PSA seem to occur at approximately T=0.25sec for El Centro and at T=0.5sec (largest peak) and T=0.25sec (second peak) for Hector 090. Given the fact that the fundamental period of the soil column is 0.13sec it is clear that the soil has yielded resulting in softening and offset of the natural periods. Moreover, the fact that the largest peak occurs at a larger period for Hector090 than ElCentro 180, indicates that the former introduces larger stains and more nonlinearity in the soil. This is verified in Figures 2-20 and 2-21, which show the maximum strains together with relative displacements and the shear stress-strain loops respectively. Both input motions introduce large shear strains, which are above 0.5%. In particular, in the case of El Centro the bottom soil layer reach 0.6%, while for Hector the max shear strain is slighlty above 1.4%. It must be also noted that in the former case only a few feet at the bottom of the soil column exceed the 0.5% shear strain, while in the latter case approximately 2/3 of the whole soil column witness shear stresses in excess of 0.5%. This justifies why for the Hector motion the peak PSA occurs at larger periods.

These figures demonstrate that the frequency content of the motion at the surface of the soil column is highly dependent on the input motion at the bottom especially when the soil behaves nonlinearly. It is important to identify/predict the motion at the surface because that will facilitate the selection of the dynamic properties of the structure that

might be tested in future SSI experiments. These properties should be selected carefully if the goal is to resonate the structure with the soil column and magnify the response.

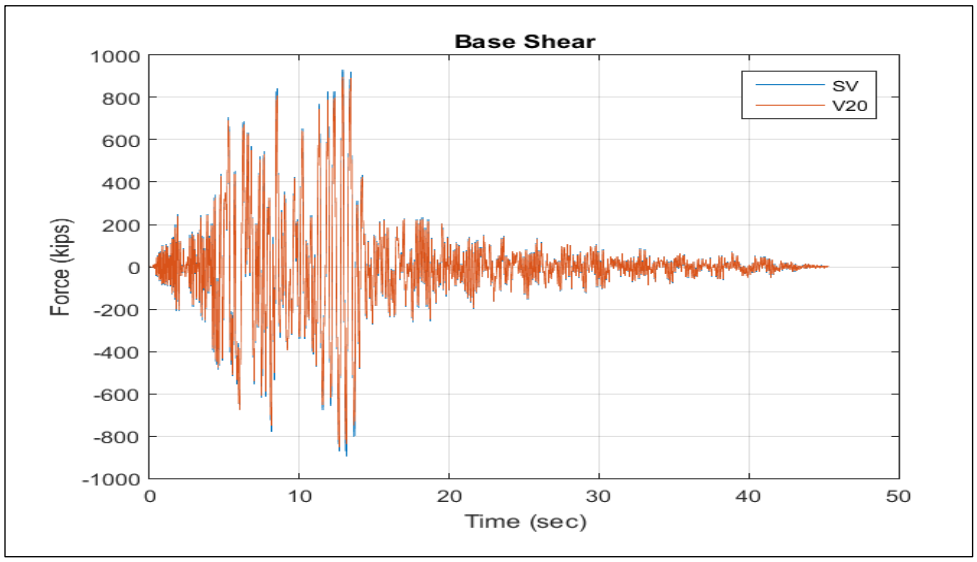

Figure 2-17: Base shear histories calculated from accelerations and shear stresses for Hector 090

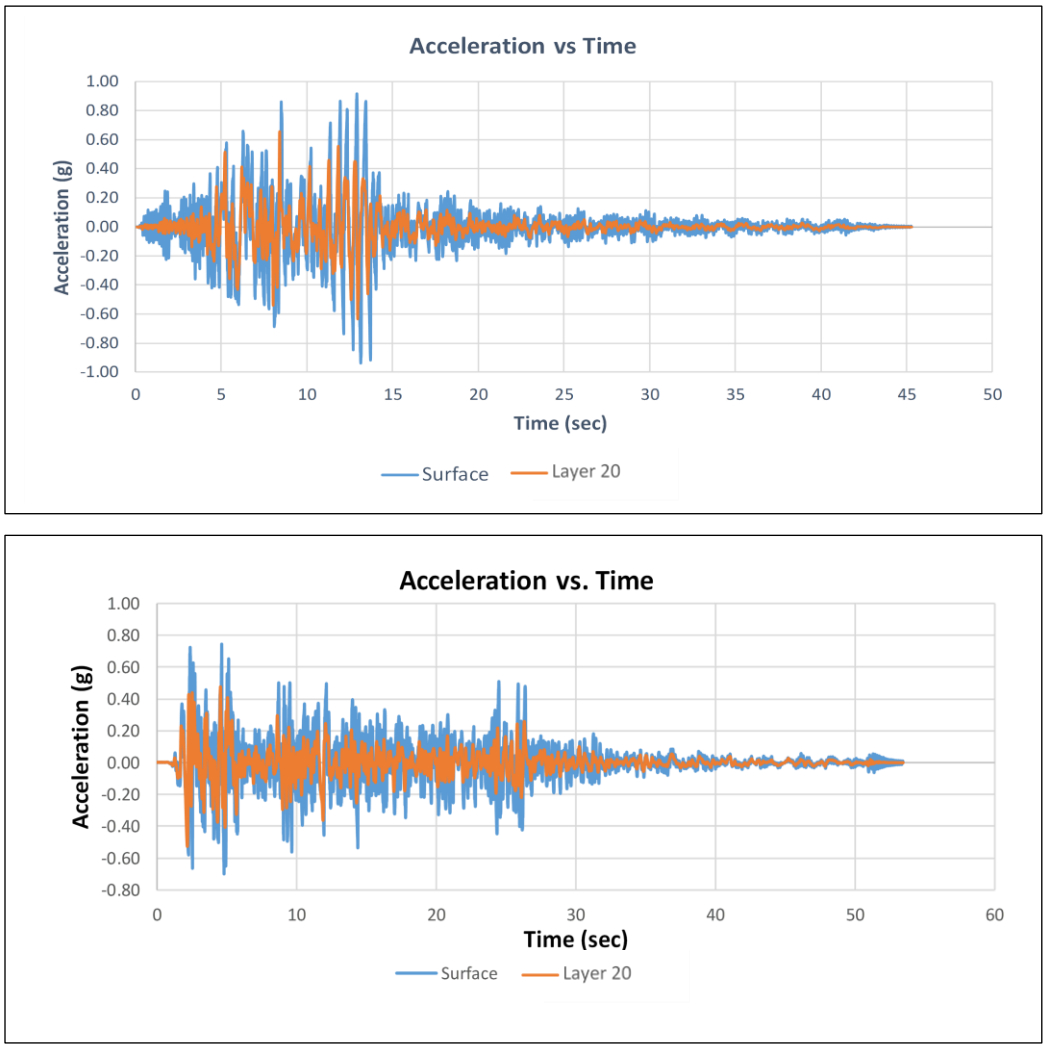

Figure 2-18: Acceleration histories for Hector 090 (top) and El Centro 180 (bottom)

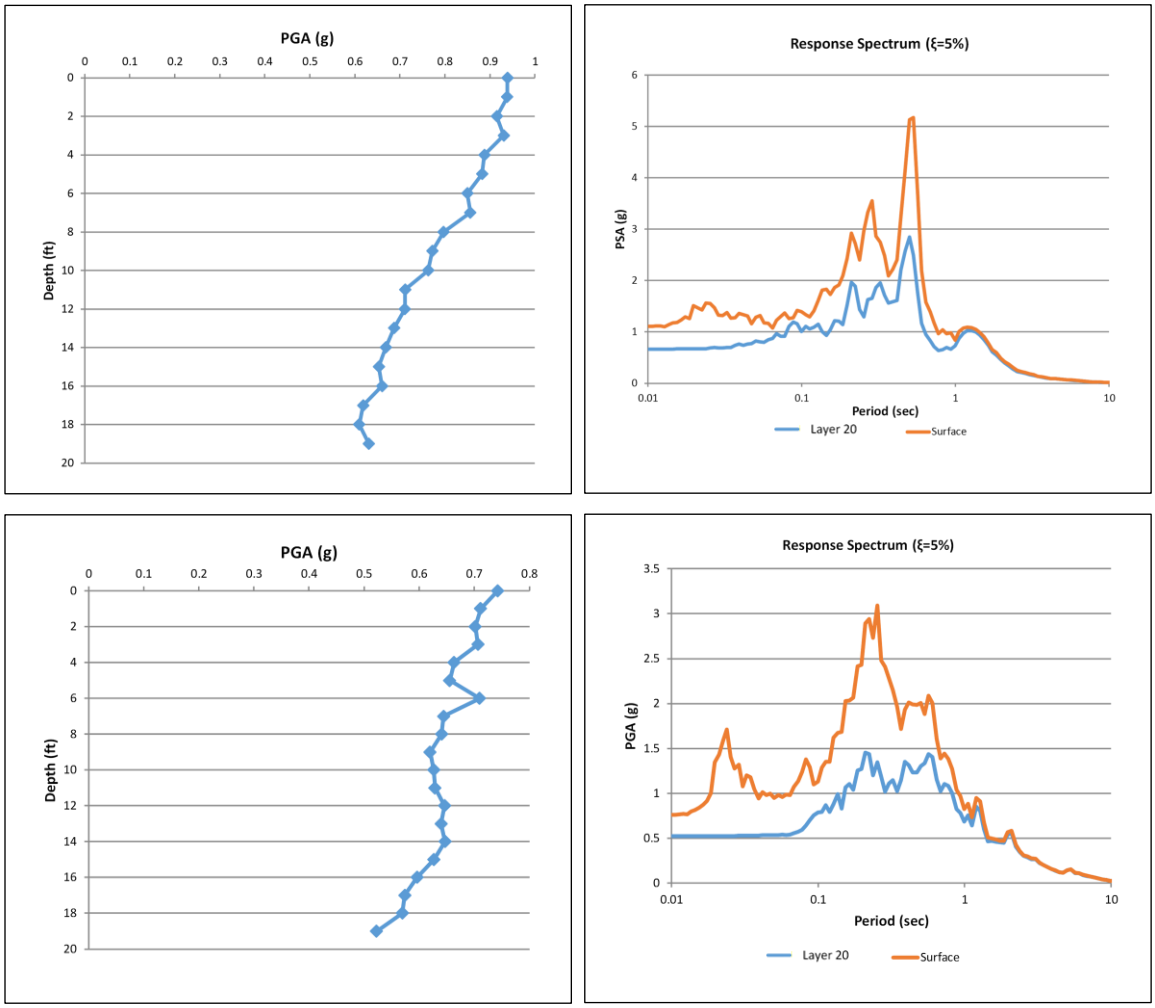

Figure 2-19: PGAs and Response Spectra for Hector 090 (top) and El Centro 180 (bottom)

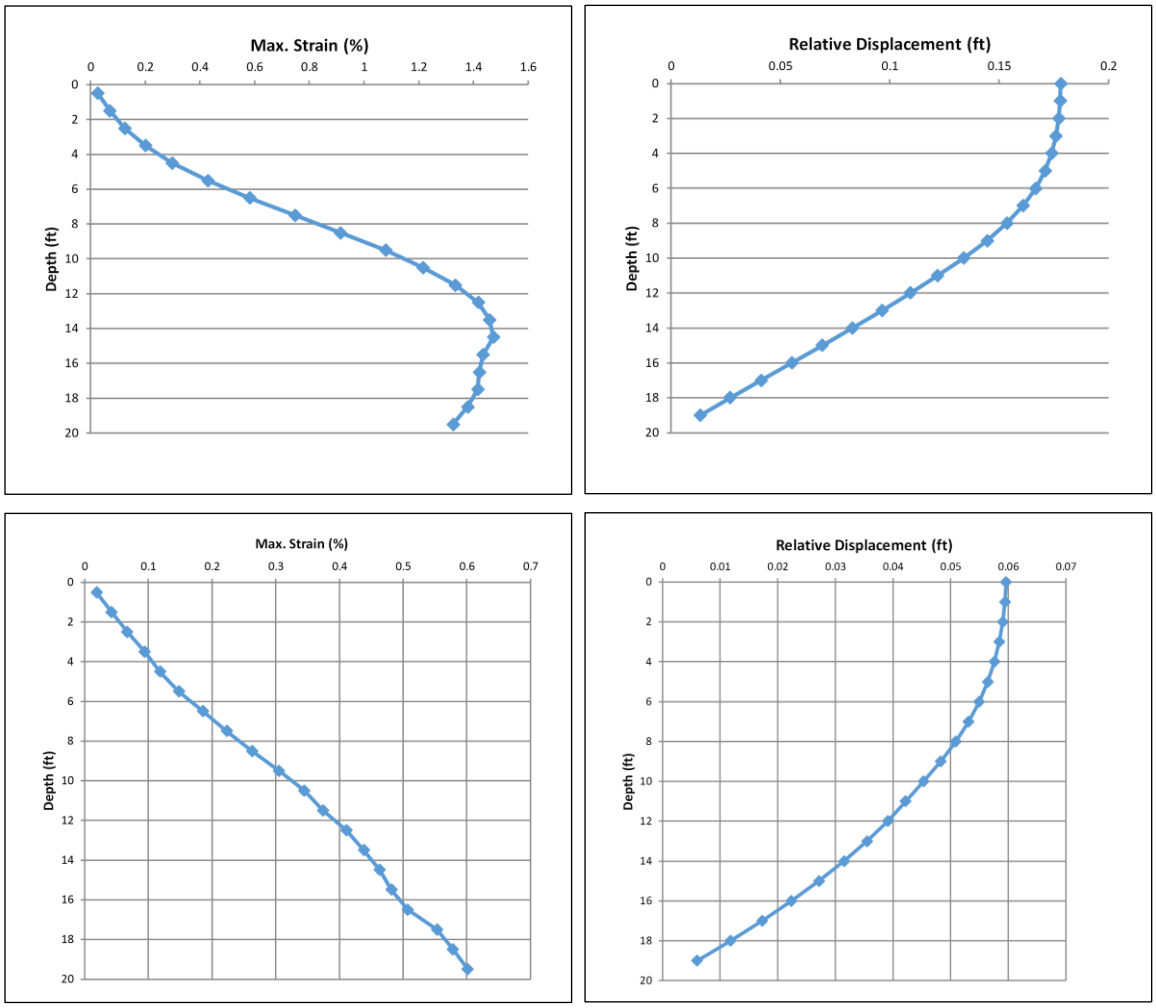

Figure 2-20: Max shear strain and Displacement profiles for Hector 090 (top) and El Centro 180 (bottom)

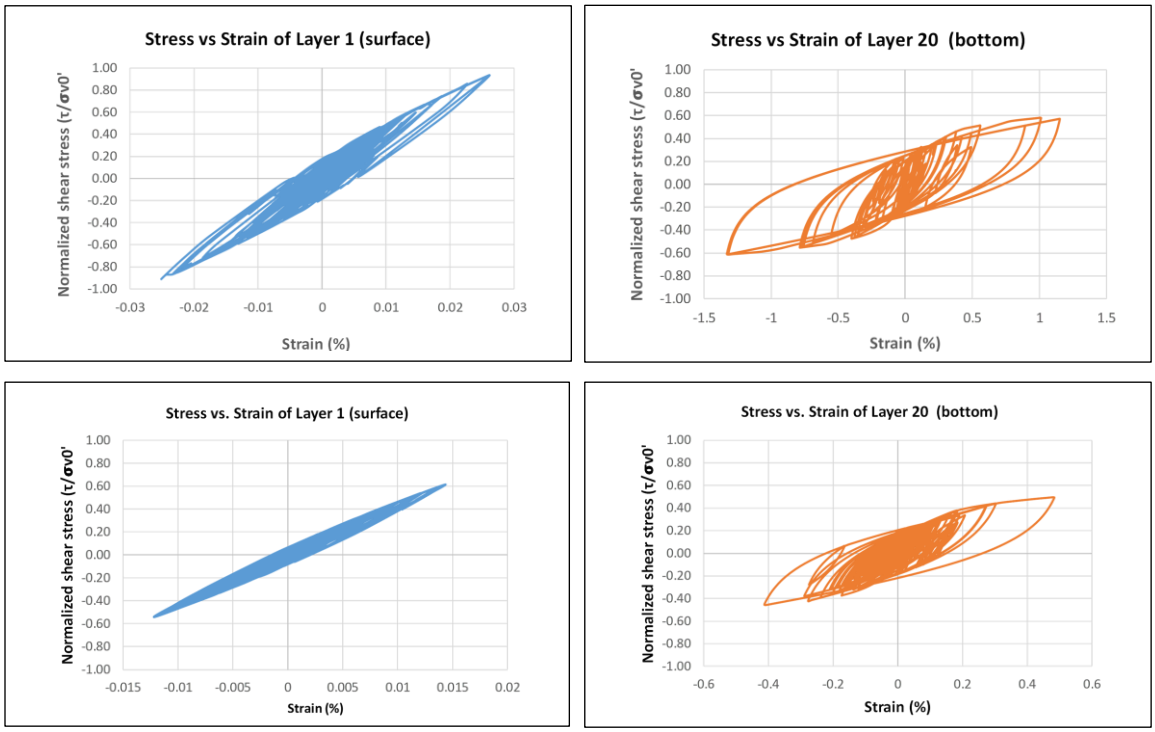

Figure 2-21: Surface and bottom stress strain loops for Hector 090 (top) and El Centro 180 (bottom)

2.3 Linear, Equivalent Linear and Nonlinear Site-Response Analyses

This section will present results from linear, equivalent and nonlinear analyses. Linear analyses were conducted to increase our understanding of the dynamic response of the soil-column and get an upper bound of the stresses and forces. Moreover, at very small shear strains the soil nonlinearity is small and linear analyses might realistically predict the response. For larger strains, a standard practice for the industry is to conduct equivalent linear analyses (e.g. in SHAKE, DEEPSOIL or other tools). This type of analyses simplify the nonlinear problem by solving it as linear problem with consecutive iterations on the shear modulus and damping values. Detailed information on how an equivalent linear analysis is performed can be found in Kramer (1996). Although, the equivalent linear analyses are very promising and have been seen in the literature to give similar results with nonlinear analyses in many cases, for other cases with very large strains the two methods can deviate from each other. Therefore, it is beneficial to compare the three methods for different levels of shaking and identify the conditions under which differences start appearing. To this end, 1D site response analyses were conducted using all three types of analyses, and for a range of scale factors between 0.5 (PGA=0.13g) and 5 (PGA=1.04g) of El Centro 180.

Table 2-5 and Figure 2-22 show the maximum shear strains and maximum base shear obtained from the three types of analyses for El Centro 180. As expected the linear analyses give an upper bound for the base shear and a lower bound for the shear strains, and even at a PGA=0.13g the linear analyses overpredict the base shear by a factor of 2. At PGA=1.04g (SF=4) this overprediction is by a factor of 5, demonstrating that linear

analyses cannot capture properly the behavior of the soil column at such high levels of shaking. On the other hand, equivalent linear analyses seem to give identical results with nonlinear analyses up to a PGA of 0.26g, and relatively close results up to PGA of 0.5g (SF=2). In particular, at SF=2 the equivalent linear analyses over-predict the base shear by 18%, while at SF=4 this over-prediction is 30%. Regarding the shear strains the equivalent linear analyses are under-predicting them as expected, however the interesting thing is that the largest difference occurs at SF=2 (44% lower) instead of SF=4 (25% lower). The fact that the equivalent linear analyses give values relatively close to the nonlinear ones, gives an extra level of confidence in the nonlinear numerical solution. It must be noted that the base shear has been calculated for a soil box of 18ft x18ft in plane dimensions and 20ft height with a total weight of 780kips (for dense soil).

Table 2-6: Max values for El Centro 180 with three different analyses types

Dense Soil						
	Nonlinear		Equivalent Linear		Linear	
Scale Factor	Max Shear Strain (%)	Max Base Shear (kips)	Max Shear Strain (%)	Max Base Shear (kips)	Max Shear Strain (%)	Max Base Shear (kips)
0	0.000	0	0.000	0	0.000	0
0.5	0.047	158	0.039	169	0.051	365
1	0.123	248	0.093	282	0.101	730
2	0.601	395	0.333	468	0.203	1460
3	2.331	513	1.401	671	0.304	2190
4	5.219	585	3.927	776	0.406	2920

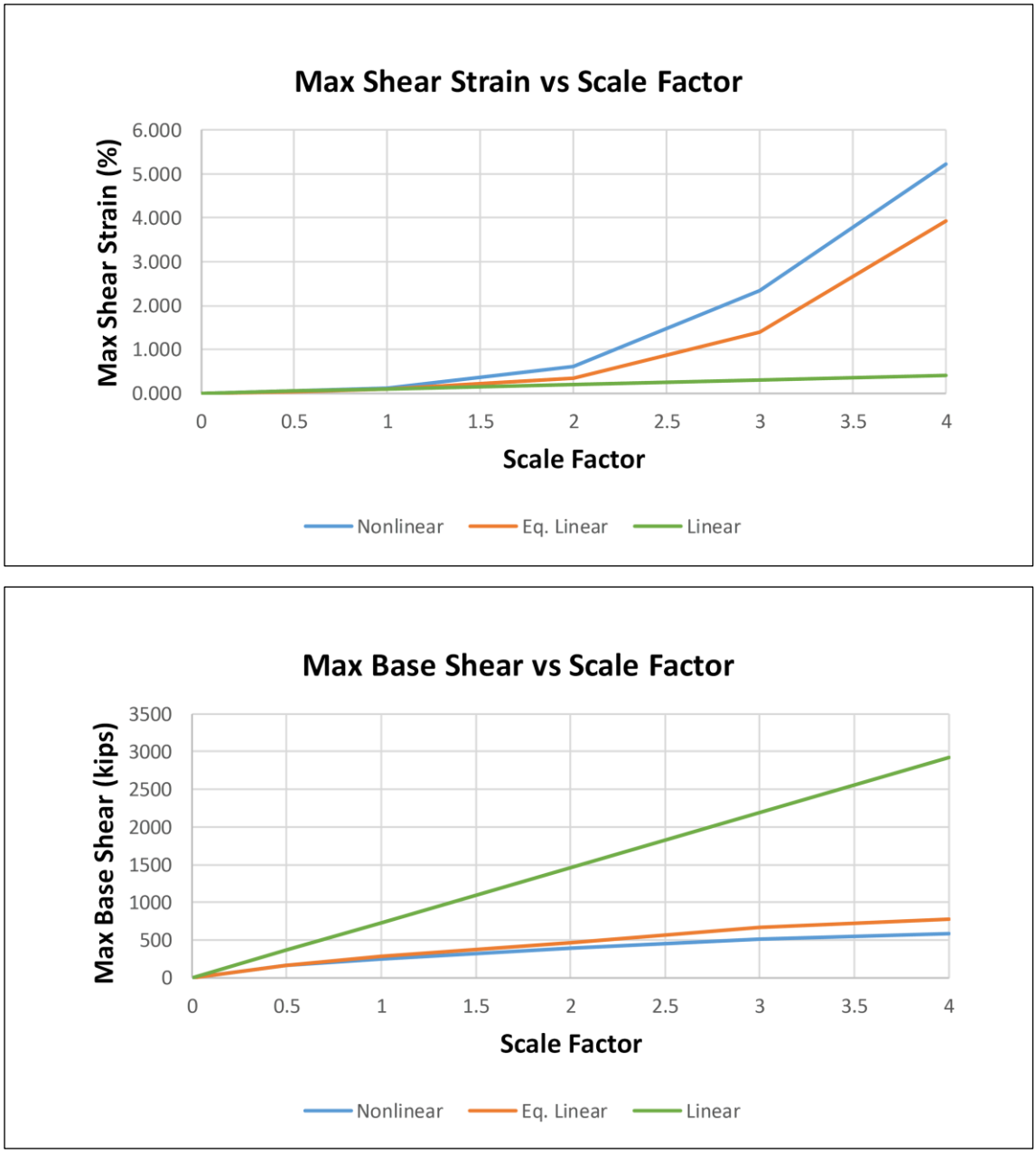

Figure 2-22: Max shear strains (top) and max base shears (bottom) for different scale factors of El Centro 180 record

2.4 Examination of the effect of soil nonlinearity

The last part of this chapter will attempt to determine the effect of soil nonlinearity on different parameters of interest such as acceleration response spectra at the surface, PGAs, soil stresses and strains, displacements and strains. To this end, Figure 2-23 shows the acceleration response spectra of the input motion and at the surface of the soil column for two levels of shaking with PGA of 0.13g (SF=0.5) and 0.52g (SF=2), for Hector 000. As expected at the lowest level of shaking, the surface acceleration response spectra is maximized at a period close to 0.15sec, which is very close to the fundamental period of the soil column, which is 0.13sec, indicating small levels of soil-strains. On the other hand, at the higher level of shaking the peak PSA occurs at approximately T=0.25sec, indicating an offset of the fundamental period of the soil column due to yielding, since the max PSA occurs when the main frequency content of the input motion coincides with the period of the soil. Figure 2-24, which shows the shear stress-strain loops demonstrate the lower level of shaking (PGA=0.13g) introduces strains at the bottom layer close to 0.04%, while the four time large shaking (PGA=0.52g) introduces shear strains larger by a factor of 10 (shear strains >0.5%).

This shifting of the natural period can also be observed in Figure 2-26 that shows the acceleration response spectra at the surface for all eight two-component selected input motions and two different scale factors (1 and 4). Although, as shown in Figure 2-24, the frequency content of each input motion is the same for both scale factors (since only linear scaling was performed), at the surface of the soil column the frequency content of the acceleration changes and the peak occurs at a different period. In particular, for SF1

(PGA=0.26g) the surface acceleration response spectra seem to be maximized somewhere between 0.15 and 0.22sec, while for SF4 (PGA=1.04g) this happens at approximately 0.5-0.6sec, indicating significant shifting of the fundamental period of the soil column due to the softening that takes places after the soil yielding. This indication is strengthened via the examination of the PGAs at different soil depths, shown in Figure 2-27. For SF2 the ground accelerations are amplified from the bottom to the surface, however for SF4 this is not happening but instead for some motions the accelerations are reduced at the top indicating significant soil nonlinearity.

Figure 7-28 shows the maximum shear strain profile, and as indicated by the previous discussion, the shear strains for SF1 are moderate (<0.2%), while for SF4 they are very large with most of the motions being in the range of 1-5%, and two of them exceeding this range (Erzincan goes up to 19%). This large strains are translated into significant horizontal relative displacements, which as shown in Figure 2-29, are in the range of 2 to 5.5 inches at the surface (Erzincan goes up to 14.5in), meaning that the walls of the soil-box should be designed to withstand such relative displacements.

Last but not least, Figures 2-30 and 2-31 show the maximum base shears and shear strains for different scale factors. These figures verify previous observations that as the level of shaking increases the soil nonlinearity increases significantly altering the response of the soil column and the effects that will introduce on the soil-box and shake-table system. The soil nonlinearity seems to limit the increase of the base shear with the increase of the shaking level for all input motions, which is good for the actuators of the shake table.

However, this nonlinearity increases significantly the shear strains meaning that the soil-box should be able to accommodate larger relative displacements.

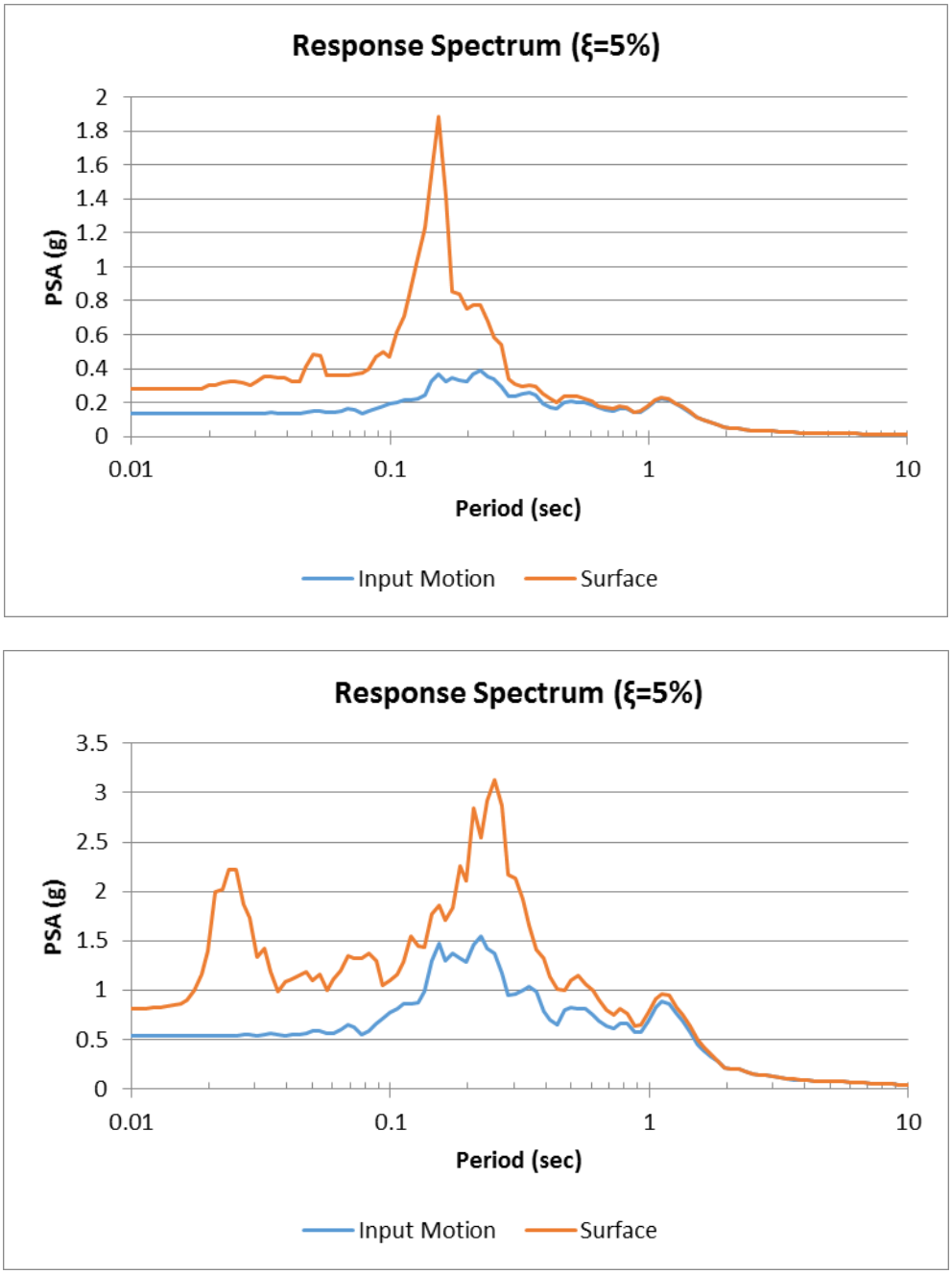

Figure 2-23: Acceleration response spectra for the Hector_000 record for SF=0.5 (top) and SF=2 (bottom)

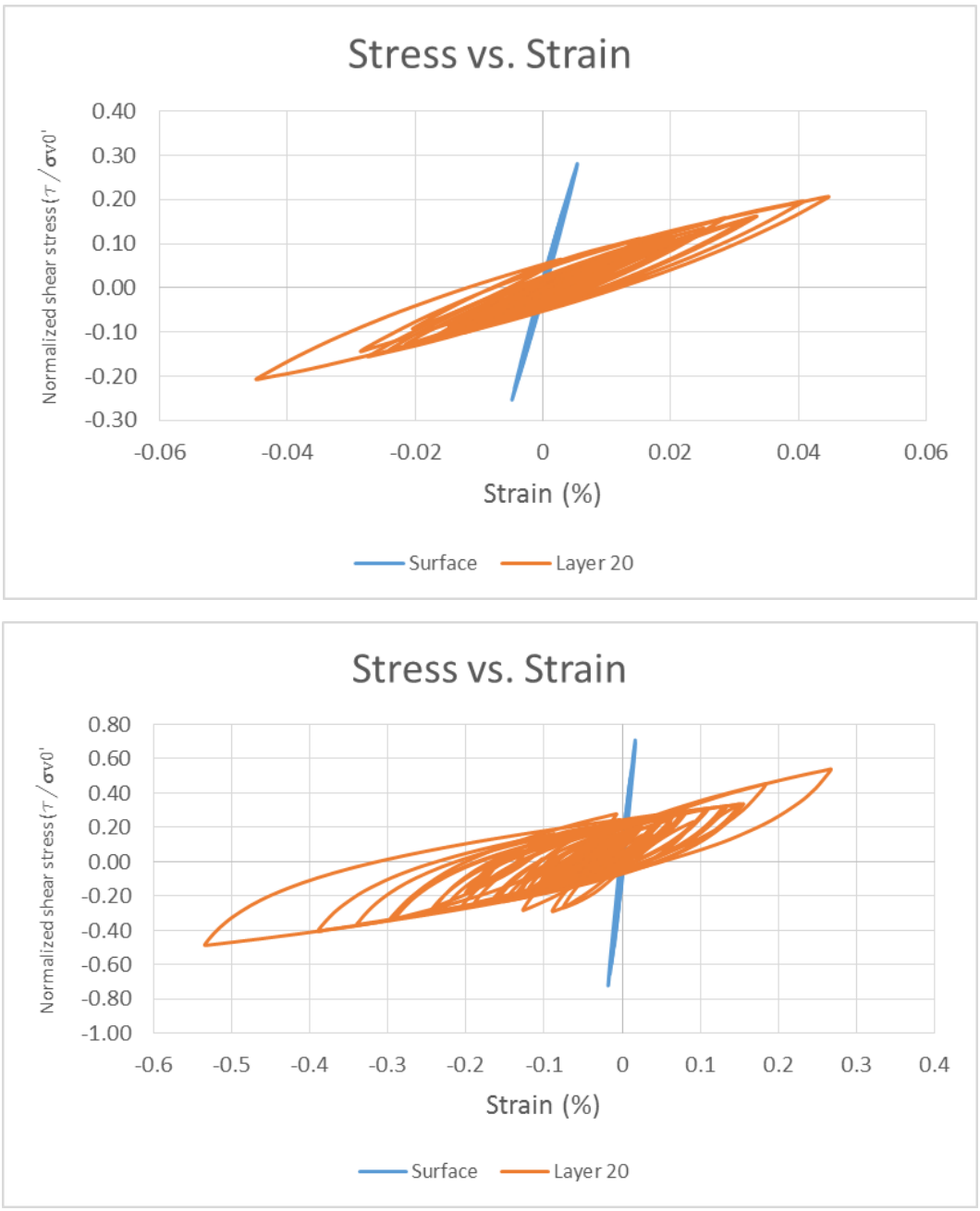

Figure 2-24: Shear stress-strain loops for the Hector_000 record for SF=0.5 (top) and SF=2 (bottom)

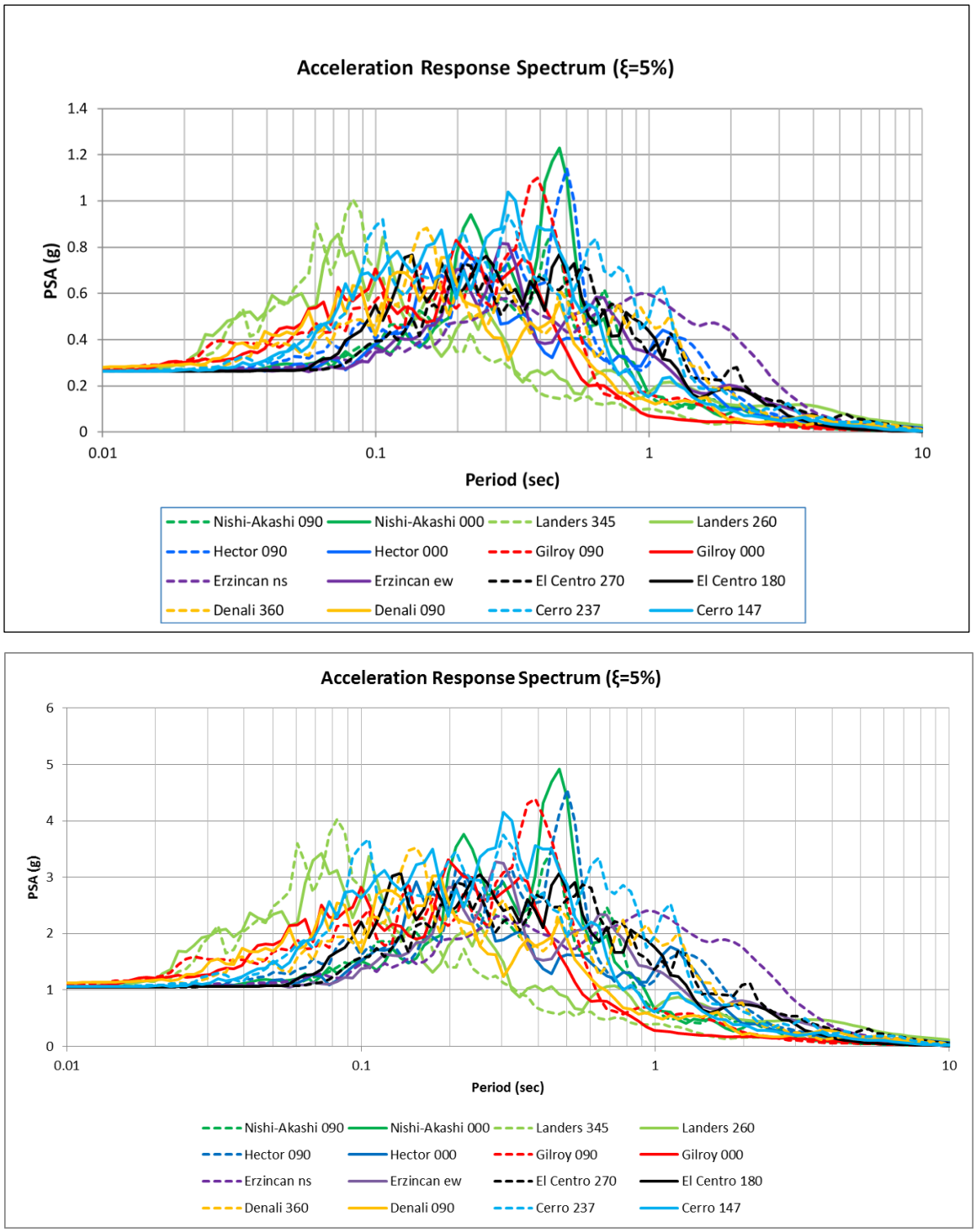

Figure 2-25: Input acceleration response spectra for selected ground motions for SF=1 (top) and SF=4 (bottom)

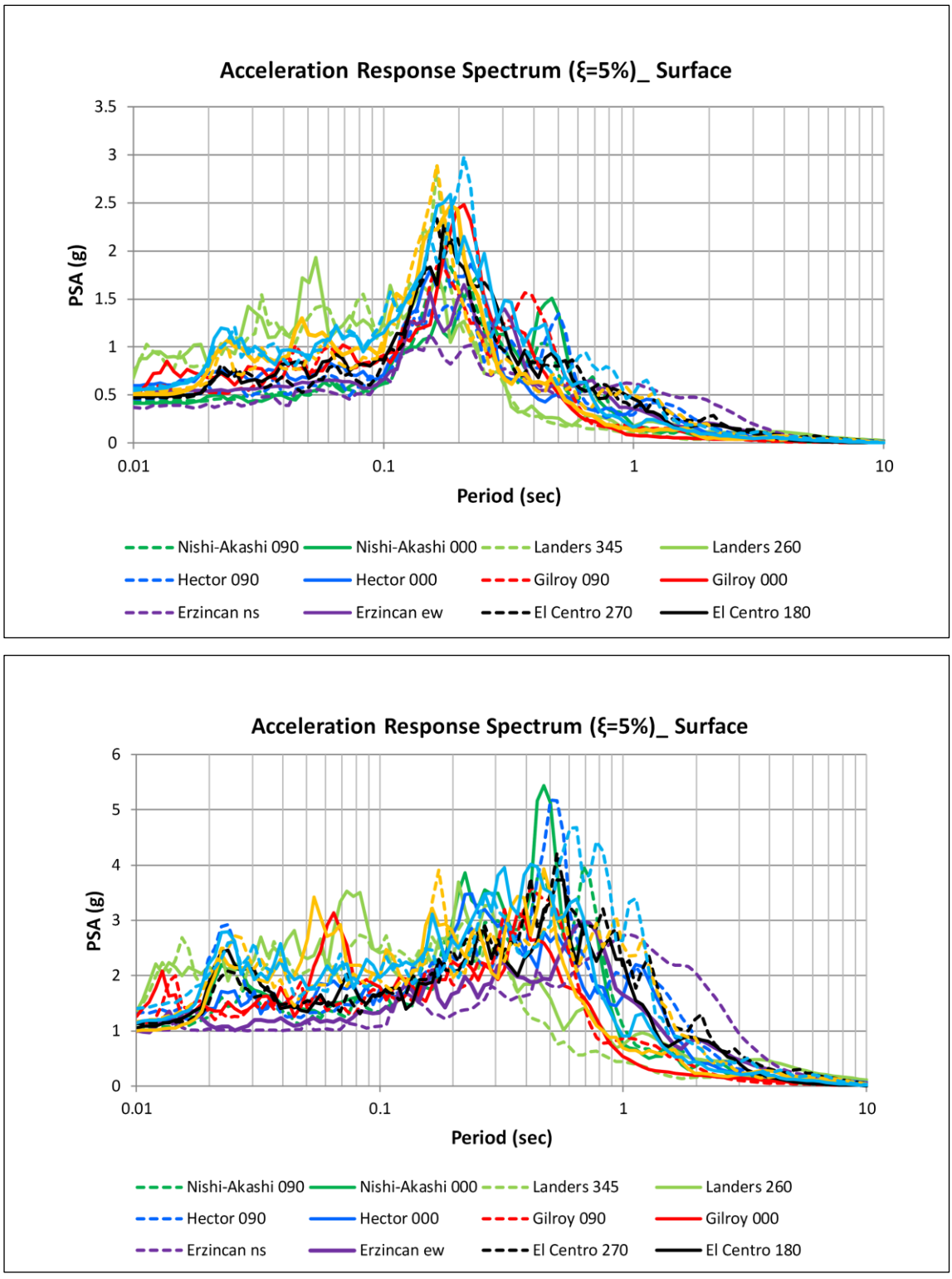

Figure 2-26: Acceleration response spectra at the surface for selected ground motions for SF=1 (top) and SF=4 (bottom)

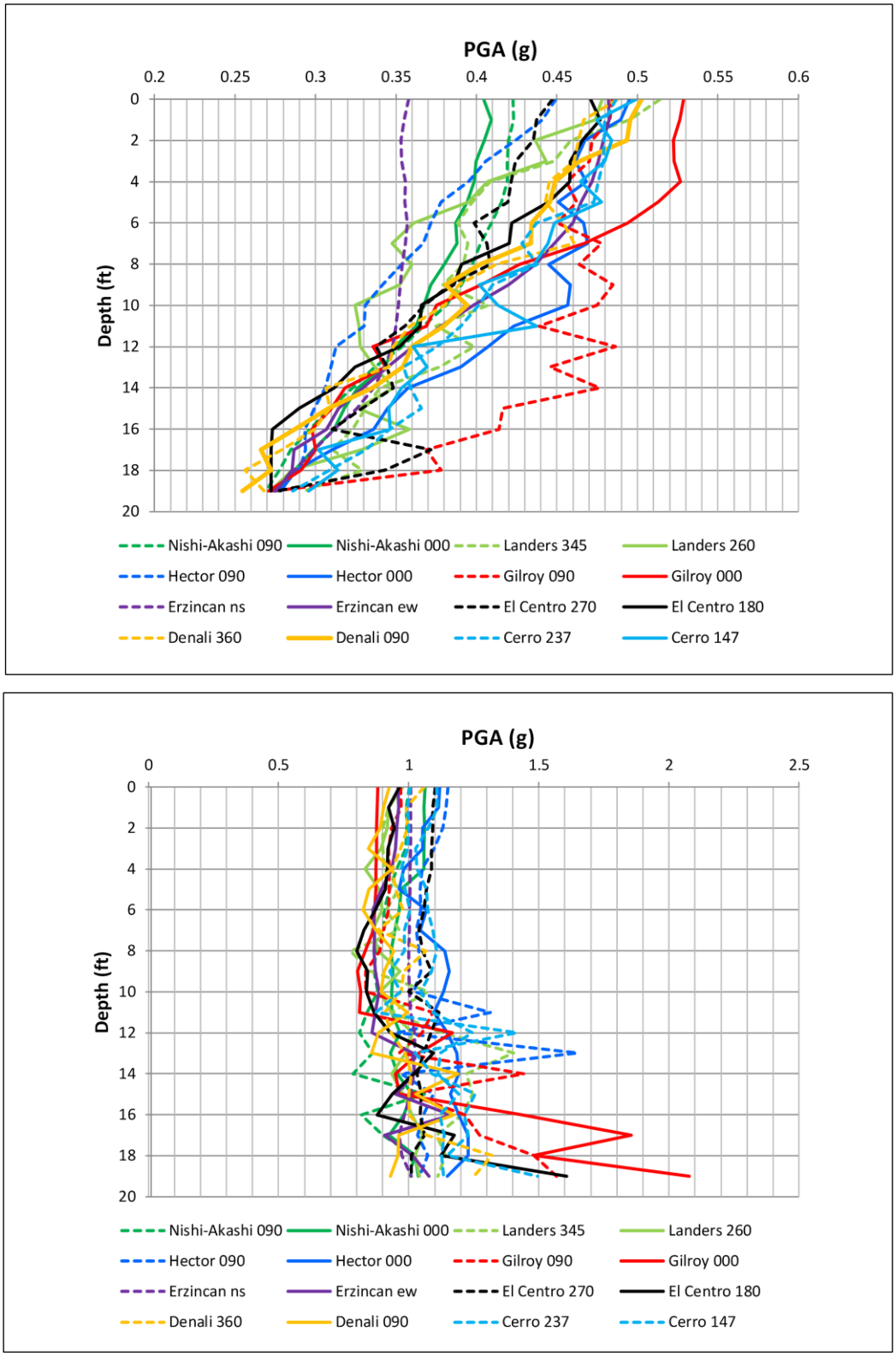

Figure 2-27: Peak ground accelerations for selected ground motions, for SF=1 (top) and SF=4 (bottom)

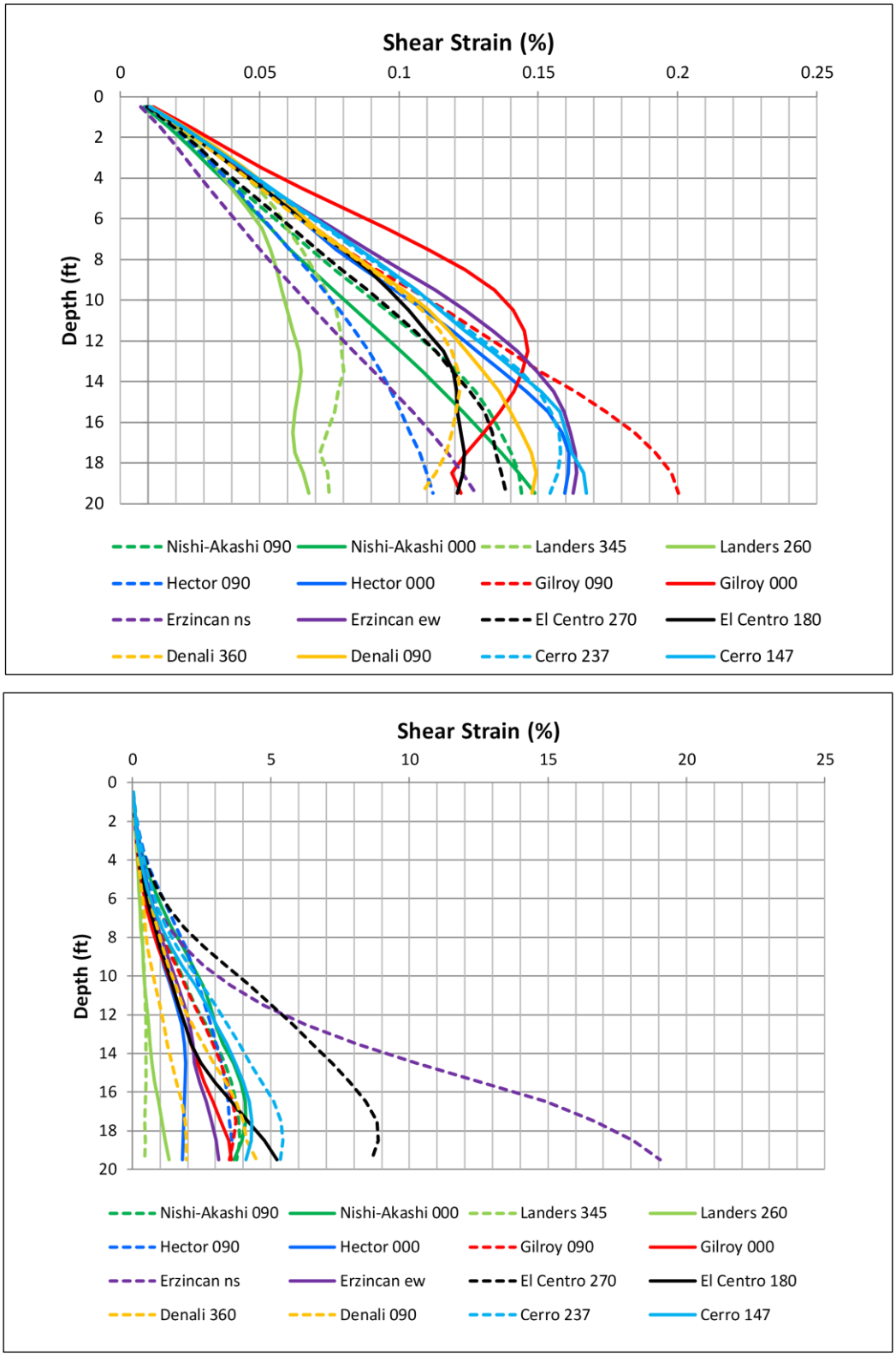

Figure 2-28: Shear strain profiles for selected ground motions for SF=1 (top) and SF=4 (bottom)

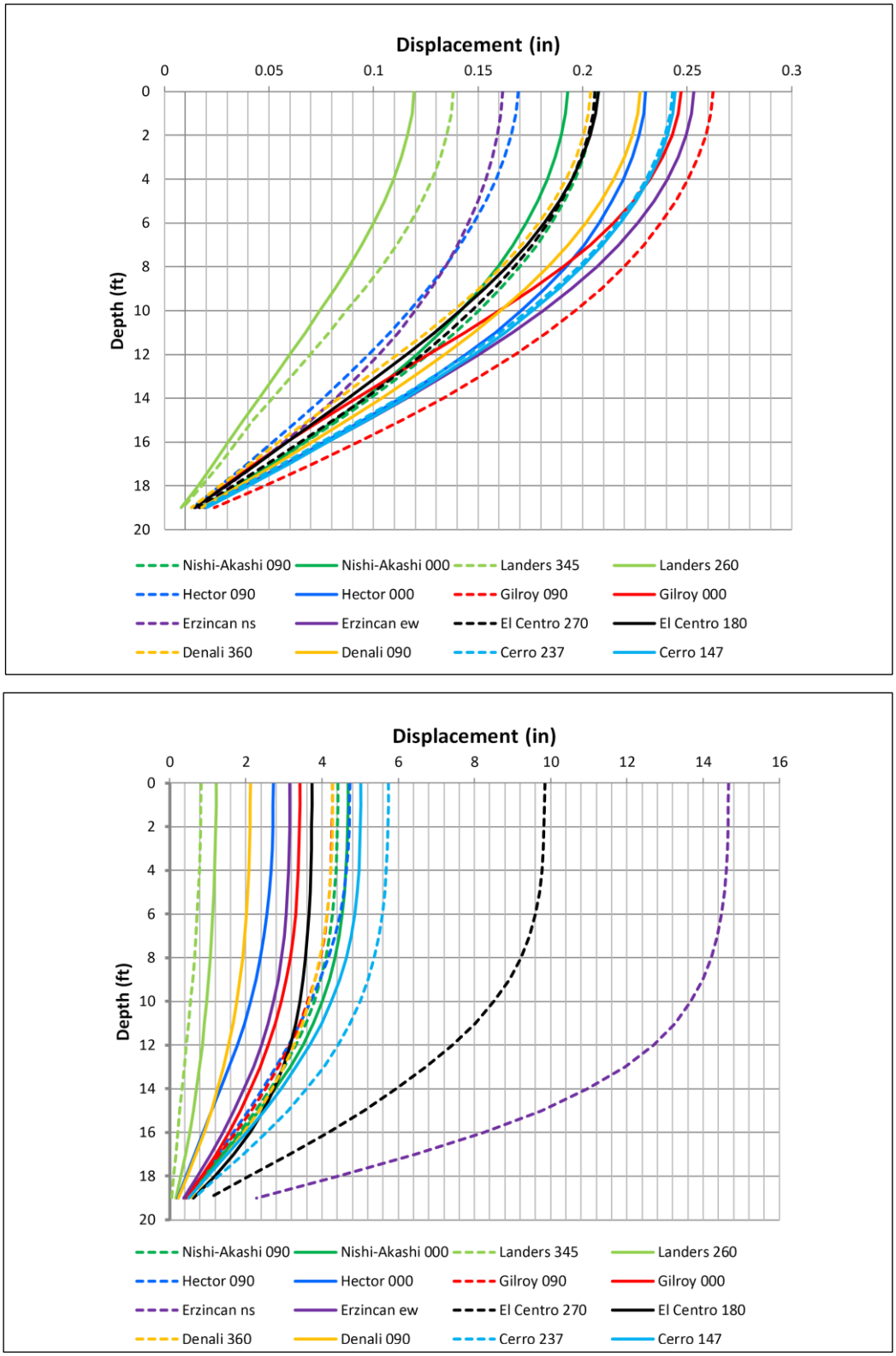

Figure 2-29: Displacement profiles for selected ground motions for SF=1 (top) and SF=4 (bottom)

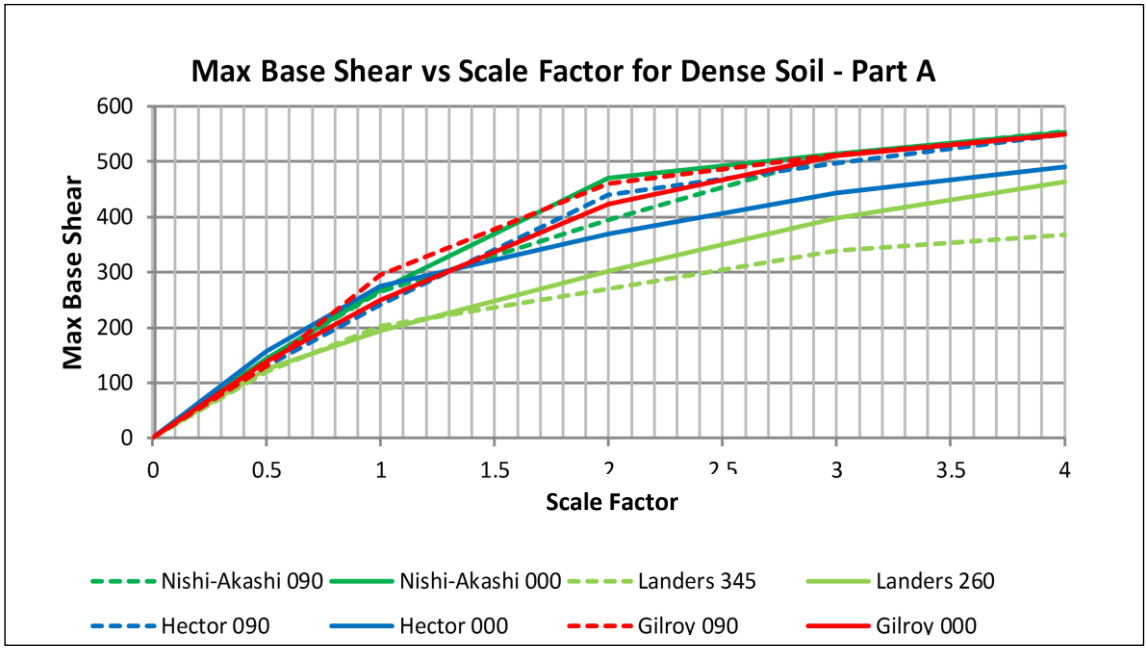

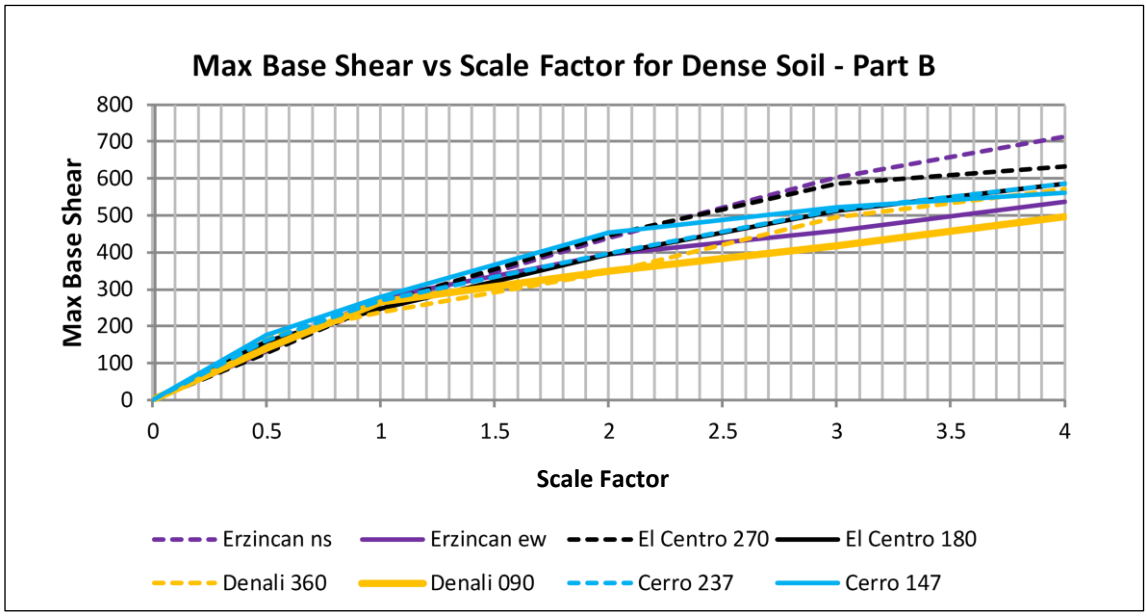

Figure 2-30: Max base shear for different scale factors of selected ground motions

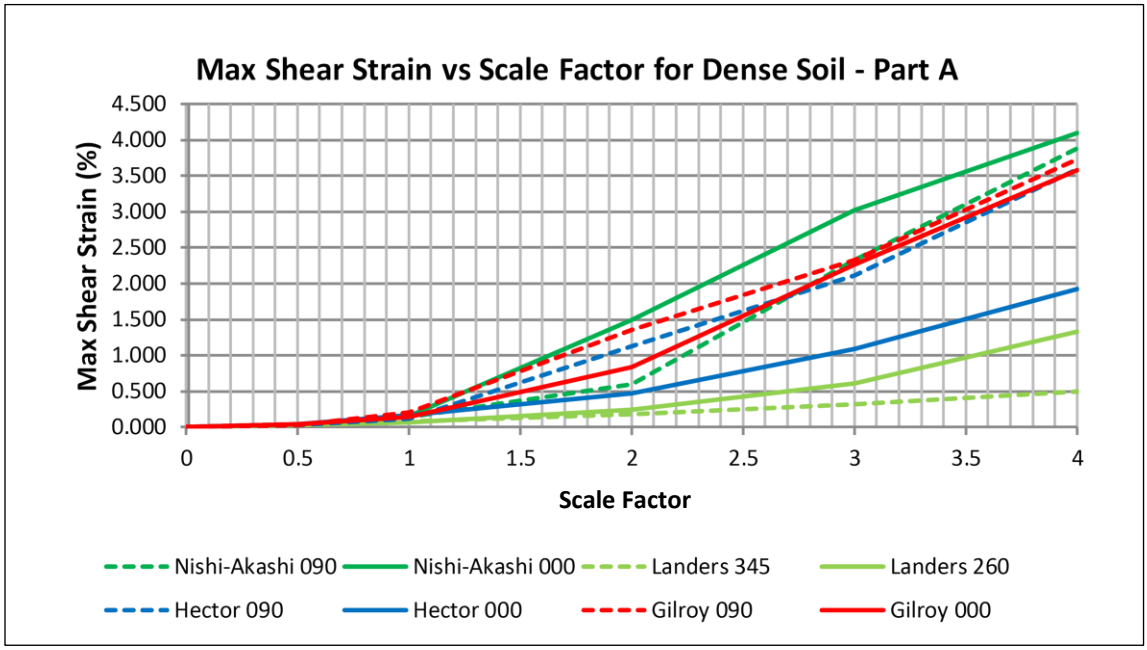

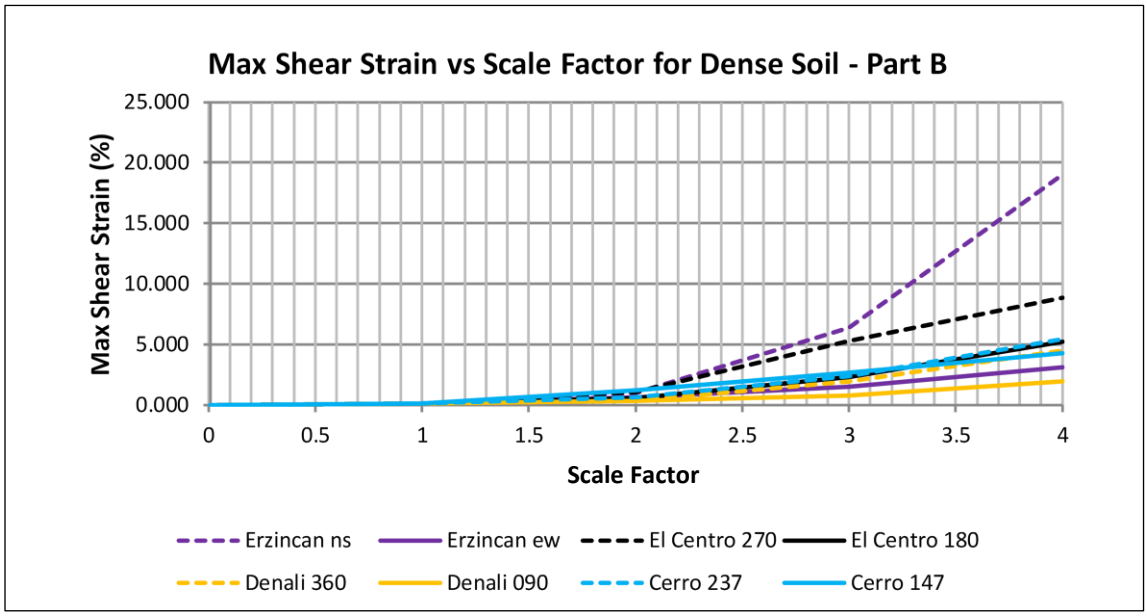

Figure 2-31: Max shear strains for different scale factors of selected ground motions

Chapter 3: Sensitivity of one-dimensional DEEPSOIL analyses to various parameters

3.1 New soil material: General Quadratic/Hyperbolic model

3.1.1 Description of the model

The one-dimensional analyses of the 20ft soil column presented in the previous chapter simulated the soil material using the Modified Kodner-Zelasko model (Matasovic, 1993), which is one of the most popular models for site response analyses. This model and most of the hyperbolic models available in the literature can be used to match the backbone (stress-strain) and damping curves as a function of shear strain, obtained from experimental tests or using existing curves as a reference (e.g. Darendeli (2001) or Menq (2003)). This means that the model can capture the soil behavior at small strains reasonable, however since it does not control the shear stresses at large strains (e.g. >0.5-1%) it can result in over-estimation or under-estimation of the shear strength of the soil. To solve this issue a new General Quadratic/Hyperbolic (GQ/H) model was developed by Groholski et al (2015) and implemented in DEEPSOIL version 6.1. (October 2015). This model is more realistic because it has the ability to simulate the soil behavior at small strains and it asymptotically approaches the shear strength at large strains. Given the initial shear modulus Gmax and the shear strength τmax, a quadratic model is used to create the backbone curve and match both the initial soil stiffness and the strength. More information about the model can be found in the aforementioned paper.

For the analyses presented in this chapter the shear strength of the soil was calculated using the vertical effective stress and the equation $\tau = c + \sigma v' * tan\varphi$. Figures 3-1 and 3-2 show the shear modulus reduction curves and the stress-strain curves respectively, for soil layer 10 and three different soil modelling approaches. In the first approach the MKZ model is used based on the Seed & Idriss reference curve. The second approach uses the same reference curve but the new GQ/H soil material. The third approach uses the GQ/H model but the Darendeli reference curve. Interestingly, for the particular soil model and depth, the MKZ model seems to give identical modulus reduction curves up to 0.3-0.5% shear strains, with differences starting appearing after that. These differences are not very obvious in the G/Gmax curves due to the logarithmic scale of the x-axis, however they become very apparent in the stress-strain curves (regular x-axis), with the GQ/H model approaching the shear strength of the soil (840psf) at large strains, and the MKZ model over-predicting the shear strength by approximately 60% at shear strains equal to 10%. Moreover, the same figures demonstrate that the reference curves (Seed&Idriss or Darendeli) selected for fitting the GQ/H model, can affect significantly the backbone curves, especially for shear strains between 0.001-3%, with the Darendeli reference curve giving smaller stresses than the Seed& Idriss curve. Therefore, it is important to determine the magnitude of the effect of the soil material and reference curve on the nonlinear analyses especially for strong shaking that will introduce large shear strains.

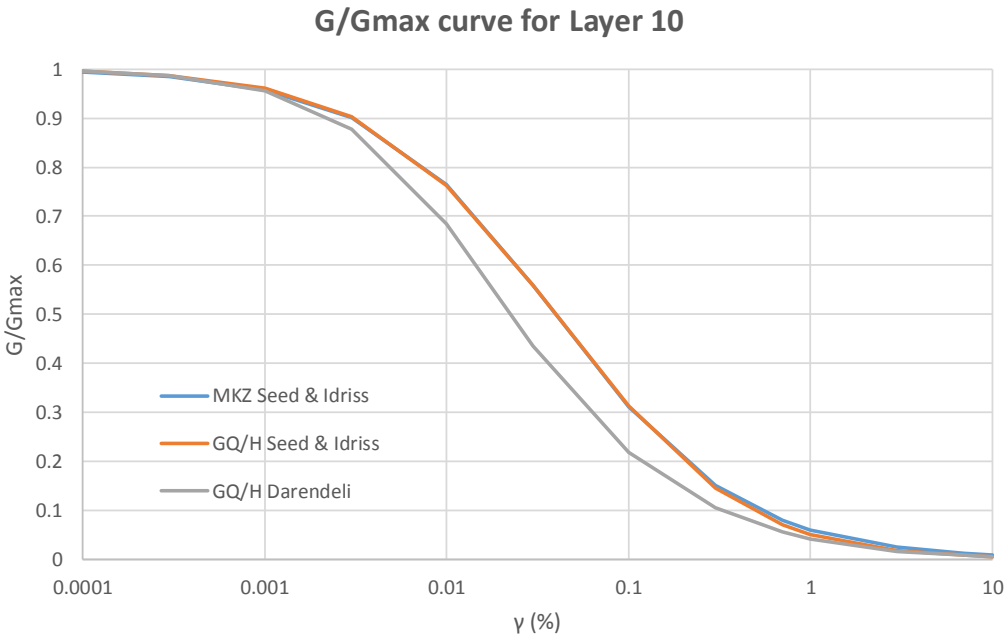

Figure 3-1: Shear modulus reduction curves for different soil materials and reference curves

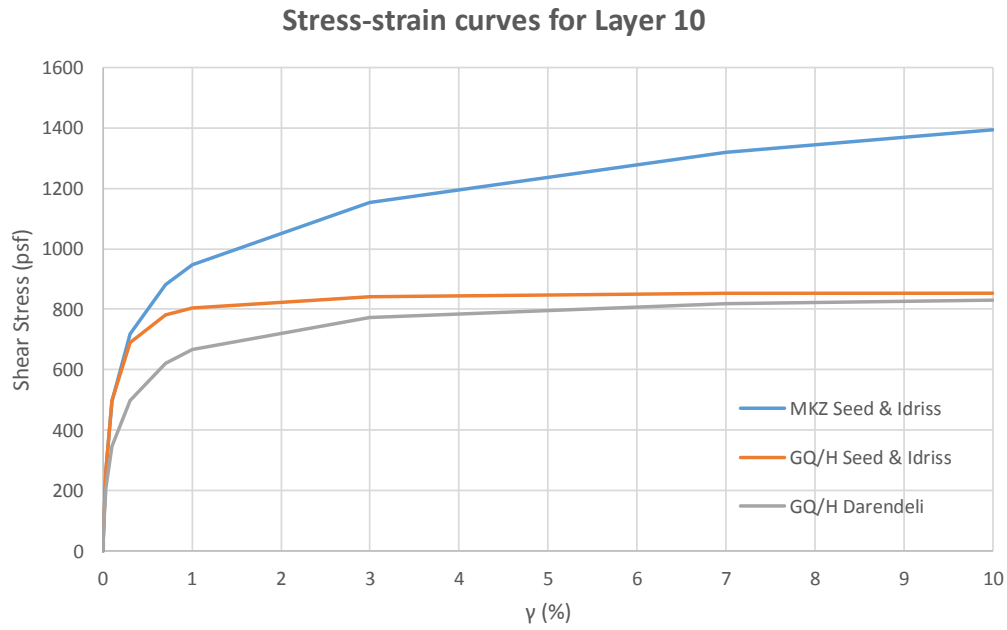

Figure 3-2: Stress-strain (backbone) curves for different soil materials and reference curves

3.1.2 Selected results

This section will present selected results from one-dimensional nonlinear dynamic analyses using the GQ/H soil material with the Darendeli reference curve. These results correspond to Cerro 237 for two scale factors, with PGAs equal to 0.26g (SF1) and 1.04g (SF4) respectively. Figure 3-3 shows the accelerations histories of the input motion and at the surface of the soil column, as well as the stress-strain loops at the mid-depth of the surface and bottom soil layer. The accelerations histories show a significant amplification of the motion as it propagates vertically towards the surface, with the PGA at surface being 75% larger than the PGA of the input motion. This is true for the lower level of shaking (SF1) but not for the high/extreme level of shaking (SF4) where the PGAs are similar at the surface and bottom, indicating significant nonlinear soil behavior. This nonlinear behavior can be clearly observed in the stress-strain loops, where significant hysteresis takes place both at the surface and bottom soil layer, with the former layer reaching 4.8% shear strains and the latter 2.7%, for SF=4. For the SF=1, the maximum shear strains at the two soil layers are smaller by approximately one or two orders of magnitude and particularly 0.037% at the surface and 0.13% at the bottom.

Figure 3-4 gives a broader view of the soil response by presenting the PGAs, maximum shear strains and maximum shear stresses recorded at different depths of the soil column. The amplification of the PGAs towards the surface that was observed in the two acceleration histories presented in the previous figure, is verified in Figure 3-4, for the input motion of SF1. When the motion is very strong (SF4) then not only the acceleration at the surface is similar to the one at the bottom, but the accelerations at several depths are

smaller than the input one (de-amplification). The max shear strain profile shows that this happens for the layers with the largest soil strains, which seem to occur in the upper third of the soil-column, with the maximum shear strain reaching 7%. The explanation of the observed behavior comes from the bottom graphs of Figure 3-4, which show both the maximum recorded shear stresses and the calculated shear strength of each soil layer. It becomes clear that although there is some soil nonlinearity and hysteresis at the low level shaking (SF1) the max shear stresses are much smaller than the shear strength (less than half of τ_{max} for most layers). On the other hand, for the strong shaking (SF4) many of the soil layers, especially the ones at smaller depths, have reached the shear strength, meaning that they have reached failure and their resistance to further shearing is minimal, explaining the recorded large strains at those locations. This also demonstrates that at the extreme levels of shaking (SF4) it is very important to use a material model that can accurately predict the shear strength and apply a cap (limit) on the shear stresses.

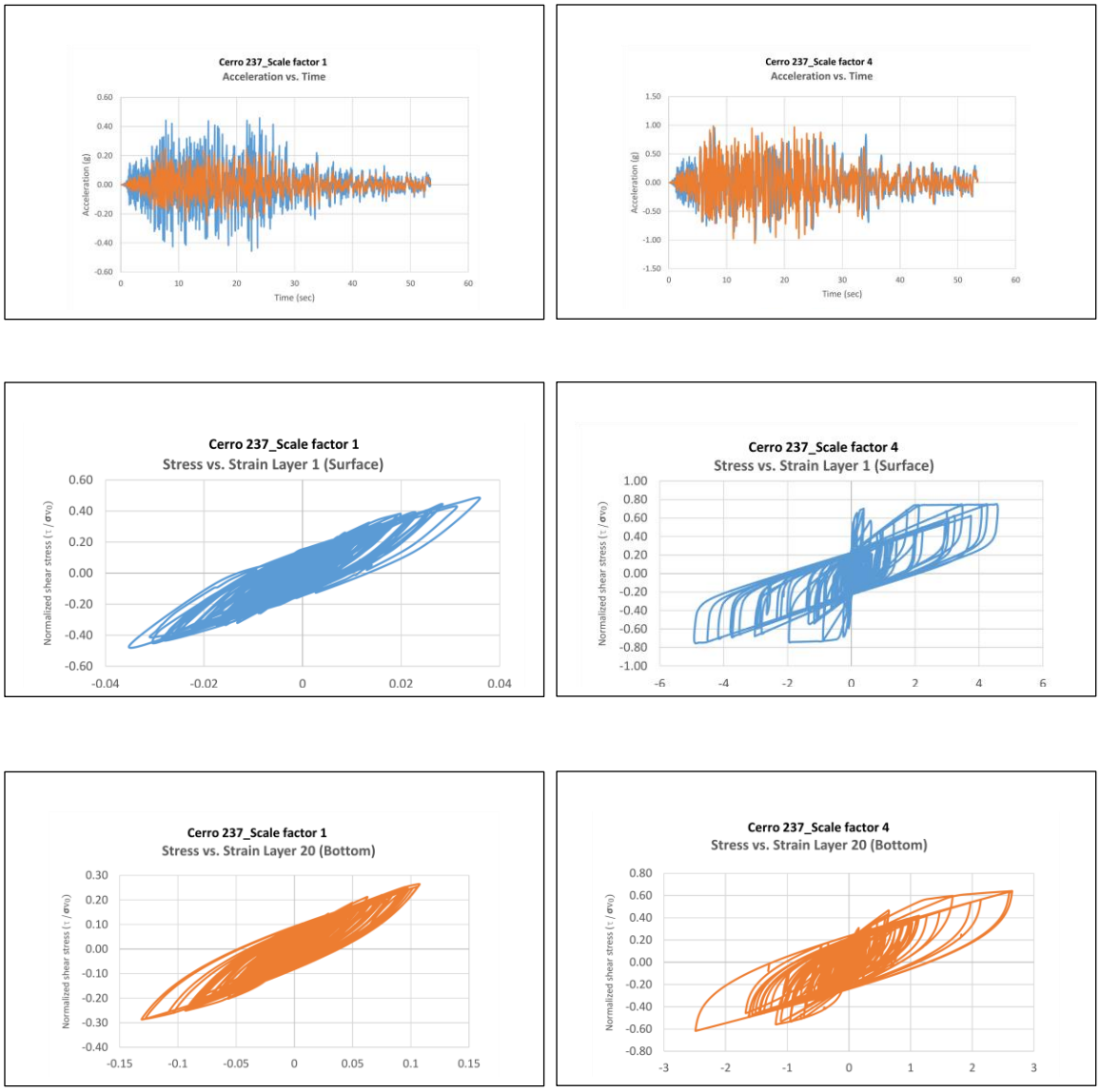

Figure 3-3: Acceleration histories (top) and stress-strain loops at the surface layer (middle) and bottom soil layer (bottom), for SF=1 (left) and SF=4 (right)

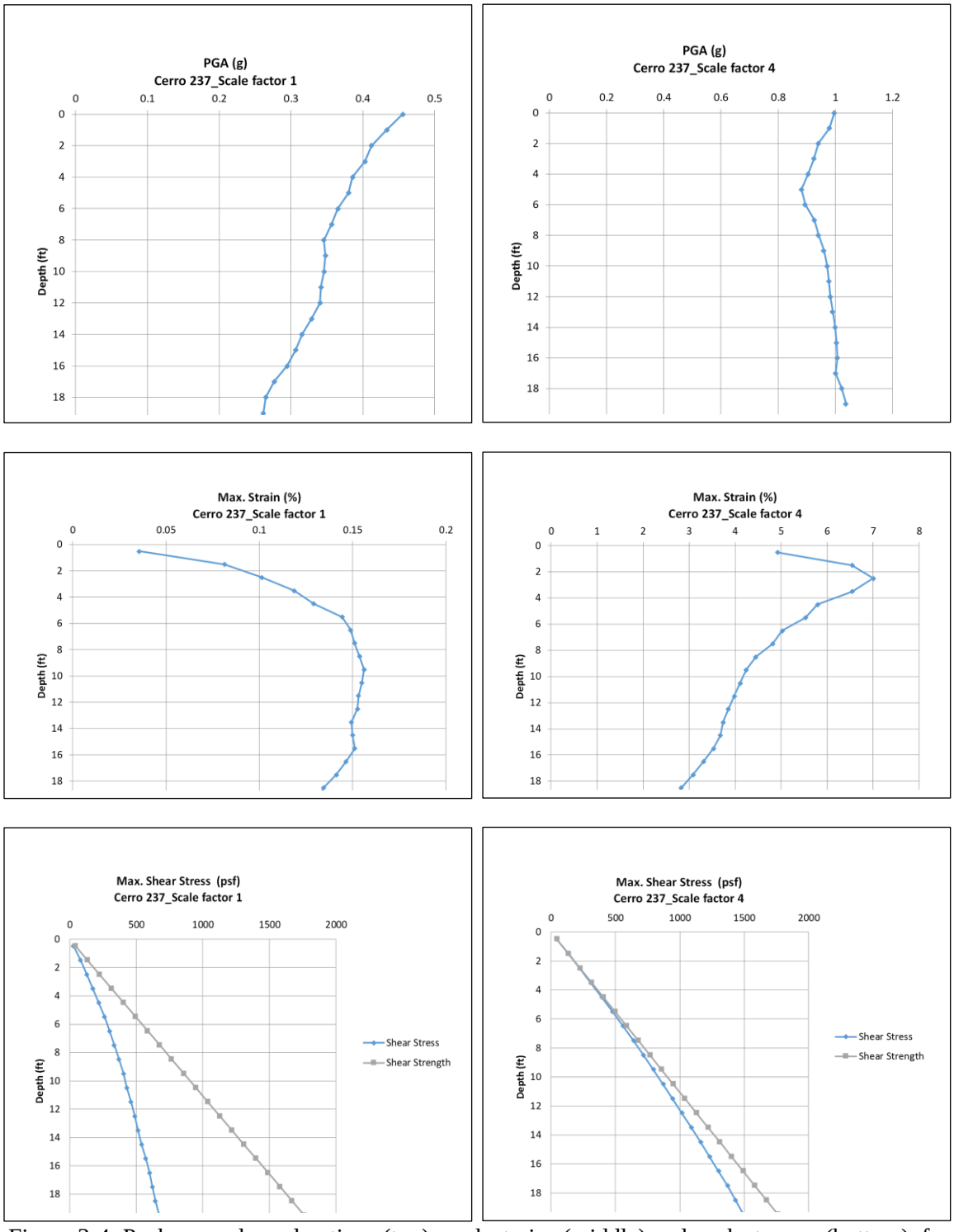

Figure 3-4: Peak ground accelerations (top), peak strains (middle) and peak stresses (bottom), for SF=1 (left) and SF=4 (right)

3.2 Effect of soil materials and reference curves

As discussed in previous sections of this chapter there are different soil materials (e.g. MKZ and GQH) and reference curves (e.g. Seed & Idriss, Darendeli, Menq) available for site response analyses, with most of them having the capability to simulate the soil response accurately at small shear strains but not at large ones. Since one of the objectives of the soil-box project is to conduct experiments for strong earthquakes that are expected to introduce significant soil nonlinearity, it is critical to examine how the numerical analyses will be affected by the different modeling parameters. In an attempt to shed light to this issue, nonlinear analyses were conducted for the three modeling approaches presented in the first section of this chapter, namely MKZ-Seed&Idriss, GQ/H-Seed&Idriss and GQ/H-Darendeli.

Figure 3-5 shows the acceleration response spectra at the surface of the soil-column for selected input motions with PGA=1.04g (SF4). Comparison of the MKZ and GQ/H models for the Seed & Idriss curves, shows that although the peak PSA is slightly above 4.5g (for Cerro 237) at approximately T=0.6sec for both models, there are several differences for the rest of the curves and spectral values. The most apparent difference is the fact the GQ/H model seems to reduce significantly the accelerations in the high-frequency range (T=0.02-0.04sec) relative to the MKZ model. Moreover, when the Darendeli curve is used as a reference for the GQ/H model then these high frequency accelerations peaks are totally eliminated. The Darendeli curve also seems to change the shape of the spectral curves and reduce the peak PSA down to 4g (from 4.5g).

Figure 3-6 presents the peak ground accelerations recorded at different depths of the soil-column for the three combinations of soil materials and reference curves. For the Seed&Idriss curves using the GQH model instead of the MKZ model results in more significant de-amplification of the motion as the waves propagates from the bottom to the surface, and smaller PGAs at the surface. The GQH model also seems to reduce the magnitude and the number of peaks observed in the PGA profile. Furthermore, switching from the Seed&Idriss to the Darendeli curve reduces/eliminates the localized jumps and abrupt changes observed in the deeper half of the soil-column, but does not necessary lead to smaller PGAs at the surface.

Three of the most significant parameters of interest for the preliminary design of the soil-box system, namely the base shear, maximum shear strains and maximum relative displacement (that the walls will need to accommodate), are presented in Tables 3-1 and 3-2. These tables show that using the GQH model, which limits the shear stress that each soil layer can reach, reduces the base shear by up to 15%, but increases the shear strains by up to a factor of 2. This demonstrates the importance of simulating the soil shear strength properly especially for input motions with PGA=1.04g that can lead to soil failure. Interestingly, although the GQH model results in a larger maximum shear strain it does not result in larger relative displacements, indicating that the significant soil nonlinearity occurs only at a few soil layers. Last but not least, switching from the Seed&Idriss to the Darendeli curve for the GQH model, causes a further reduction of the base shear by 12%, indicating that this modelling approach can lead to a more economical design of the actuators of the shake-table.

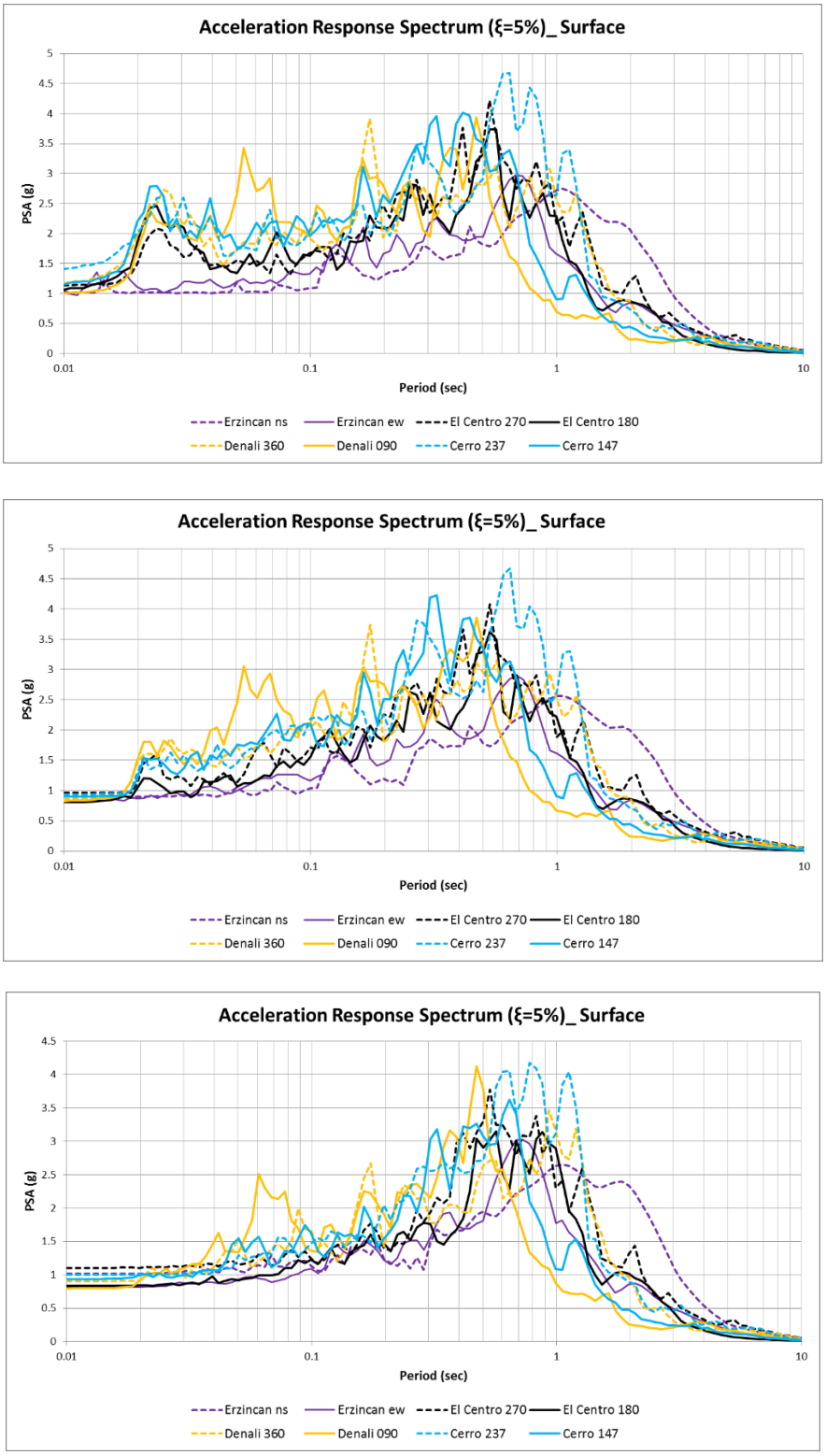

Figure 3-5: Acceleration response spectra at the soil surface for MKZ_Seed&Idriss (top), GQH_Seed&Idriss (middle), and GQH_Darendeli (bottom)

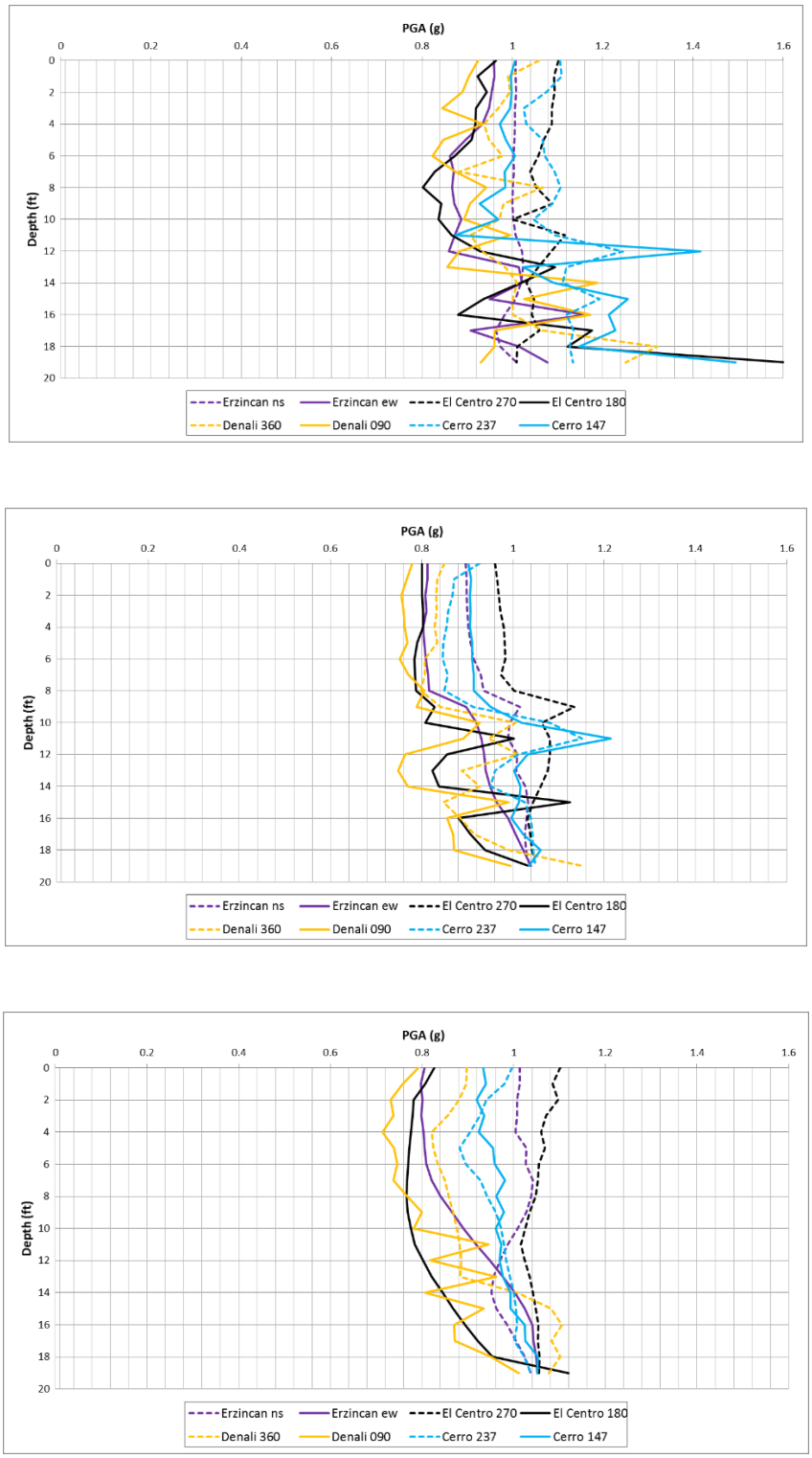

Figure 3-6: Peak ground accelerations for MKZ_Seed&Idriss (top), GQH_Seed&Idriss (middle), and GQH_Darendeli (bottom)

Table 3-1: Maximum shear strains, relative displacements and base shears for different soil materials and reference curves.

Input Motion	MKZ_Seed&Idriss			GQH_Seed&Idriss			GQ_Darendeli		
	γ (%)	Base Shear (kips)	Displ. (in)	γ (%)	Base Shear (kips)	Displ. (in)	γ (%)	Base Shear (kips)	Displ. (in)
Erzincan ew	3.110	750.67	3.157	6.139	679.02	2.603	2.711	631.33	4.821
El Centro 270	8.880	882.78	9.843	14.327	750.21	9.002	6.870	696.25	11.596
El Centro 180	5.219	816.03	3.735	5.320	743.58	3.276	4.007	709.32	5.478
Denali 360	4.486	796.66	4.280	7.633	720.96	3.826	4.314	684.84	7.526
Denali 090	1.954	692.72	2.118	3.176	654.66	1.762	1.493	576.59	2.928
Cerro 147	4.299	784.97	5.021	8.652	714.48	4.581	3.388	631.79	5.675

Table 3-2: Ratios of maximum shear strains, relative displacements and base shears for different soil materials and reference curves.

Input Motion	GQH Seed&Idriss/ MKZ Seed & Idriss			GQH Darendeli/ GQH Seed & Idriss		
	γ	Base Shear	Displ.	γ	Base Shear	Displ.
Erzincan ew	1.974	0.905	0.825	0.442	0.930	1.852
El Centro 270	1.613	0.850	0.915	0.479	0.928	1.288
El Centro 180	1.019	0.911	0.877	0.753	0.954	1.672
Denali 360	1.701	0.905	0.894	0.565	0.950	1.967
Denali 090	1.625	0.945	0.832	0.470	0.881	1.662
Cerro 147	2.012	0.910	0.912	0.392	0.884	1.239

3.3 Sensitivity of nonlinear dynamic analyses to time-step

One of the most common numerical parameter that can affect the accuracy of a time domain analysis is the selected time-step to be used in the numerical integration. DEEPSOIL offers the capability to define either a fixed or a flexible time-step. In the first approach the user can directly limit the time-step (via adjustment of the number of sub-increments), while in the second approach the time-step can be variable and automatically limited based on whether the computed strain increment at a particular time-step exceeds the user-defined maximum shear-strain increment. In this thesis, both approaches were implemented and the sensitivity to them was examined. This section will present results from four different models that used a fixed time-step, which ranged between 0.01sec and 0.002sec.

Figure 3-7 shows the peak ground accelerations, maximum strains and maximum stress ratios at different soil depths, for El Centro scaled at PGA=0.52g (SF2). Significant differences seem to occur in the PGAs of all soil layers, in the max strains of the lower half of the soil-column, and the stress ratios of the upper half column, when the time-step is reduced from 0.01sec to 0.005sec and 0.0025sec. However, when the time-step is reduced to 0.002sec then there are no significant differences indicating that the solution is converging to a steady value at approximately 0.002 to 0.0025 sec. This can also be verified in the acceleration response spectra at the soil surface, shown in Figure 3-8. Although the acceleration response spectra at the bottom soil layer do not seem be very sensitive to the time-step, the one at the surface is highly sensitive especially at higher frequencies.

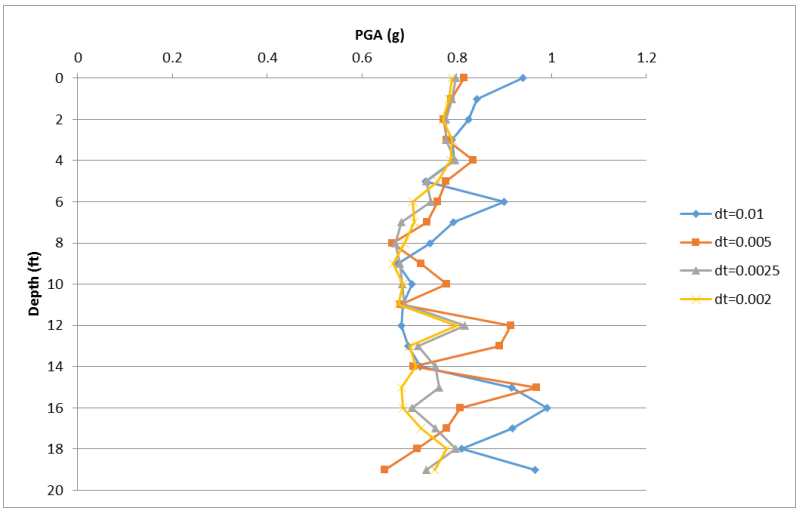

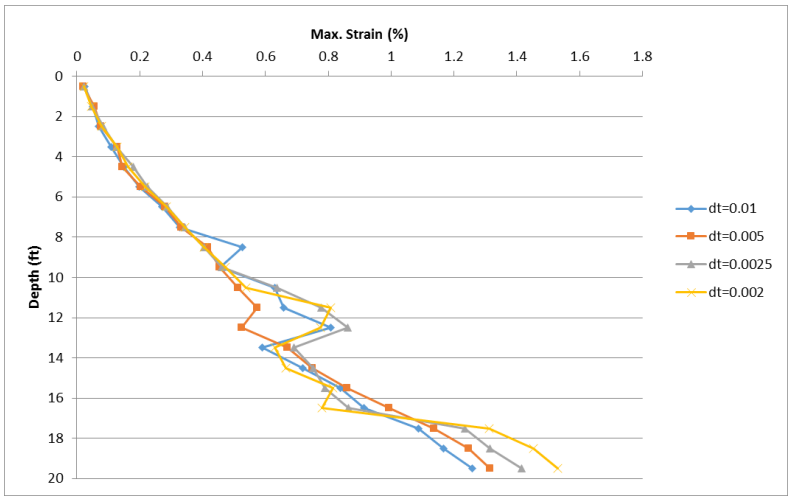

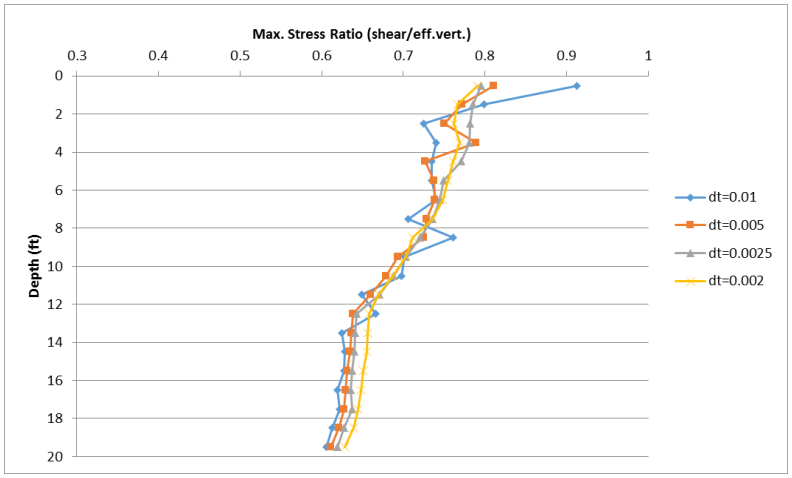

Figure 3-7: Peak ground accelerations (top), peak strains (middle) and peak stress ratios (bottom), for different time-steps and El Centro with SF=2

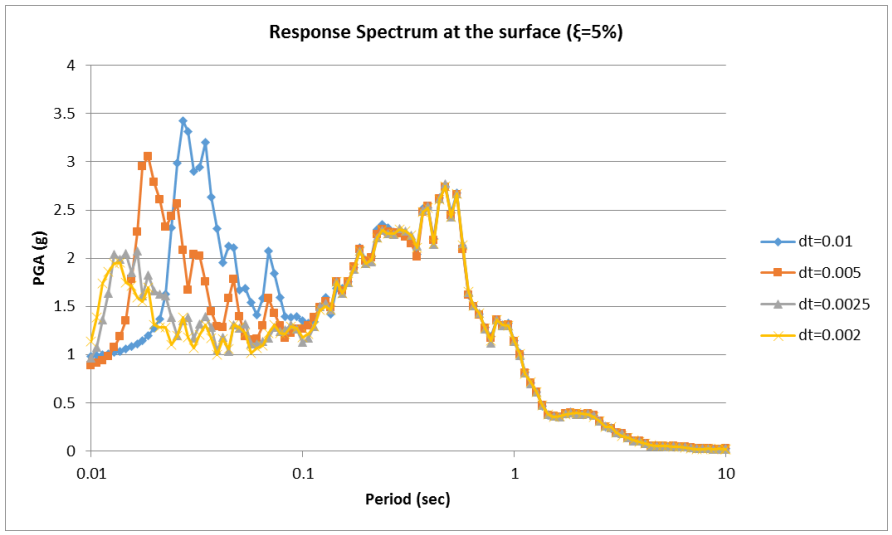

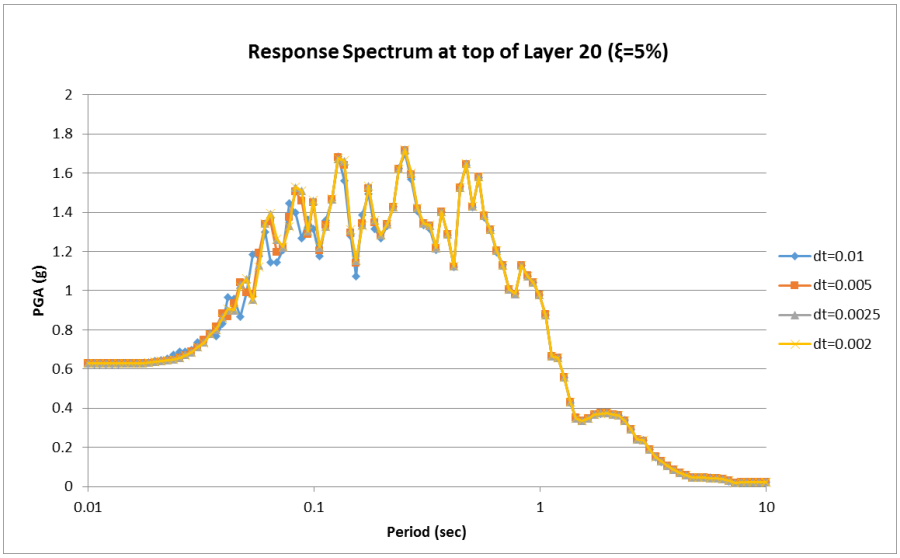

Figure 3-8: Acceleration response spectra at surface (top) and layer 20 (bottom), for different time-steps and El Centro with SF=2

3.4 Effect of time-scaling

The last section of this chapter will focus on the effect of the time-scaling of the input motion. In experimental testing it is common to scale the properties of the specimen in order to obtain the correct response. This is done both in (a) structural earthquake engineering testing (1-g shake-table tests), where the geometry and mass of the structure together with the magnitude and time-scale of the input motion are scaled accordingly, and (b) in geotechnical earthquake engineering (e.g. centrifuge tests), where the properties of the model and the soil, the vertical soil stresses and the input motion are scaled accordingly (via the adjustment of the gravitational and lateral acceleration). In 1-g shake-table Soil-Structure-Interaction experiments, it is possible to scale the structural properties but it is almost impossible to scale the vertical stresses (unless artificial weight is applied at the top surface), which can affect the response of the soil. That is why it is important to test at the largest possible scale in order to minimize the scale effects, which is one of the objectives of the new large-scale UNR soil-box. One of the question that naturally arises for such SSI experiments, is how to scale the input motion. In all the numerical analyses presented in this study the time-scale of the input motions was not modified, just the magnitude.

This section will examine the effects that a time-scaling of the ground motions would have on the response of the soil column. Two different geometric scales were selected, particularly 1:5 and 1:10. This means that the time will be scaled by the square root of 5 and 10 respectively, according to Froude scaling laws. Figure 3-9 shows the PGAs recorded at different soil-depths for the ElCentro270 and Hector090 records at SF1 (PGA=0.26g) for three cases, unscaled and scaled to the two previous scales. It is

interesting to see that although the scaled motions for ElCentro270 give significantly larger PGAs for the whole soil than the unscaled motion, this trend is not true for Hector 090. For the latter motion, the 1:10 scale gives similar results to the unscaled motion, while the 1:5 scale increases the PGAs for the 2/3 of the upper soil layers. This behavior can also be observed in the maximum strains and maximum relative displacements, with ElCentro consistently resulting in higher values when it is scaled, and Hector having an inconsistent effect depending on the exact scale. The different trends observed for the two motions, indicate that the frequency content of each motion influences the effect of time-scaling.

To understand the reasons behind the observed effect, Figure 3-12 shows the acceleration response spectra at the bottom soil layer. As expected scaling the time of the input motion, results on an offset of the spectral accelerations at the bottom layer towards the left. Given the fact the fundamental period of the soil-column is 0.13sec (linear) and the soil undergoes some yielding at SF1, the period could increase and get close to 0.18-0.2sec. At this period range, the response spectrum of the scaled motion at the bottom soil-layer gives larger values than the unscaled one for the ElCentro motion. On the other hand, for the Hector090, the 1:5 scale can give larger accelerations than the 1:10 scale and the unscaled motion, providing a possible explanation of the effect of time-scaling on the response of the soil-column. Last but not least, Figure 3-13 shows the acceleration response spectra at the surface of the soil and reveals that depending on the periods of interest and the input motion the time scaling can have a positive, negative or minimal effect of the surface accelerations.

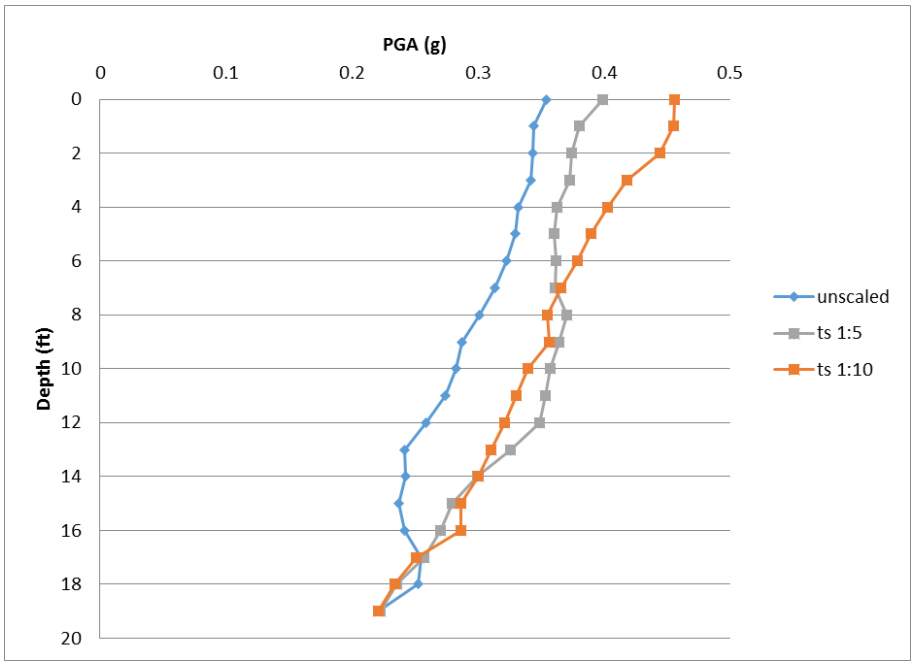

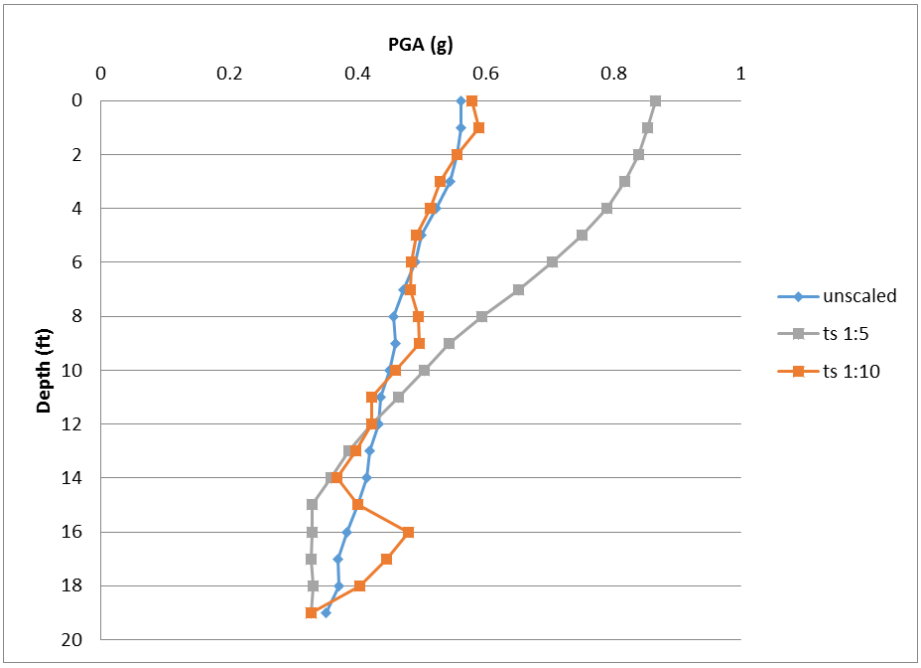

Figure 3-9: PGAs for ElCentro270 (top) and Hector090 (bottom) with SF1

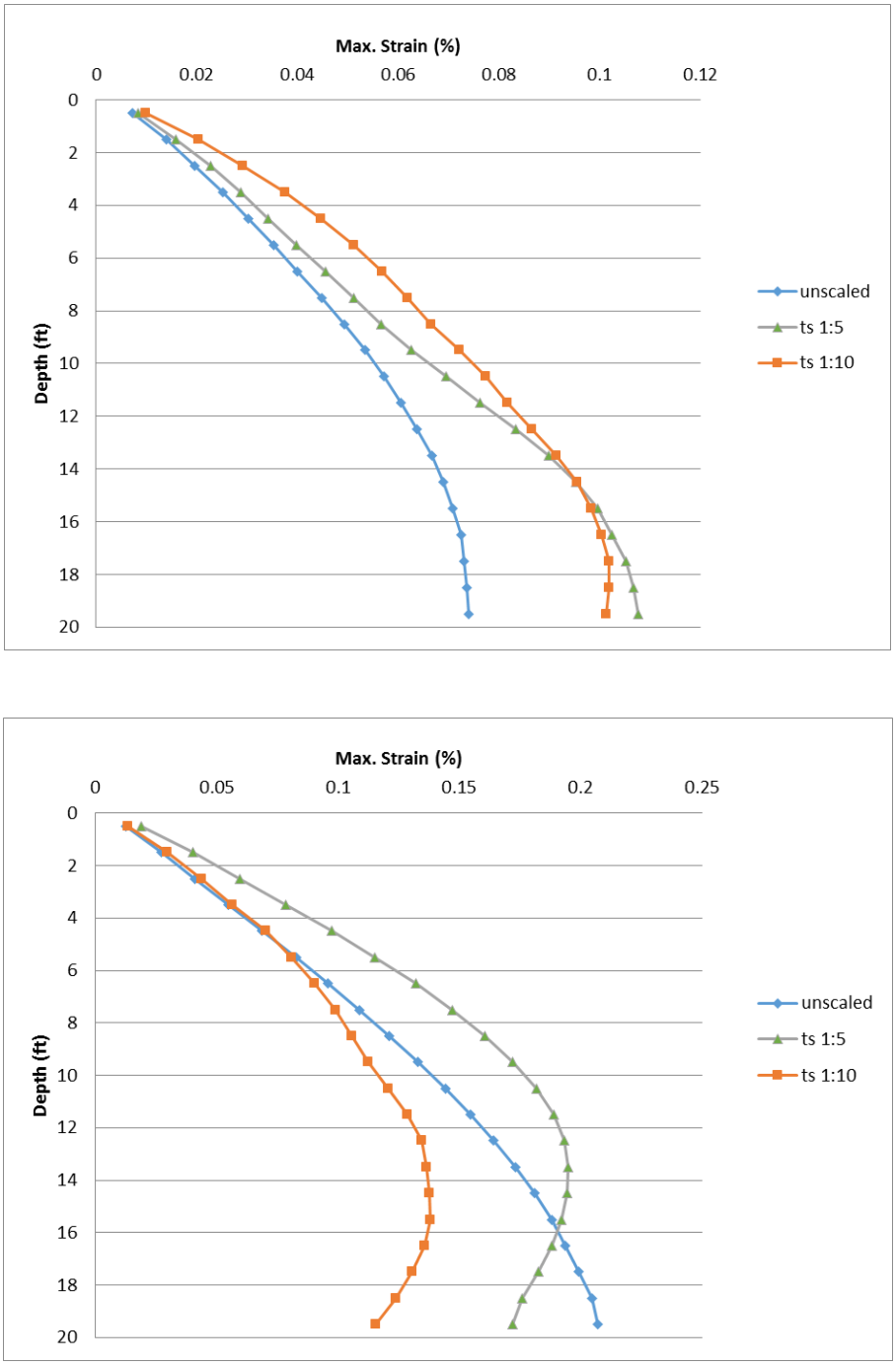

Figure 3-10: Max strains for ElCentro270 (top) and Hector090 (bottom) with SF1

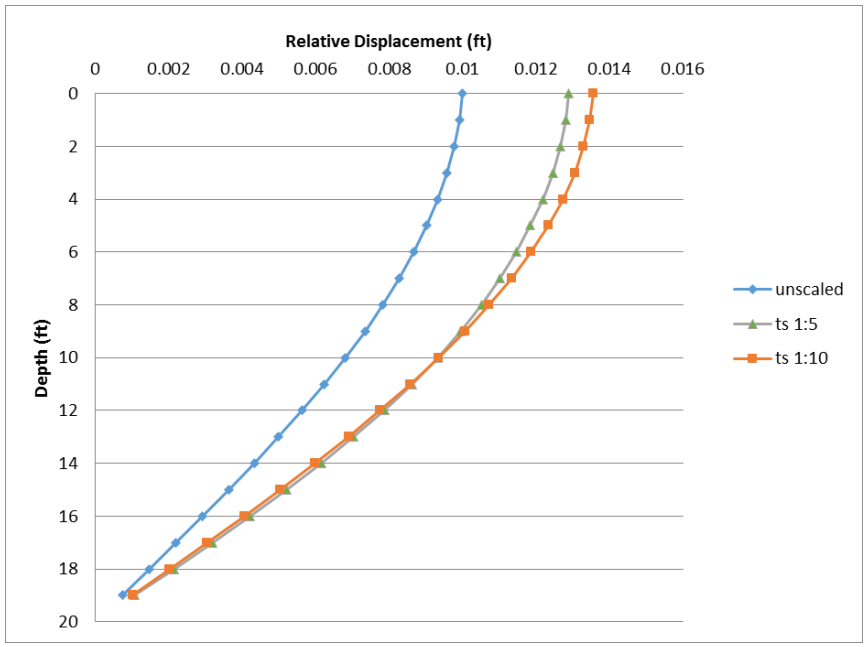

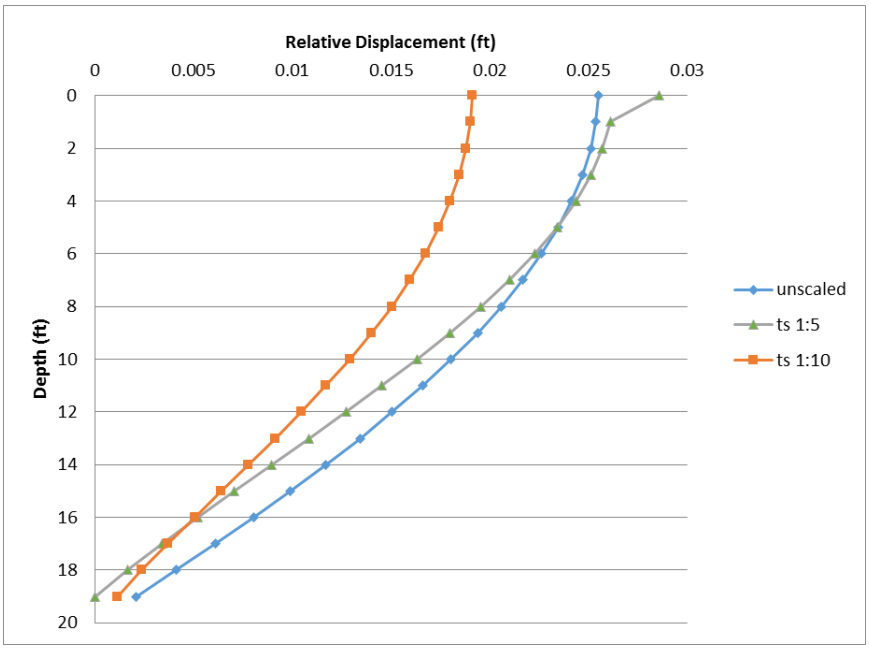

Figure 3-11: Max relative displacements for ElCentro270 (top) and Hector090 (bottom) with SF1

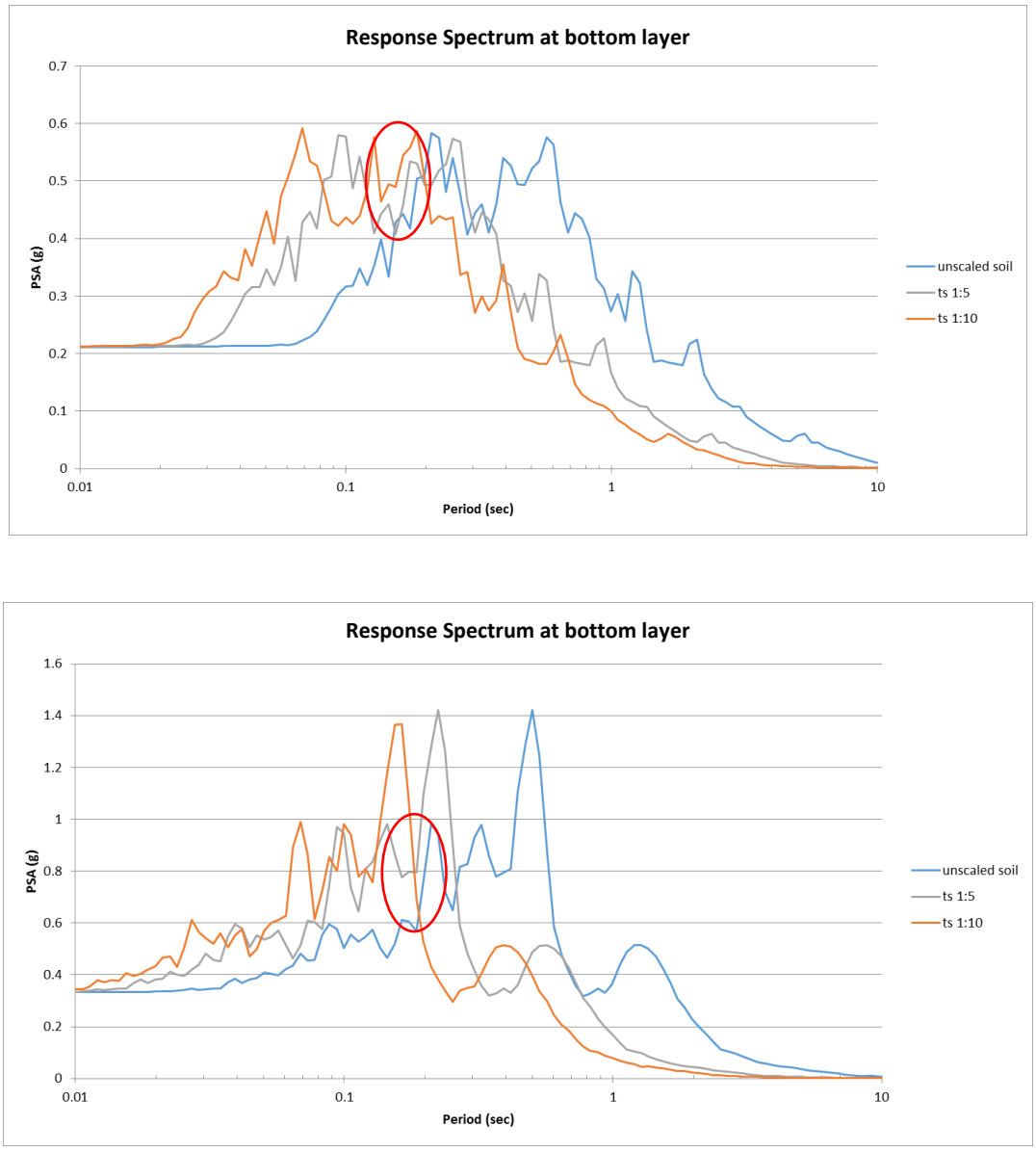

Figure 3-12: Acceleration response spectra at the bottom soil layer for ElCentro270 (top) and Hector090 (bottom) with SF1

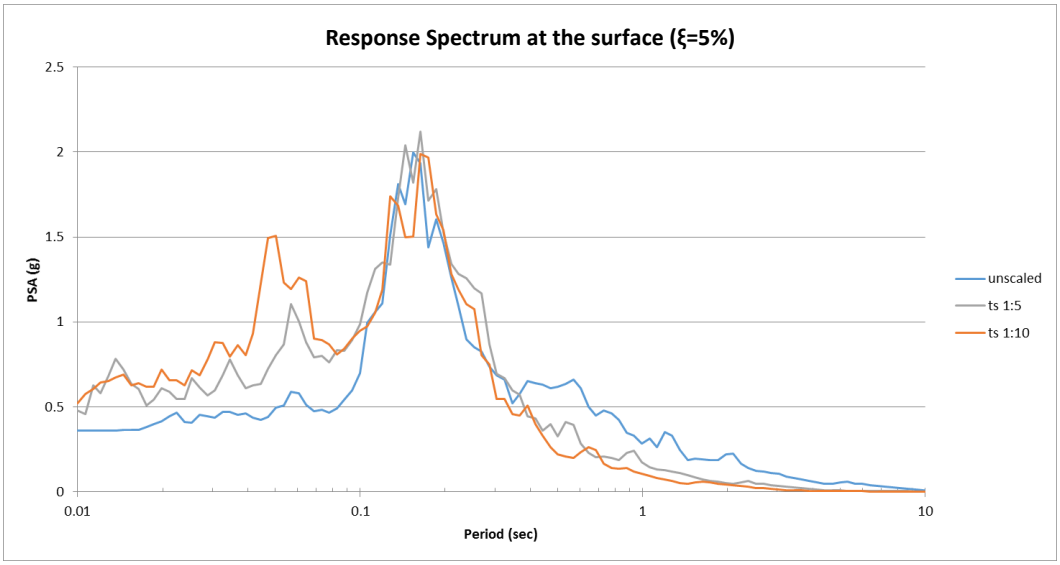

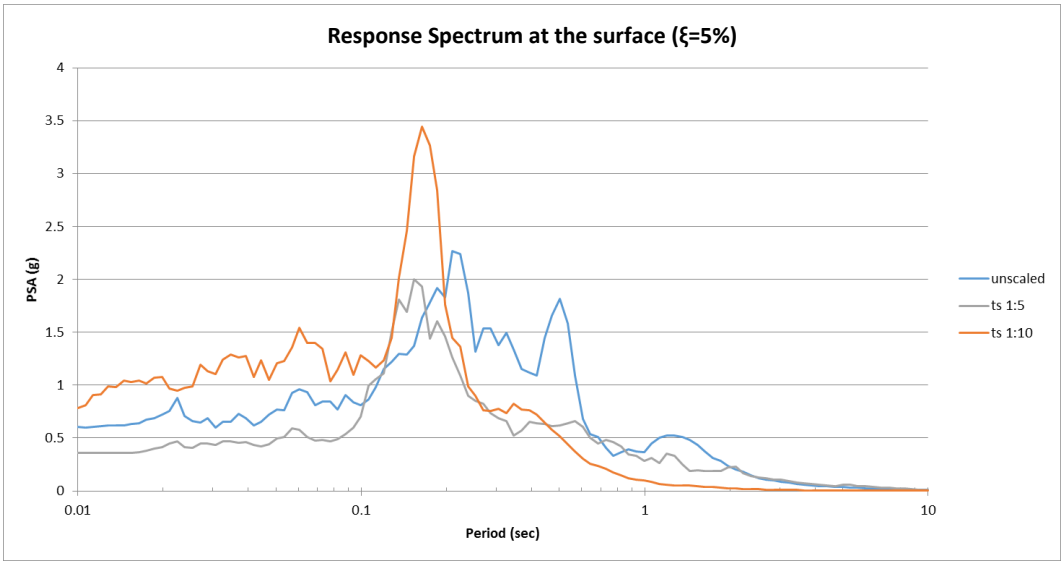

Figure 3-13: Acceleration response spectra at the surface for ElCentro270 (top) and Hector090 (bottom) with SF1

Chapter 4: Site Response Analyses in LS-DYNA

4.1 Model Description

In previous chapters, extensive 1D site response analyses were conducted in DEEPSOIL to get a basic insight into the behavior of a 20ft soil column. However, in order to advance the understanding of the behavior of the actual soil-box and provide information for its design more advanced type of analyses are required. In particular complex Finite Element models, which simulate the soil and the walls of the box should be developed. To this end, the general purpose commercial finite element software LS-DYNA (LSTC 2014) was selected for the development of advanced finite element models. Before the development of these models however it was deemed critical to simulate in LS-DYNA the same soil column that was simulated in DEEPSOIL and compare the results between the two software tools. Therefore, a 20ft height soil column was simulated using 8-node 3D solid elements with dimensions 1ftx1ftx1ft, as shown in Figure 1.

LS-DYNA has been widely used for automotive/crash applications, impact problems and generally very transient phenomena due to its robust explicit solver and the wide variety of contact formulations. It addition, the software is versatile and can be conveniently used to study multi-physics phenomena, with several studies having recently used it for site response (Bolisetti et al 2014, Motamed et al 2016) and soil-structure analyses (e.g. Bolisetti 2015). The software provides also a variety of soil materials, with one commonly used material being the MAT_HYSTERETIC_SOIL, which was also used

in the current study. This material model allows the direct input of the backbone curve via specification of ten points in the curve and it employs the Masing rules. The input curves were adjusted to account for the ultimate shear strength of the soil using an automated Excel spreadsheet described in Motamed et al (2016). According to the LS-DYNA manual (LSTC 2014), MAT_HYSTERETIC_SOIL is a nested surface model that consists of ten elastic-perfectly plastic layers superimposed, which generate hysteretic energy every-time that a layer yields. To determine the yielding the stress invariant J2 is calculated for each layer based on the deviatoric stresses and then compared to the maximum shear stress calculated using the assumption of a uniaxial stress state for each layer ($J2 < (4 * \tau \overset{2}{\max})/3$).

For simulating the seismic input motion prescribed boundary conditions and particularly acceleration time histories were applied at the bottom nodes of the last soil layer. SPC constraints were used to constrain the out-of-plane displacements of all the nodes of the soil column, as well as the vertical displacements of the bottom nodes. Moreover, in order to make this model to behave in shear, horizontal constraints were applied to the 4 nodes of each solid element that have the same elevation. Two construction stages were defined, with the first one applying the gravity loading to develop the correct vertical soil stresses, and the second one applying the lateral seismic motion. In addition to the hysteretic damping automatically calculated by the nonlinear material model, viscous damping equal to 2% was applied via the use of the keyword DAMPING_FREQUENCY_RANGE_DEFORM in order to simulate the frequency-independent damping of soils at small strains. The current implementation in LS-DYNA

applies the damping only to a range of frequencies and in this study the range was selected to be between 1Hz and 30Hz in order to capture the frequency content that might be of interest to nuclear power plants and facilities.

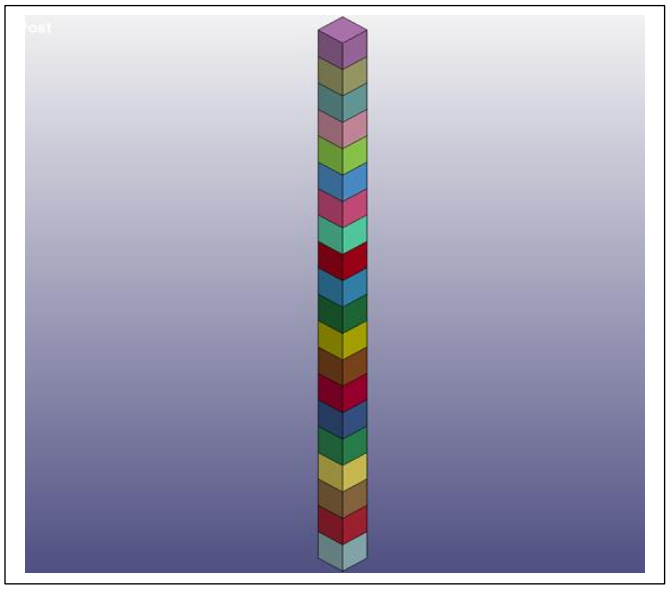

Figure 4-1: 20ft soil column in LS-DYNA

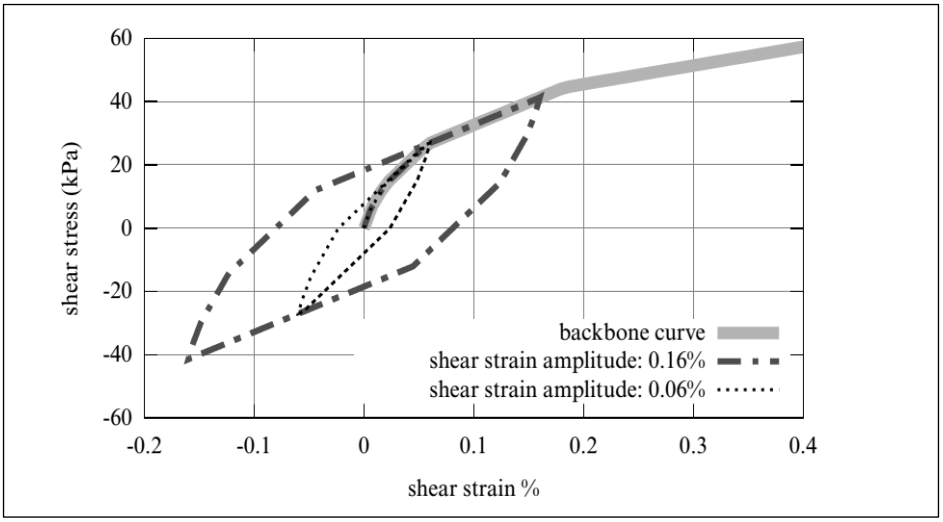

Figure 4-2: Shear stress-shear strain loop for MAT_HYSTERETIC_SOIL in LS-DYNA (from LSTC manual)

4.2 Results: LS-DYNA vs DEEPSOIL

This section will present a comparison of LS-DYNA and DEEPSOIL for two types of analyses, a linear and a nonlinear one. In the nonlinear analyses the soil was simulated with the nonlinear MAT_HYSTERETIC_SOIL material model described in the previous section, while in the linear analyses this was done with an elastic material model that required the input of the elastic modulus and Poisson's ratio for each soil layer. Both types of analyses were conducted for the Cerro_237 record, the magnitude of which was scaled to a PGA of 1g (no frequency scaling).

4.2.1 Linear Analyses

Figure 4-3 shows the peak ground accelerations (PGAs), the maximum strains and the maximum stresses as a function of the depth, obtained from linear analyses. It can be observed that both programs show a significant amplification of the PGAs as the wave propagates vertically towards the surface, and this is because the fundamental natural period of the soil column (0.13sec or 7.6Hz) is close to the frequency content of the ground motion. The PGAs obtained from LS-DYNA and DEEPSOIL seem to have a reasonable agreement for all the soil layers, apart from the surface where DEEPSOIL gives noticeably smaller PGA. Regarding the maximum shear strain and shear stress values, both software tools give general smaller values at smaller depths. Although the trends in the maximum strains and stresses are similar in DEEPOIL and LS-DYNA, the latter one gives generally larger values. Possible reasons for the differences between the two programs are presented in a following section of this chapter.

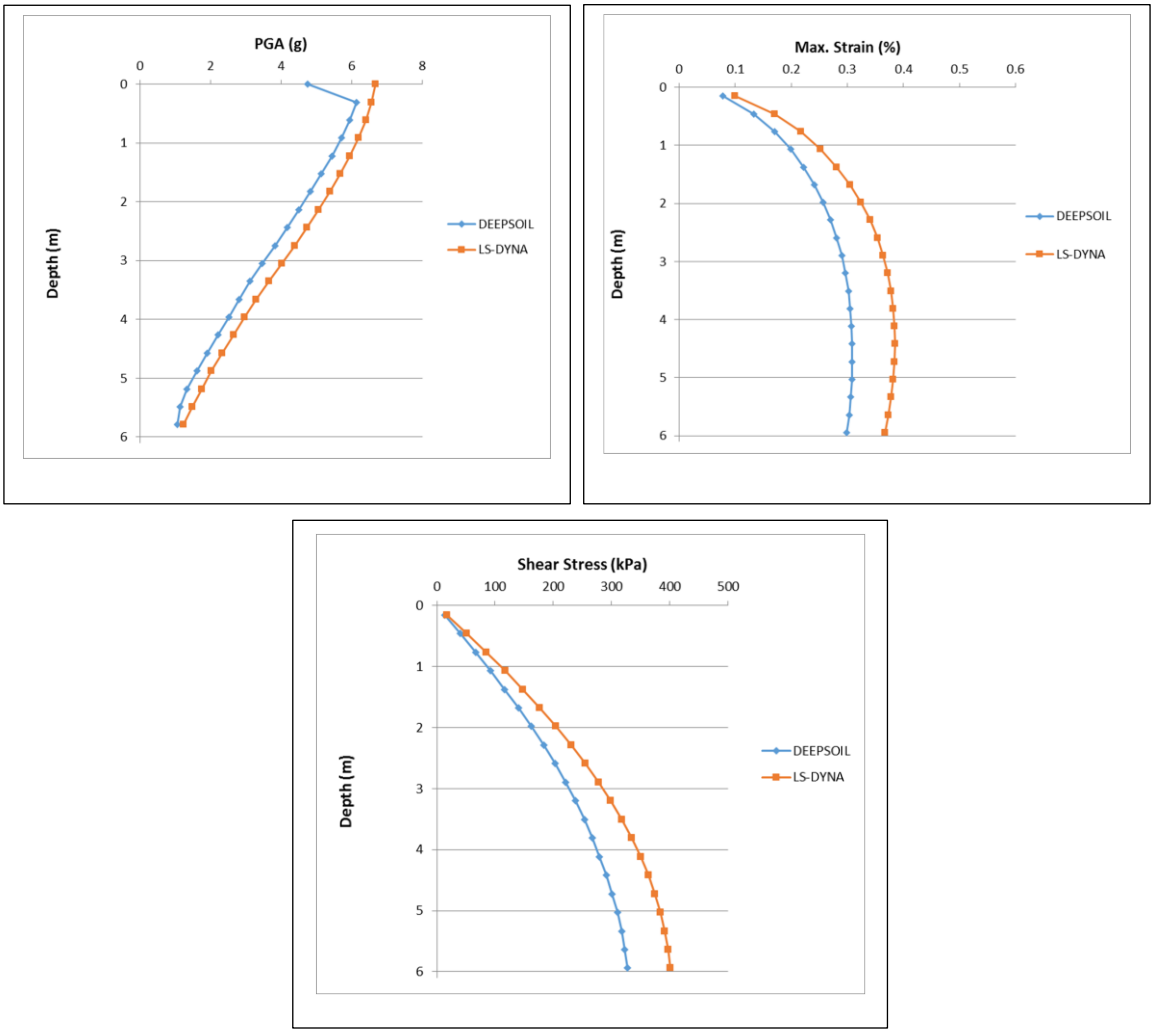

Figure 4-3: PGAs (top-left), peak shear strains (top-right) and peak shear stresses (bottom) as function of depth from linear analyses

4.2.2 Nonlinear Analyses

This section will present a thorough comparison of nonlinear analyses conducted in DEEPSOIL and LS-DYNA. Figures 4-4 and 4-5 show the acceleration histories recorded at the soil surface and at the mid-depth (layer 10) respectively, for two levels of shaking with PGAs equal to 0.25g (S.F.=1) and 1.0g (S.F.=4). The two graphs reveal that there is a very good agreement between the results from the two programs, with LS-DYNA generally introducing some higher frequency accelerations in the model than DEEPSOIL. These high frequency components can be also observed in the acceleration response spectra shown in Figure 4-6. Interestingly, the PSAs from the two software tools are similar, both at the surface and at the mid-depth, especially for periods larger than 0.1sec. The largest differences occur for large amplitude shaking (S.F.=4) and in the small-period range (<0.1sec) with LS-DYNA giving larger accelerations, which is consistent with the high-frequencies observed in the acceleration histories.

Figures 4-7 and 4-8 show the shear stress and shear strain histories respectively for the two soil layers mentioned previously. A generally good agreement is observed for the shear stresses but this is not true for the shear strains. Although, the trends in the histories of the shear strains are similar in the two software tools, however the magnitudes are different, with LS-DYNA giving significantly larger residual shear strains. The good agreement of shear stresses and the bad agreement of the shear strains, implies that the soil has yielded meaning that the shear stresses have reached the shear strength, and although in both numerical codes the soil shear strength is the same the respective strain histories are not the same due to the different soil material and its hysteretic behavior. This

assumption can be backed up by the fact that the maximum shear strains for an input motion with S.F.=4 seem to reach 0.6% at the surface (low confinement) and 2% at the mid-depth, which puts the soil in the post-yielding range. In addition, this can be verified by examining the shear stress-strain loops calculated by DEEPSOIL and LS-DYNA, and are shown in Figure 4-9, which have the same maximum shear stresses, however they look significantly different with different levels of dissipated hysteretic energy that result in a different dynamic behavior of the soil. One of the major differences between the analyses conducted in DEEPSOIL and LS-DYNA is the fact that in the former one Non-Masing rules were selected for the material model while in the latter the Masing rules are automatically used.

The profiles of the peak ground accelerations, peak shear strains and peak shear stresses with depth are shown in Figures 4-10, 4-11 and 4-12 respectively, for the two levels of seismic shaking. For a scale factor of 1, the agreement of the PGAs is overall good with the best agreement occurring for lower depths and the agreement worsening for soil layer at shallower depths. As the level of shaking increases (S.F.=4) then the differences between the two software tools increase. Figure 4-12 shows that for S.F.=1 approximately only the upper 8ft (2.4m) of the soil have reached the shear strength, while for S.F.=4 all the soil layers have reached the shear strength, demonstrating that indeed the agreement of DEEPSOIL and LS-DYNA is better as the soil nonlinearity decreases, and strengthening the assumption that the differences between the two software programs arise

from the different hysteretic behavior of the soil materials. This could also possibly explain the differences in the peak shear strains seen in Figure 4-11.

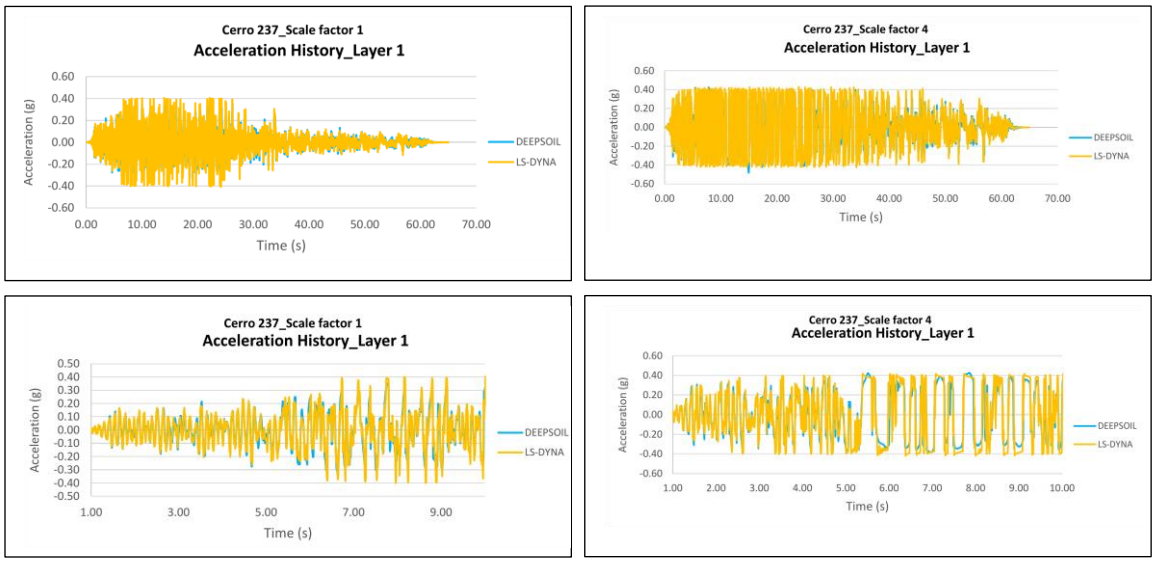

Figure 4-4: Acceleration histories at the surface of the soil column, whole history (top) and zoom in (bottom), for S.F.=1 (left) and S.F.=4 (right)

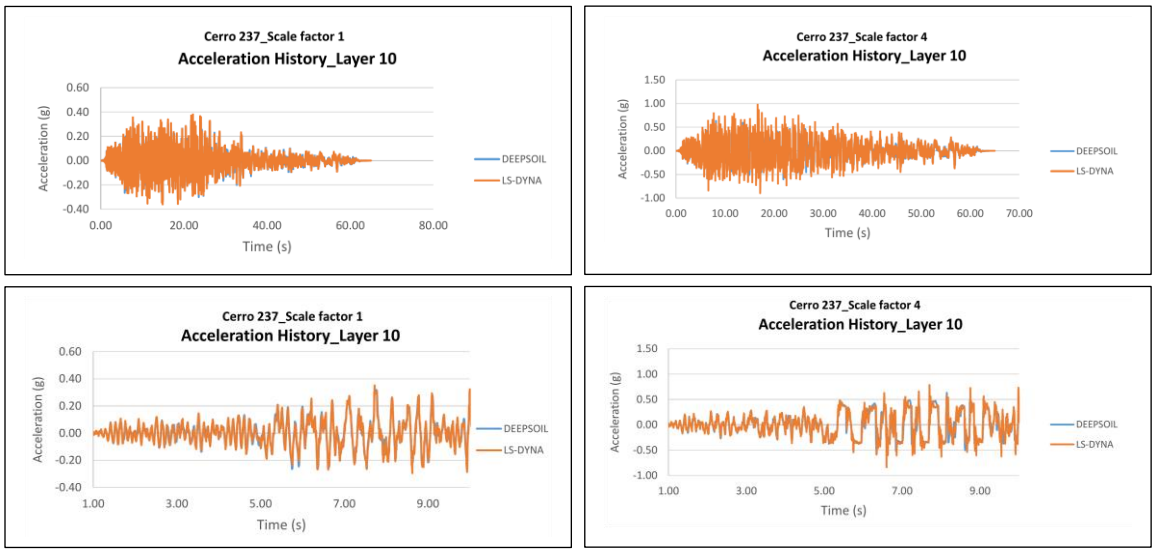

Figure 4-5: Acceleration histories at the mid-depth of the soil column, whole history (top) and zoom-in (bottom), for S.F.=1 (left) and S.F.=4 (right)

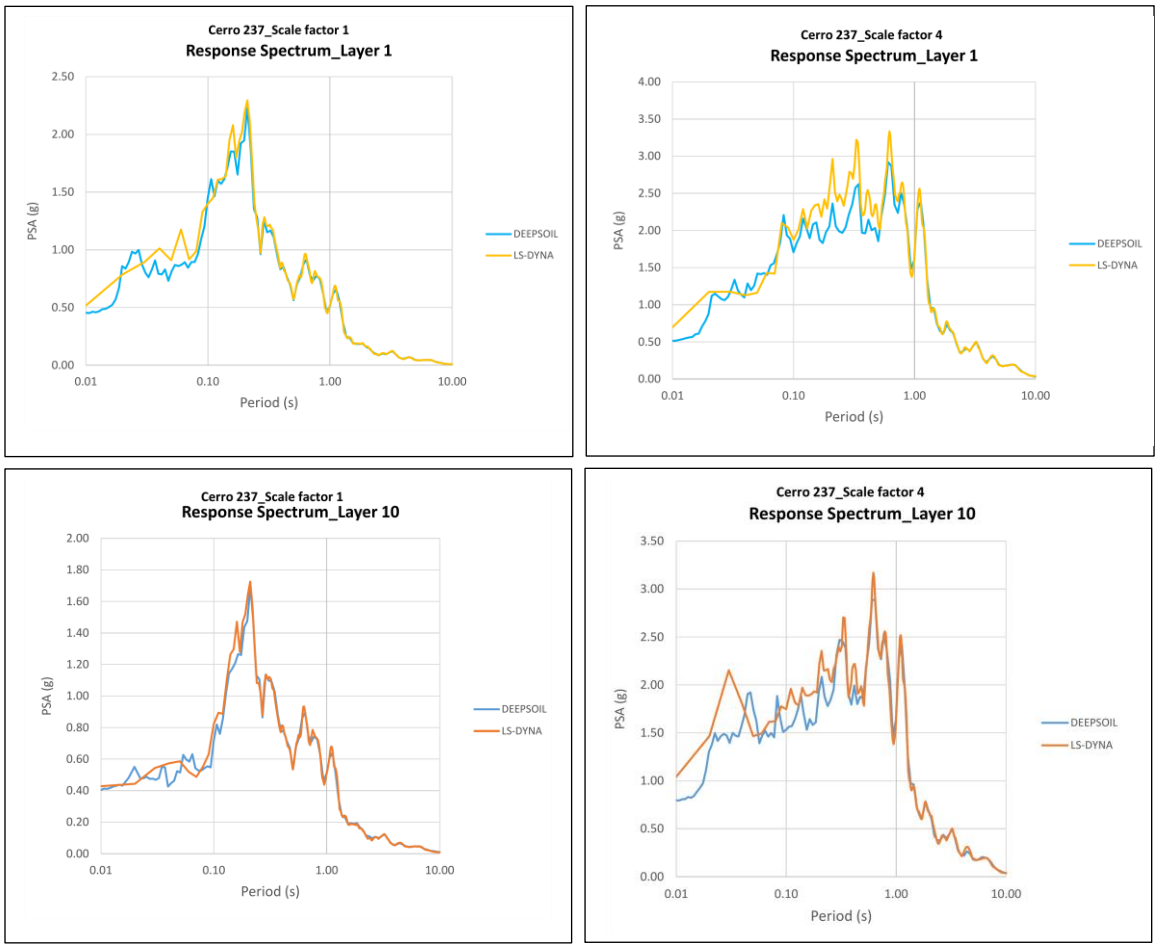

Figure 4-6: Acceleration response spectra at the surface (top) and mid-depth (bottom) of the soil column, for S.F.=1 (left) and S.F.=4 (right)

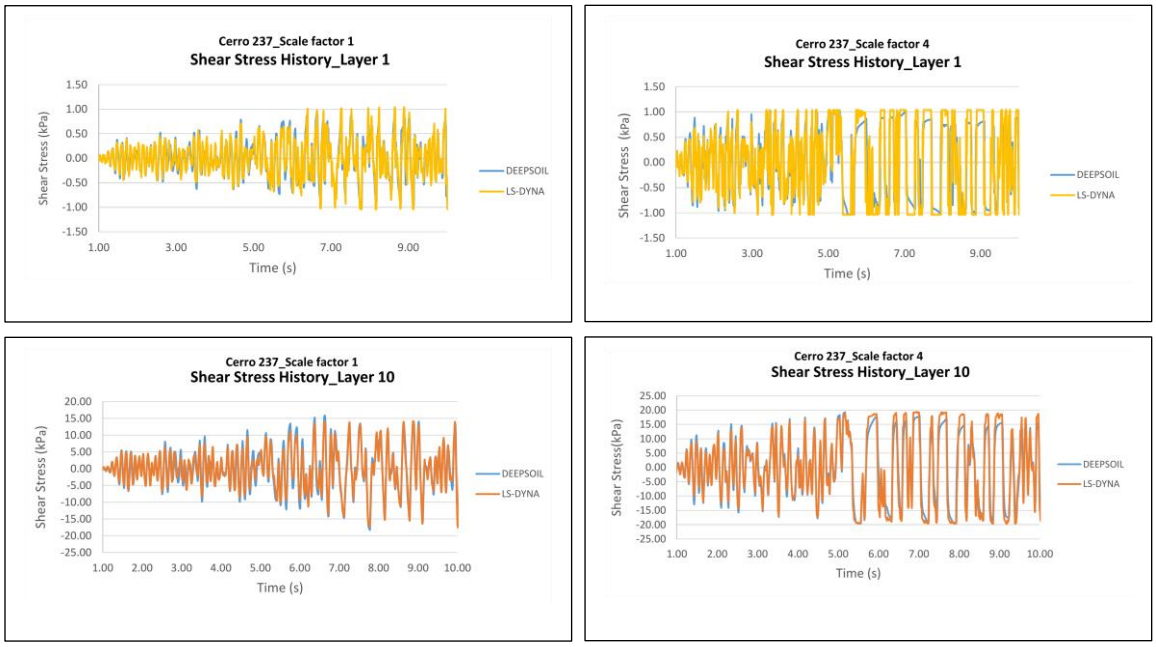

Figure 4-7: Shear stress histories at the surface layer (top) and at layer 10 (bottom), for S.F.=1 (left) and S.F.=4 (right)

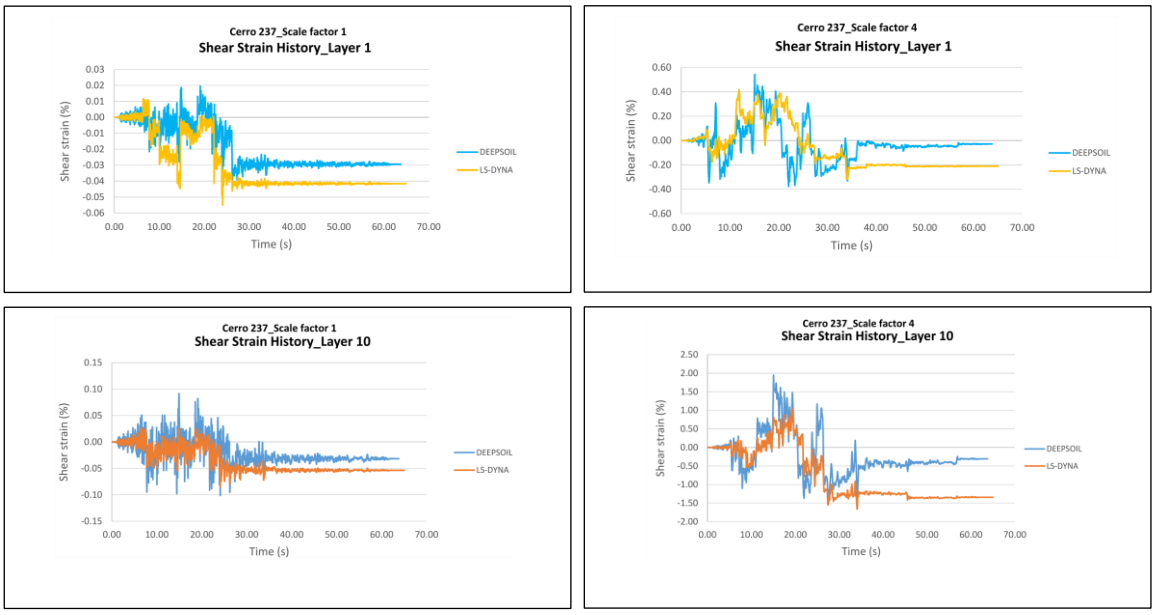

Figure 4-8: Shear strain histories at the surface layer (top) and at layer 10 (bottom), for S.F.=1 (left) and S.F.=4 (right)

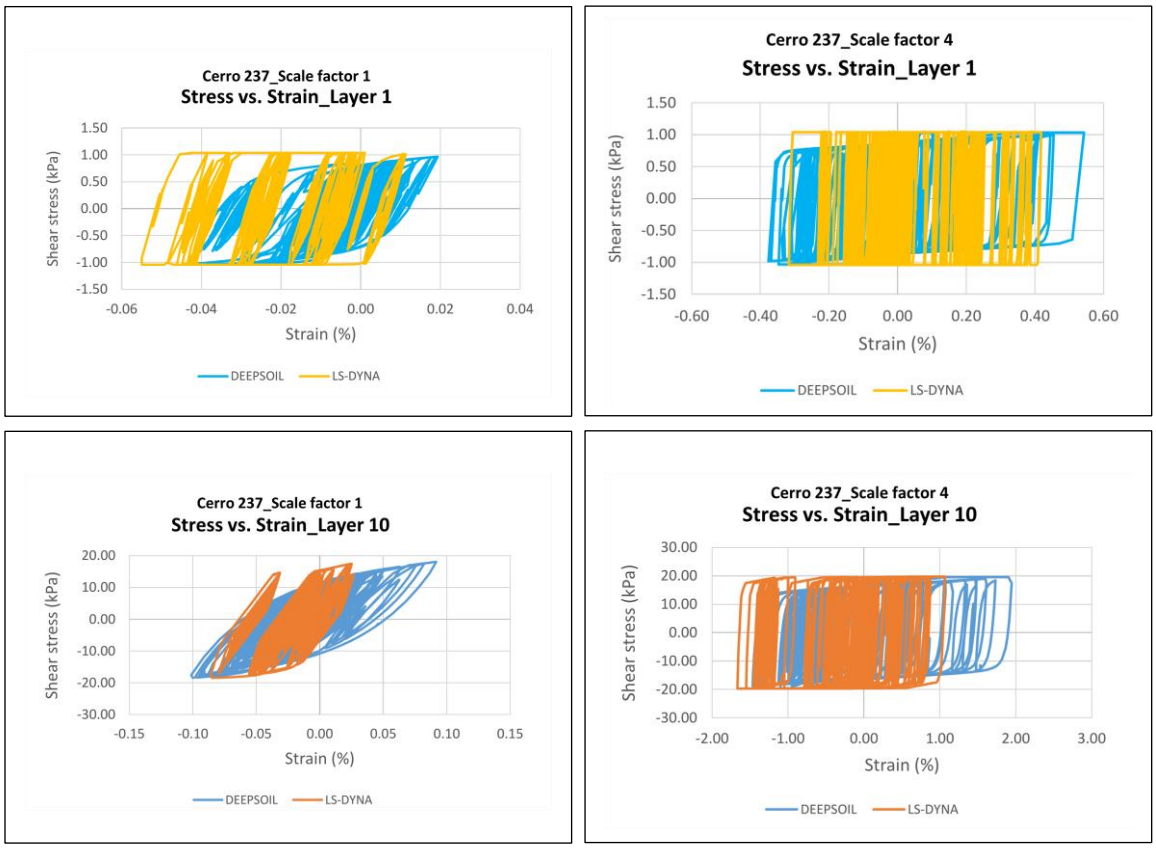

Figure 4-9: Shear Stress-strain loops at the surface (top) and mid-depth (bottom) of the soil column, for S.F.=1 (left) and S.F.=4 (right)

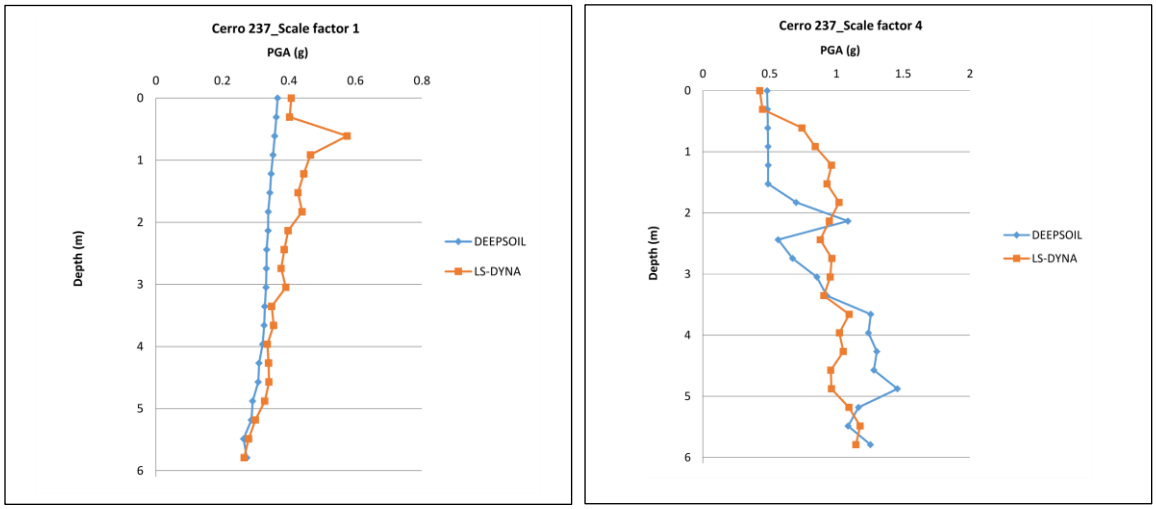

Figure 4-10: PGA of the soil column as a function of the depth, for S.F.=1 (left) and S.F.=4 (right)

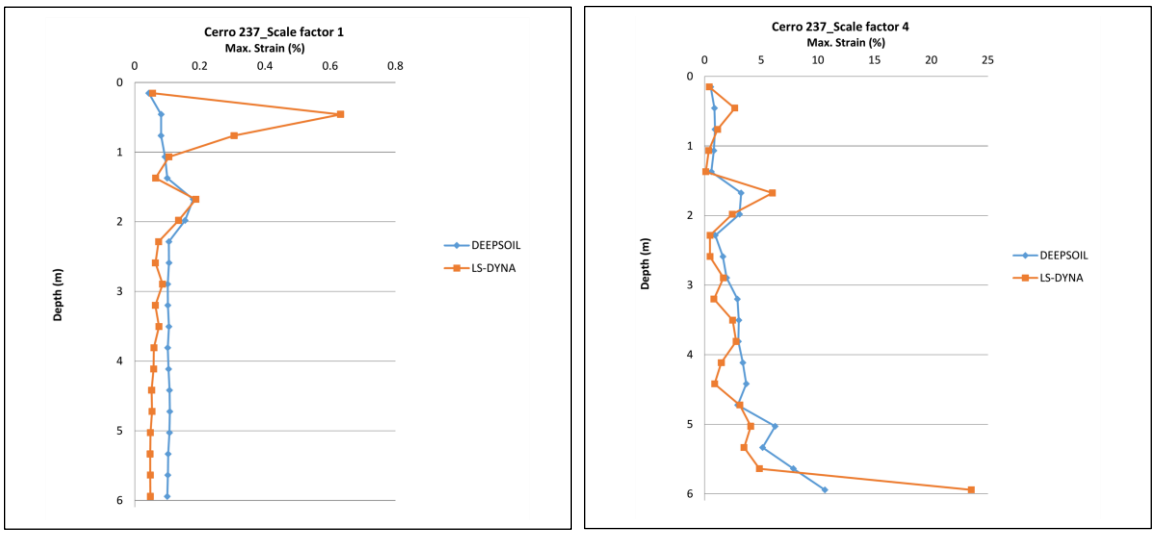

Figure 4-11: Peak shear strains of the soil column as a function of the depth, for S.F.=1 (left) and S.F.=4 (right)

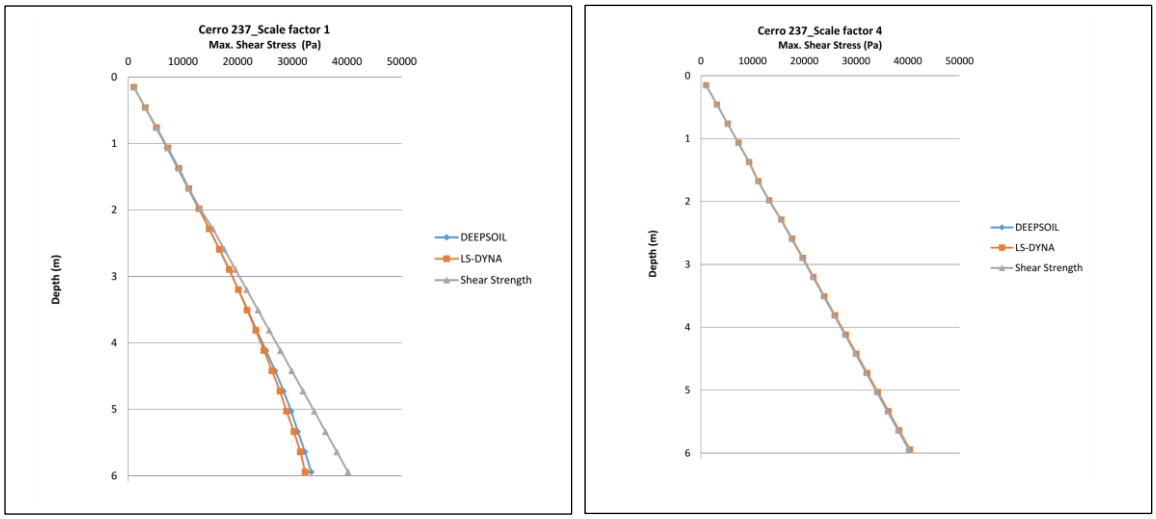

Figure 4-12: Peak shear stresses of the soil column as a function of the depth, for S.F.=1 (left) and S.F.=4 (right)

4.3 Discussion on differences between the two software tools

This section will identify reasons that could have contributed to the differences observed in the numerical results obtained from DEEPSOIL and LS-DYNA. The differences could be divided in four groups including (1) analysis options, (2) small-strain damping formulation, (3) material models, and (4) stress-strain curves. More information is presented below.

1. *Analysis Options:*

   DEEPSOIL uses lumped mass interconnected with shear springs, the Finite Difference Method, and either a fixed time-step that is defined by the user or a flexible time-step based on the user defined maximum acceptable shear strain increment calculated at each integration step. On the other hand LS-DYNA uses

3D solids, the Finite Element Method, and an Explicit Numerical Integration Method with the time-step always defined by the program (implicit integration methods are also available).

2. *Small-Strain Damping Formulation:*

   DEEPSOIL has a frequency independent viscous damping for all range of frequencies, while in LS-DYNA the small-strain damping is truly frequency independent only in a certain range of frequencies specified by the user. The larger the frequency range the larger the error that is introduced in the dynamic stiffness of the soil column. Therefore, the LS-DYNA results can be sensitive to the frequency range of the small-strain damping selected by the user.

3. *Material Models:*

   DEEPSOIL allows the use of a nonlinear material model (GQ/H) with Non-Masing Rules and an automatically determined G/Gmax and damping curves based on the shear modulus (shear velocity) and the user defined shear strength. In addition, the software has a reduction factor for the damping curves, which is activated at large strains in order to reduce the hysteretic damping calculated from the hysteretic loop. On the other hand, the MAT_HYSTERETIC_SOIL material in LS-DYNA is a nested surface material that automatically uses Masing rules. These differences affect the shape of the hysteretic loop and consequently the hysteretic damping generated by the two material models.

4. *Backbone Curves:*

In the numerical analyses presented in this chapter, strength adjusted backbone curves (calculated based on mean effective stress) were used in both DEEPSOIL and LS-DYNA. In DEEPSOIL these curves were automatically generated by the GQ/H material model, while in LS-DYNA the curves were generated using an automated Excel spreadsheet following the procedure described in Motamed et al (2016). Although these curves have the same initial slope (shear modulus) and the same shear strength, they are not exactly the same between the linear part and the ultimate strength due to the different process used for developing the intermediate part of the curve. Moreover, in DEEPSOIL the backbone curve is described by a continuous equation while in LS-DYNA the backbone curve of each layer has only 10points. Previous research (Bolisetti 2015) has shown that the abrupt change of the slope in the backbone curve of LS-DYNA can cause high-frequency 'noise' that can lead to overestimation of the accelerations.

4.4 Effect of soil shear strength

The shear strength of soils can be calculated based on equation (4.1), where c is the cohesion (equal to zero for cohesion-less soils/sands), φ is the angle of friction and σv' is the effective stress normal to the failure plane. The Mohr-Coulomb failure criterion can be used in order to calculate the c and φ values by employing eq. (4.2) and results from multiple triaxial tests (at different σ_3' values), and the ultimate shear strength for a given condition of σ_1' and σ_3'. This means that the ultimate shear stress that a soil can take

depends on the two principal effective stresses (σ_1' and σ_3'). Despite this fact, in 1D site response (e.g. Yee et al 2013), it is assumed that the shear strength depends only on the vertical effective stress, and equation (4.1) is used again to calculate the shear strength. Therefore, there are two ways to calculate the shear strength of soils, either by considering the mean effective stress (based on σ_1' and σ_3') or by considering the vertical effective stress. For this study both ways were examined in order to determine the effect on the numerical results.

$$\tau = c + \sigma v' * tan\varphi \tag{4.1}$$

$$\frac{\sigma_1 - \sigma_3}{2} = \frac{\sigma_1 + \sigma_3}{2} * sin\,\phi + c * cos\varphi \tag{4.2}$$

Figure 4-13 shows the G/Gmax and backbone curves created by the GQ/H material model in DEEPSOIL for both the vertical and mean effective stress. Although, there do not seem to be significant differences in the G/Gmax curve (with a logarithmic x-axis), major differences can be observed in the backbone curve after the initial linear part with the vertical effective method resulting in larger magnitudes of shear stresses. This is reasonable since the vertical effective stress is larger than the mean effective stress by approximately a factor of 2, meaning that the shear strength calculated by eq. (4.1) is twice as high in the former case than in the latter one.

To determine the sensitivity of the numerical results to the soil shear strength, the peak PGAs, shear strains and shear stresses for Cerro 237 and S.F.=4 are plotted in Figure

4-14 as a function of depth. As expected the larger shear strength (based on vertical stress) resulted in larger PGAs for all soil layers. However, the PGAs did not increase linearly with the shear strength and although the shear strength doubled when the vertical effective stress was used, the PGAs did not double. The different shear strength affected the dynamic behavior of the soil column significantly because at a scale factor of 4 all the soil layers reached the shear strength when the mean effective stress was used, however this was not true for vertical effective case where only the soil layers from the surface to 12ft depth actually reached the ultimate strength (bottom graph in Figure 4-14). Apart from the significant effect on the PGAs, the smaller shear strength resulted also in larger shear strains, especially at larger depths where the soil reached the ultimate strength for the mean effective case but it did not reach it for the vertical effective one.

The above comparison gave an insight into the effect of the shear strength on the expected response of the soil. Since for the design of the soil-box and shake table system one of the main parameters of interest is the base shear that the actuators of the shake table should be able to take, the maximum base shear was calculated based on the results obtained from the 1D analyses. Interestingly, for the above input motion the maximum base shear was 715kips and 365kips for the case with the vertical effective and mean effective stress respectively. Doubling the shear strength almost doubles the base shear of the soil-column, which is consistent with the shear stresses measured at the bottom layer. To ensure a conservative design of the new soil-box and shake table it was decided that in the following chapters all the analyses will be conducted for the upper bound of the shear strength (based on vertical effective stress). It must be noted that the smaller shear strength

resulted in increased shear strains and relative displacements but this shall not be a concern for the walls of the soil box since these strains are minor relatively to the capacity of the elastomeric bearings that compose the walls of the box.

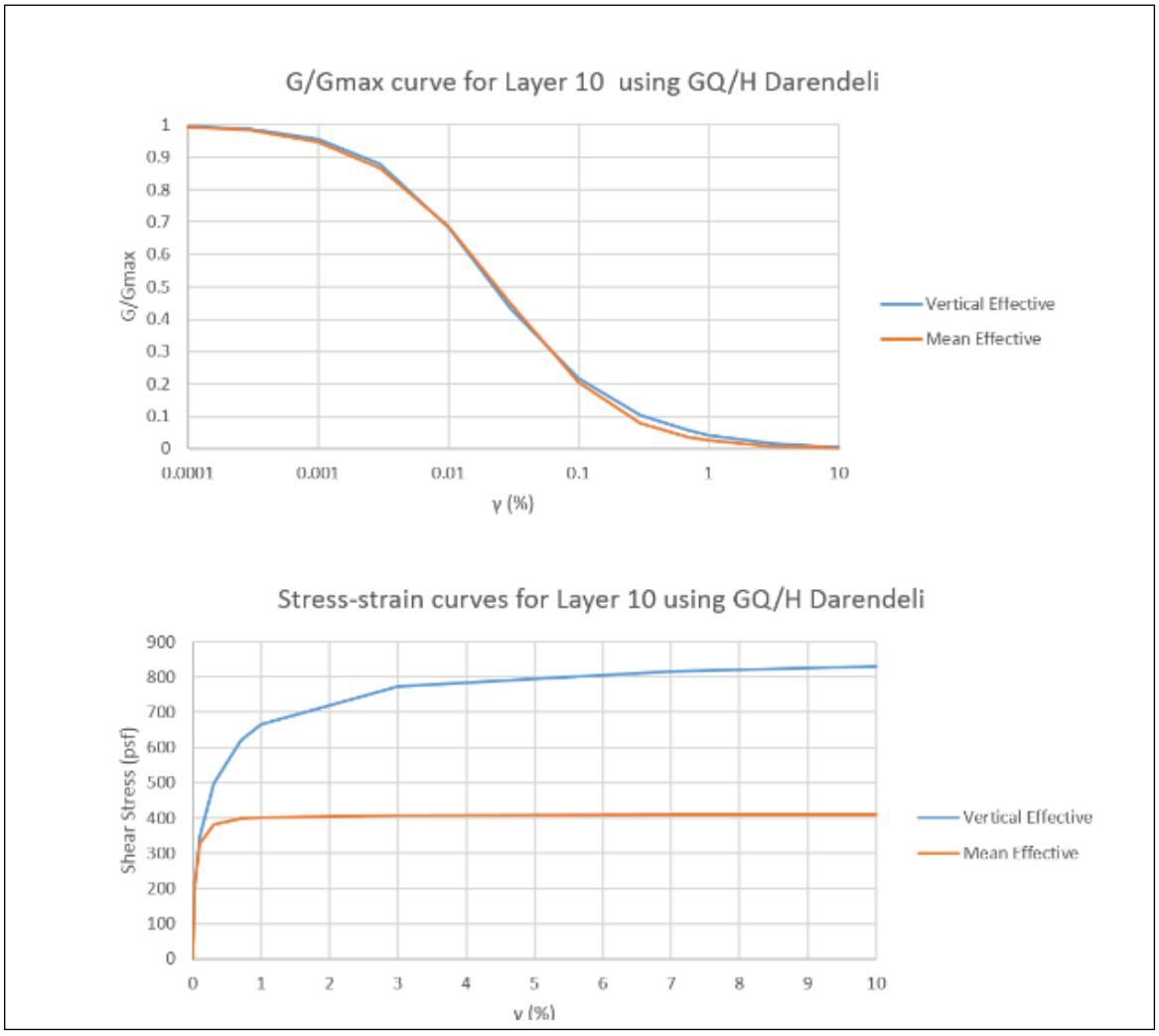

Figure 4-13: G/Gmax curves (top) and backbone curves (bottom) for soil layer 10, as a function of the shear strain

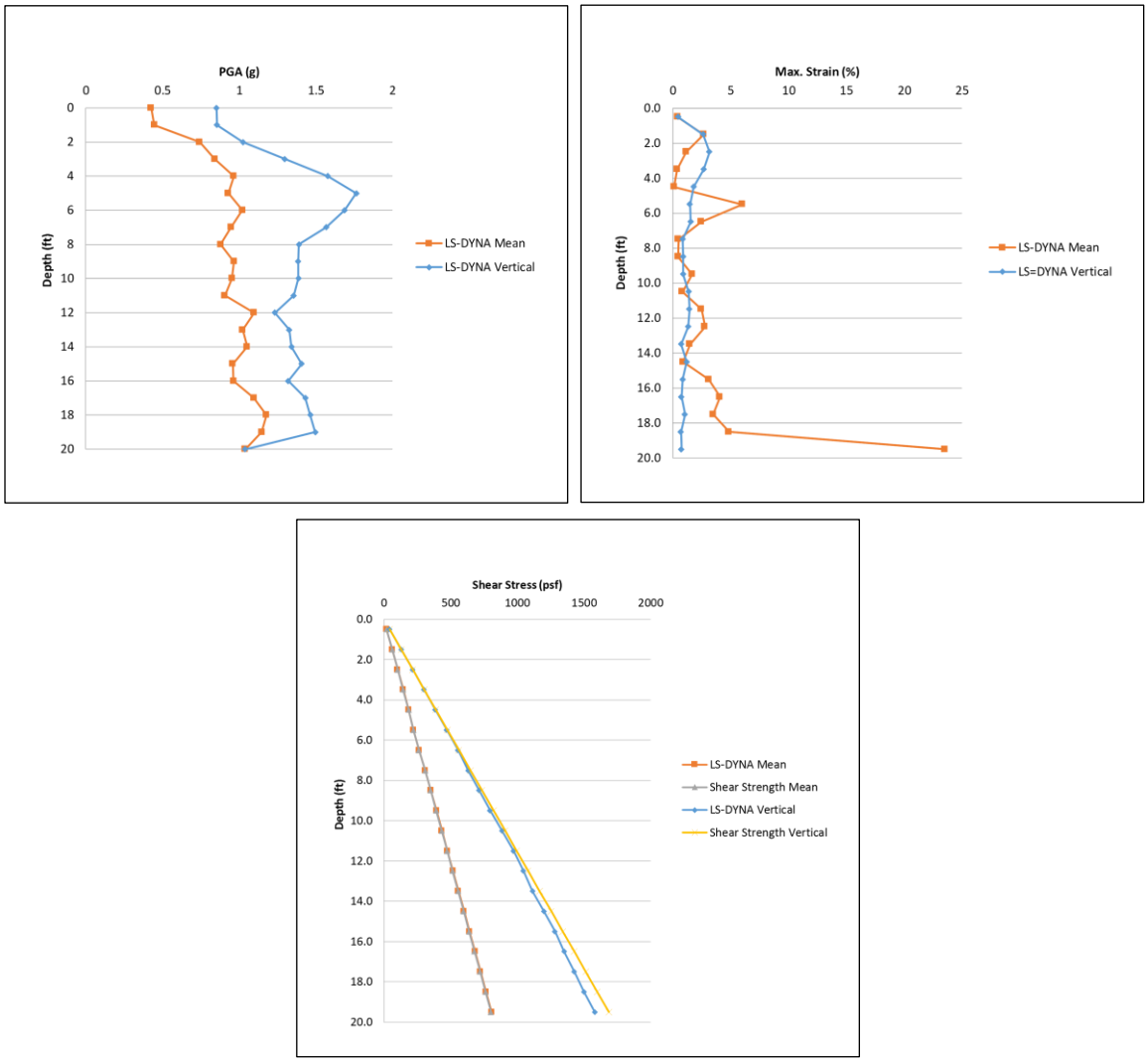

Figure 4-14: PGAs (top-left), peak shear strains (top-right) and peak shear stresses (bottom) as function of depth from nonlinear analyses with different soil strengths

4.5. Summary

This chapter presented a comparison of DEEPSOIL and LS-DYNA for 1D site response analyses of a 20ft soil column. Both linear and nonlinear analyses were conducted for a selected ground motion (Cerro 237), and for the nonlinear analyses two different magnitudes (0.25g and 1.0g) were examined. For linear analyses LS-DYNA generally resulted in larger PGAs, stresses and strains compared to DEEPSOIL, however both software programs showed similar trends and significant amplification of the PGAs from the bottom of the column to the soil surface, due to resonance of the frequency content of the ground motion with the fundamental period of the column (0.13sec).

The results from nonlinear analyses revealed that there was a good matching of the accelerations histories, acceleration response spectra and stress histories, at the surface and at mid-depth, with LS-DYNA generally introducing higher frequencies in the dynamic response of the soil column. Generally, the matching of the results seemed to be better for smaller magnitude shaking (S.F.=1), which resulted in reduced soil nonlinearity. The largest differences occurred in the shear strains, which were associated with significantly different stress-strain loops, indicating a different hysteretic soil behavior. Possible reasons for the observed differences could be the (i) analysis options, (ii) small-strain damping formulation, (iii) soil material models, and (iv) backbone curves.

The last part of the chapter examined the role of the shear strength by comparing results from nonlinear analyses conducted for two different shear strength values, with the first one calculated based on vertical effective stress and the second one based on mean effective stress. For large magnitude ground motions (PGA=1) the results were seen to be

very sensitive to the value of the shear strength, and this happened because for such significant shaking most of the soil layers underwent a very nonlinear behavior and the response was governed by the ultimate soil strength. In particular, the large shear strength resulted in a major increase of the PGAs and stresses along the whole depth of the soil column, and approximately doubled the base shear. For the purpose of the design of the soil-box it was decided to use the shear strength obtained using the vertical effective stress since it lead to the upper bound for the forces.

Chapter 5: Two-Dimensional Nonlinear Dynamic Analyses in LS-DYNA

5.1 2D soil slice vs 1D soil column

Following the extensive 1D analyses conducted in previous chapters, this chapter will present analyses from more complicated models that attempt to simulate the behavior of the soil-box more realistically and provide an insight into the interaction of the walls of the box with the soil. The first step in this attempt was to develop in LS-DYNA a 2D slice model consisting of multiple soil columns and compare the results with a 1D soil column. The 2D slice consisted of 3D solid elements, as shown in Figure 5-1, which had shared nodes between them in order to simulate a soil layer with a finite length. Boundary conditions (SPC constraints) were applied at the bottom nodes of each solid element of the bottom soil layer to prevent any vertical movement. At the same nodes, the input ground motion was applied in the lateral direction. All the nodes of the model had SPC constraints that did not allow any out-of-plane deformation. Similar to the 1D model, horizontal constraints were assigned to all the nodes of a soil layer that had the same elevation in order to force a shear behavior of the 2D slice.

Different parameters were output in the 2D soil slice and the results recorded at the center soil column were compared with the ones obtained from the 1D model. Figure 5-2 shows the results of this comparison for Cerro 237 and SF=4. Interestingly, similar PGAs, shear strains and shear stresses seem to be output by the two models, giving confidence in the 2D model.

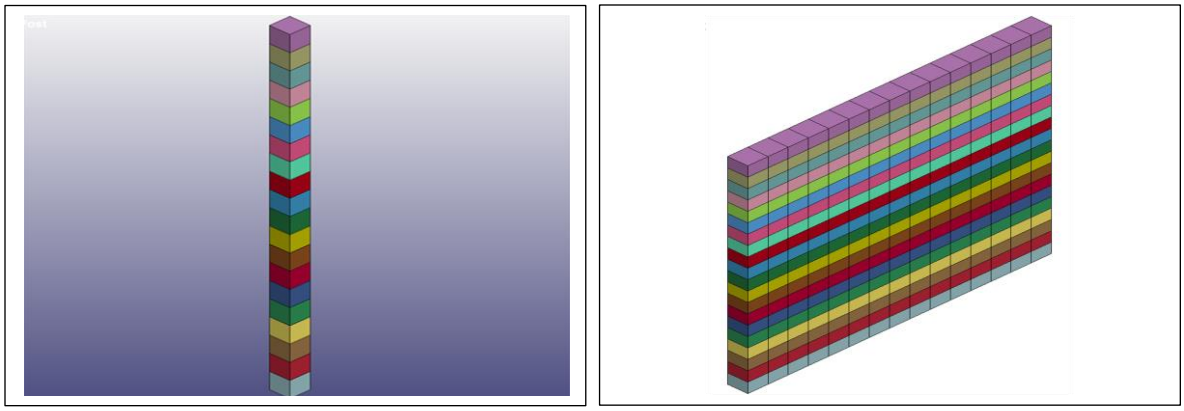

Figure 5-1: 1D Soil column (left) and 2D soil-slice (right) in LS-DYNA

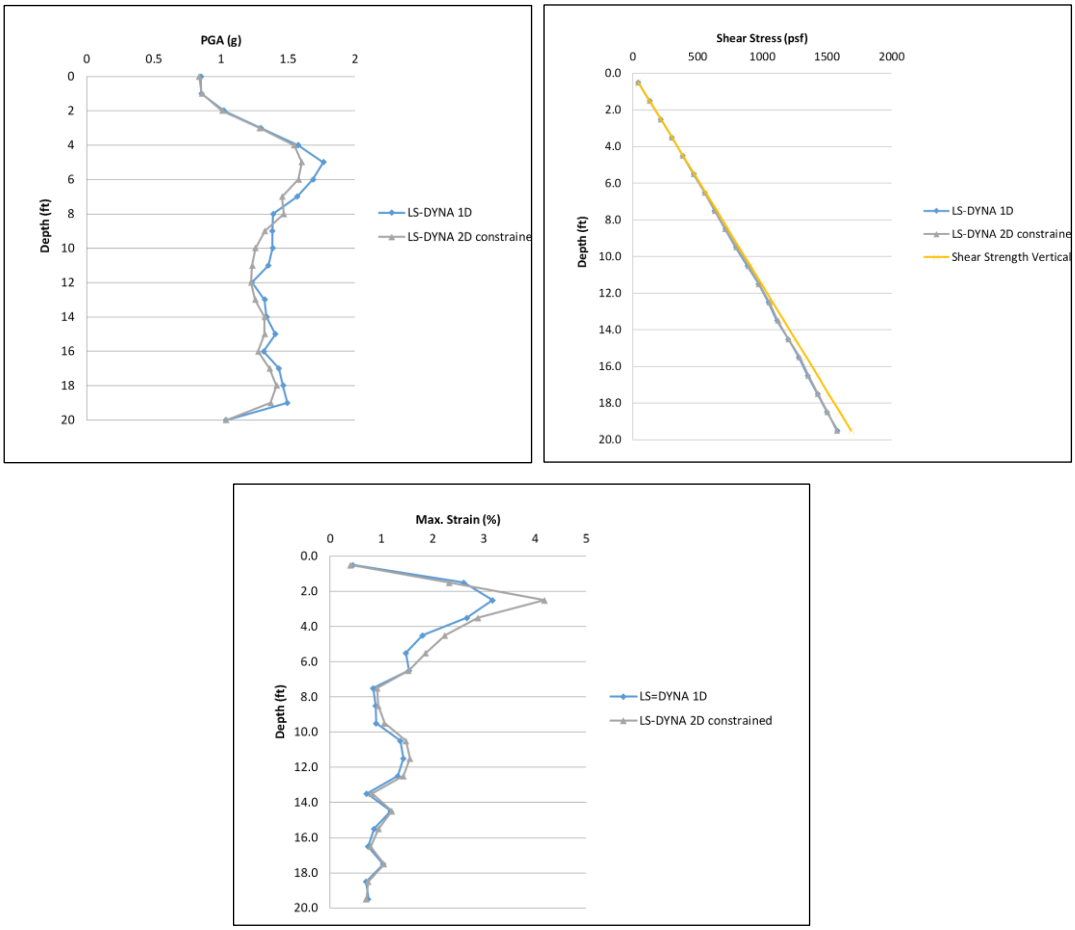

Figure 5-2: Peak ground accelerations, peak shear stresses and peak strains for the 1D Soil column and 2D soil-slice in LS-DYNA

5.2 2D model of the soil-box

5.2.1 Model Description

During the design process of the soil-box different shapes were examined including a square shape, a circular shape and an octagonal shape. For the development of the 2D soil slice presented in the previous section the length of the slice was selected to be equal to the length of the 3D square box or equal to the diameter of the 3D circular box (Figure 5-3). This soil slice was used as a basis for the development of a more advanced model that included the actual walls of the box, as shown in Figure 5-4. The walls consisted of interchangeable layers of a very stiff material –steel/aluminum- and a very soft/flexible material, namely rubber. These interchangeable layers of the walls were simulated via 3D solid elements with two elastic materials, and these elements were assumed to be perfectly connected to the soil elements next to them. This means that all the complementary shear at the edge of the soil columns would be taken by the walls of the box. Since in reality it was expected that the elongation of a certain layer of the walls would be minimal/negligible, this was simulated in the 2D slice model by assigning horizontal constraints at the external nodes of the walls that had the same elevation.

Figure 5-5 shows the nodes and elements that were selected for output. The nodes and elements corresponded to a left, center and right soil column. For all these locations the accelerations, displacements, stresses and strains were examined. Moreover, the forces in the walls, the base shear, the forces/pressures at the bottom nodes below the box and the overturning moment were also calculated in order to provide data for the design of the box.

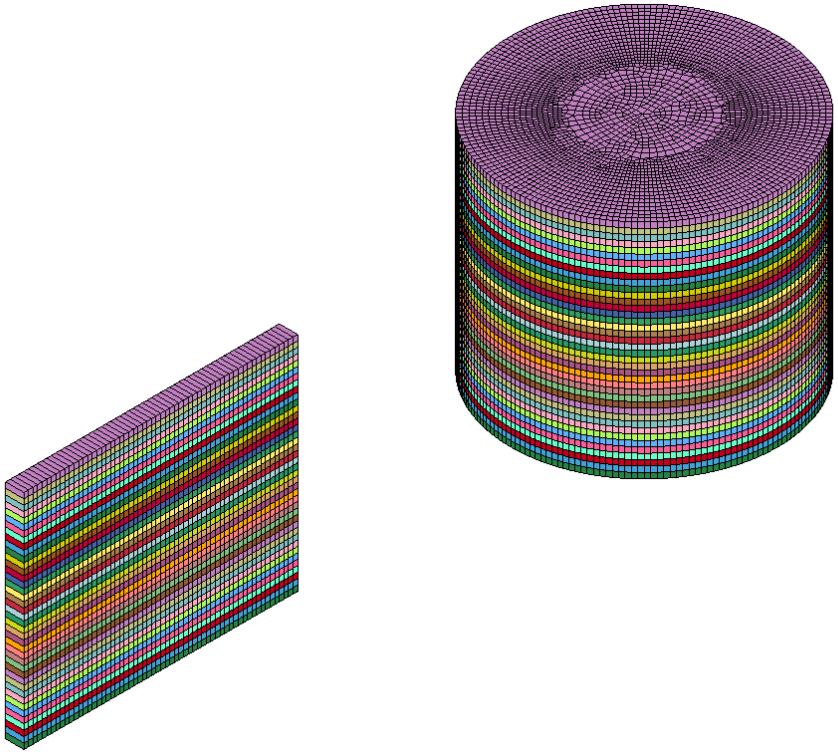

Figure 5-3: 3D view of the full circular soil box (extracted from Istrati et al 2018) and the 2D slice in LS-PrePost

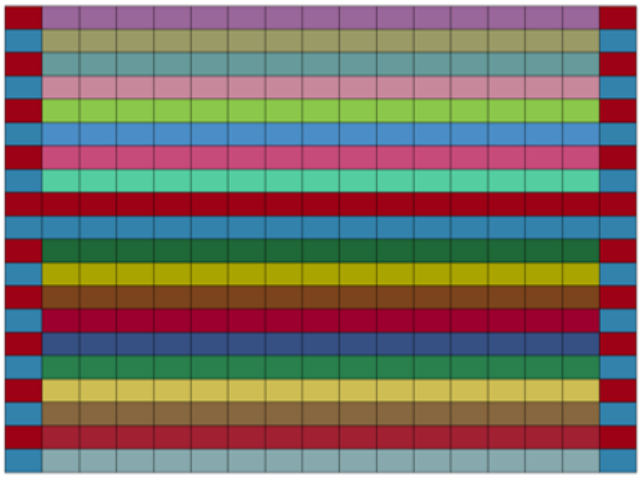

Figure 5-4: Side view of the 2D model of the soil-box in LS-PrePost

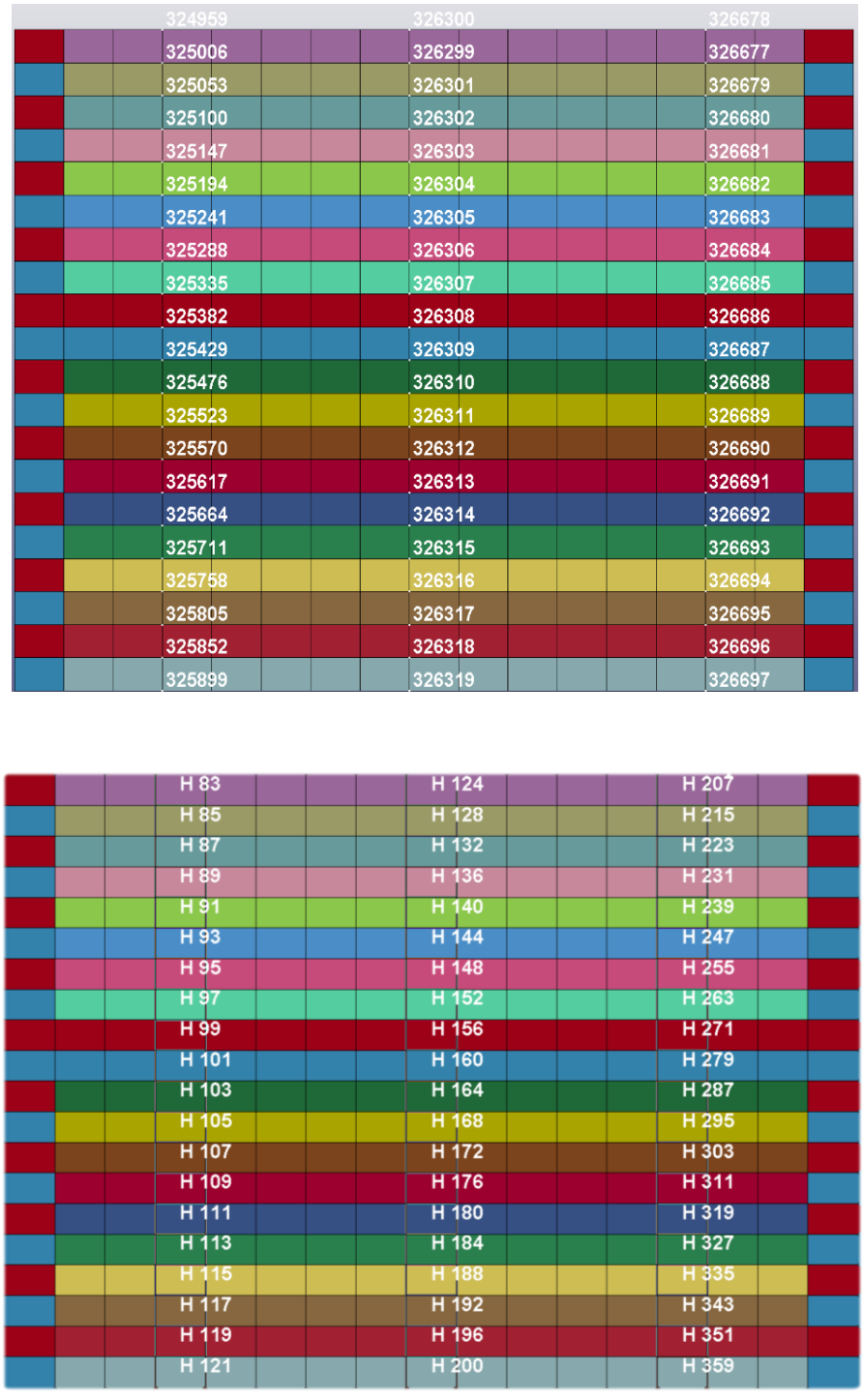

Figure 5-5: Location of nodes and elements selected for output

5.2.2 Numerical Results

This section will present results from the 2D numerical model of the soil with the walls obtained from nonlinear dynamic analyses. Figure 5-6 shows the deformed shape and the shear stresses in the model at t=22.4sec. From the deformed shape it can be observed that there are some vertical displacements close to the walls of the box, indicating that the box does not behave purely in shear. Moreover, for a certain soil layer the stresses are not uniform along the whole length of the layer, with the two-three soil columns closer to the walls witnessing different stresses than the ones close to the center of the box, demonstrating the existence of a boundary effect caused by the walls.

To get a more quantitative insight, Figure 5-7 shows the acceleration histories in the lateral direction recorded at the nodes of the left, center and right soil column, for three different depths. As expected the acceleration histories at the bottom nodes are identical, which is reasonable since all these nodes were assigned the input motion. However, as the shaking propagates from the bottom to the surface of the soil, differences in the acceleration of the left and right column relatively to the center one start appearing. These differences can be further witnessed in the peak ground accelerations shown in Figure 5-8. Clearly, the left and right soil column witness different PGAs than the middle column, and for most soil layers the former PGAs are larger than the latter ones. It is interesting though that the two soil columns (left and right) close to the walls of the box witness very similar PGAs. Despite the consistent trend in the PGAs, there is no consistency in the maximum shear strains with the soil layers of the left and right columns below the mid-depth witnessing

smaller strains than the center column, and the ones above the mid-depth witnessing larger strains.

Figures 5-9 and 5-10 show the histories of the vertical forces recorded at the boundary nodes and particularly at two nodes of the walls and two nodes of the soil respectively. An interesting observation that can be made by examining the two nodes of the walls, the location of which is symmetric to the center of the box, is that the vertical forces histories are out-of-phase, meaning that when one is maximized the other one is minimized, indicating that overturning moment is introduced at the bottom of the soil-box during lateral shaking. This overturning moment can be so significant that the uplift forces that introduces in a certain well can significantly exceed the counter-acting weight resulting in large tensile bearing forces. This means that the bearings of the walls should be designed to take this tension. The existence of the overturning moment is verified via the examination of the vertical forces at the two soil nodes shown in Figure 5-10, which are out-of-phase during shaking but they always stay in compression (positive), and at the end of the shaking the permanent weight on each node is slightly different than the pre-shaking weight (although the total weight of the soil-box remains the same) indicating an offset of the center of mass due to the significant soil nonlinearity.

Figure 5-11 shows the vertical forces in all the boundary nodes at the bottom, at three different instants, (a) after the application of gravity and pre-shaking, (b) close to the maximum shaking, and (c) after the maximum shaking. This figure verifies that although the nodes below the walls are taking a larger weight than the nodes of the soil, during the maximum shaking, where the overturning moment is maximized, significant uplift is

introduced in one side of the box (walls and soil) resulting in reduced compression force in the soil and in tension in the walls. This moment seems to distort the soil areas close to the walls and to alter the shear strains relative to the soil at the center of the box, for the case of the perfect contact between the walls and the soil.

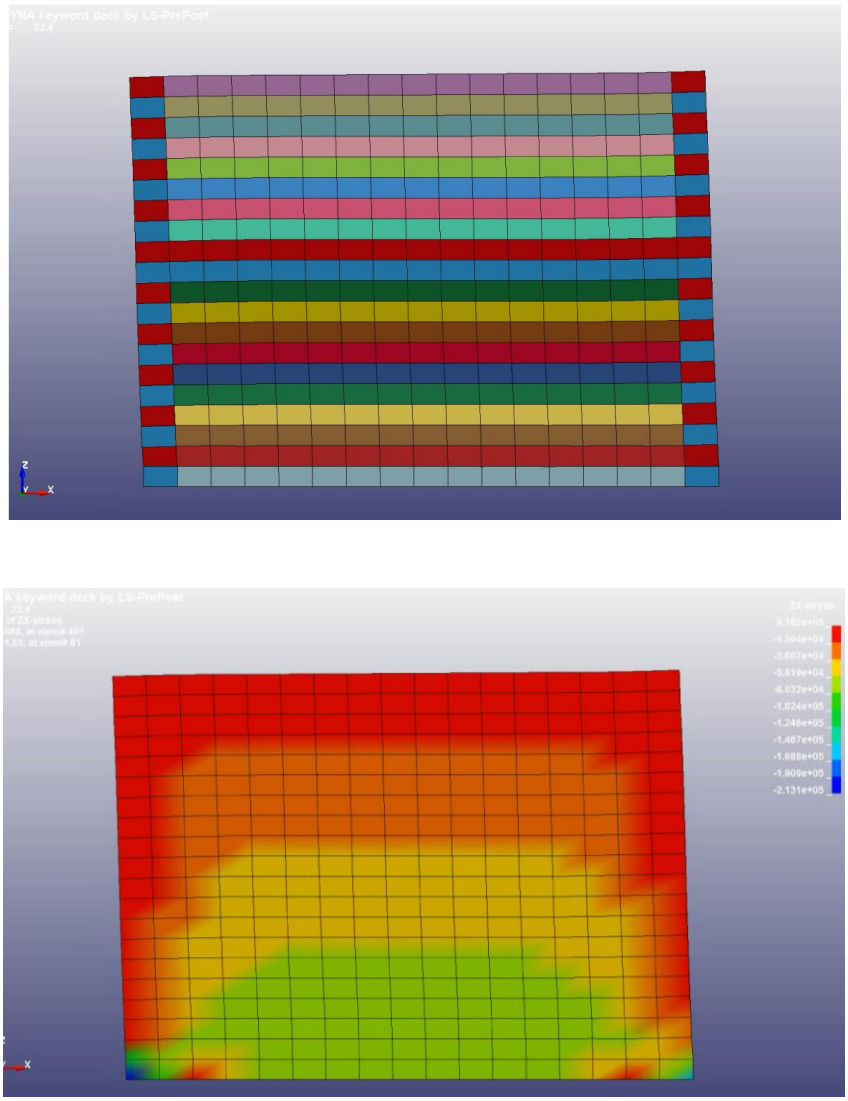

Figure 5-6: Snapshot of the deformations (top) and the shear stresses (bottom) of the 2D soil-box model at t=22.4sec

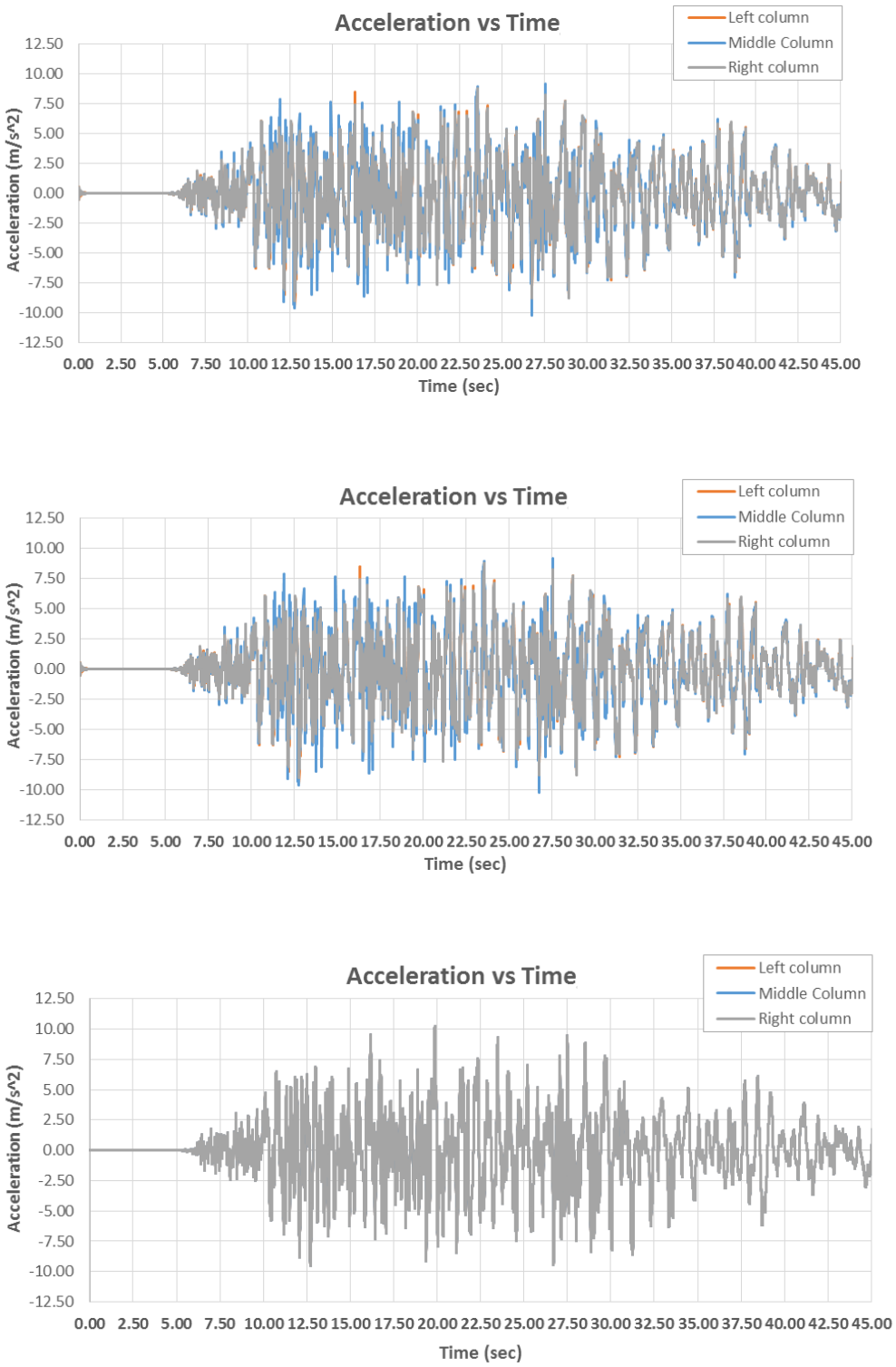

Figure 5-7: Acceleration histories recorded at surface (top), mid-depth (middle) and bottom soil layer (bottom) of the 2D model

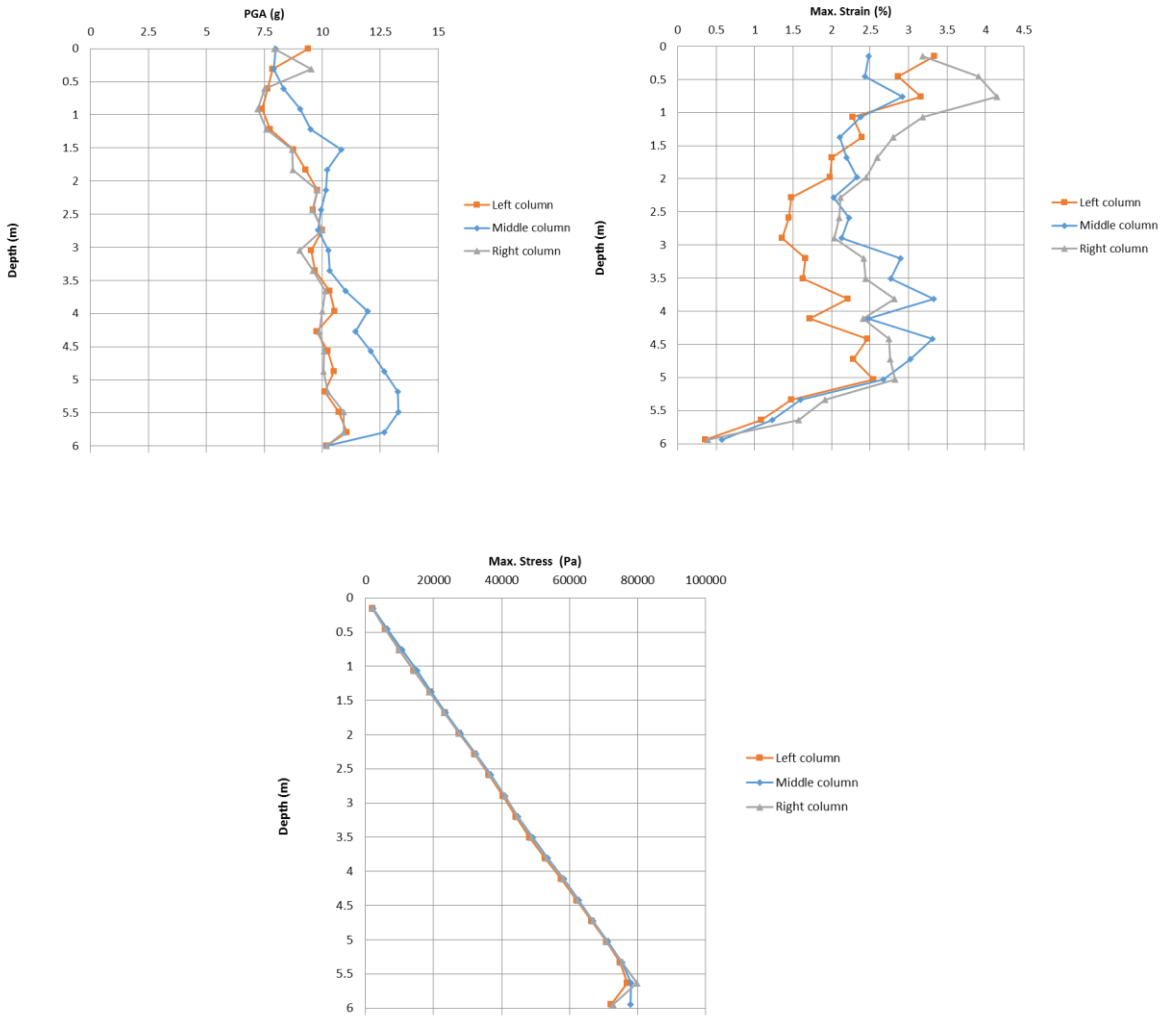

Figure 5-8: Peak ground accelerations (top-left), peak shear strains (top-right) and peak shear stresses (bottom) recorded at the left, middle and right soil column of the 2D model

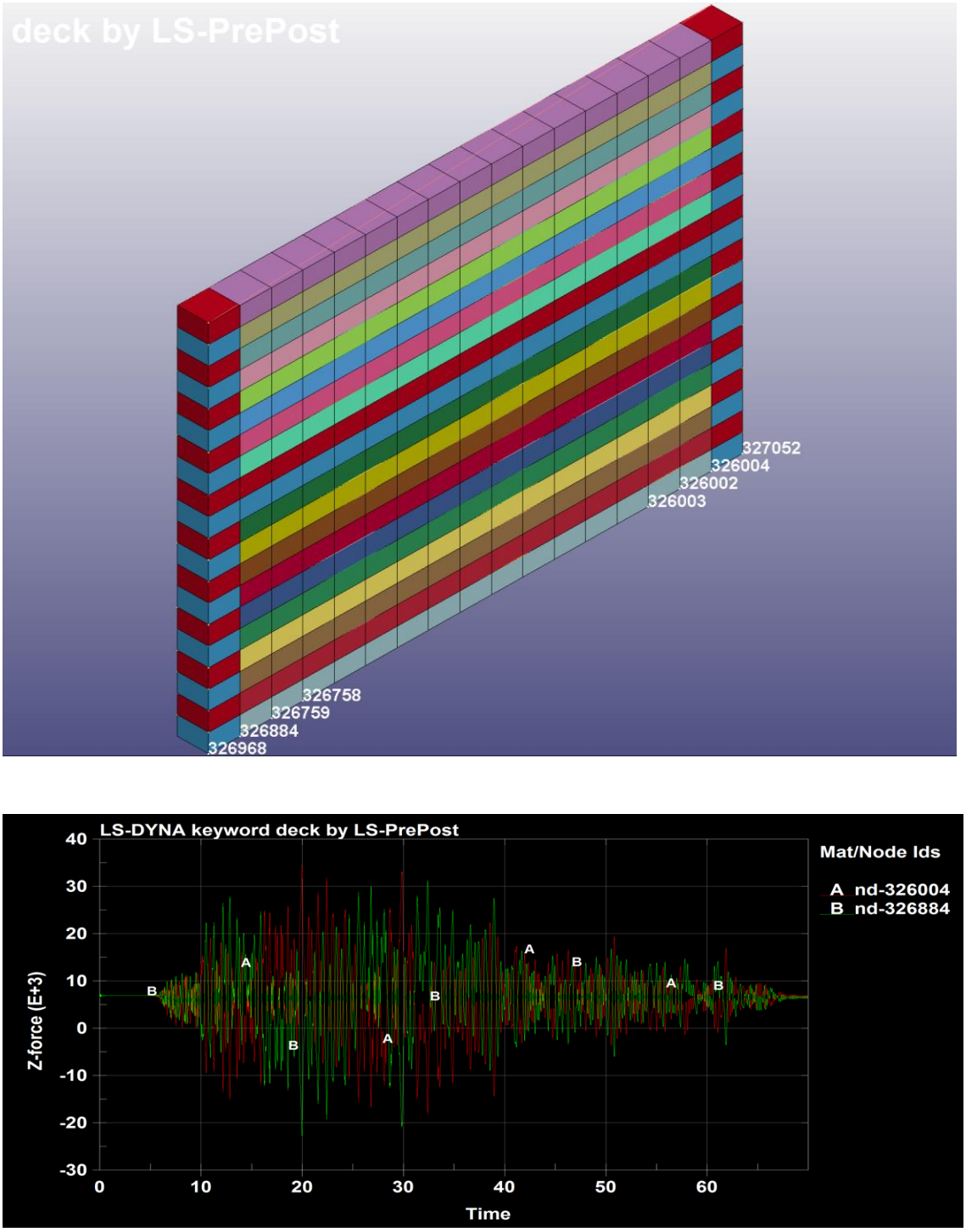

Figure 5-9: 2D model with selected boundary nodes (top) and vertical force histories of two selected nodes of the walls of the box (bottom)

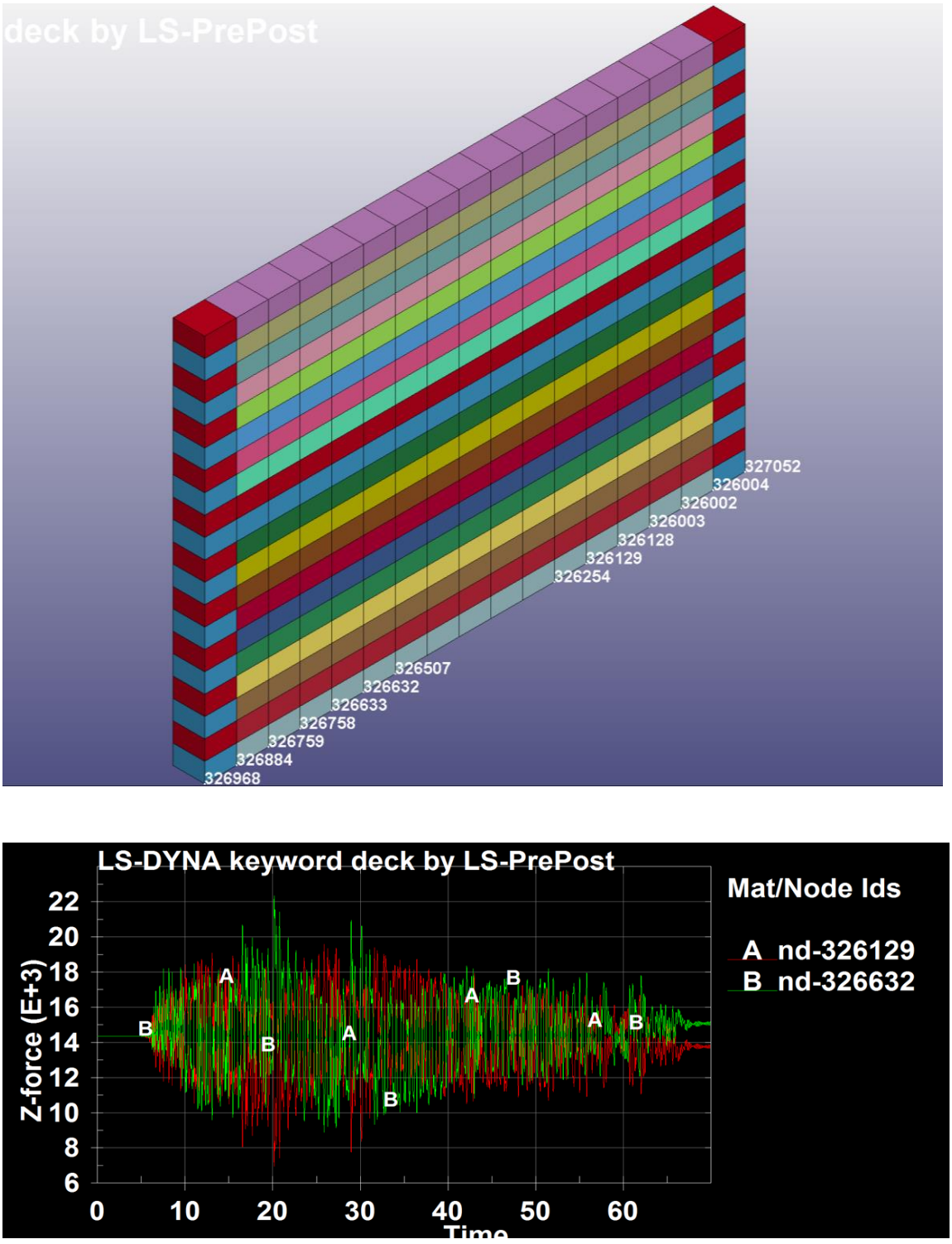

Figure 5-10: 2D model with selected boundary nodes (top) and vertical force histories of two selected nodes below the bottom soil layer (bottom)

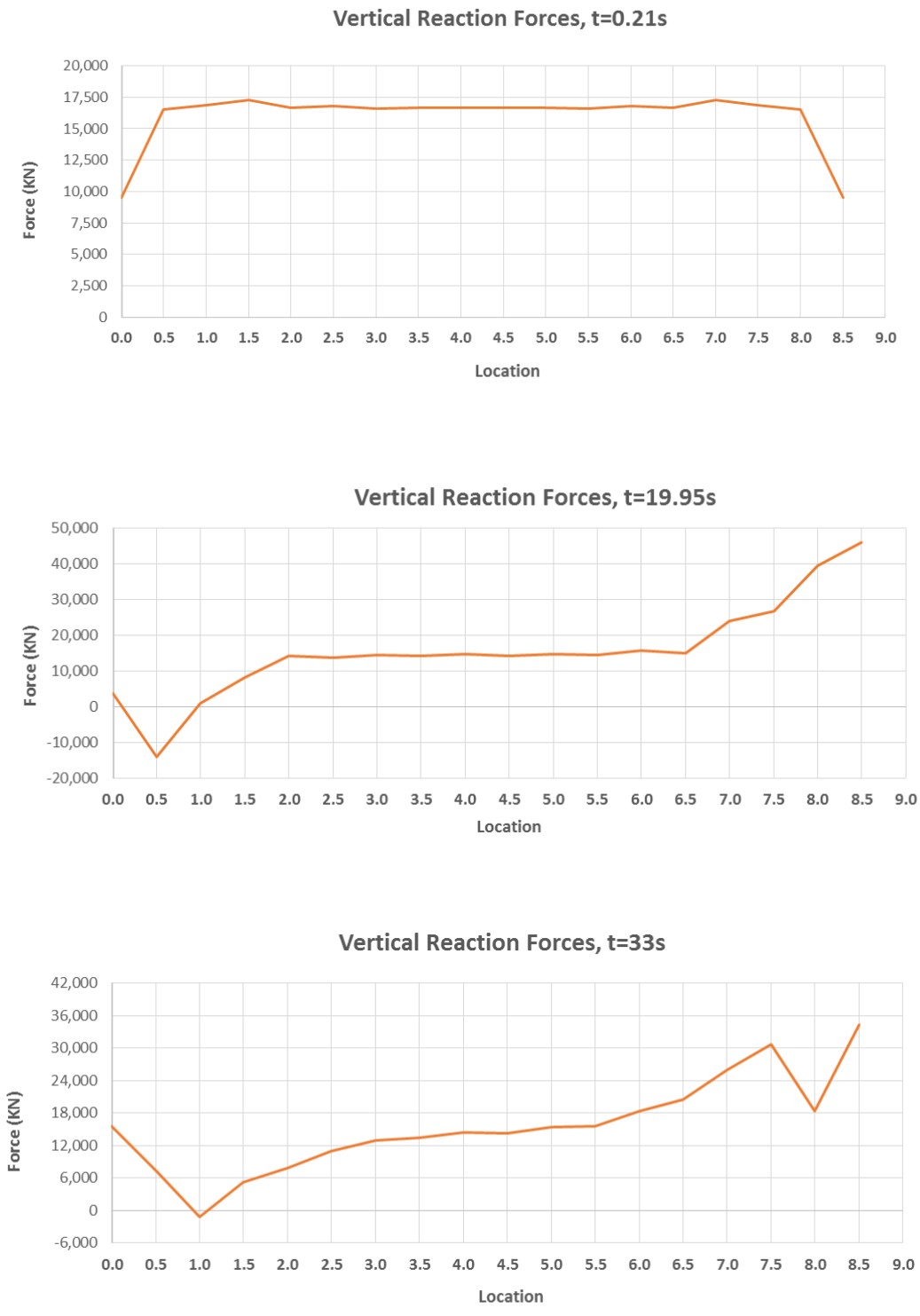

Figure 5-11: Vertical reaction forces at the boundary nodes below the box at different locations along the length of the 2D model, recorded at three different instants

5.3 Mesh Sensitivity

5.3.1 Horizontal Mesh Size

The previous results revealed interesting facts, among which was the existence of significant overturning moment at the bottom of the box, tension in the walls, and non-uniform shear stresses along the length of a soil-layer due to boundary effects generated by the walls of the box. However, in order to increase the confidence in these numerical results, it should be made sure that these solutions are not affected by different numerical parameters, such as the mesh size. To verify these, four models with different horizontal mesh sizes were developed, by starting from a coarse mesh and then reducing the size in half and then in quarter of the initial size, as shown in Figure 5-12.

Figure 5-13 shows the accelerations and absolute displacement histories in the lateral direction at the surface nodes of the left and center soil column. It can be observed that there are minor differences in the absolute displacements at both locations, and in the accelerations at the center column, however there are more noticeable differences in the accelerations at the surface of the left column (close to the walls), with the smaller mesh size generally giving smaller values. The displacement profile shown at two different time instants in Figure 5-14, reveals that the horizontal mesh size does affect the displacement of the soil-box and actually leads to different response of the box. Interestingly, the vertical displacements seem to be very sensitive to the mesh size, however as the mesh size becomes smaller and smaller these displacements are consistently being reduced. All these four models are showing some uplift (positive z-displacement in the range of 2cm) of the soil close to the walls of the box followed by settling, during the lateral shaking, however

at the center of the box the soil is always settling. The most important perhaps conclusions for the design of the soil-box can be reached based on Figures 5-15 and 5-16. These figures demonstrate that the base shear is totally insensitive to the horizontal mesh size, while the vertical forces in the walls are the most sensitive, and particularly as the mesh becomes smaller these forces reduce significantly. Therefore, it is critical to use an adequately small horizontal mesh size in order to capture the distribution of the overturning moment and complementary shear in the walls of the box.

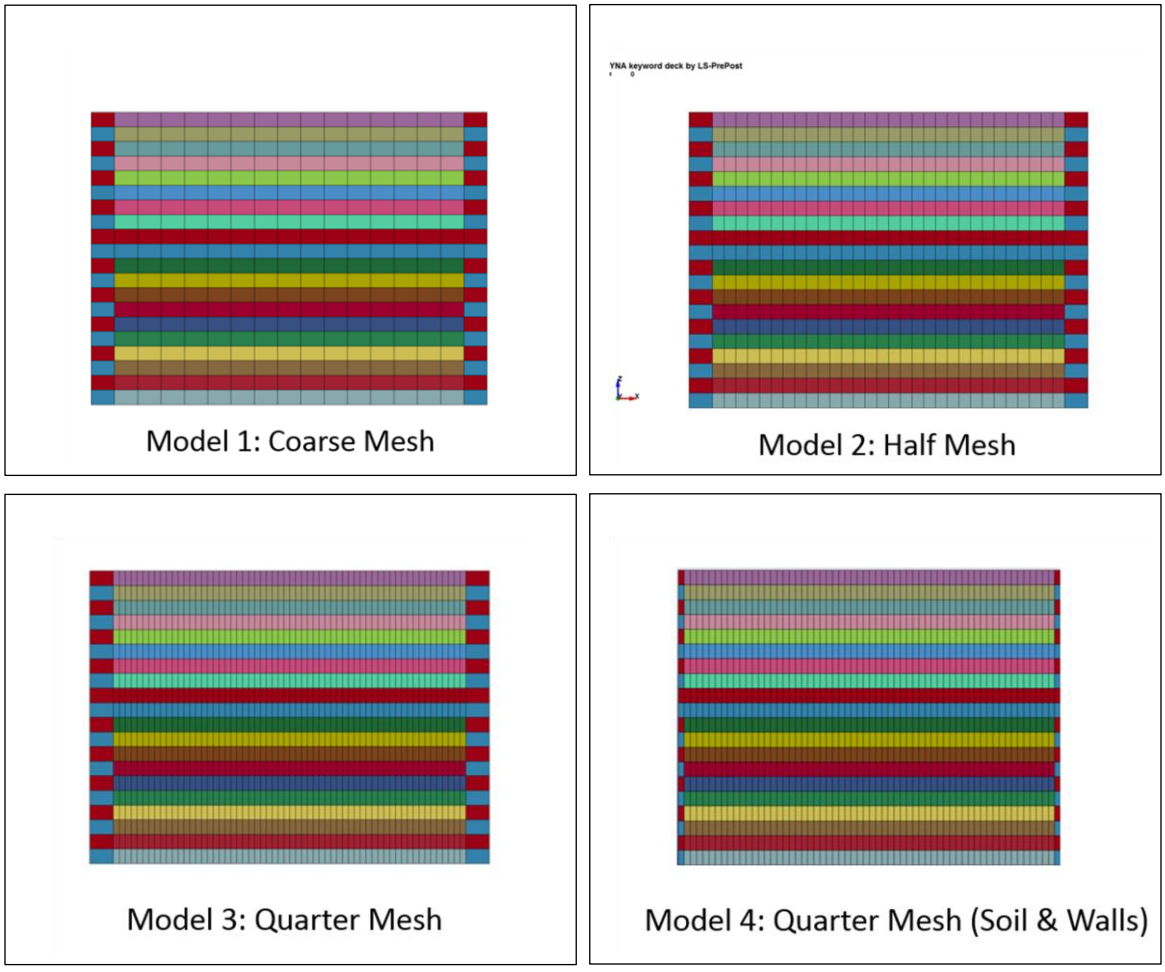

Figure 5-12: 2D models of the soil-box with four different mesh configurations

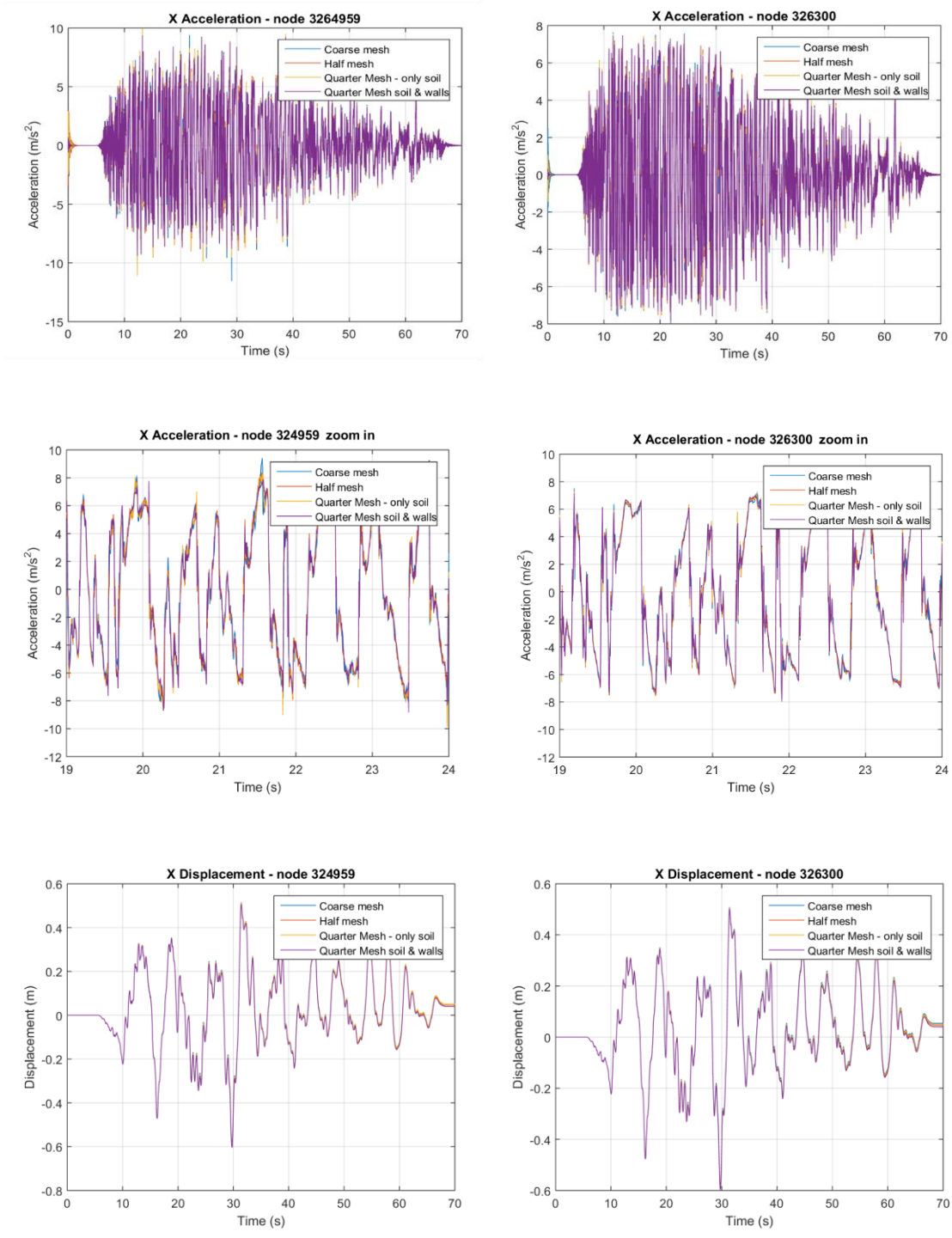

Figure 5-13: Lateral accelerations (top and middle) and lateral absolute displacements (bottom) at the surface of the left (left) and of the center (right) soil column, for four mesh configurations

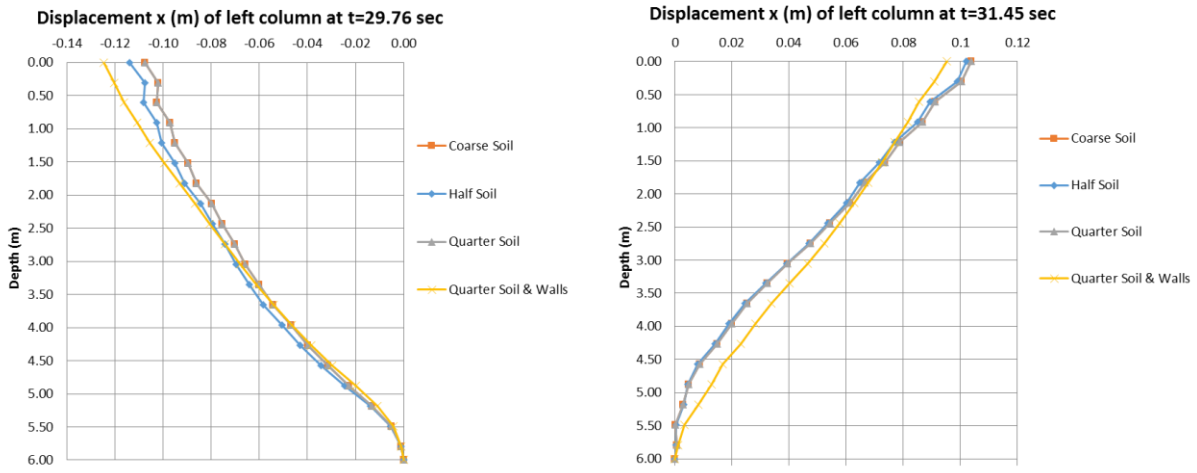

Figure 5-14: Displacement profile at two different instants during the shaking, for four mesh configurations

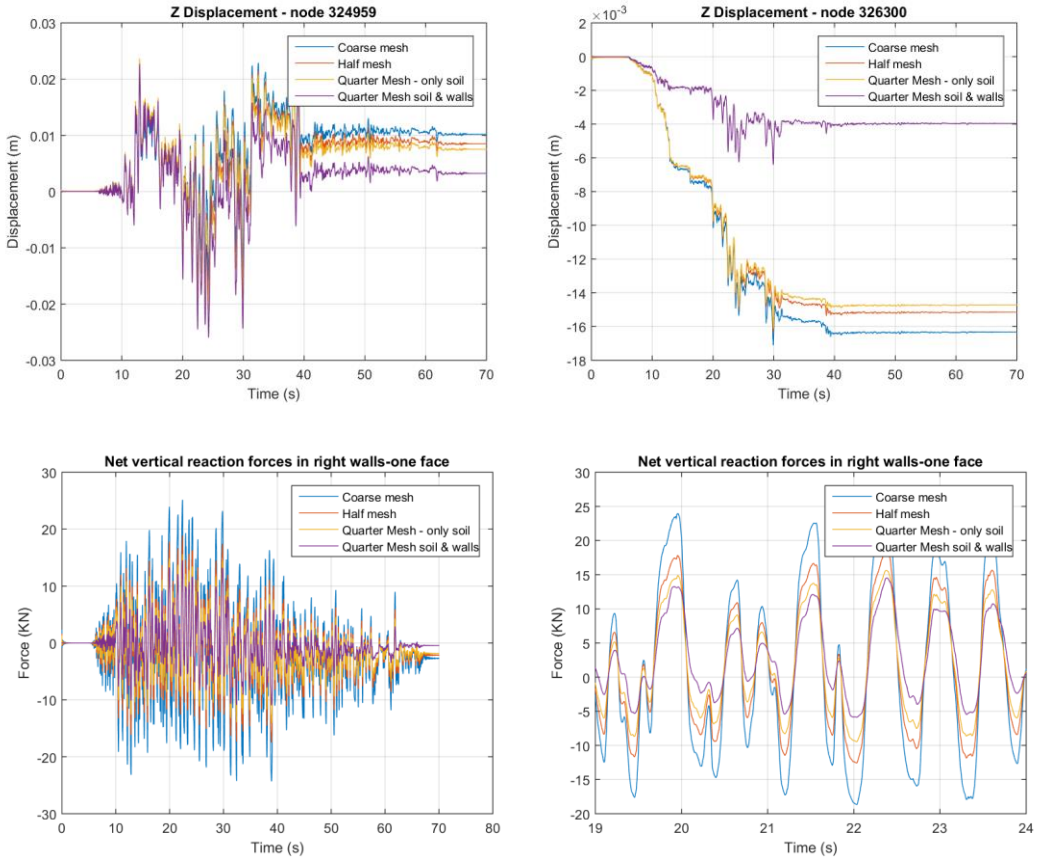

Figure 5-15: Absolute z-displacement histories at the surface of the left (top-left) and the center (top-right) soil column, and net vertical reaction forces (bottom), for four mesh configurations

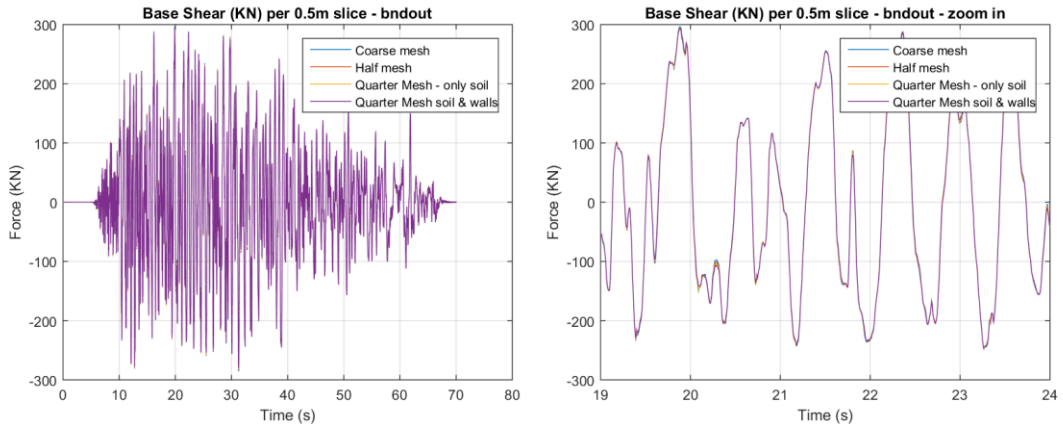

Figure 5-16: Base shear histories for four mesh configurations

5.3.2 Vertical Mesh Size

The previous section showed that some response parameters of the soil-box were sensitive to the horizontal mesh size, which led to the decision to use the model with the smallest horizontal mesh size in subsequent analyses (model 4). Based on model 4, two additional models were created where the vertical mesh was divided in half and in a quarter of the one in model 4. That meant now that model 4 had 10 rubber layers, model 5 had 20 rubber layers and model 6 had 40 rubber layers, resulting in a more accurate representation of the properties of the walls. It must be noted that the stiffness of the rubber layers in the three models was adjusted accordingly so that all models have the same global lateral wall stiffness.

Similar to the case with the horizontal mesh size, the vertical mesh size also seems to have a small effect on the horizontal displacement histories at the surface and the acceleration at the surface of the center column, and a larger effect on the soil accelerations

close to the walls, as shown in Figure 5-18. The next figure (Figure 5-19) shows that the vertical mesh size does have an effect on the base shear, contrary to the horizontal mesh size. This effect is even more significant on the vertical wall forces and vertical displacements, shown in Figure 5-19. This comparison demonstrates that a sufficiently refined mesh size is required in both the horizontal and vertical direction in order to properly capture the interaction of the walls with the soil and the physical effects generated during the ground shaking. Therefore, model 6 will be used for further parametric analyses.

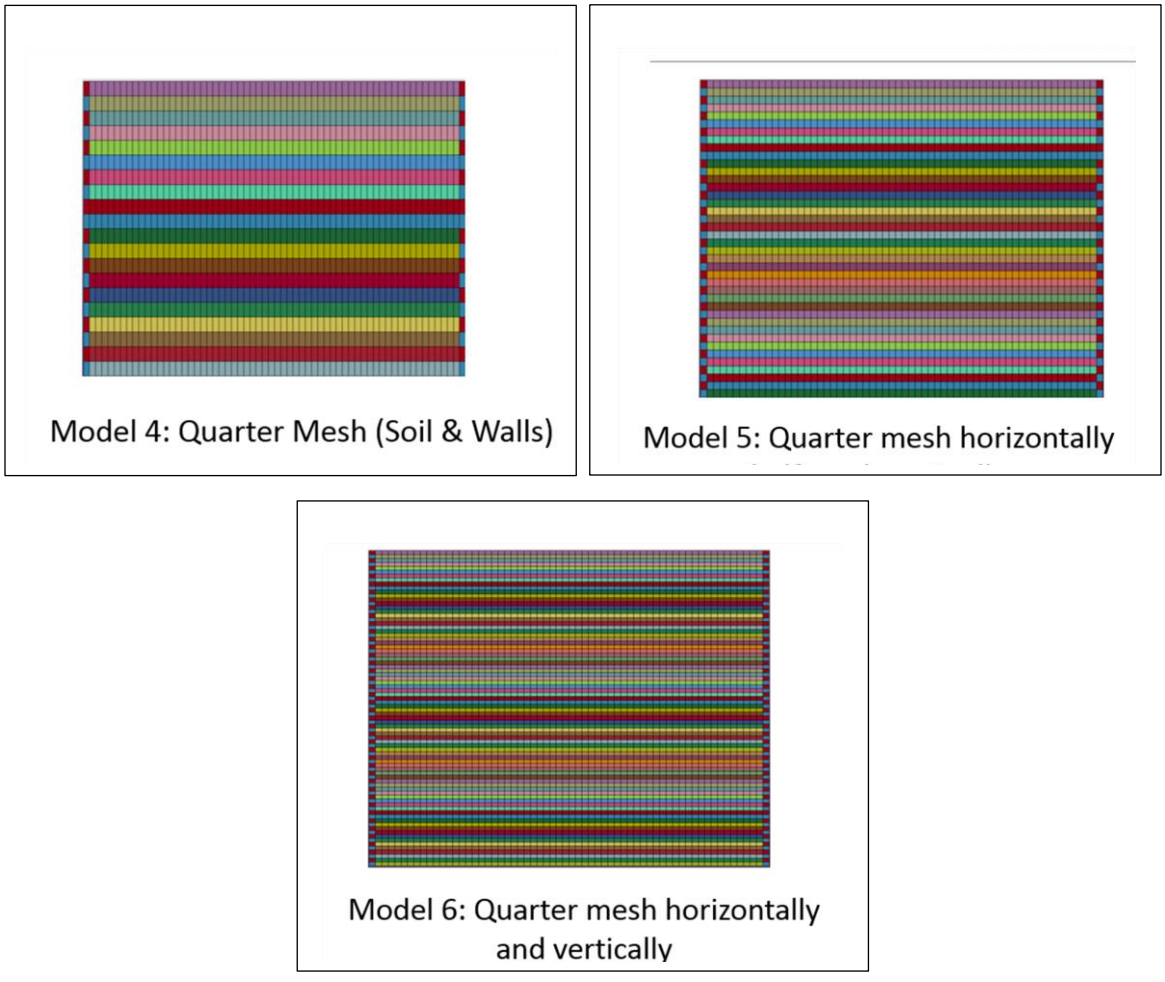

Figure 5-17: 2D models of the soil-box with three different vertical mesh sizes

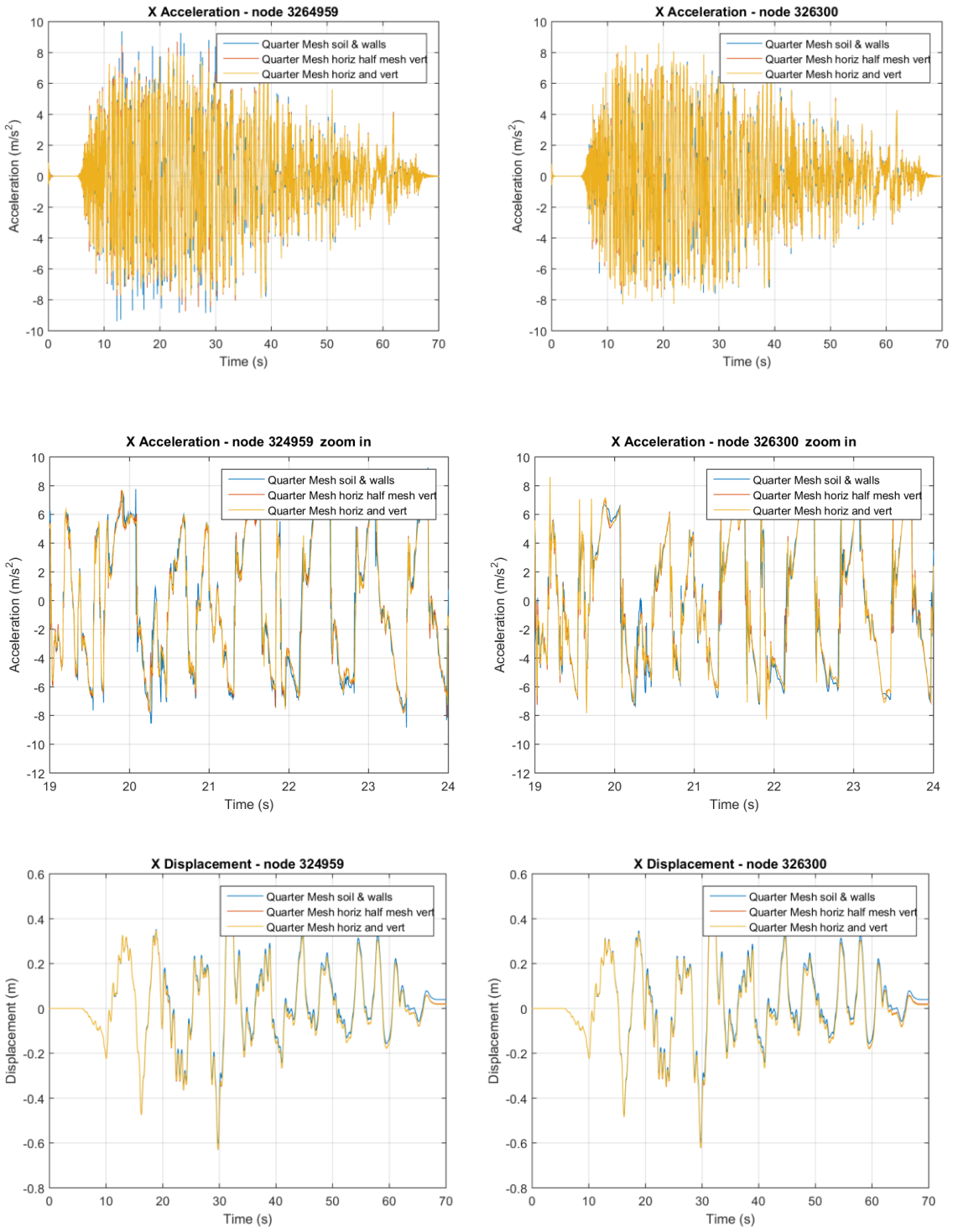

Figure 5-18: Lateral accelerations (top and middle) and lateral absolute displacements (bottom) at the surface of the left (left) and of the center (right) soil column, for three vertical mesh sizes

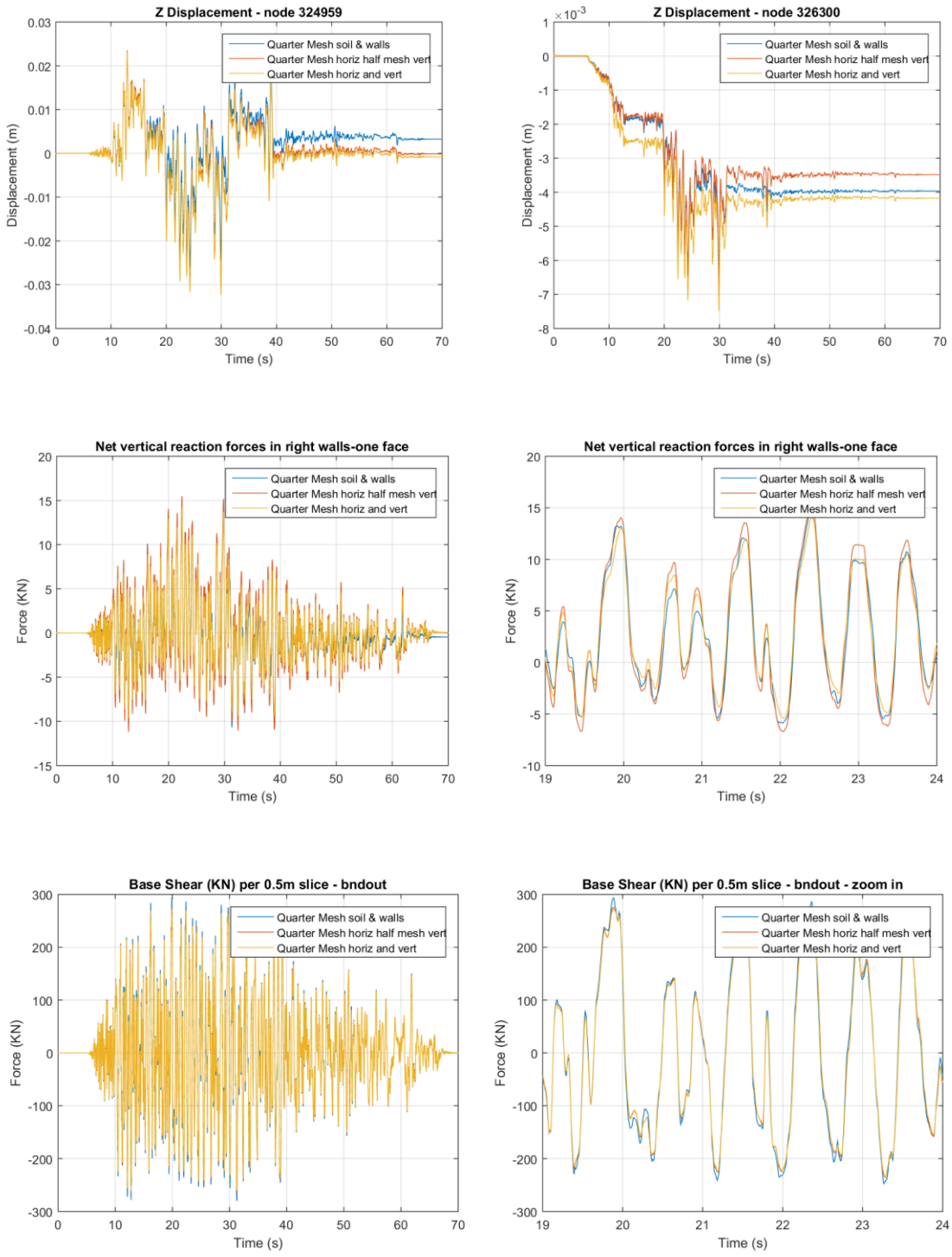

Figure 5-19: Absolute z-displacement histories at the surface of the left (top-left) and the center (top-right) soil column, net vertical reaction force histories (middle), and base shear histories (bottom), for three different vertical mesh sizes

5.4 Effect of Wall Vertical Stiffness

5.4.1 Description of wall configurations

The preliminary nonlinear analyses that were conducted using models 1 to 6 revealed the existence of a boundary effect that resulted in the creation of disturbed regions of soil close to the walls with shear stresses/strains different than the ones close the center of the box. In all these models the walls of the box consisted of steel and soft rubber, with the latter resulting in a very small shear stiffness of the box, which was one of the desired features of the box. However, this small shear stiffness of the rubber which was achieved via the use of a small shear modulus resulted also in small axial and bending stiffness of the rubber layers, which coupled with the significant overturning moment and complementary shear resulted in noticeable vertical displacements during the horizontal ground shaking. These vertical displacements affected the attached soil and nearby range resulting in a complex stress state of the soil, different from the targeted pure shear. To deal with this issue different design alternatives were considered by the UNR research team, three of which are shown in Figure 5-20. The first type of the wall included continuous layers of soft rubber with small shear stiffness and rigid balls inside the rubber that would increase the axial-compressive stiffness of the walls. The second type of the wall was similar to the first type but it had a plug instead of a ball. Both of these types had a large compressive stiffness due to the existence of the rigid ball or the very stiff plug, but they had a small tensile stiffness that was coming directly from the soft rubber. The third type of the wall included discrete elastomeric bearings with a small shear stiffness and a large axial stiffness in both compression and tension.

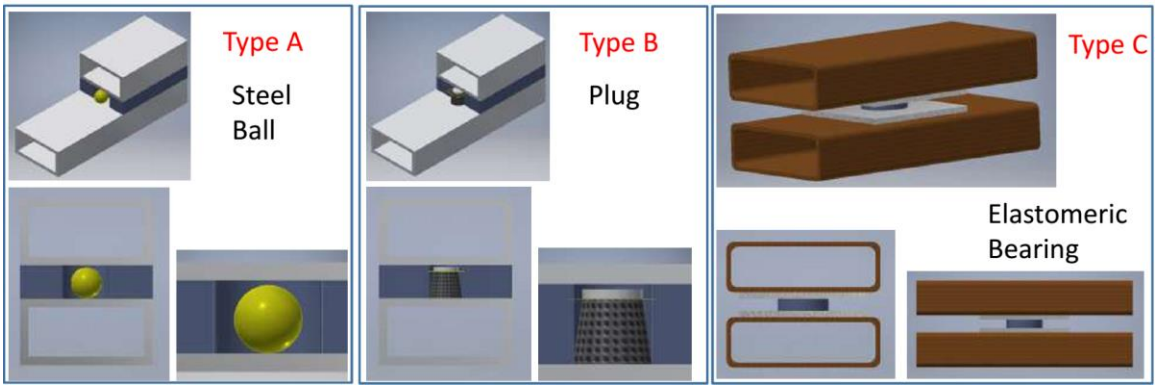

Figure 5-20: Three different design alternatives for the walls of the box (credit: Dr. Elfass)

5.4.2 No Vertical Constraints vs Vertical Constraints

To simulate the different wall properties numerically, model 6 was used and modified accordingly. The first modification was the addition of vertical constraints to all the nodes of the left and right wall respectively (model 6B). This meant that the walls were now allowed to deflect horizontally based on the lateral stiffness of the laminar walls, however they were not allowed to undergo vertical displacements, leading consequently to the elimination of flexural effects.

Figure 5-21 shows a snapshot of the contours of shear stresses for the 2D soil-box model with and without vertical constraints, obtained from LS-PrePost. It is very interesting that although the boundary effect and the non-uniform shear stresses in the case of the model without the constraints seem to extend to a distance from the wall equal approximately to 15% of the total length of the slice, the respective distance is minimized when vertical constraints are used. Uniform shear stress seems to appear along the length of a soil layer, and only part of the first soil column that is in direct contact with the walls (perfect contact) is affected by the walls, demonstrating that the soil is now in pure shear.

This demonstrates that the significant boundary effect observed in the previous section was due to the flexural behavior of the walls (small axial and bending stiffness of the rubber) and the existence of a perfect contact between the soil and the walls, which transferred all the flexural effects to the soil (numerical effect).

Figure 5-22 shows the acceleration and the absolute displacement histories at the surface of the soil, both close to the wall and the center of the box. At both locations the addition of vertical constraints, which seem to put the soil-box in pure shear, increase also the acceleration histories and it makes them be the very similar at the two locations (close to the walls and the center). Obvious differences exist also in the absolute lateral displacements, with the model with the vertical constraints witnessing significantly larger residual lateral displacements. The pure shear behavior of the model with vertical constraints can also be verified via examination of Figure 5-23, which shows that in this case the soil close to the walls does not uplift anymore and does not fluctuate between uplift and settlement, but there is only some small settlement (in the range of 2mm) similar to the one observed at the center of the box. The same figure shows that the base shear increases with the addition of vertical constraints, which is consistent with the increase noticed in the horizontal accelerations.

One of the most interesting conclusions that can be reached from Figure 5-23 is that although the base shear increases slightly with the addition of vertical constraints, the axial forces in the walls increase by an outstanding factor of 3. This result becomes even more interesting since Figure 5-24 shows that the overturning moment in the model with the vertical constraints is smaller. This can be possible explained by the fact that in the case

where there were no vertical constraints the larger overturning moment was taken partially by the walls of the box and a soil region close to the walls that is highly disturbed and in a complex stress state. On the other hand, when vertical constraints are present in the walls, the axial and flexural stiffness of the walls is very high (almost rigid), most of the soil is in pure shear, and the overturning moment is translated into axial forces in the walls. This is in agreement with the fundamental knowledge (e.g. statics, strength of materials) that in the case of a structure subjected to an external loading, the stiffer the structural element the larger the force it attracts.

The previous observations can be also verified in Figure 5-25 that shows the vertical forces recorded in the boundary nodes at the bottom of the box, for the model with the vertical constraints. After the application of the gravity load all the nodes seem to be in compression and carrying a similar load which is equal to the weight of the soil column above. However, during the horizontal shaking significant uplift and downward forces are introduced in the walls of the box, which can exceed the corresponding weight of the walls (and shared weight from the nearby soil column due to the perfect contact) by several times. Despite these large axial forces in the walls, the vertical forces in the nodes below the soil seem to remain unaffected and equal to the weight if the soil above, demonstrating again the soil is in pure shear. Last but not least, Figure 5-22 had shown that additional vertical constraints increase the absolute lateral displacements at the surface of the box, and Figure 5-26 reveals that this increase is generated by significant shear deformations in the upper third of the soil-box, probably due to the reduction of the confinement in these area.

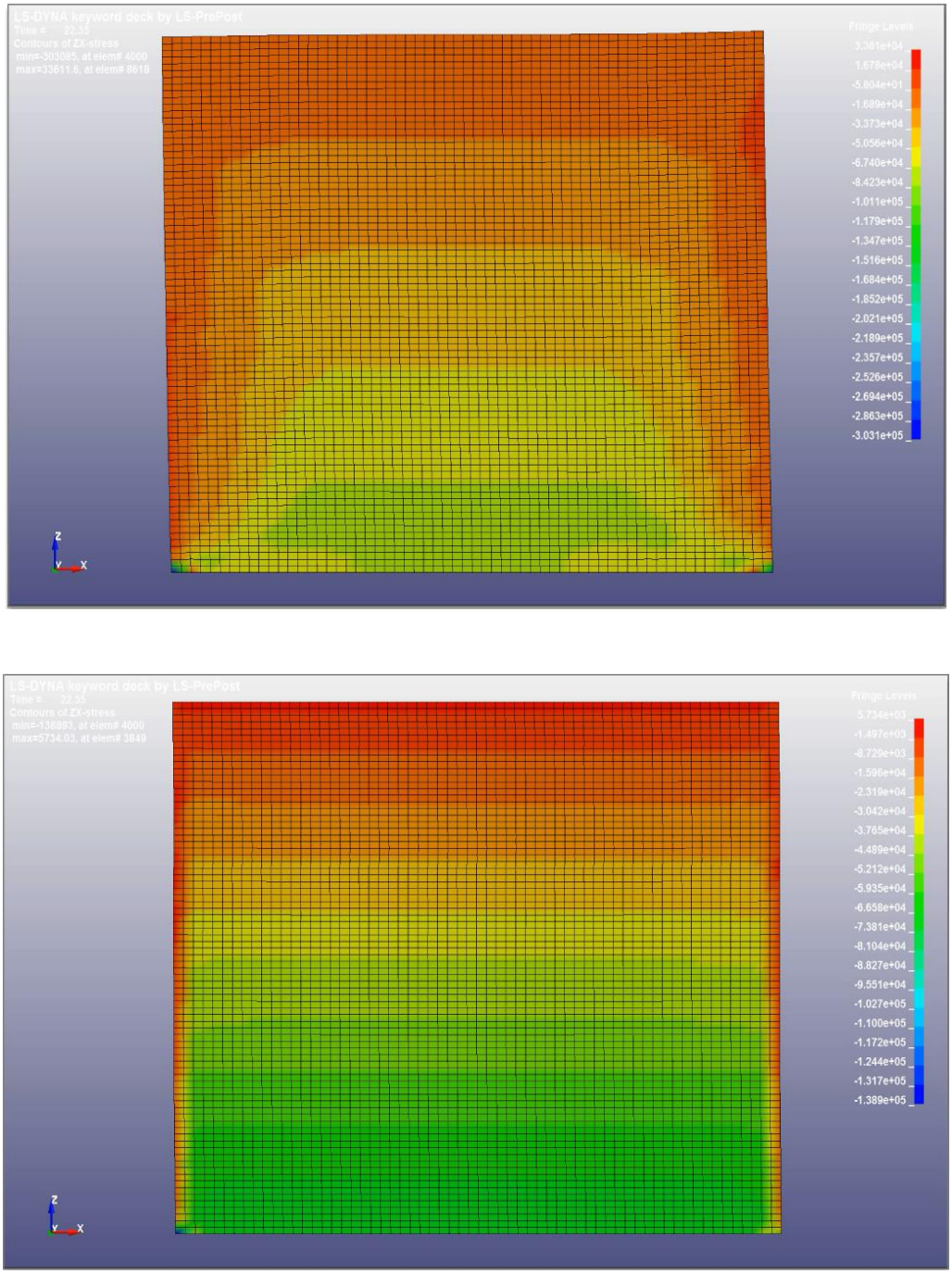

Figure 5-21: Contours of shear stresses at t=22.35sec for the 2D model without vertical constraints (top) and with vertical constraints (bottom)

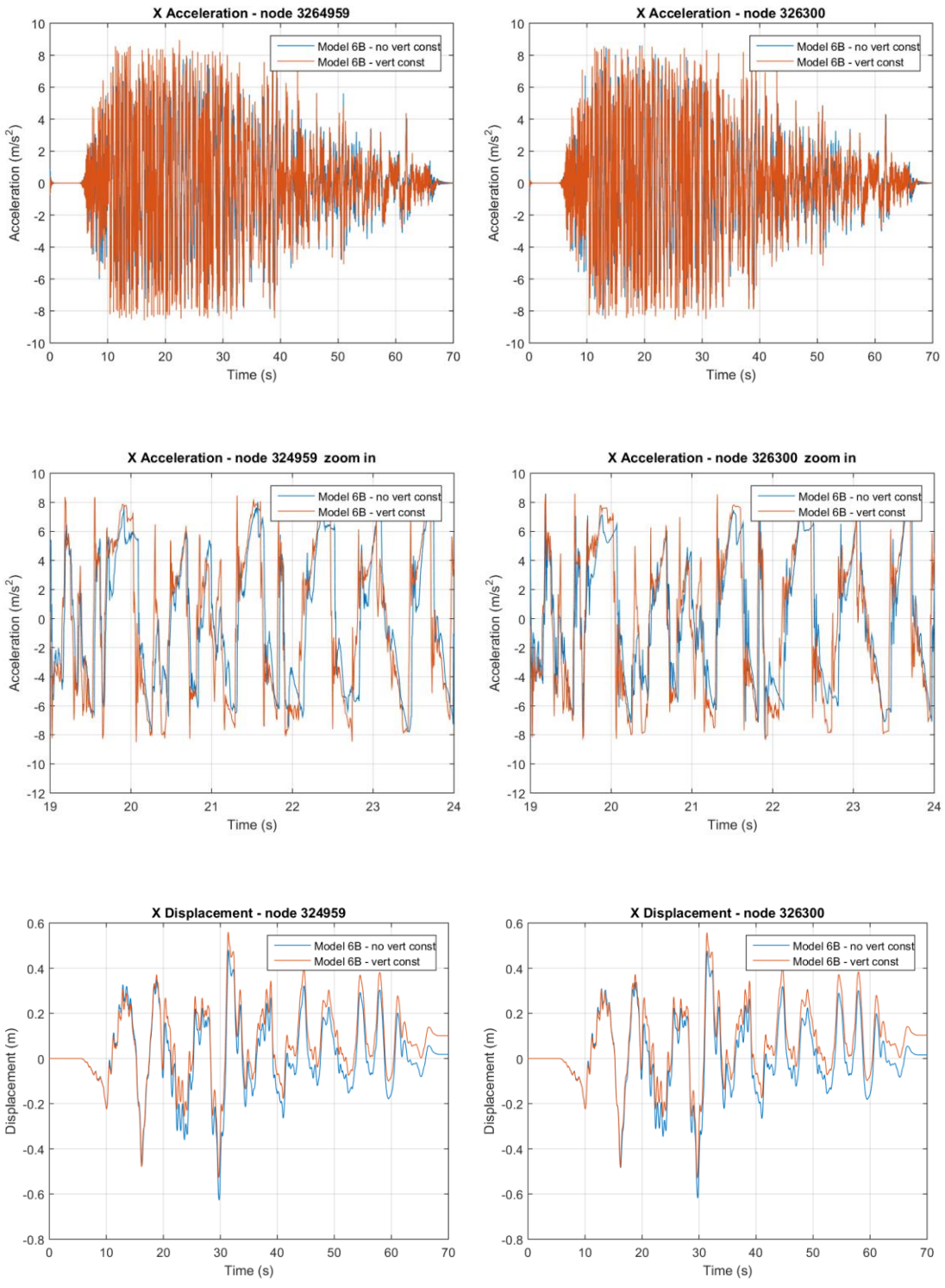

Figure 5-22: Lateral accelerations (top and middle) and lateral absolute displacements (bottom) at the surface of the left (left) and of the center (right) soil column, for the 2D models with and without vertical constraints in the walls

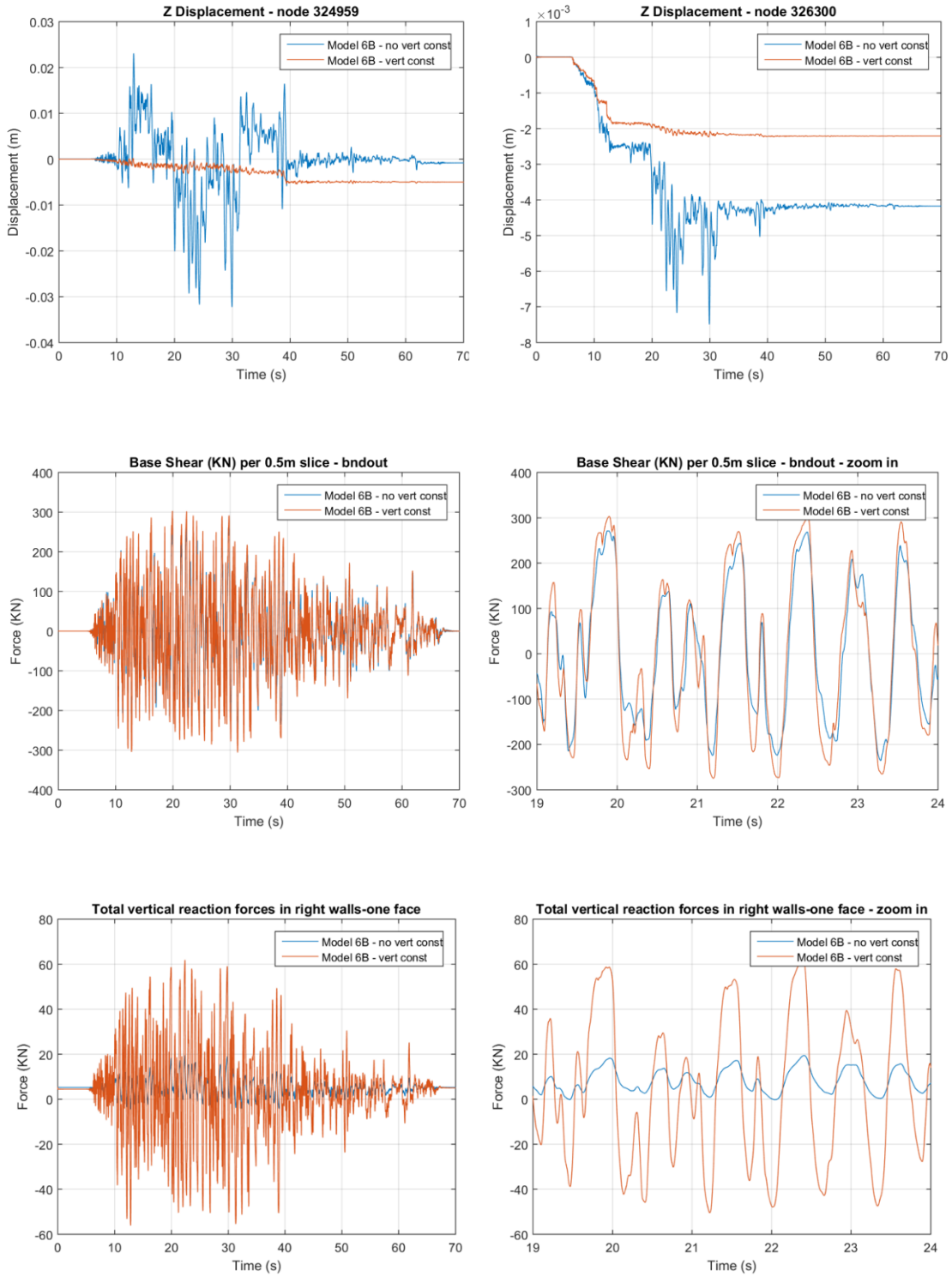

Figure 5-23: Absolute z-displacement histories at the surface of the left (top-left) and the center (top-right) soil column, base shear histories (middle), and net vertical reaction force histories (bottom), for the 2D models with and without vertical constraints in the walls

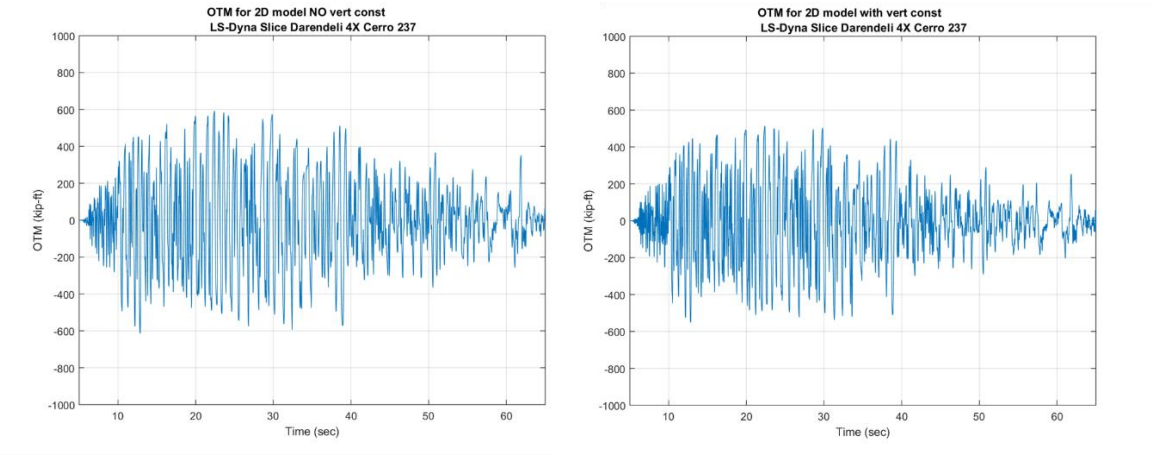

Figure 5-24: Overturning moments at the bottom of the soil-box, for the 2D model without vertical constraints (left) and with vertical constraints (right)

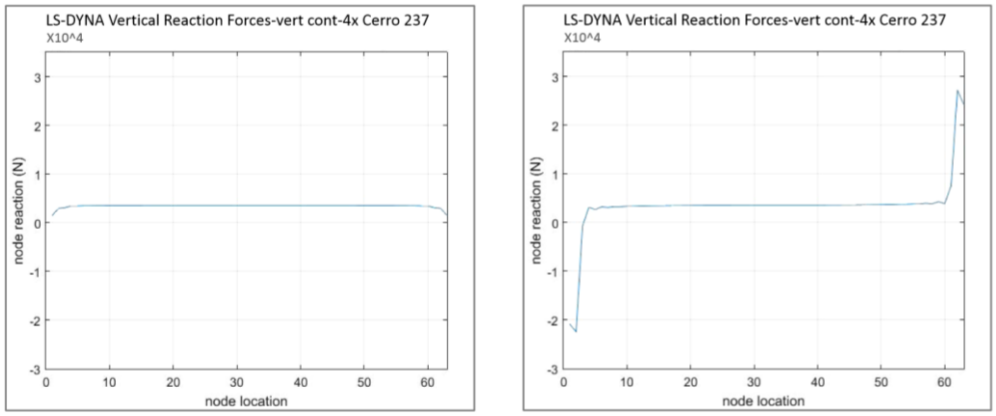

Figure 5-25: Vertical reaction forces at the boundary nodes at the bottom of the box, at two instants, during the gravity application stage (left) and during the shaking (right)

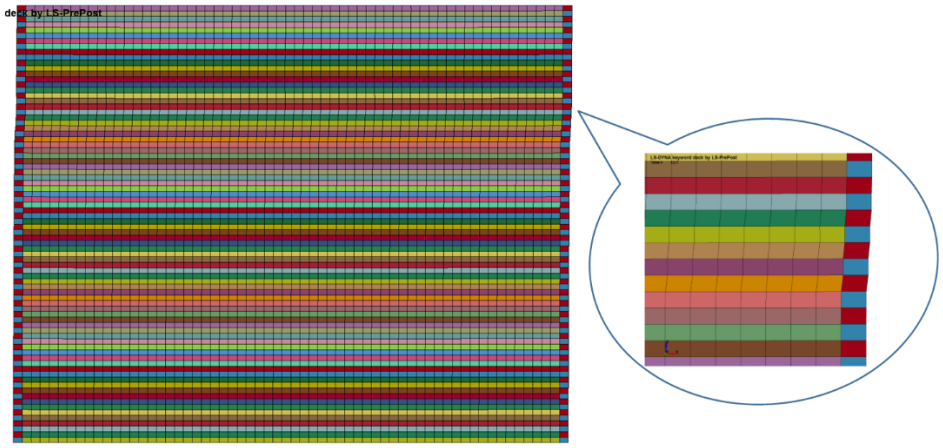

Figure 5-26: Deformed shape of the soil-box during shaking

5.4.3 Vertical Constraints: Comparison of three configurations

The previous section gave an insight into the response of the 2D soil-box when vertical constraints are applied to the wall. However, this model might have exaggerated the effect of the vertical constraints because they were applied at all the nodes of the wall. In reality the two first wall configurations had a rigid ball or a stiff plug respectively only at the middle of the wall section, meaning that a certain rubber layer would still be allowed to bend/rotate depending on the bending stiffness of the rubber. To create a more realistic representation more refined models were developed based on model 6, and particularly models 7, 8 were used for further analyses. In model 8, the wall mesh is broken in half resulting in the creation of a new node at the mid-width of each layer of the wall, as shown in Figure 5-27. Based on this model three variations were created, with each of them having vertical constraints at different locations. In particular, the vertical constraints were

assigned to all the nodes of each wall (model 8B), just the new nodes at the mid-width of each wall and all the layers together (model 8C), and only to the nodes at the mid-width of each wall and one set of constraints for each rubber layer. It was expected beforehand that model 8B will not allow any vertical displacement of the wall, model 8C will allow the vertical displacement of the edges of the walls (exterior and interior nodes) but not of the middle nodes, and model 8D would be similar to model 8C but in addition it will allow also the middle nodes to displace vertically depending on the stiffness of the steel.

Figure 5-29 shows that all three configurations yield similar horizontal accelerations at the surface, however this is not true for the horizontal displacements and mainly the residual displacements at the end of the shaking. The largest differences occur in the vertical displacements at the surface of the soil column close to the walls, with model 8D demonstrating significant uplift and model 8C a smaller uplift. This is reasonable because although the two models have vertical constraints that make the walls axially extremely stiff, the fact that these constraints are located at the mid-width of the walls means that these constraints do not affect the bending stiffness of the rubber layer, which continues to be small since it is provided only by the soft rubber. The small bending stiffness of the rubber layers consequently lead to a small flexural stiffness of the whole wall, resulting in significant flexural effects during shaking, which move up and down the nodes at the edges of the walls (interior and exterior) and this movement is transferred to the nearby soil via the perfect contact at the soil-wall interface. Figure 5-30 shows that the three models have similar base shears, but significantly different vertical forces in the walls of the box, with model 8D that had both the smallest axial and the smaller bending stiffness,

witnessing the smallest forces. This is consistent with the discussion in the previous section that suggested that the flexural effects of the box reduce the forces in the walls but introduce significant disturbance to the soil next to the walls. It must be noted that for the calculation of the vertical forces in the walls the forces in the three nodes below the walls (of one face) are summed together as shown in Figure 5-31. This section demonstrated that in order to achieve a pure shear of the soil in the box it is important the walls to have both a large axial as well as a large bending stiffness.

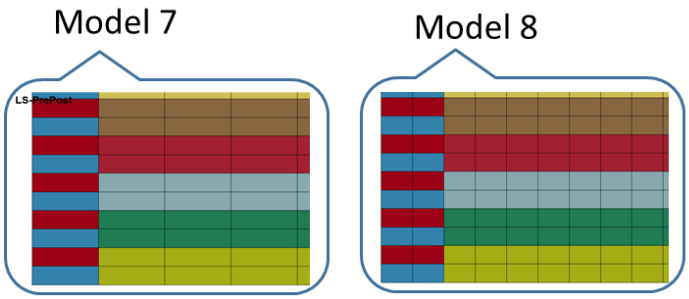

Figure 5-27: Zoom-in of two different mesh configurations for the walls of the box

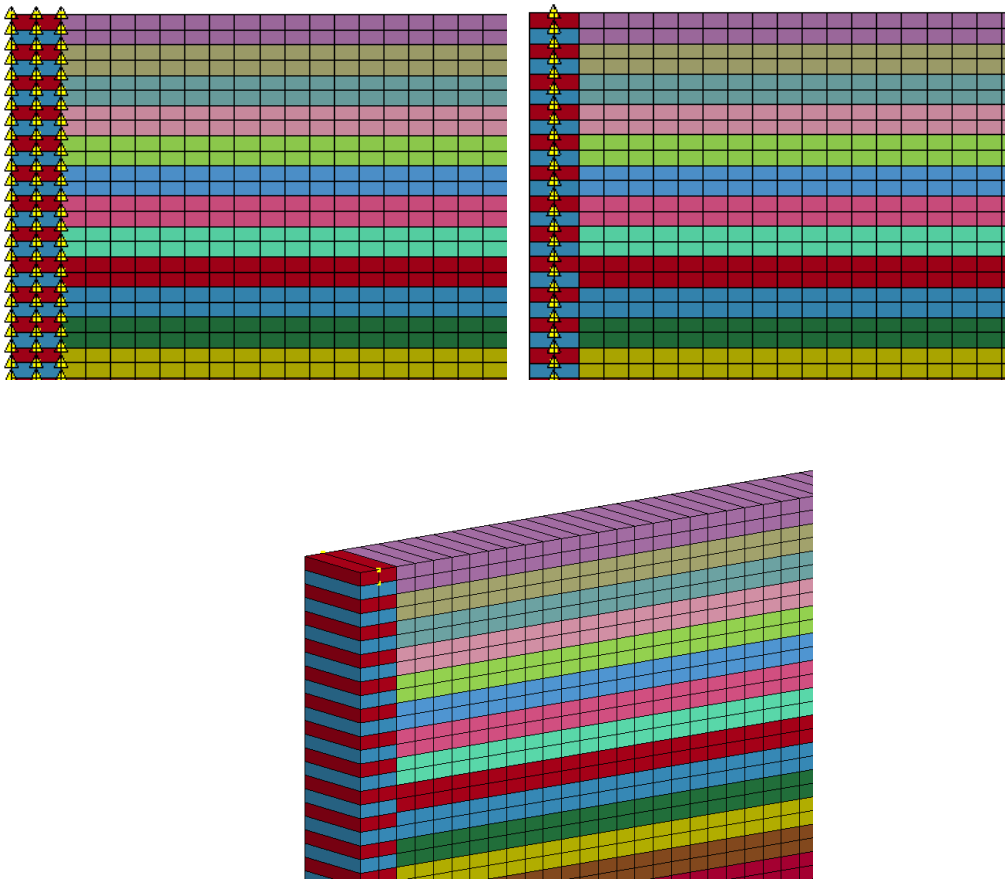

Figure 5-28: Models 8B (top-left), 8C (top-right) and 8D (bottom)

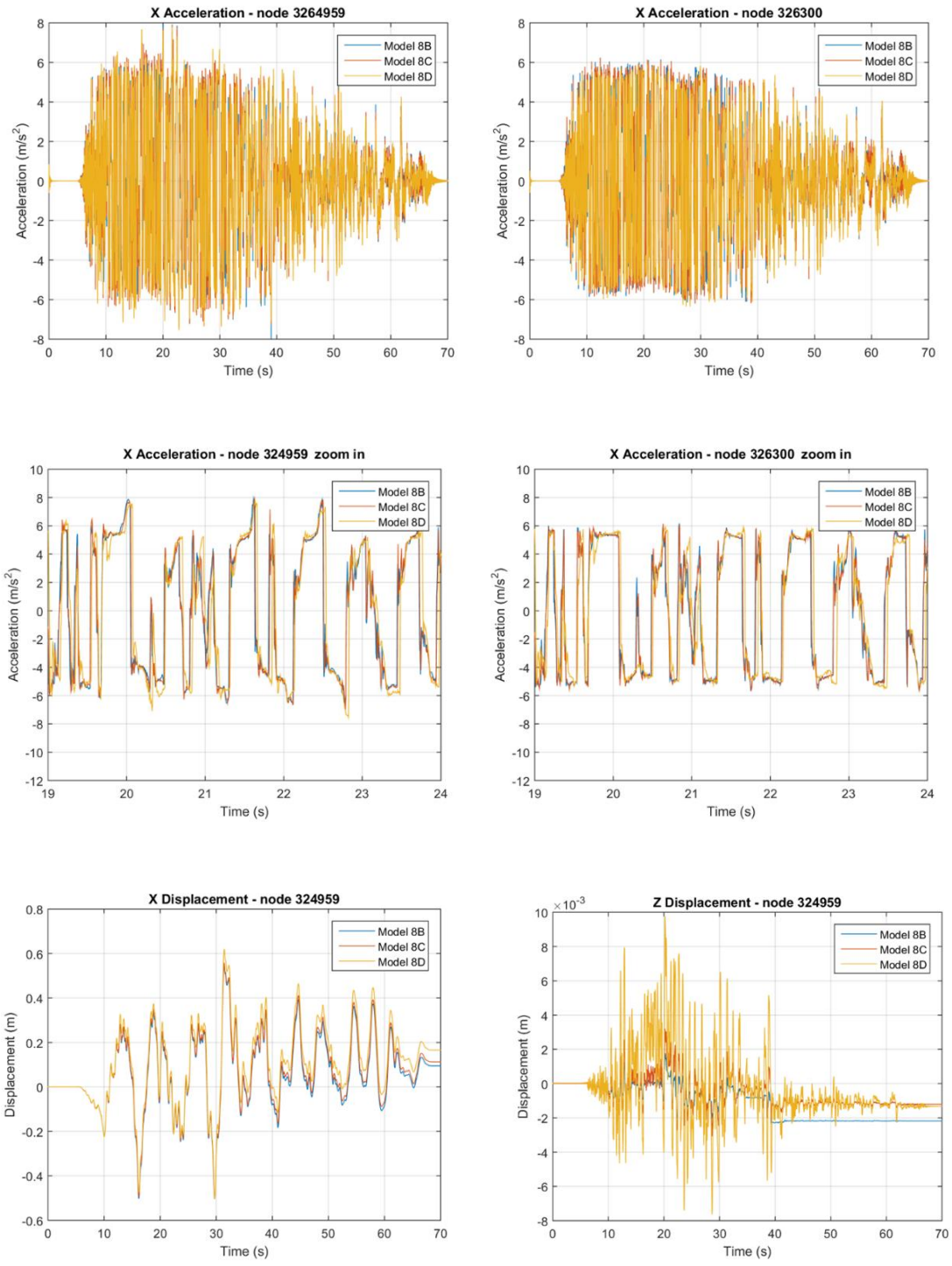

Figure 5-29: Lateral accelerations (top and middle) at the surface of the left (left) and of the center (right) soil column, absolute lateral displacement (bottom-left) and absolute vertical displacement (bottom-right) at the surface of the left soil column, for 2D models with different configurations of the vertical constraints

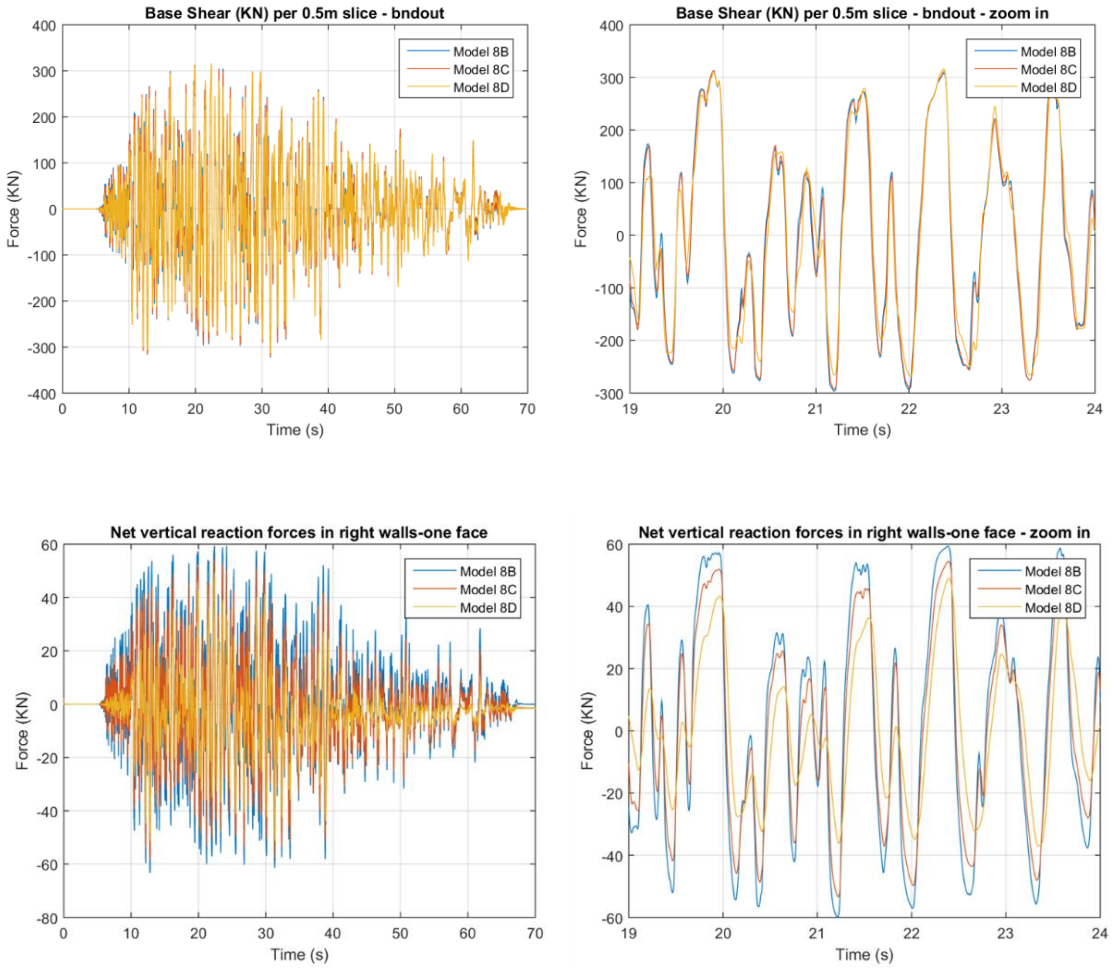

Figure 5-30: Base shear histories (top) and net vertical reaction force histories (bottom), for 2D models with different configurations of the vertical constraints

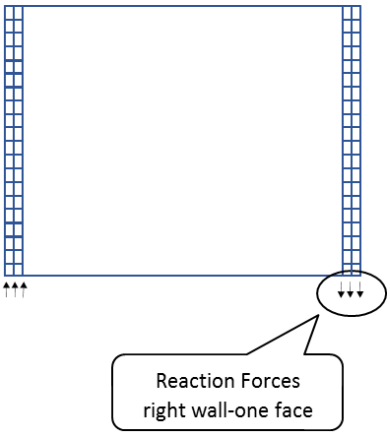

Figure 5-31: Sketch showing the nodes used to calculate the reaction forces in the right wall

5.4.4 Constraints vs Springs

Up to this point the effect of the wall axial and bending stiffness was examined via the use of vertical constraints. Although this is a reasonable approach for simulating the increased stiffness of the walls generated by the stiff element inside the rubber layer (ball/plug) it has the disadvantages that (i) it over-predicts the stiffness (zero relative displacements between the constrained nodes), (ii) it is not possible to assign different stiffness in tension and compression, and (iii) it is not possible to output the forces developed between the end nodes. An alternative approach that eliminates all these three drawbacks is the use of uniaxial vertical springs between two nodes of the same rubber layer. This approach was implemented in model 8E, as shown in Figure 5-32. An elastic material was assigned to the springs and the stiffness in both tension and compression was determined to be equal to 1000 times higher than the largest stiffness in the system, which was the axial stiffness of the steel.

Figure 5-33 shows the location of several springs that were selected for output and will be further discussed in this section. In particular, the member forces in the springs at the surface, ¼ depth, ½ depth, ¾ depth and bottom rubber layer were output and are presented in Figure 5-34. As expected the member forces increase for the springs with larger depths, and this is because the springs have to transfer the complementary shear generated by all the soil layers above it. Interestingly, this increase is not linear with the depth, since for example at approximately t=12.8sec the tension in the bottom spring of the left wall is 23kN while the respective tension in the spring at mid-depth is only 7.5kN (which is less than 50%). Moreover, Figure 5-35, shows that the net vertical forces in the bottom springs of the left and right wall are out-of-phase, and when one wall is in tension the other one is in compression, verifying the generation and significance of overturning moment during the lateral shaking.

Figure 5-36 shows the acceleration and displacement histories at the surface of the left soil column, while Figure 5-37 the net vertical in the walls, for three models and particularly 8B, 8D and 8E. These figures demonstrate that models 8D and 8E, which correspond to vertical constraints and springs respectively, give identical results, as expected, giving confidence in the numerical results. It must be noted that although the use of springs has certain benefits relative to the constraints, it has the main disadvantage that it can reduce the time-step of explicit analyses and consequently increase the required computational time by orders of magnitude depending on the exact stiffness of the springs. The other disadvantage of using very stiff springs is that they seem to introduce very high frequencies/numerical “noise” in the results.

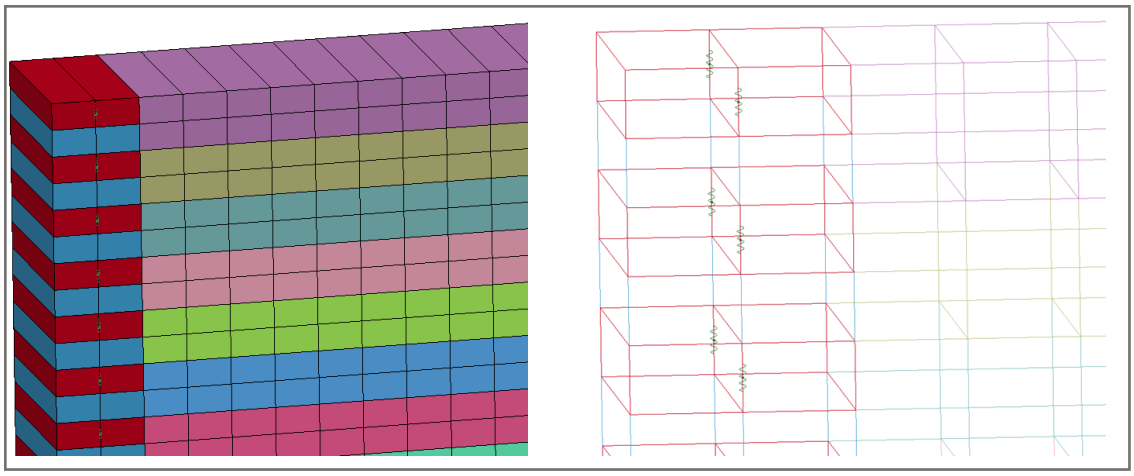

Figure 5-32: Axial springs attached between the nodes of the rubber layers of the walls

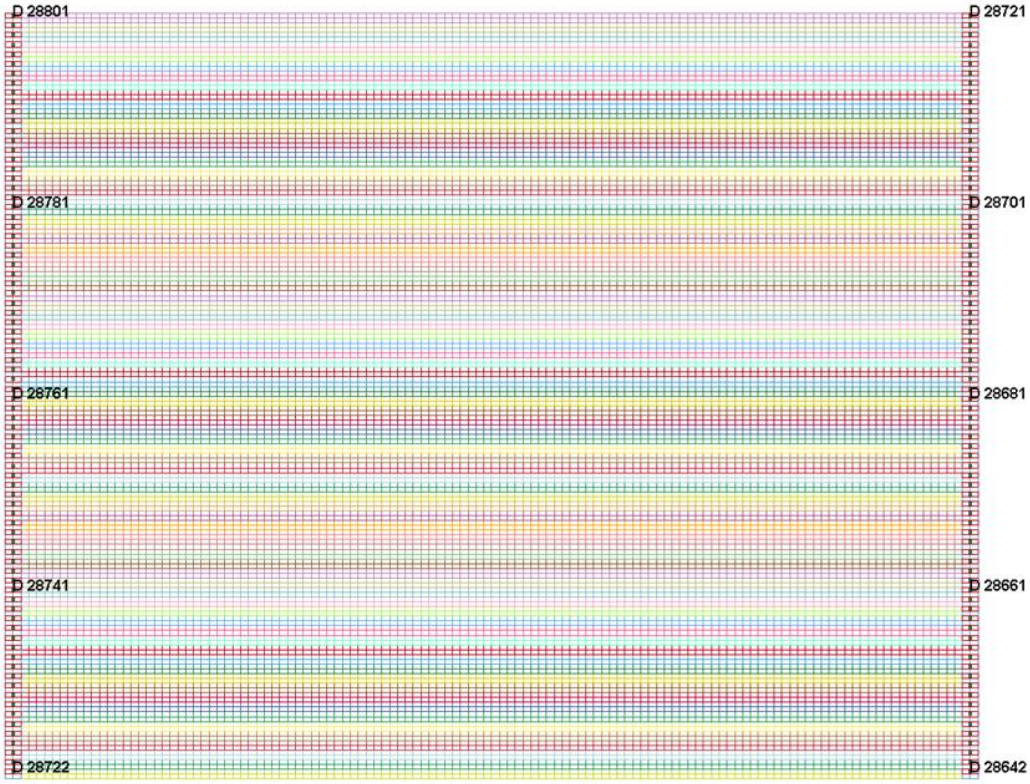

Figure 5-33: Location of the springs selected for output in model 8E

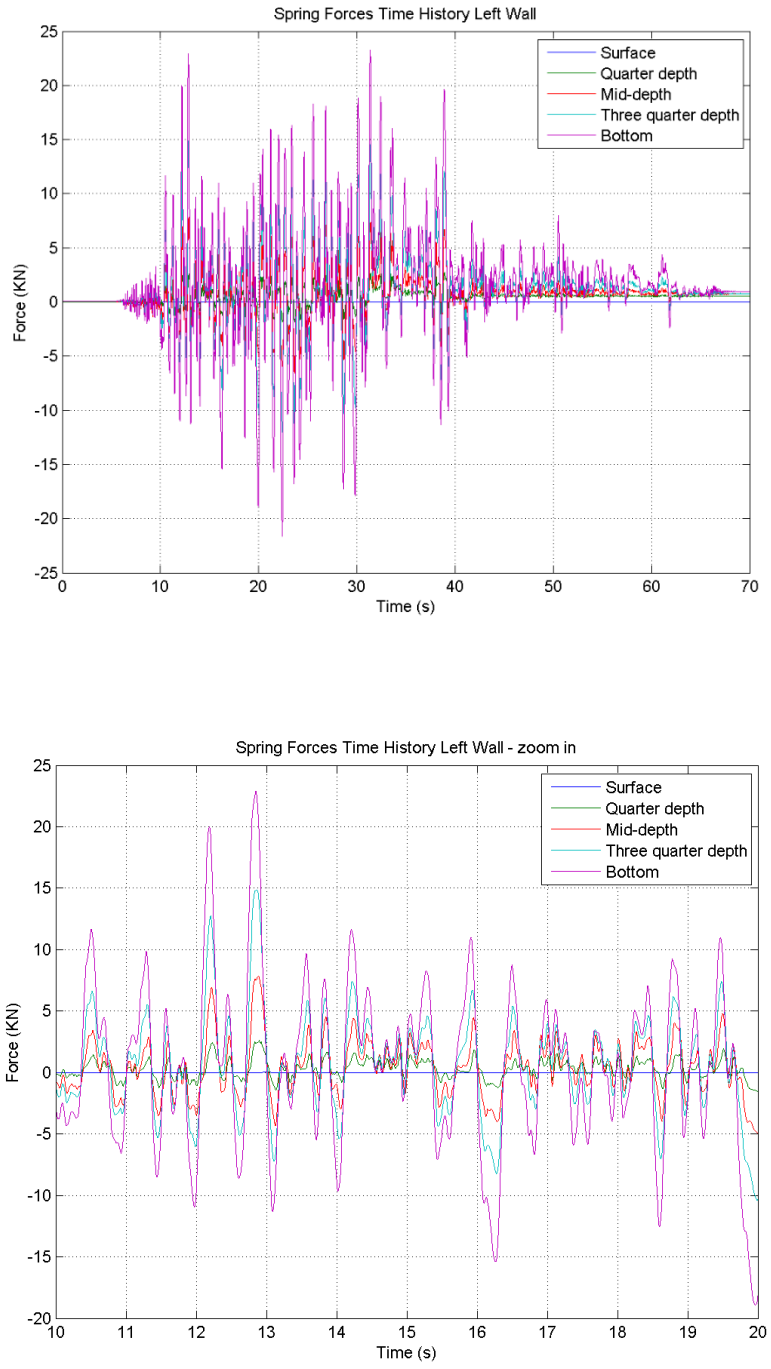

Figure 5-34: Vertical spring forces at five different heights of the left wall of the soil-box

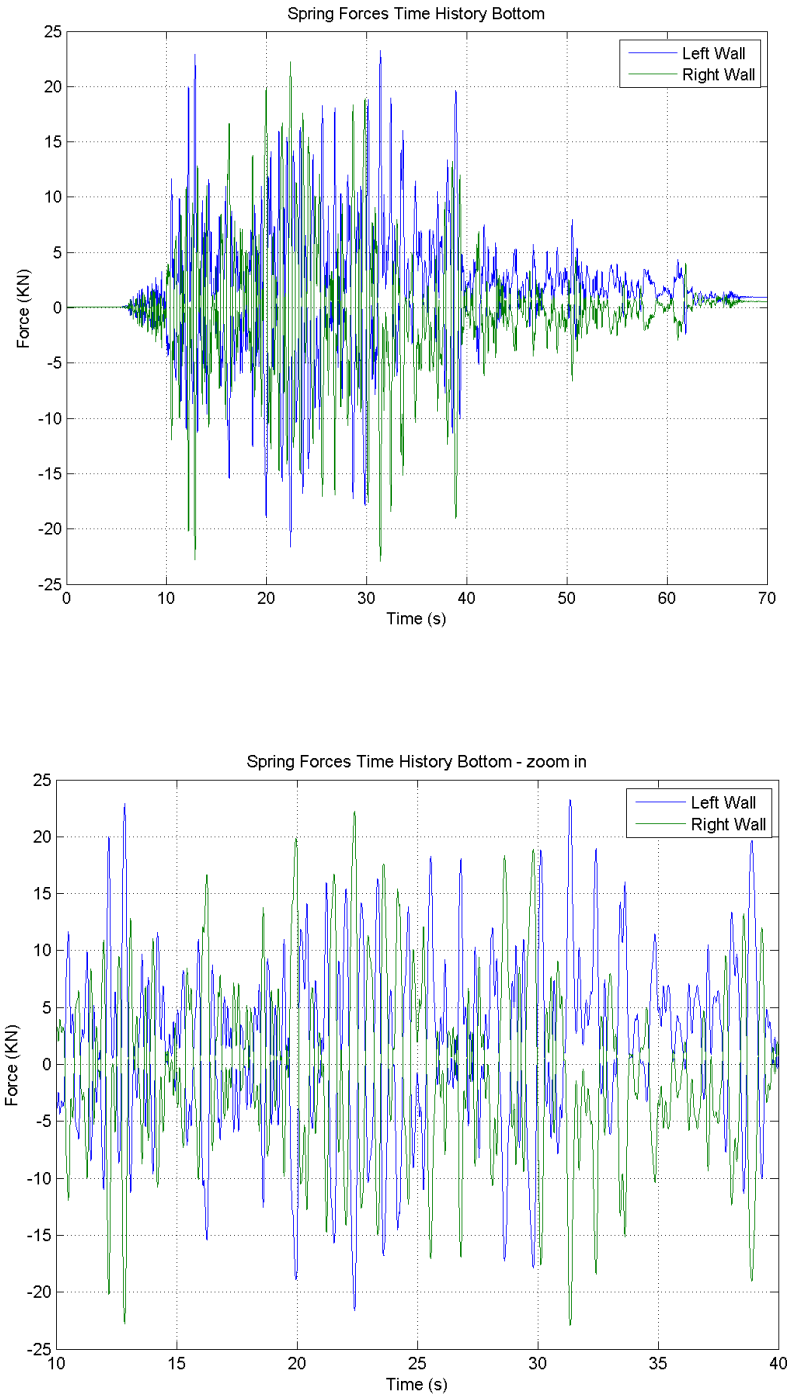

Figure 5-35: Vertical spring forces at the bottom rubber layer of the two walls of the soil-box

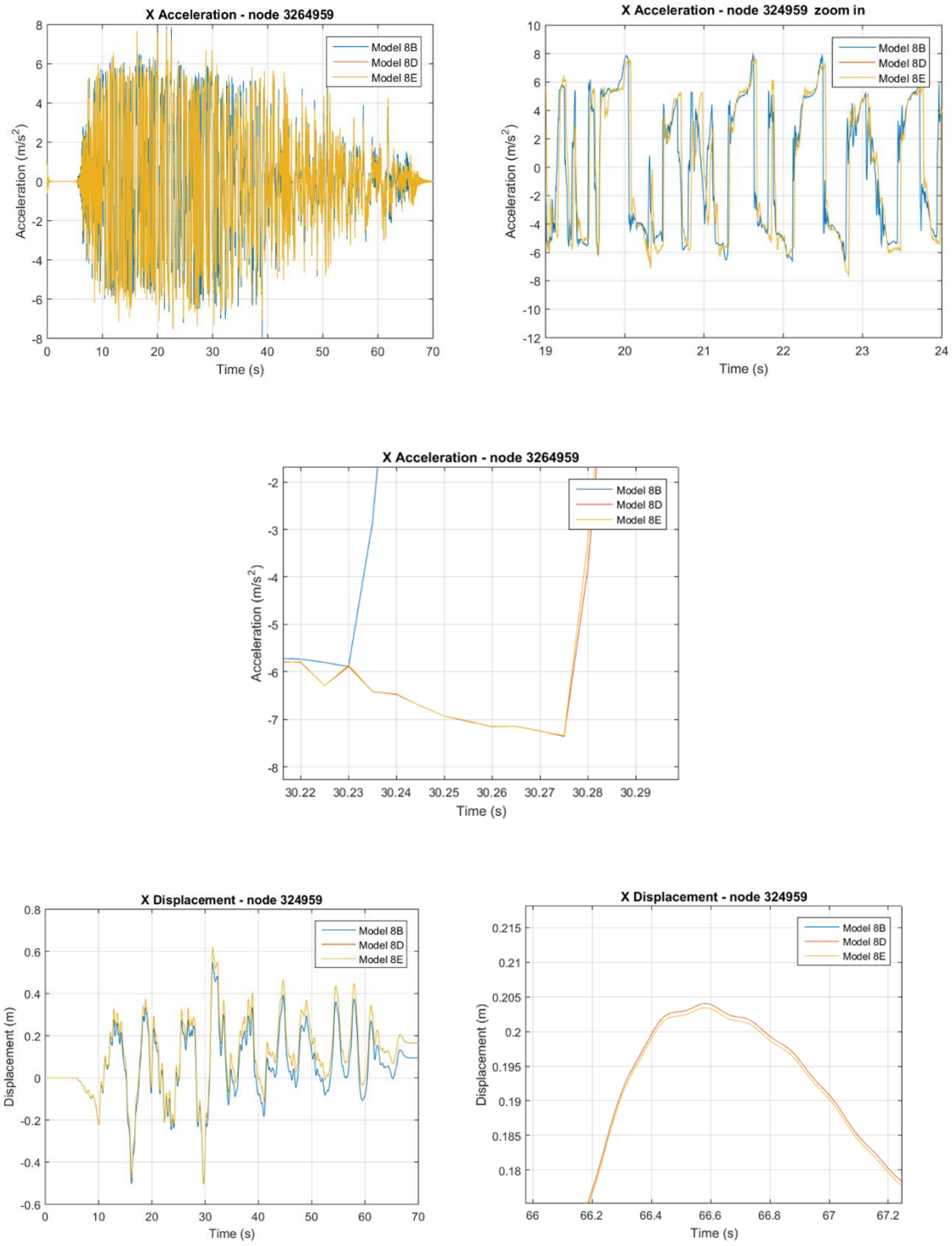

Figure 5-36: Lateral accelerations (top and middle) and lateral absolute displacements (bottom) at the surface of the left (left) soil column, for the 2D models with constraints and springs

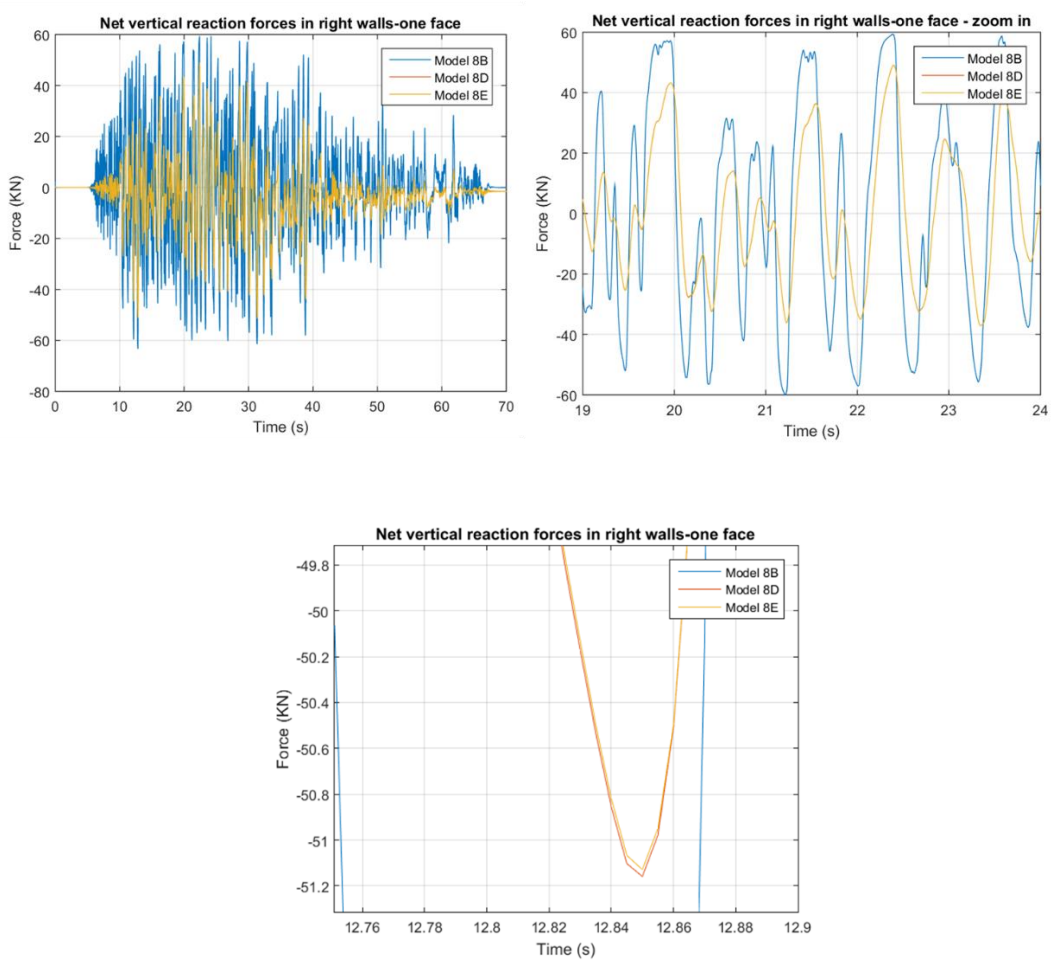

Figure 5-37: Net vertical reaction forces in boundary nodes below the soil-box, for the 2D models with constraints and springs

5.5 Effect of Spring Type: Linear vs Compression only Springs

The last section of this chapter will examine the differences generated in the response of the soil-box by the use of compression only springs (represents the rigid ball inside the rubber layers), relative to the case that the springs have the same stiffness in both tension and compression. To this end, model 8E was modified and the material of the spring was changed to another elastic material where only the compression stiffness was defined

(model 8G). The 2D models with two different spring types seem to have similar horizontal accelerations and displacements at the surface of the left soil column (close to the walls), however, this is not true for the vertical displacements, with the compression only springs giving larger vertical movement/uplift for the nearby soil, which is reasonable since in this case the wall stiffness is very small and comes only from the soft rubber. Similarly, to the horizontal accelerations and displacements, the base shear is not affected significantly by the spring type, however this is not true for the net vertical forces in the walls. When compression-only springs are used, the tensile forces at the bottom of the walls are significantly reduced, which is reasonable/expected, and the compressive forces are increased, which was not expected beforehand. In particular, the maximum tension at the bottom of the walls, in the model with the linear springs is 51.4kN and in the model with the compression-only springs is 18.2kN, while the respective values for the compression are 49 and 90.6kN respectively.

The larger compression forces are also observed in the member forces of the springs at different depths shown in Figure 5-40, 5-41 and 5-42. Even in the case of compression-only springs the distribution of the maximum compression spring force is not linear with depth. Figure 5-42 also demonstrates that for both-types of vertical springs in the walls the axial forces in the walls are out-of-phase, with the compression-only springs of one wall giving a zero force when the other wall gives a large compression force.

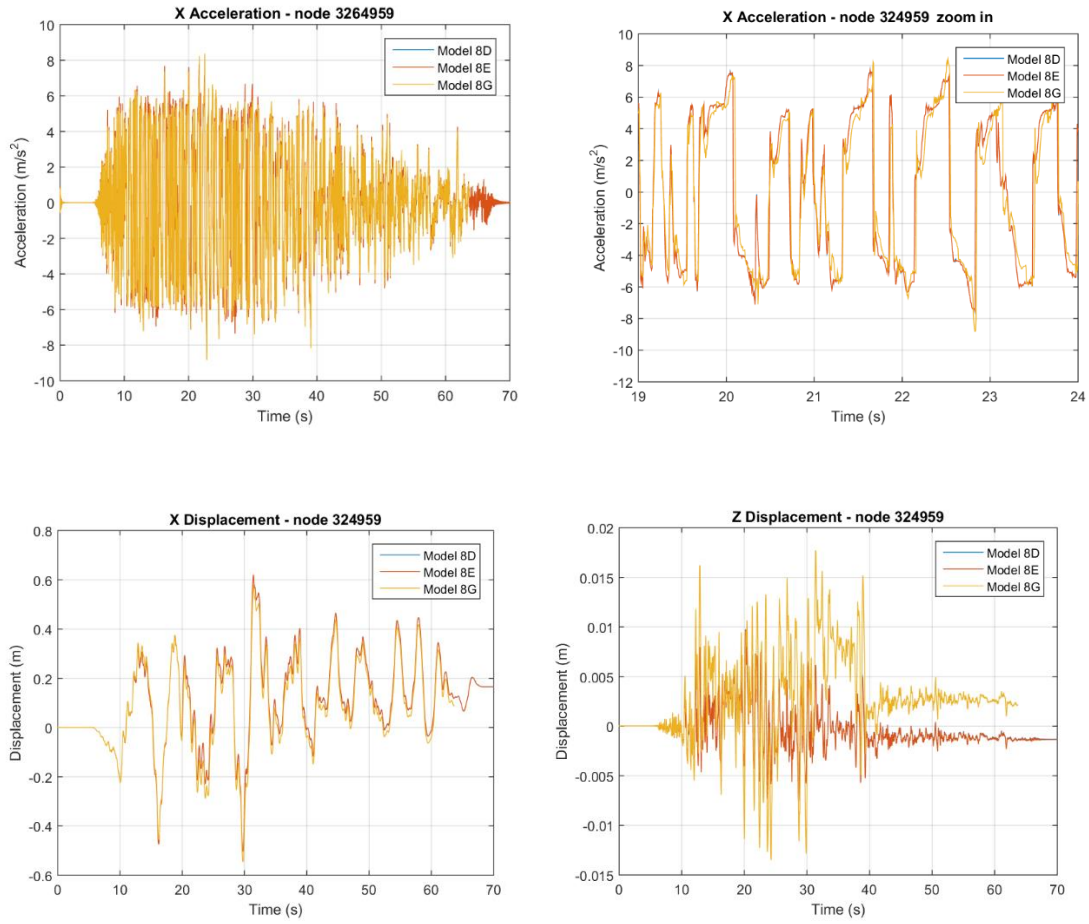

Figure 5-38: Lateral accelerations (top), lateral absolute displacements (bottom-left) and vertical absolute displacements (bottom-right) at the surface of the left soil column, for the 2D models with constraints, linear springs and compression-only springs

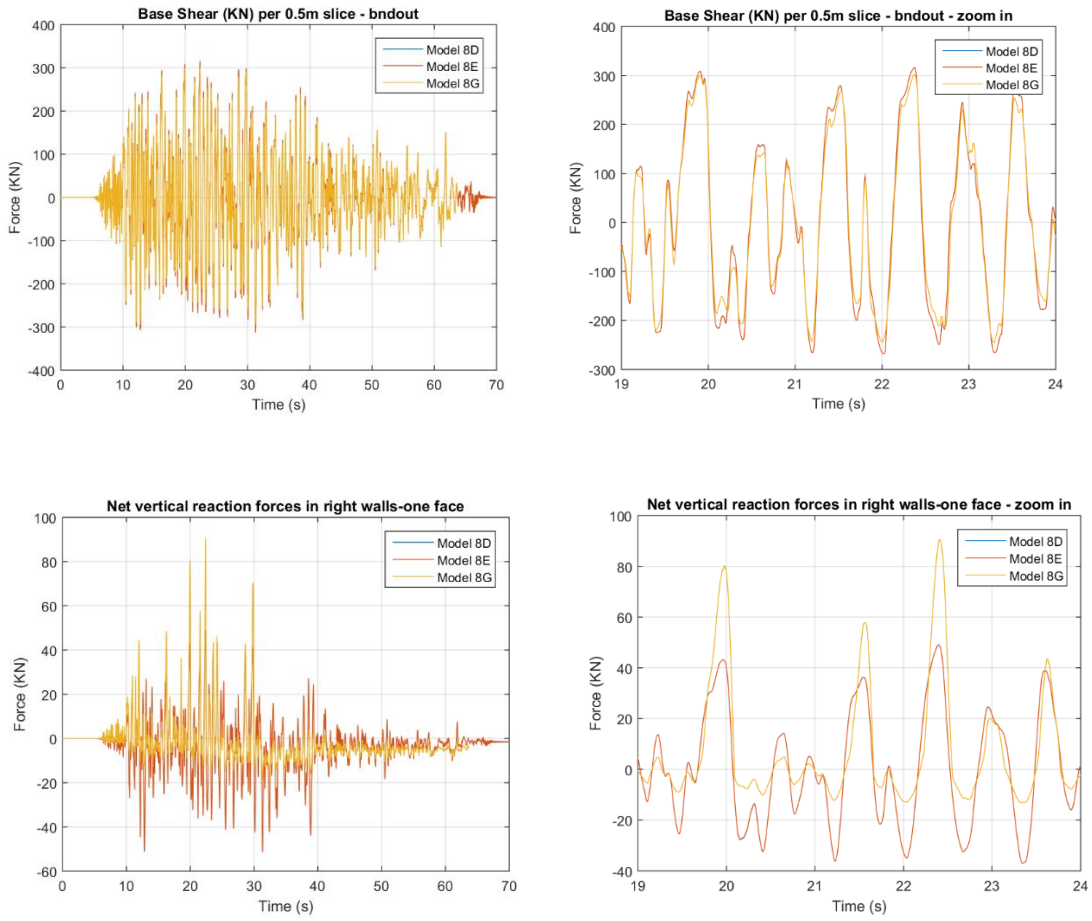

Figure 5-39: Base shear histories (top) and net vertical reaction force histories (bottom), for the 2D models with constraints, linear springs and compression-only springs

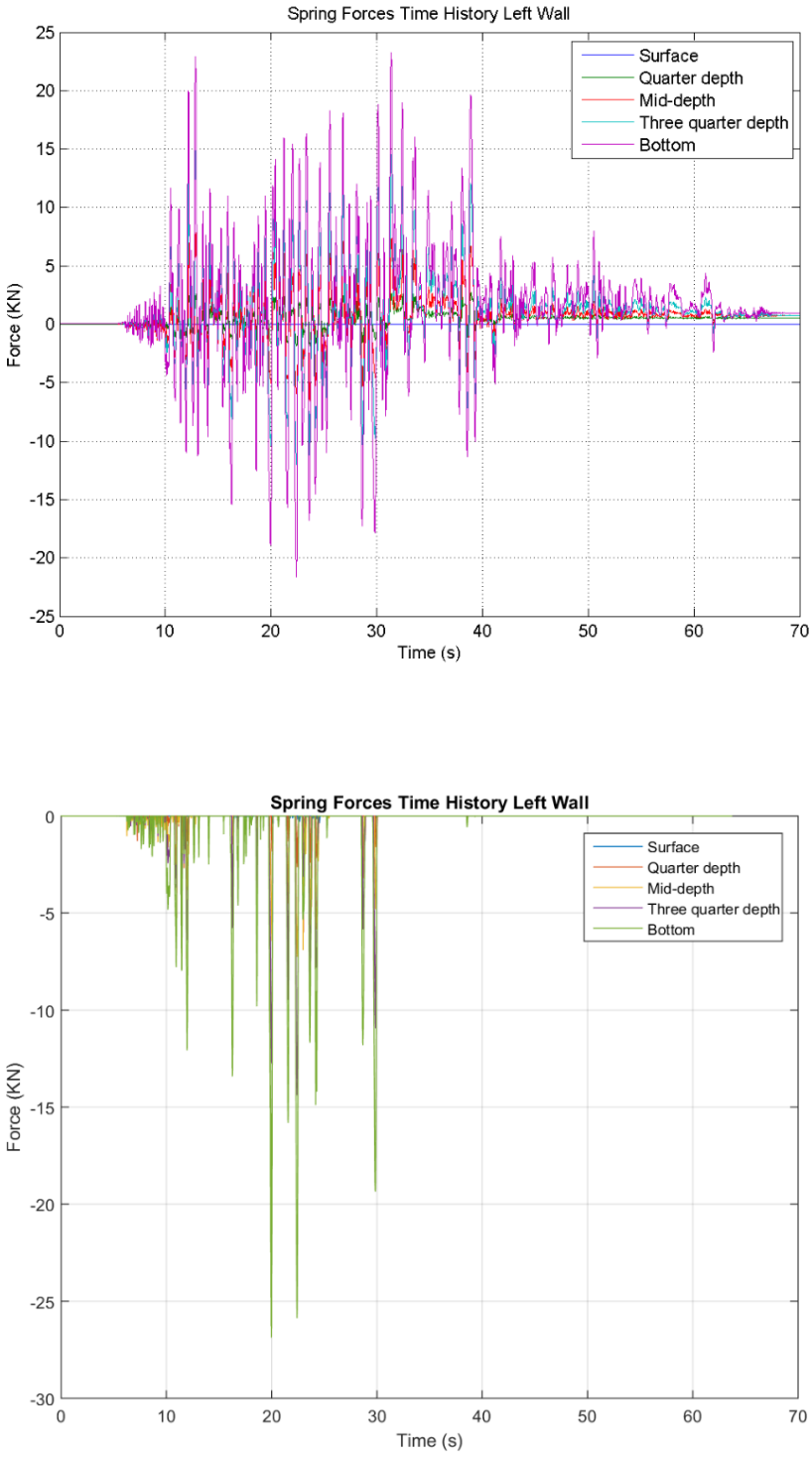

Figure 5-40: Vertical spring forces at five different heights of the left wall of the soil-box, for the model with linear springs (top) and compression only springs (bottom)

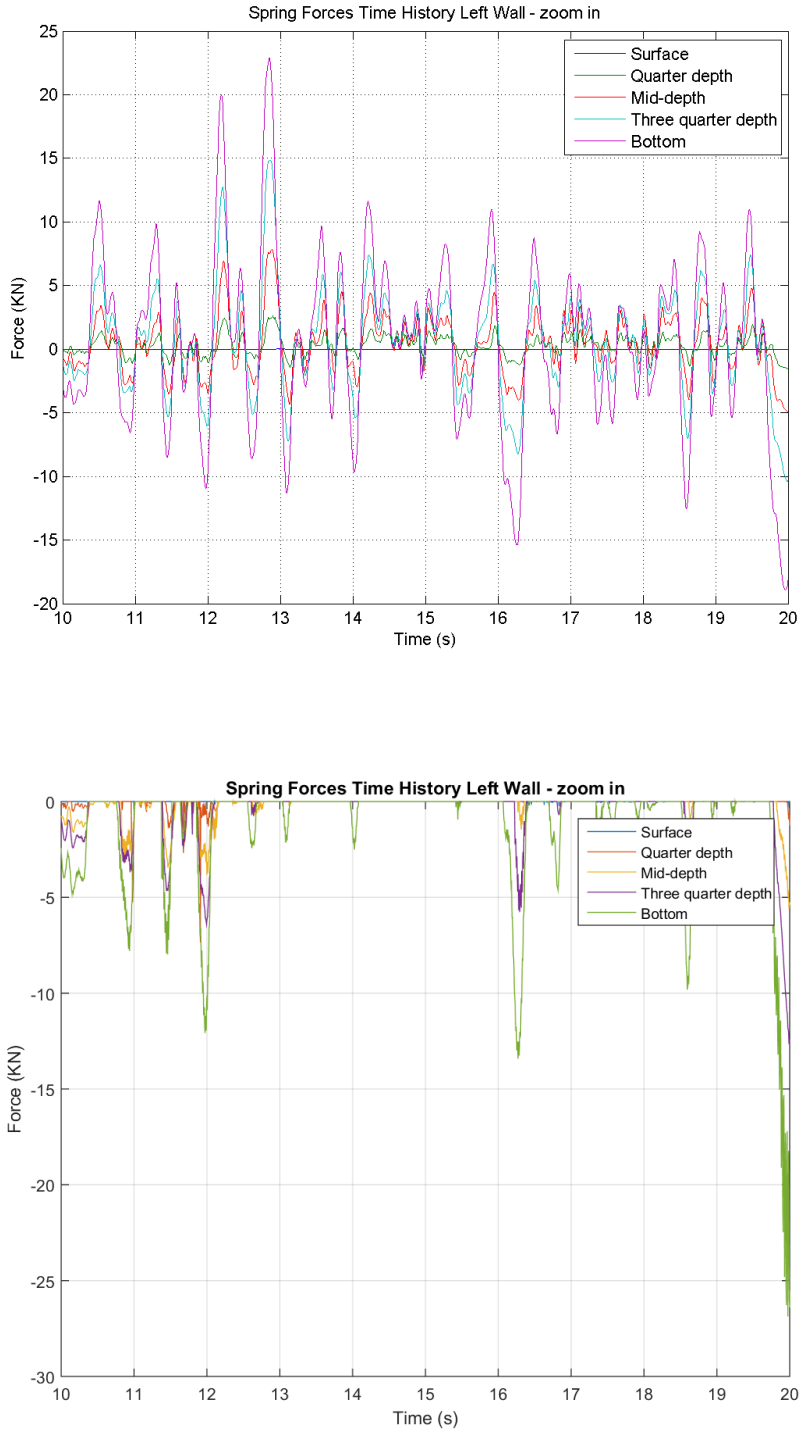

Figure 5-41: Zoom-in of vertical spring forces at five different heights of the left wall of the soil-box, for the model with linear springs (top) and compression only springs (bottom)

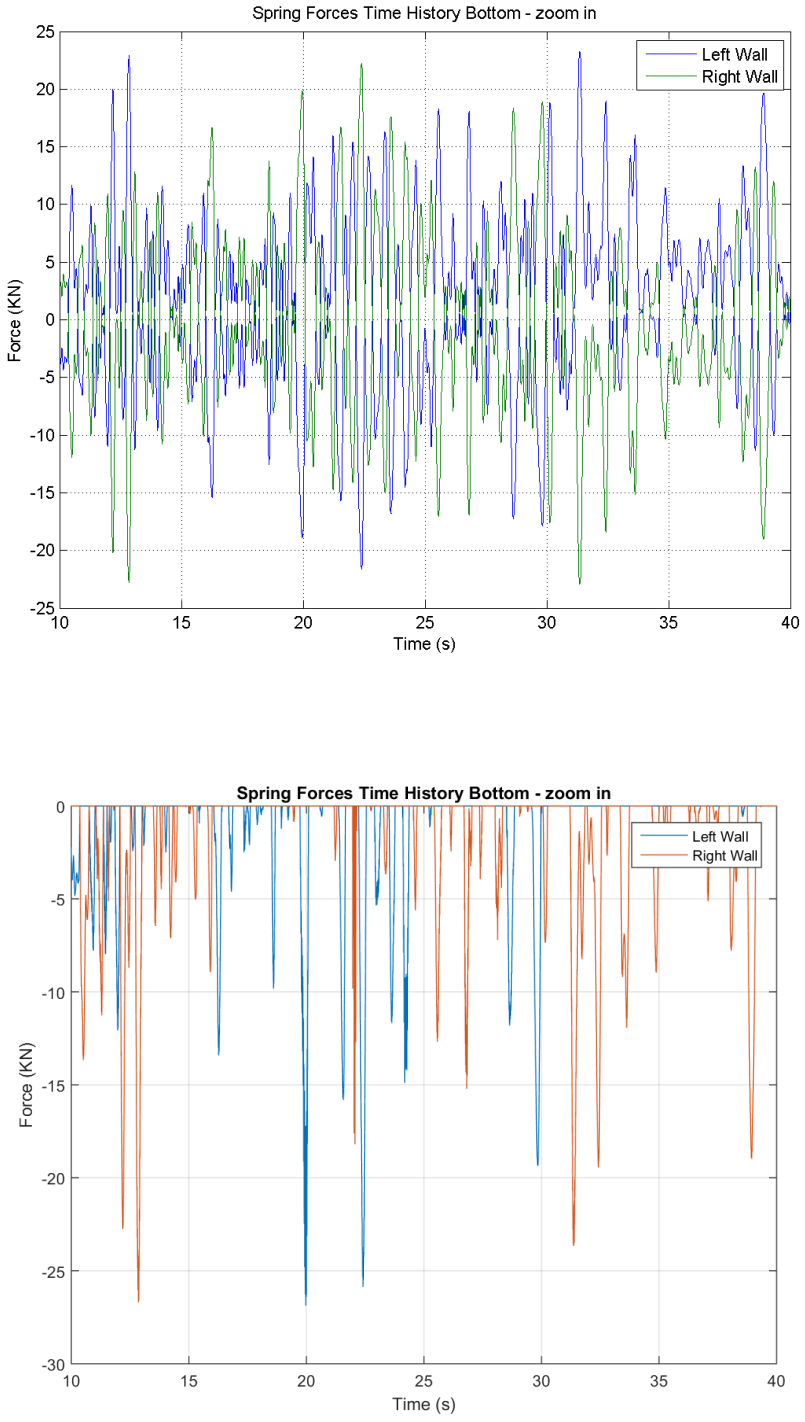

Figure 5-42: Vertical spring forces at the bottom rubber layer of the two walls of the soil-box, for the model with linear springs (top) and compression only springs (bottom)

Chapter 6: The role of contact conditions at the interface of soil and laminar walls

6.1 Description of 2D numerical models

The extensive 2D nonlinear dynamic analyses presented in the previous chapters increased the understanding of the dynamic behavior of the soil-box and how this is affected by several numerical and modeling parameters. However, all the models presented in the previous chapter were developed based on the assumption that the soil will not detach from the walls meaning that there was a perfect contact between the walls and neighboring soil column. In this chapter, models with different contact conditions at the interface of the soil and laminar walls will be presented.

To this end, the first model to be examined is one that decouples the soil from the walls and allows it to slide freely in the vertical direction without any friction (model 10E). To achieve this condition the shared nodes between the walls and the soil were detached, meaning that there were now collocated/duplicate nodes at the same location (Figure 6-1), with the first set of nodes belonging to the walls and the second one to the neighboring soil. If no other conditions would have been specified then the walls and the soil would move independently from each other, which is unrealistic. To avoid penetration of the solid elements of the soil into the ones of the wall, horizontal constraints (or springs) were specified between every four duplicate nodes (two on each face), as shown in Figure 6-2, which made the wall and the soil at the interface have the same lateral displacement during

shaking. This meant that gapping was not permitted, however frictionless sliding was allowed in the vertical direction.

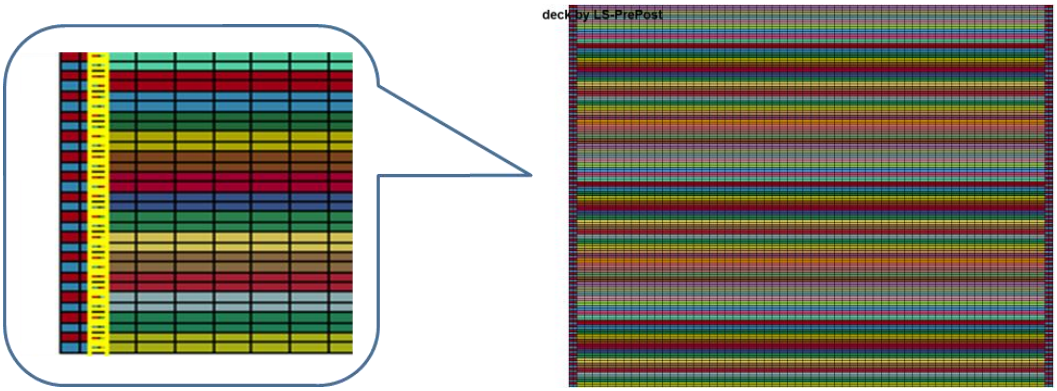

Figure 6-1: 2D soil-box model with duplicate nodes

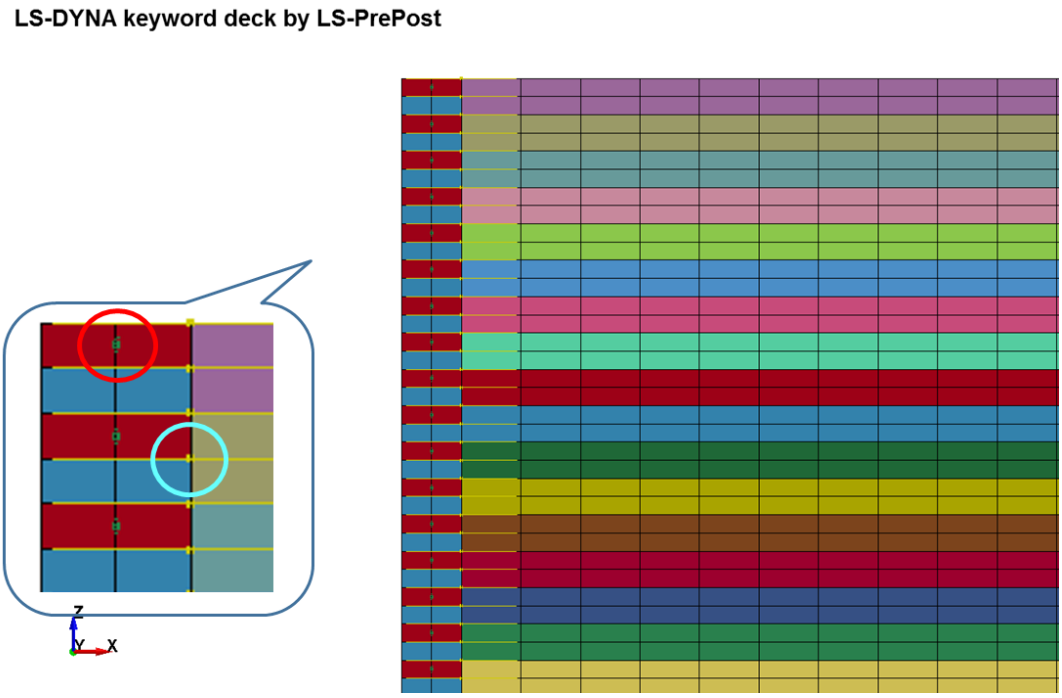

Figure 6-2: Location of vertical and horizontal springs/constraints in the 2D soil-box model with duplicate nodes

6.2 Effect of sliding at the soil-wall interface

The previous model with frictionless sliding at the wall-soil interface was subjected to lateral shaking and particularly to Cerro 237 at a scale factor of 4 (PGA=1g). Two snapshots of the deformation of the soil-box were generated at two different instants (t=14.15sec and 24.15sec) and are shown in Figures 6-3 and 6-4. It must be noted that this model had also vertical constraints at the mid-width nodes of the walls, one set of constraints for each rubber layer. The snapshots reveal that the soil is uplifting at one side of the box and is settling at the other side of the box, and this behavior is reversed during shaking. It becomes clear from the visualized deformed shape that the soil does not behave in pure shear anymore and that a more complex soil stress state is developed especially in the soil regions close to the walls, which could potentially result in non-uniform shear stresses along the width of a soil layer.

To quantify the effect of the sliding, certain parameters were output at the two locations shown in Figure 6-5. Both locations are at the mid-depth of the soil-box, however one is at the mid-width of the walls and the other one at the center soil-column. Figure 6-6 shows the acceleration histories in the horizontal and vertical direction. The model with the frictionless sliding seems to witness noticeably smaller horizontal accelerations than the model with perfect contact, an observation that is in agreement with the results presented in chapter 5, according to which the horizontal accelerations were larger in the soil-box when the box responded in pure shear. Moreover, the decoupling of the soil from the walls eliminates the vertical accelerations in the walls, demonstrating that the reason for the generation of the acceleration in the walls was not only the existence of overturning

moment but also the idealized perfect contact which transferred the dynamic complementary shears of the soil to the walls of the box.

Figure 6-7 shows the shear stress histories and shear strains at the mid-depth of the center soil column, the total vertical forces in right and the base shear for the models with perfect contact (10B) and frictionless sliding (10E). Although the shear stresses seem to be very similar in the two models, this is not true for the shear strains, where larger differences can be observed. The largest difference occurs in the vertical forces that the walls have to withstand, since in the model with the frictionless sliding the walls seem to be getting only a very small compressive force, which is equal to their own weight, and the force is not affected by the complementary shears generated during the lateral shaking. Moreover, the same model is witnessing smaller base shears and overturning moments, than the model with perfect contact.

This comparison demonstrated that allowing the soil to slide vertically at the interface with the walls is beneficial for the design of the soil-box and shake table system because it reduces (a) the vertical forces in the walls of the box, (b) the overturning moments on the table, (c) the local pressures on the platen, and (d) the base shear that the actuators have to introduce/withstand. However, the major disadvantage is the fact that the sliding at the interface results in very distorted soil regions in a large portion of the box, as shown in Figure 6-9, resulting a complex stress state of the soil and not pure shear. Since this is an undesired soil behavior and physically unrealistic, the frictionless sliding at the wall-soil interface is not recommended.

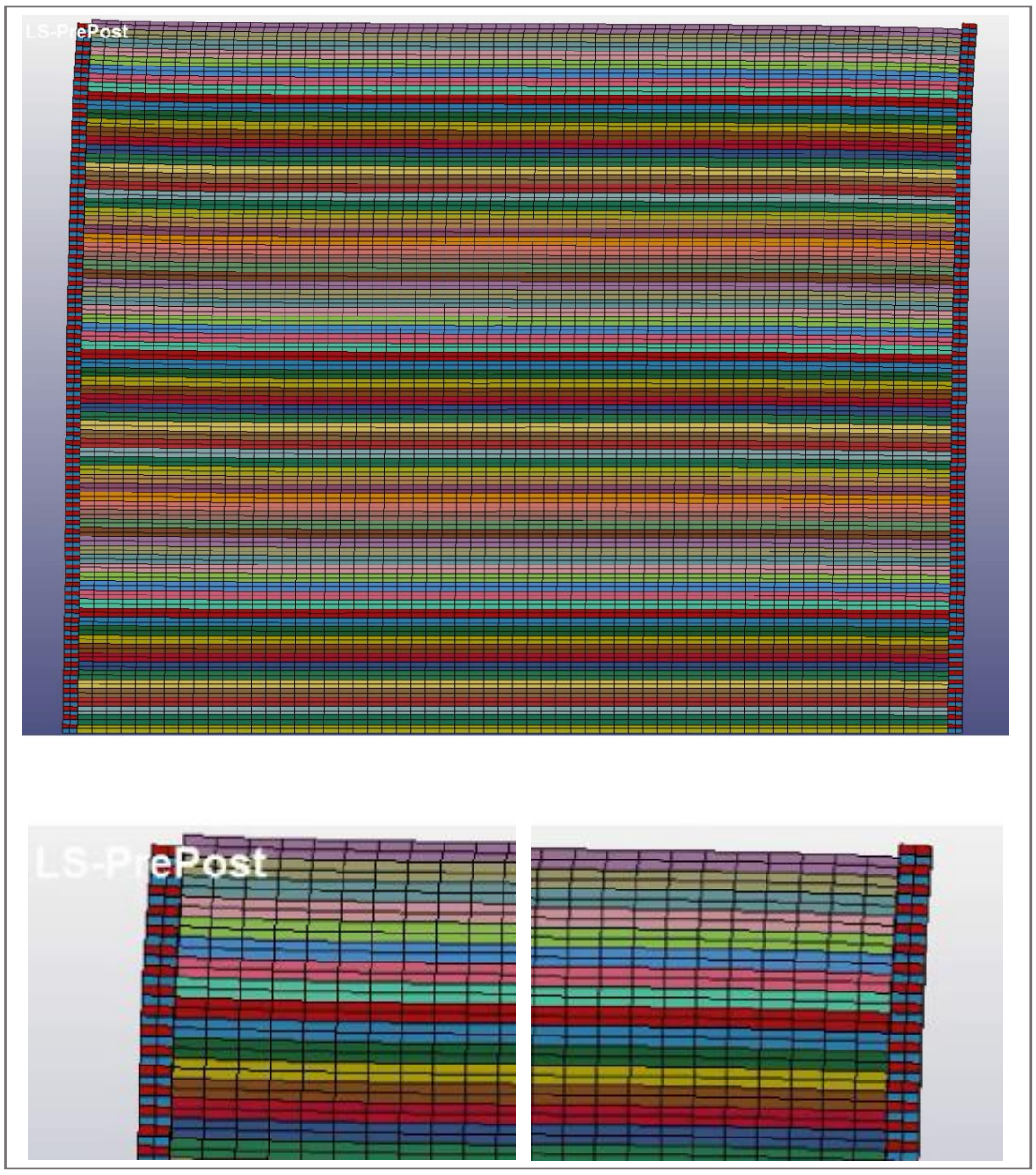

Figure 6-3: Snapshot of deformed soil-box (top) and zoom-in at the top corners (bottom) at t=14.15sec during lateral shaking

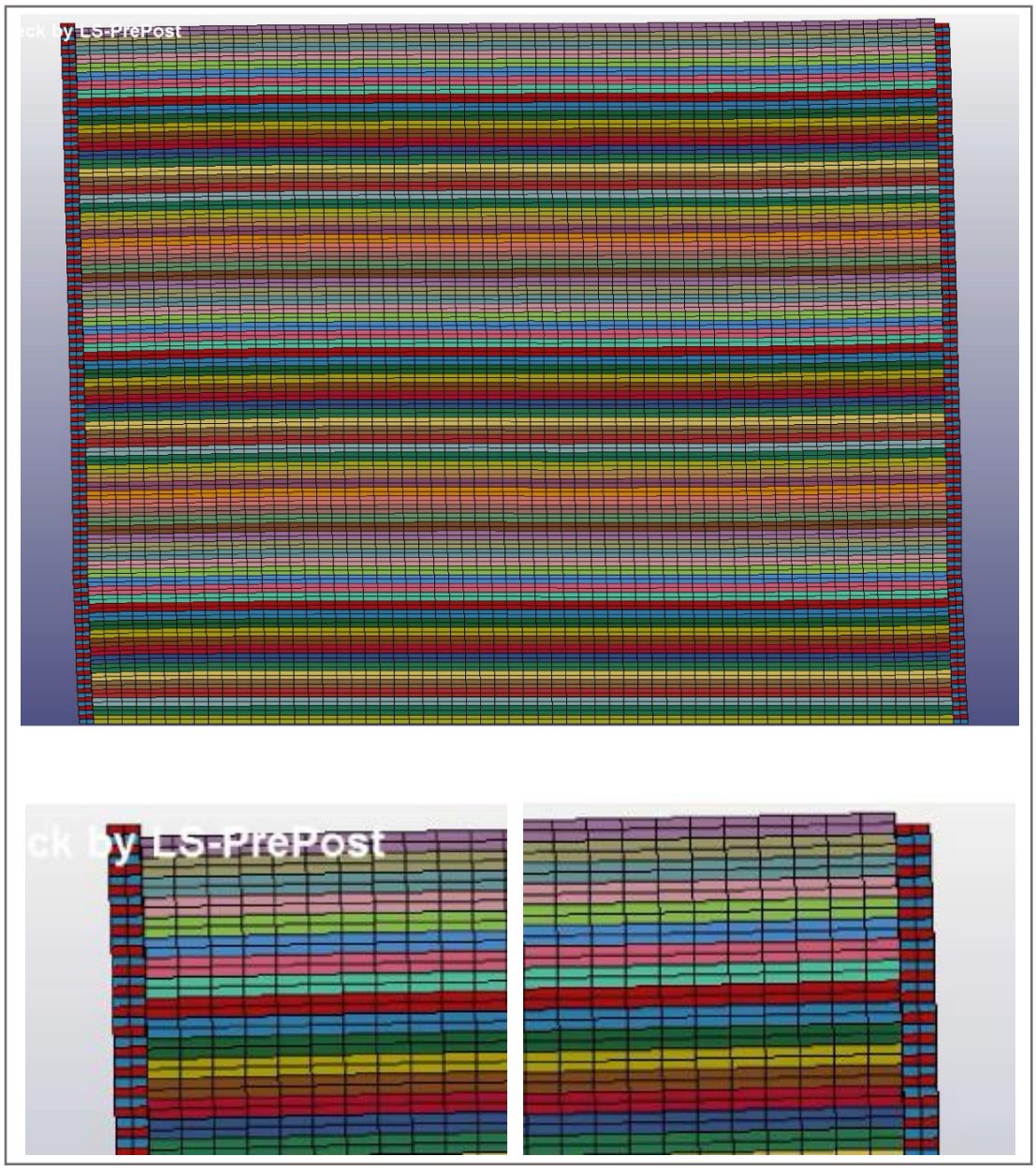

Figure 6-4: Snapshot of deformed soil-box (top) and zoom-in at the top corners (bottom) at t=24.15sec during lateral shaking

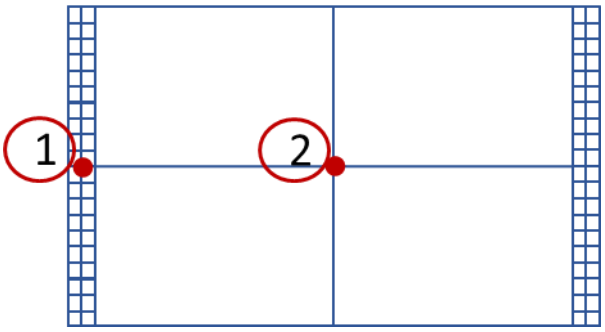

Figure 6-5: Location of nodes used for comparison of models 10B and 10E

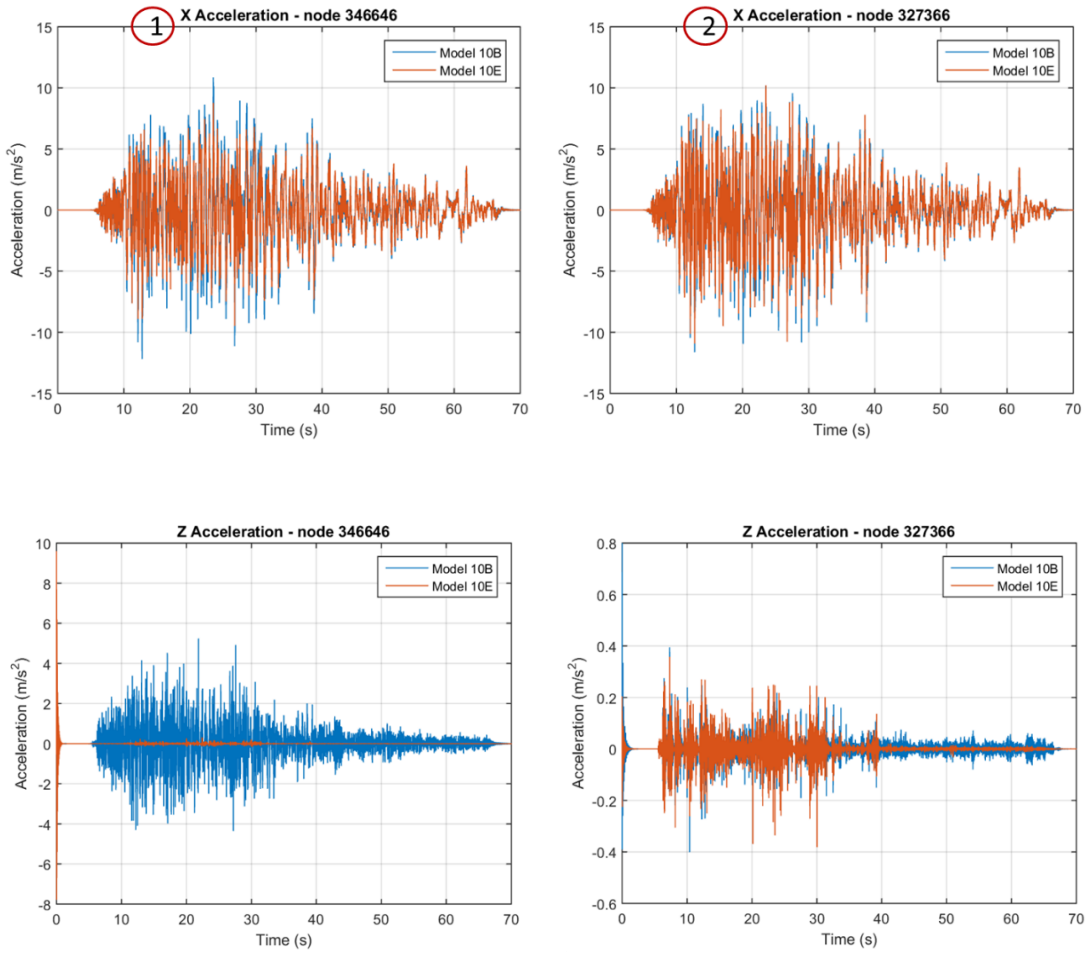

Figure 6-6: Accelerations histories in the horizontal (top) and vertical (bottom) direction, at the mid-depth of the left wall (left) and mid-depth of the center soil column (right)

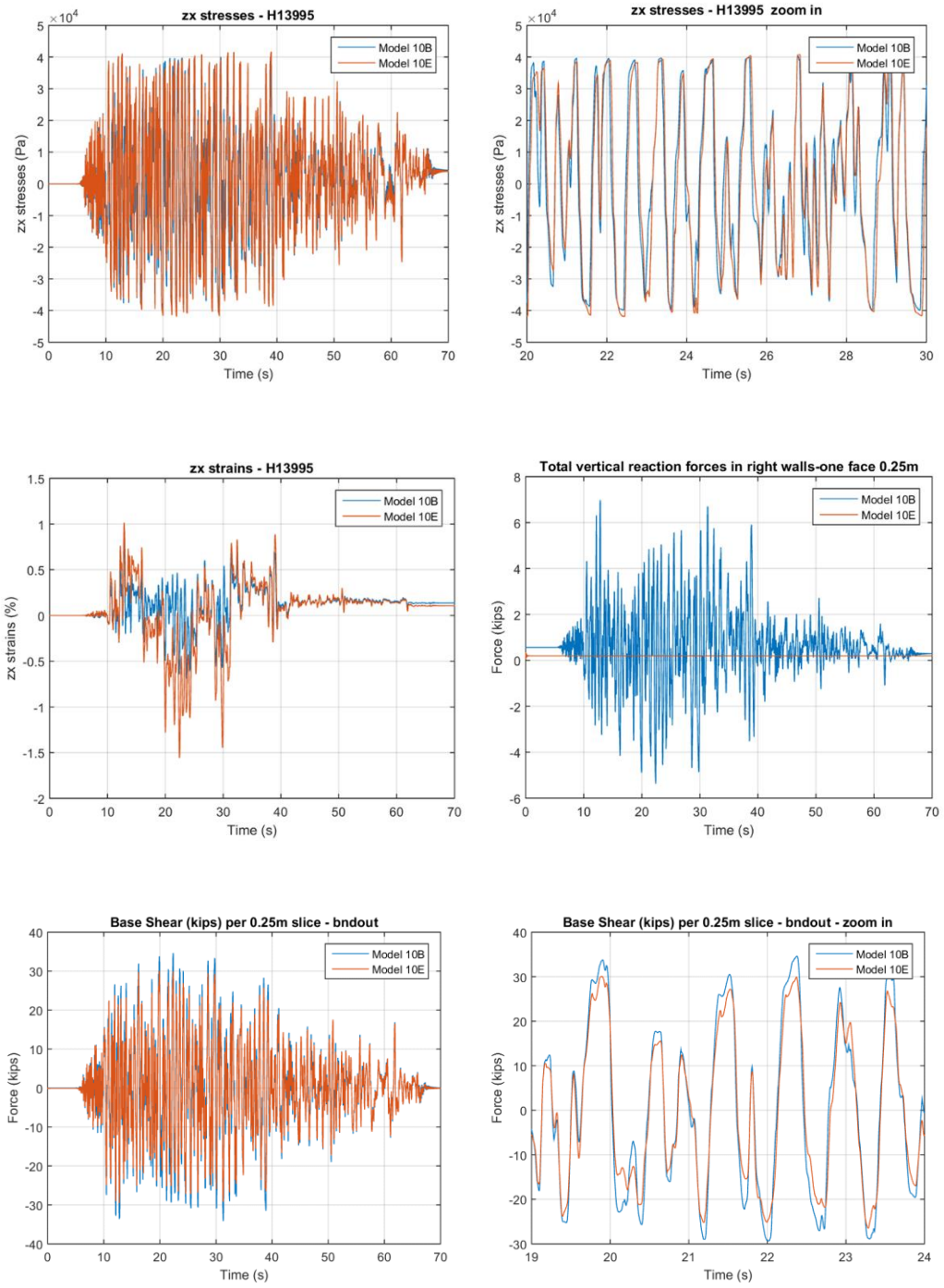

Figure 6-7: Shear stress histories (top) and shear strains (middle-left) at the mid-depth of the center soil column, total vertical forces in right walls (middle-right), and base shear (bottom), for the models with perfect contact (10B) and frictionless sliding (10E)

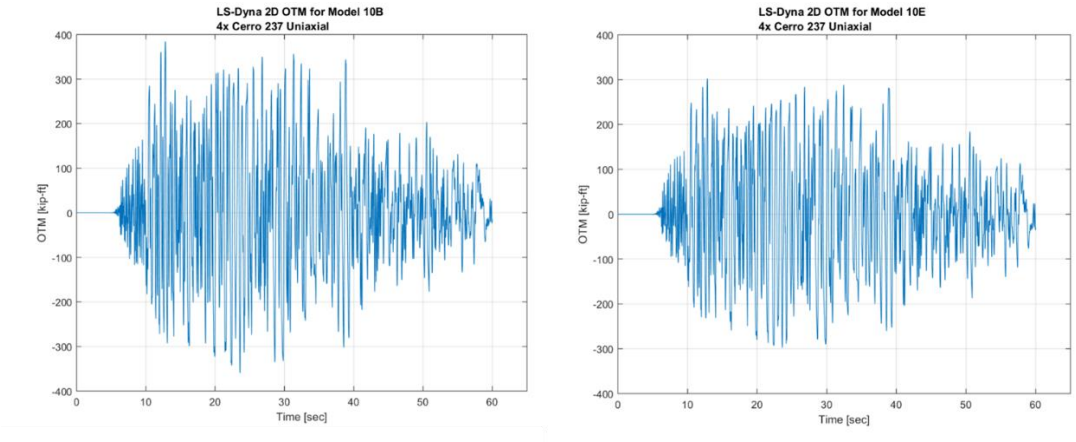

Figure 6-8: Overturning moment at the bottom of the box for the models with perfect contact (left) and frictionless sliding (right)

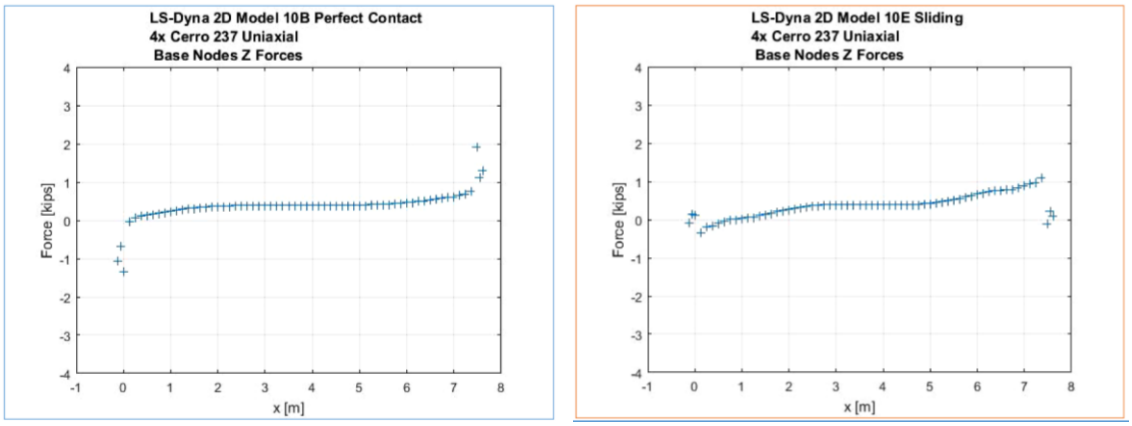

Figure 6-9: Vertical forces in the boundary nodes at the base of the box, for the models with perfect contact (left) and frictionless sliding (right)

6.3 Effect of gapping between soil and laminar walls

6.3.1 Description of 2D models with gapping

To simulate the soil-wall interaction even more realistically the contact conditions at the interface of the two materials should be adjusted in order to permit not only the vertical sliding but the formation of a gap in the horizontal direction. This means that the horizontal constraints applied between the duplicate nodes of soil in model 10E should be removed. Once the removal is completed then contact interfaces/nodes can be defined in LS-DYNA to allow for the simulation of the opening/closing of the gap between the wall and the soil, as well as the friction between them.

LS-DYNA has a wide range of robust contact types among which are one-way contacts, two-way contacts and single-surface contacts. The implementation of the contact can be based either on a penalty-stiffness formulation or a constraint-based formulation. In this study a segment-based frictional contact with a penalty-stiffness formulation was used, which allowed the specification of a coefficient of friction that is developed only when the soil is in contact with the walls. Since the materials in contact (soil and steel/aluminum) have significantly different material properties special consideration was given to the calculation of the penalty stiffness, and a "soft" formulation was selected. To advance our understanding of the role of gapping only, a numerical model with zero friction was developed (10I) and compared with the previous model (10E) that did not allow the soil to separate from the walls. Moreover, in order to understand the role of friction, the friction coefficient was varied between zero and 1, and additional models were created, namely models 10K and 10L, as shown in Table 6-1. It is useful to note that there are numerous

parameters in the definition of the *CONTACT, which can affect the behavior and numerical stability of the contact, meaning that sensitivity studies and comparisons with simpler models are always required.

Table 6-1: Description of 2D numerical models used for the investigation of the role of the contact conditions at the soil-wall interface

2D Models	Perfect Contact	Sliding at wall-soil	Wall-soil friction coeff	Gap
10B	Y			
10E		Y	0.00	
10I		Y	0.00	Y
10K		Y	0.33	Y
10L		Y	1.00	Y

6.3.2 Numerical Results

Figure 6-10 shows the base shear, overturning moment at the bottom of the box, and vertical force histories in the walls, for the models 10E and 10I, with and without gapping at the interface of the laminar walls and the soil respectively. These figures reveal that allowing the soil to separate from the walls does not seem to have significant effect on the aforementioned parameters, but this observation is applicable only to the case with the zero friction. Nonetheless, the comparison of the two models is very useful because it demonstrates that the more complex model with automatic contact (10I) gives similar results to the simpler model (10E), a fact that increases the confidence in the advanced model and allows us to use it for further parametric analyses focusing on the role of friction.

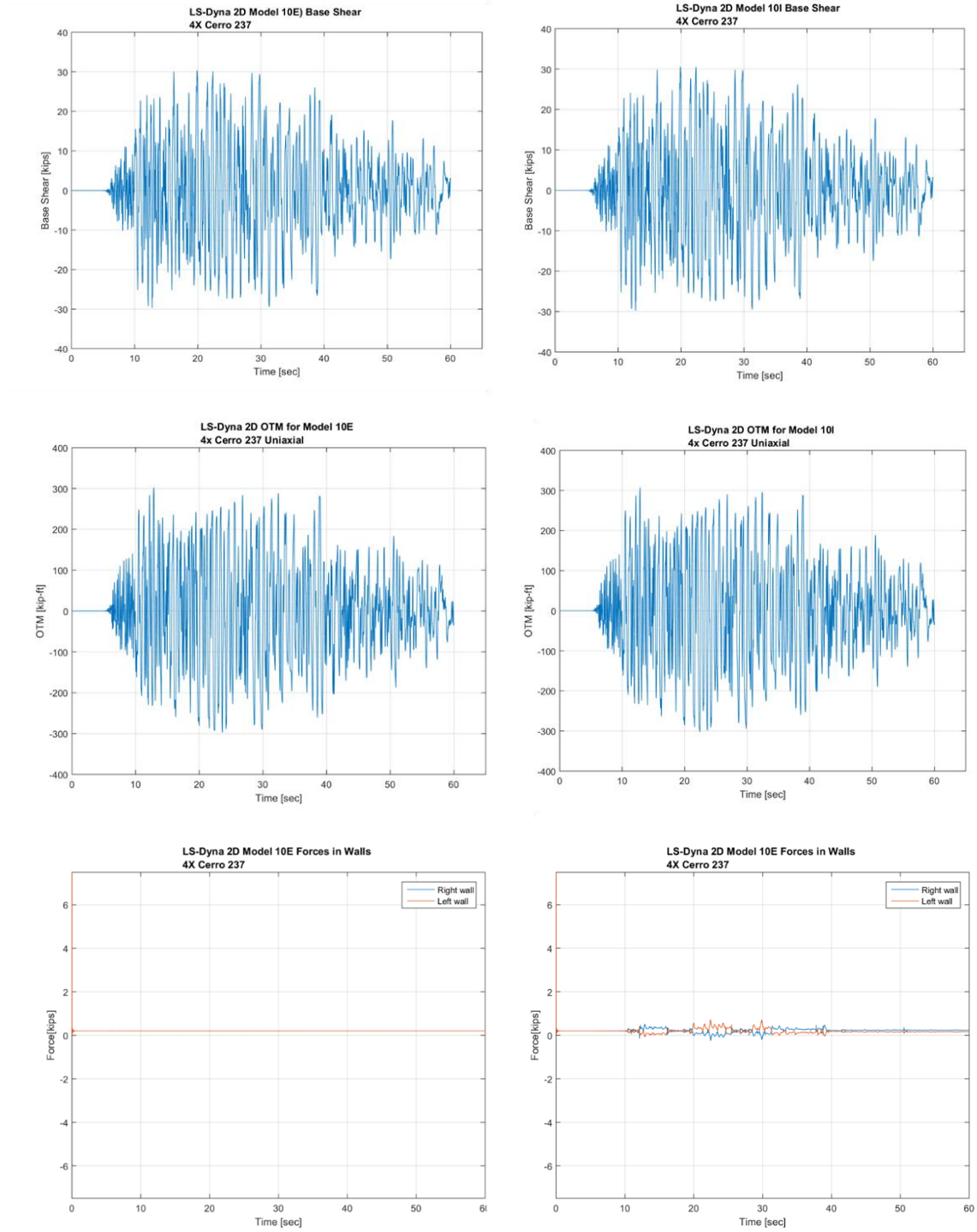

Figure 6-10: Base shear histories (top), overturning moment histories at the bottom of the box (middle) and vertical force histories in the walls, for the models without gapping (left) and with gapping (right) at the interface of the laminar walls and the soil

6.4 Effect of friction at soil-wall interface

Figure 6-11 shows the overturning moment histories for models 10I, 10K, 10L, with contact interfaces, gapping and corresponding friction coefficients equal to 0, 0.33 and 1.0 respectively, and for model 10B that has a perfect contact between the soil and the walls of the box. This figure reveals that the overturning moment (OTM) increases as the friction coefficient increases, and when the coefficient becomes 1.0 then the OTMs become similar to the ones obtained by the model with the perfect contact, which is reasonable. A similar trend is also observed in the vertical walls forces shown in Figure 6-12, where the increase of the friction coefficient increases the forces in the walls significantly demonstrating that the friction coefficient is a key parameter. As the friction coefficient increases (10L) the model approaches the behavior of the perfect contact (10B). This fact increases again the confidence in the advanced models with the contact interfaces.

Figure 6-13 and Table 6-2 show the maximum base shear, overturning moment at the base of the box, and max tension in the walls for 2D models 10E, 10I,10K, 10L and 10B. Interestingly, all the aforementioned parameters are increasing with the increase of the friction at the soil-wall interface, with the most sensitive parameter being the walls forces and the least sensitive being the base shear. Even more interesting is the fact that as the friction reduces the wall force do not reduce in a linear fashion, and for a reduction of μ from 1 to 0.33 the tensile forces in the walls reduces by 27%. Another notable observation is the fact that the simpler models 10E and 10B that have a frictionless sliding contact with no gapping (implemented via horizontal constraints) and a perfect contact (implemented

via shared nodes), provide an upper and lower bound for the base shear, OTMs and wall forces. The more advanced models with automatic contact give results in the range specified by the two simpler models, increasing again the confidence in the former models, and the conclusions that have been reached via their comparison. This indicates that it is possible to use the advanced models with contact to determine the exact values of the parameters of interest for the design of the soil-box. More complex 2D models, which simulate also the bottom steel plate and the contact with the soil, can be found in Bitsani et al (2018).

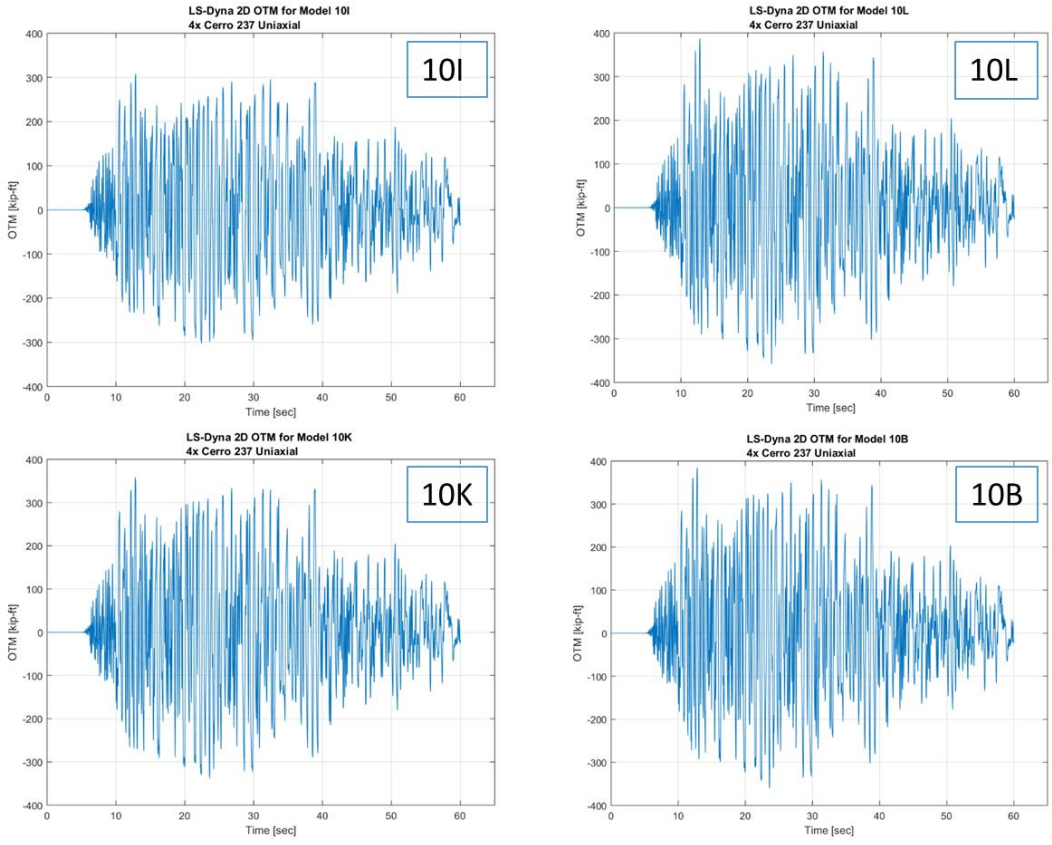

Figure 6-11: Overturning moment histories at the bottom of the box for the models with (a) zero friction (top-left), (b) frictional contact and μ=0.33 (bottom-left), (c) frictional contact and μ=1 (top-right), and (d) perfect contact (bottom-right), at the interface of the laminar walls and the soil

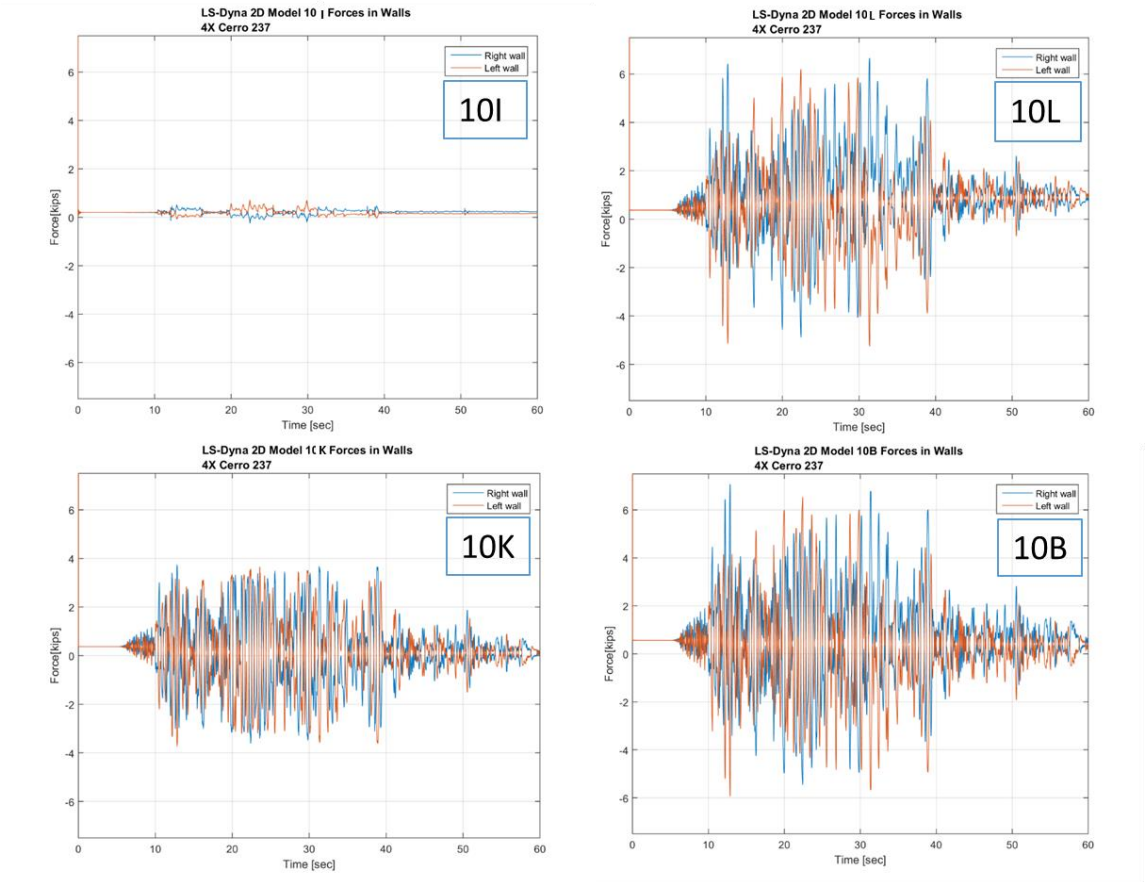

Figure 6-12: Vertical force histories in the walls of the box for the models with (a) zero friction (top-left), (b) frictional contact and μ=0.33 (bottom-left), (c) frictional contact and μ=1 (top-right), and (d) perfect contact (bottom-right), at the interface of the laminar walls and the soil

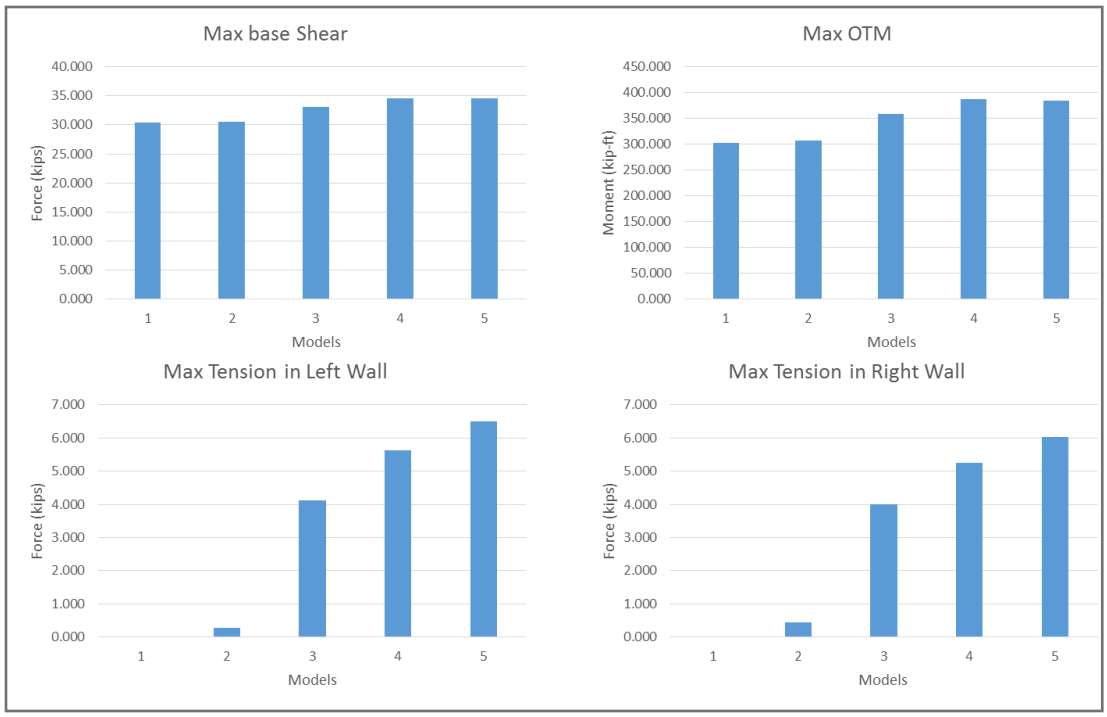

Figure 6-13: Maximum base shear (top-left), overturning moment at the base of the box (top-right), and max tension in walls (bottom), for 2D models 10E, 10I,10K, 10L and 10B

Table 6-2: Summary of results from 2D numerical models used for the investigation of the role of the contact conditions at the soil-wall interface

Models	Max Base Shear	Max OTM	Right wall Max Net	Left wall Max Net	Right wall Max Net Tension	Left wall Max Net Tension	Max Net Tension
	(kips/slice)	(kip-ft/slice)	(kips/slice)	(kips/slice)	(kips/slice)	(kips/slice)	(kips/slice)
10E	30.337	302.220	0.006	0.006	0.003	0.003	0.003
10I	30.580	307.160	0.325	0.517	0.451	0.269	0.451
10K	33.086	358.040	3.377	3.284	3.990	4.115	4.115
10L	34.541	387.030	6.289	5.826	5.259	5.639	5.639
10B	34.623	384.590	6.506	5.979	6.028	6.500	6.500

6.5 Numerical 2D vs 3D models

This thesis has focused on 1D and 2D finite element modelling and different types of dynamic analyses (linear, equivalent linear and nonlinear) in order to decipher the behavior of the soil-box, understand the interaction of the walls with the soil and provide data for the design of the box and shake table system. However, apart from the analyses conducted by the author of the thesis, the UNR research team that was involved in the design of the box developed also advanced 3D models that could simulate more accurately certain phenomena. These 3D models and analyses are presented in Istrati et al (2018), and have been included in this document in order to show possible differences between 2D and 3D results.

Figure 6-14 shows two 3D models of a circular box with different mesh sizes and shapes, which have been developed for both the case of a perfect contact and a frictional contact at the soil-wall interface. Table 6-3 compares the 2D and 3D results for both contact cases. For the perfect contact the 2D and 3D models give closer results and the 2D models under-predict the maximum tension in the walls by 12%, however when frictional contact (equal to 0.85) is used in both the 2D and 3D models, then the under-prediction is between 16% and 23%. This comparison shows that although the 2D analyses can capture the effect of frictional contact reasonably, they might under-estimate the demand on certain components of the soil-box and shake table system due to the significance of 3D effects.

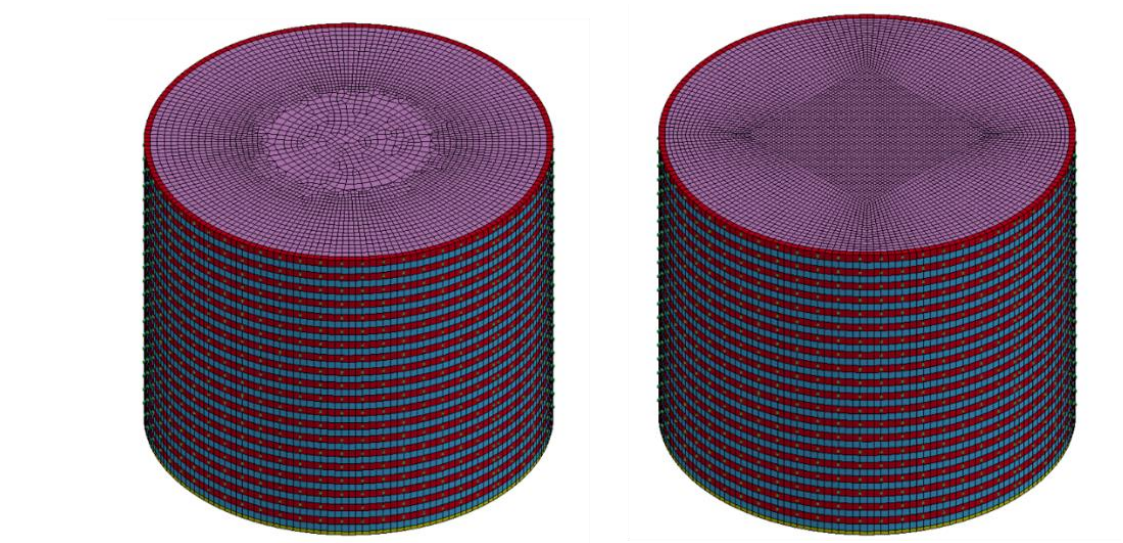

Figure 6-14: 3D models of the circular 20ft high soil box with different in-plane mesh sizes and configurations (source: Istrati et al 2018)

Table 6-3: Comparison of tension forces in the walls of the box obtained from 2D and 3D models for two different contact conditions at the soil-wall interface (source: Istrati et al 2018)

2D Models	Bottom plate	Contact soil-wall	Ground Motion	Max Net Tension	3D Models	Max Spring Tension H	Ratio 2D/3D
				kips/ft		kips/ft	
11MM	Y	μ=0.85	4x Cerro 237	12.61	**3D_2Mx**	16.43	0.77
					3D_4Mx	15.10	0.84
10B		perfect	4x Cerro 237	15.85	**3D_1Bx**	18.00	0.88

Chapter 7: Summary and Conclusions

7.1 Summary

This thesis is part of a DOE sponsored multi-institutional research project called “A Modern Computational Framework for the Nonlinear Seismic Analysis of Nuclear Facilities and Systems”. As part of this project UNR will design and build a large-scale biaxial soil-box that will be used to understand soil-structure interaction (SSI) phenomena for nonlinear soils during strong earthquakes, and validate the ESSI nonlinear computational framework developed by UC Davis. This thesis focused on extensive numerical analyses that provided an insight into the dynamic behavior of the soil-box, the role of soil nonlinearity, the interaction of the walls with the neighboring soil columns, and the effect of friction and gapping at the soil-wall interface. The numerical analyses also generated data useful for the design of the whole soil-box shake table system, such as shear and axial forces for the design of the walls, base shear and demands on stroke and velocity for the design of the actuators, overturning moment and pressures at the bottom of the box for the design of the shake table components.

During the design phase of the soil-box system several numerical models were developed, including 1D models of a soil-column, 2D model of a soil slice, 2D models of a slice of the soil-box and 3D models of the whole box, with this thesis focusing on the 1D and 2D models. The first part of the numerical work focused on one-dimensional site

response analyses in DEEPSOIL and the second part included more advanced finite element analyses in LS-DYNA.

The first step of the research work presented herein included the simulation of a free-field vertical array near the Kashiwazaki-Kariwa Nuclear Power Plant in Japan, the response of which was recorded during the Niigataken Chuetsu-oki earthquake. The good agreement of the DEEPSOIL model with the recorded data increased the confidence in the modelling skills of the user and gave an insight into the accuracy of equivalent linear and nonlinear numerical analyses. Following this quality assurance study, a one-dimensional soil column model with a height equal to the expected height of the soil-box was developed, and extensive site response analyses were conducted for a suite of eight recorded ground motions obtained from the PEER database, and different scale factors, with scaled PGAs between 0.25g and 1.0g. Linear, equivalent linear and nonlinear analyses were conducted for increasing levels of shaking and the effect of soil nonlinearity was investigated. Moreover, the effect of several parameters, such as the hysteretic soil material, the reference curve, the time-step and the time-scaling of the input motion, on the results of the nonlinear dynamic analyses was also evaluated.

The second part of the thesis presented the finite element models and results from nonlinear dynamic analyses that were conducted in LS-DYNA. An equivalent 1D soil model was developed in LS-DYNA using 3D solid elements and a nested surface plasticity model with direct input of shear stress-strain curves for each soil layer. Linear and nonlinear analyses were conducted and the results were compared with the ones obtained from DEEPSOIL. Following this comparison, the 1D LS-DYNA model was used to

investigate the effect of the soil shear strength on the response of the soil-column. Furthermore, the one-dimensional model was used as a basis for building a two-dimensional soil-slice with multiple soil-columns, which was later on modified in order to add the walls of the box. Several 2D models of the soil-box with different (a) mesh sizes, (b) wall configurations, and (c) contact conditions at the soil-wall interface, ranging from a perfect contact to frictionless contact were examined in order to decipher the role of sliding, friction and gapping on the behavior of the box. Wall configurations with and without vertical constraints, with linear axial springs, and with compression-only springs were investigated. The boundary effect close to the walls was also examined and the area of uniform soil stresses was identified for different design alternatives. These 2D analyses were used to quantify the base shear, overturning moment, pressures below the box, response spectra at different locations of the soil surface (and various depths), forces in the walls and the accelerations, displacements, strains and stresses of the soil and the box.

7.2 Observations and conclusions

The advanced numerical analyses and iterations presented in this thesis give an insight into the seismic behavior of the soil-box and are expected to be useful to other research teams designing their own soil-box. In particular, the main observations and conclusions developed based on the one-dimensional (1D) analyses in DEEPSOIL can be summarized below:

- The base shear calculated via the summation of the inertia forces of all soil layers is more accurate than calculating it directly from the shear force in the bottom soil-layer, because part of the base shear force comes from the force transferred via the dashpot (damping force) of the bottom soil-layer, and therefore neglecting it will under-predict the base shear force.
- Linear analyses gave an upper bound for the base shears and a lower bound for the shear-strains in the soil, while nonlinear analyses gave a lower bound for the base shear and an upper bound for the shear strains. At a PGA=0.13g the linear analyses over-predicted the base shear by a factor of 2 while at PGA=1.04g (SF=4) this over-prediction is by a factor of 5, demonstrating that linear analyses cannot capture properly the behavior of the soil column at such high levels of shaking
- Equivalent linear analyses fell in between the linear and nonlinear analyses. These analyses seem to give identical results with nonlinear analyses up to a PGA of 0.26g, and relatively close results up to PGA of 0.5g (SF=2). However, for larger levels of shaking the equivalent linear analyses over-predict the forces and under-predict the shear strains more significantly, indicating the need to use nonlinear analyses for such conditions.
- Nonlinear analyses showed that ground motions with same PGA introduced significantly different shear strains (larger by a factor of 2) in the soil-column due to the different frequency content of the motion relative to the natural period of the column (Hector090 vs ElCentro 180).
- For all the input motions with scale factors equal to 1 (PGA=0.26g) and 2 (PGA=0.52g), amplification of the motion is observed as the wave propagates from

the bottom to the surface. For larger levels of shaking the motion is de-amplified due to significant soil-nonlinearity/hysteretic behavior.

- At the lowest level of shaking with a PGA=0.13g (SF=0.5), the surface acceleration response spectra are maximized approximately at a period of 0.15sec, which is very close to the fundamental period of the soil column (0.13sec), indicating small levels of soil-strains and limited nonlinearity. On the other hand, as the level of shaking increases the peak SA occurs at larger periods indicating shifting of the fundamental period of the soil column due to the softening that takes places after the soil yielding. In particular, at a scale factor equal to 2 (PGA=0.52g) the max SA occurs at approximately T=0.25sec, while at a scale factor of 4 (PGA=1.04g) this happens at approximately 0.5-0.6sec.
- For the lower level of shaking (PGA=0.13g) the shear strains were close to 0.04%, for PGA=0.52 the shear strains were in the range of 0.5% and for the largest shaking with PGA=1.04g the shear strains were large and in the range of 1-7% for most of the motions (and up to 19% for one motion). The large strains were translated into significant horizontal relative displacements, which were in the range of 2 to 5.5 inches at the surface (up to 14.5in for one motion), meaning that the walls of the soil-box should be designed to withstand such relative displacements.
- Using the new General Quadratic/Hyperbolic model instead of the Modified Kodner Zelasko model for simulating the soil behavior, has a significant effect on the backbone curves especially at large strains (>0.5%). The GQ/H model can simulate not only the soil behavior at small-strains but also the behavior at large-strains by forcing the backbone curve to reach the shear strength at such strains.

The MKZ model on the other hand, simulates properly the behavior of the soil at small strains but leaves the stresses uncontrolled at large-strains, which for the 20ft soil-column and the selected soil material (dense) investigated here causes over-prediction of the shear strength of all soil layers. For example, for the soil layers at mid-depth the MKZ model over-predicts the shear-strength by 60%.

- The nonlinear analyses with the GQ/H soil model revealed that although there is some soil nonlinearity and hysteresis at lower levels of shaking (SF1) the max shear stresses are much smaller than the shear strength (less than half of τ_{max} for most layers). On the other hand, for the strong shaking (SF4) many of the soil layers reach the shear strength, meaning that their resistance to further shearing is minimal, explaining the recorded large strains at those locations.
- Using the GQH model instead of the MKZ models results in more significant de-amplification of the motion as the waves propagates from the bottom to the surface, and smaller PGAs at the surface. The GQH model also seems to reduce the magnitude and the number of peaks observed in the PGA profile. One of the most apparent differences is the fact the GQ/H model reduces significantly the accelerations in the high-frequency range (T=0.02-0.04sec) relative to the MKZ model.
- The GQ/H model reduces the base shear by up to 15%, but increases the shear strains by up to a factor of 2 (for the Seed & Idriss reference curves) for strong shaking (PGA=1.04g). This demonstrates that at high levels of shaking it is very important to use a material model that can accurately predict the shear strength and apply a cap (limit) on the shear stresses. Interestingly, although the GQH model

results in a larger maximum shear strain it does not result in larger relative displacements, indicating that the significant soil nonlinearity occurs only at a few soil layers.

- The reference curves used as a basis for development of the backbone curve in the GQ/H model can also affect significantly the behavior of the soil-column. Switching from the Seed&Idriss to the Darendeli reference causes the (a) elimination of high-frequency accelerations in the surface response spectra, (b) modification of the shape of the spectral curves and reduction of the peak PSA from 4.5 to 4g, (c) reduction of localized jumps and abrupt changes observed in the PGAs of the deeper half of the soil-column, (but not necessarily lead to smaller PGAs at the surface), (d) reduction of the maximum shear strain recorded in the soil-column, and (e) reduction of the base shear by up to 12%, indicating that this modelling approach can lead to a more economical design of the actuators of the shake-table. The GQ/H model with the Darendeli reference curve gives a maximum base shear of approximately 700kips for a circular box with 25ft diameter and 20ft height.
- The time-step had a significant effect on the PGAs of all soil layers and on the max strains of several soil layers, as well as on the acceleration response spectra at the surface. At dt=0.002sec the results seemed to converge at certain values, indicating that this is the required time-step for further numerical analyses.
- The time-scaling of the input motion had a variable effect depending on the frequency content and the exact scale. For certain motions and scales, the time-scaling increases the response of the soil-column (PGAs, strains, displacements), but for other cases it decreased it. This was due to the fact that the time-scaling

switched the acceleration response spectra of the input motion towards the left, and the effect on the soil-column depended on whether the SA peaks occurred at periods close to the natural period of the soil. For some motions the scaling brought the SA peaks closer to the period of the soil-column and in for other motions it moved them further apart.

The main observations and conclusions developed based on the two-dimensional (2D) analyses in LS-DYNA are shown below:

- The differences in the analysis options and small-strain damping formulations can cause noticeable differences in the results from linear analyses conducted in LS-DYNA and DEEPSOIL, resulting in over-prediction of the response by LS-DYNA. These differences together with differences in the nonlinear soil material model and backbone curve can also cause differences in the nonlinear analyses. Generally, the two codes presented similar trends in the response and the quantitative agreement of the results was better for lower levels of shaking. As the soil nonlinearity increased the differences seemed to increase.
- For large magnitude ground motions (PGA=1.04g) the results were very sensitive to the value of the shear strength, and this happened because for such significant shaking most of the soil layers underwent a very nonlinear behavior and the response was governed by the ultimate soil strength. In particular, the large shear strength resulted in a major increase of the PGAs and stresses along the whole depth of the soil column, and approximately doubled the base shear. For the purpose of

the design of the soil-box it was decided to use the shear strength obtained using the vertical effective stress (instead of the mean stress) since it leads to the upper bound for the forces.

- For the 2D soil-box model with walls consisting of interchangeable layers of steel and soft rubber that has a very small stiffness (and perfect contact), the deformed shapes show that there are some vertical displacements close to the walls of the box, indicating that the box does not behave purely in shear. The intent of such walls is to have a very small lateral shear flexibility so that the walls do not constrain the soil (but the soil drives the response), however the small shear modulus G means a small elastic modulus which leads to a small axial as well as bending stiffness. This small stiffness seems to allow the generation of vertical displacements.
- Moreover, in the case of the walls with a small shear, axial and bending (flexural) stiffness, for a certain soil layer the stresses are not uniform along the whole length of the layer, with the two-three soil columns closer to the walls witnessing different stresses than the ones close to the center of the box, demonstrating the existence of a boundary effect caused by the walls. This boundary effect causes also differences in the peak ground accelerations and max shear strains witnessed by the soil-column located close to the walls and the once at the center.
- The vertical forces histories of the nodes below the left and right wall of the box, are out-of-phase, meaning that when one is maximized the other one is minimized, indicating that overturning moment is introduced at the bottom of the soil-box during lateral shaking. This overturning moment can be so significant that the uplift

forces that introduces in a certain wall can significantly exceed the counter-acting weight resulting in large tensile bearing forces. This means that the bearings of the walls should be designed not only for shear but also for tension.

- The four models with different sizes of the horizontal mesh revealed that some parameters are more sensitive to the mesh size than other. In particular, this size had a minor effect on the lateral accelerations, displacements and base shear, however it had a major effect on the vertical displacements and the vertical forces in the walls. As the mesh becomes smaller the later displacements and forces reduce significantly. Therefore, it is critical to use an adequately small horizontal mesh size in order to capture the distribution of the overturning moment and complementary shear in the walls of the box.
- The vertical mesh size has a small effect on the horizontal displacement histories and the acceleration at the surface of the center column, and a larger effect on the soil accelerations close to the wall. Contrary to the horizontal mesh size, the vertical mesh size does have an effect on the base shear. It also has an effect on the vertical wall forces and vertical displacements, indicating that a sufficiently refined mesh size is required in both the horizontal and vertical direction in order to properly capture the interaction of the walls with the soil and physical effects generated during the ground shaking.
- Introduction of vertical constraints in all the nodes of each wall, which actually eliminated any axial or flexural deformations of the walls and made them behave in pure shear, had a significant effect on the response of the soil. The most apparent effect is the fact that the vertical constrains minimized/eliminated the boundary

effect, and although in the model without vertical constraints the region of disturbed soil and non-uniform soil stresses extended to a distance from the wall equal to about 15% of the total length of the slice, this distance is very negligible in the model with the constraints. The vertical constrains also increased the lateral accelerations, residual lateral displacements of the box and the base shears. Moreover, the soil close to the walls does not uplift anymore but just undergoes some minimal settlement during shaking.

- One of the most interesting conclusions from the comparison of the models with and without vertical constrains is that although the base shear increases slightly with the addition of vertical constraints, and the overturning moment is slightly decreases, the axial forces in the walls increase by an outstanding factor of 3. This could be explained by the fact that in the case where there were no vertical constraints the large overturning moment was taken partially by the walls of the box and a soil region close to the walls that is highly disturbed, while when vertical constraints are present in the walls, the very high axial and flexural stiffness of the walls attracts all the vertical forces generated by the overturning moment.
- The two additional configurations of vertical constraints, according to which the constraints were applied only at the middle nodes of the walls, increased the axial stiffness but they did not affect the bending stiffness. The small bending stiffness of these two models resulted in significant flexural effects during shaking, which introduced vertical displacements at the sides of the walls and the neighboring soil. Although all three models with vertical constrains had similar lateral accelerations, lateral displacements and base shears, the models with vertical constraints at the

middle nodes (high axial but small bending stiffness) witnessed smaller vertical forces in the walls.

- Switching the vertical constraints with very stiff linear springs did not affect the numerical results, but it increased the computational time of the analyses by at least an order of magnitude, since the spring stiffness enters into the calculation of the time-step of explicit analyses. The model with springs in the walls presented the advantage of calculating the forces in the springs, which were seen to increase as the depth increases, which is reasonable since the springs have to transfer the complementary shear generated by all the soil layers above it. However, this increase was not linear with depth, with the spring at mid-depth witnessing an axial force that was smaller than 50% of the force of the spring at the bottom layer.
- The use of compression-only stiff springs instead of linear stiff springs, did not affect the horizontal accelerations, displacements and base shears, however, the vertical displacements close to the wall were significantly larger in both directions (upwards and downwards). Since the tensile stiffness of the walls was very small (the spring increased only the stiffness in compression) that resulted in smaller tensile forces in the walls, which was expected, however it also caused a significant increase in the compression force of both the springs and the support nodes below the walls, which was not expected beforehand. Similarly to the linear springs, the compression-only springs at large depths witnessed larger forces (compression) than the ones closer to the surface, but the increase was not linear from the surface to the bottom of the box.

- The model with frictionless sliding and no gapping at the soil-wall interface, allowed the soil to uplift at one side of the box and settle at the other side of the box, (and the opposite) during shaking. In this case the soil did not behave in pure shear anymore (despite the large axial stiffness of the walls) and a more complex soil stress state was developed in the soil regions close to the walls, which could potentially result in non-uniform shear stresses along the width of a soil layer. The model with the frictionless sliding witnessed noticeably smaller horizontal accelerations than the model with perfect contact, and negligible vertical accelerations and walls forces. This demonstrated that the reason for the generation of the vertical acceleration in the walls and large walls forces was not only the existence of overturning moment but also the idealized perfect contact which transferred the dynamic complementary shears of the soil to the walls of the box.
- Allowing the soil to slide vertically at the interface with the walls is beneficial for the design of the soil-box and shake table system because it reduces (a) the vertical forces in the walls of the box, (b) the overturning moments on the table, (c) the local pressures on the platen, and (d) the base shear that the actuators have to introduce/withstand. However, the major disadvantage is the fact that the sliding at the interface results in very distorted soil regions in a large portion of the box, which is not in pure shear anymore. Since this is an undesired soil behavior and physically unrealistic, the frictionless sliding at the wall-soil interface is not recommended.
- The advanced and more realistic 2D numerical models with frictional contact between the soil and the walls of the box revealed that the increase of the coefficient of friction results in a noticeable increase of the base shear and the overturning

moment (OTM), and a major increase of the axial forces in the walls. When the coefficient of friction becomes 1.0 then these parameters become similar to the ones obtained by the model with the perfect contact.

- The simpler 2D models 10E and 10B that have a frictionless sliding contact with no gapping (implemented via horizontal constraints) and a perfect contact (implemented via shared nodes), provide an upper and lower bound for the base shear, OTMs and wall forces. The more advanced models with automatic contact give results in the range specified by the two simpler models, increasing the confidence in the former models. This indicates that it is possible to use the advanced models with contact to determine the exact values of the parameters of interest for the design of the soil-box.
- Comparison of the results from 2D numerical models presented in this thesis with the ones from 3D models of the whole soil-box obtained from Istrati et al (2018), reveals that the 2D models can capture properly the effect of frictional contact between the soil and the wall. However, the 2D models might under-predict the tensile forces in the walls of the box, by up to 12% in the case of a perfect contact and about 20% for the case of a frictional contact with μ=0.85.

7.3 Future work

This thesis presented a wide range of numerical analyses that gave an insight into the behavior of the soil column and soil-box, and provided useful information for the preliminary design on the whole system. However, these analyses made certain assumptions regarding the soil properties, and focused only on 1D and 2D dynamic behavior. Therefore, future work should focus on:

- Validation of the assumed soil properties with laboratory tests, which will provide the actual backbone and damping curves of the soil that will be used in the large-scale experiments during the commissioning phase of the soil-box.
- Two-dimensional analyses of the final design of the soil-box that will have the exact wall dimensions and properties.
- Three-dimensional modelling and analyses of the final design of the 400-ton octagonal soil-box (Figure 7-1) that will allow for simulation of biaxial shaking and investigation of 3D effects.

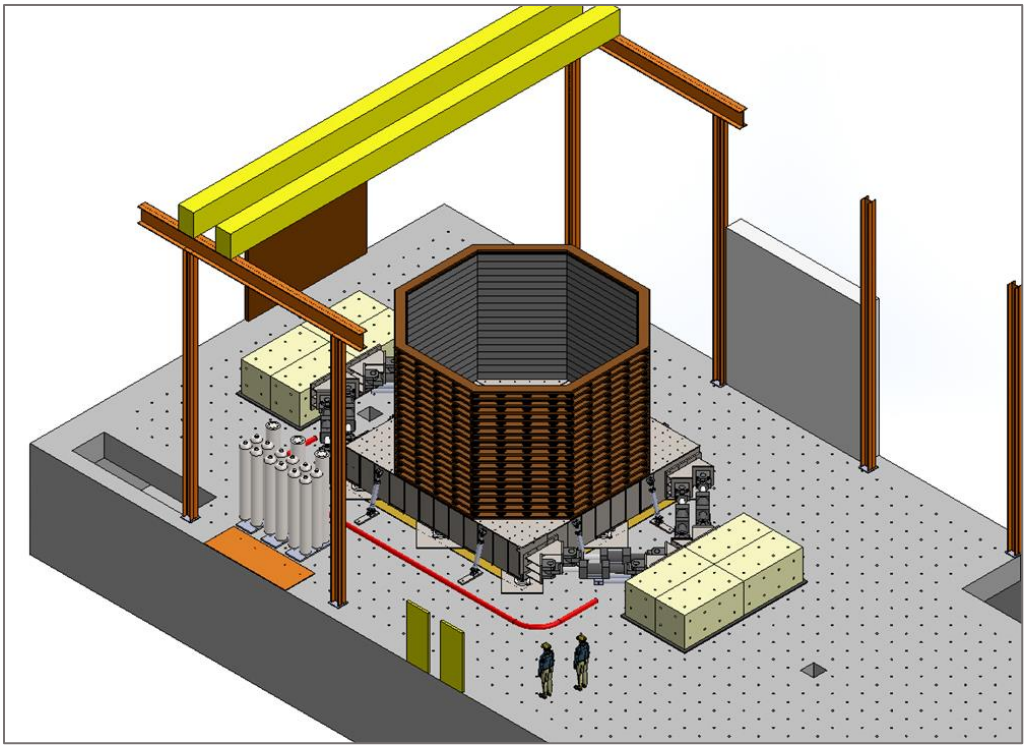

Figure 7-1: Conceptual drawing of octagonal biaxial soil-box and shake table system (credit: P. Laplace)

References

Antonellis, G., Gavras, A. G., Panagiotou, M., Kutter, B. L., Guerrini, G., Sander, A. C., & Fox, P. J. (2015). Shake table test of large-scale bridge columns supported on rocking shallow foundations. Journal of Geotechnical and Geoenvironmental Engineering, 141(5), 04015009.

Bitsani A., Istrati D., Buckle I.G, Motamed R., Elfass S., Laplace P., Siddharthan R. (2018). Design of a Large-Scale Biaxial Soil-Box for Seismic Soil-Structure-Interaction Studies. 11th National Conference on Earthquake Engineering, June 25-29, 2018, Los Angeles, USA (in press)

Bolisetti, C. (2015). Site response, soil-structure interaction and structure-soil-structure interaction for performance assessment of buildings and nuclear structures. State University of New York at Buffalo.

Bolisetti, C., Whittaker, A. S., Mason, H. B., Almufti, I., & Willford, M. (2014). Equivalent linear and nonlinear site response analysis for design and risk assessment of safety-related nuclear structures. *Nuclear Engineering and Design*, *275*, 107-121.

Chunxia, H., Hongru, Z., Guoxing, C., & Zhilong, S. (2008). DESIGN AND PERFORMANCE OF A LARGE-SCALE SOIL LAMINAR SHEAR BOX IN SHAKING TABLE TEST.

Darendeli, M. B. (2001). Development of a new family of normalized modulus reduction and material damping curves Ph. D., University of Texas at Austin.

Dihoru L., Crewe A. J., Dietz M., Bhattacharya S., Taylor C.A. (2010). Laminar Shear Box Design for Soil-Structure Interaction Studies. *SERIES Workshop, Seismic Engineering Research Infrastructures for European Synergies*, Role of Research Infrastructures in Performance-Based Earthquake Engineering, University of Bristol, UK
http://www.series.upatras.gr/userfiles/15_Dihoru.pdf

Groholski, D. R., Hashash, Y. M. A., Musgrove, M., Harmon, J., & Kim, B. (2015, November). Evaluation of 1-D non-linear site response analysis using a general quadratic/hyperbolic strength-controlled constitutive model. In 6ICEGE: 6th International Conf. on Earthquake Geotechnical Engineering.

Hashash, Y. M., & Park, D. (2001). Non-linear one-dimensional seismic ground motion propagation in the Mississippi embayment. *Engineering Geology*, *62*(1), 185-206.

Hashash, Y., Phillips, C., & Groholski, D. R. (2010). Recent advances in non-linear site response analysis.

Hashash, Y.M.A., Musgrove, M.I., Harmon, J.A., Groholski, D.R., Phillips, C.A., and Park, D. (2015) "DEEPSOIL 6.1, User Manual"

Istrati D., Bitsani A., Buckle I.G, Motamed R., Elfass S., Laplace P., Siddharthan R. (2018). Design of a Large-Scale Biaxial Soil-Box for Studying Seismic Soil-Structure-Interaction. 16th European Conference on Earthquake Engineering, June 18-21, 2018, Thessaloniki, Greece (in press)

Jafarzadeh, B. (2004, August). Design and evaluation concepts of laminar shear box for 1G shaking table tests. In Proceedings of the 13th world conference on earthquake engineering, Vancouver, paper (No. 1391).

Kawamata, Y., Nakayama, M., Towhata, I., Yasuda, S., & Tabata, K. (2012). Large-scale experiment using E-Defense on dynamic behaviors of underground structures during strong ground motions in urban areas. In *15th World Conference of Earthquake Engineering, Lisbon*.

Kramer, S.L., 1996. Geotechnical Earthquake Engineering Prentice Hall. New York.

Kwok, A. O., Stewart, J. P., & Hashash, Y. M. (2008). Nonlinear ground-response analysis of Turkey flat shallow stiff-soil site to strong ground motion. *Bulletin of the Seismological Society of America*, *98*(1), 331-343.

Kwok, A. O., Stewart, J. P., Hashash, Y. M., Matasovic, N., Pyke, R., Wang, Z., & Yang, Z. (2007). Use of exact solutions of wave propagation problems to guide implementation of nonlinear seismic ground response analysis procedures. *Journal of Geotechnical and Geoenvironmental Engineering*, *133*(11), 1385-1398.

Lai, C. G., & Rix, G. J. (1998). *Simultaneous inversion of Rayleigh phase velocity and attenuation for near-surface site characterization* (p. 258). Georgia: School of Civil and Environmental Engineering, Georgia Institute of Technology.

Livermore Software Technology Corporation (LSTC), (2014). "LS DYNA Keyword User's Manual. Version R 7.1. Volume II". Livermore, California.

Matasovic, N. (1993). Seismic response of composite horizontally-layered soil deposits Ph.D. Thesis, University of California, Los Angeles.

Menq, F. Y., 2003. Dynamic Properties of Sandy and Gravelly Soils, Ph.D. Dissertation, University of Texas, Austin.

Motamed, R., Stanton, K. V., Almufti, I., Ellison, K., & Willford, M. (2015, November). Effects of Multi-directional Shaking in Nonlinear Site Response Analysis: Case Study of 2007 Niigata-ken Chuetsu-oki Earthquake. In *Proceeding of the 6th International Conference in Earthquake Geotechnical Engineering, Christchurch, New Zealand*.

Motamed, R., Stanton, K., Almufti, I., Ellison, K., & Willford, M. (2016). Improved Approach for Modeling Nonlinear Site Response of Highly Strained Soils: Case Study of the Service Hall Array in Japan. *Earthquake Spectra*, *32*(2), 1055-1074.

Motamed, R., Towhata, I., Honda, T., Tabata, K., & Abe, A. (2013). Pile group response to liquefaction-induced lateral spreading: E-Defense large shake table test. *Soil Dynamics and Earthquake Engineering*, *51*, 35-46.

Phillips, C., & Hashash, Y. M. (2009). Damping formulation for nonlinear 1D site response analyses. *Soil Dynamics and Earthquake Engineering*, *29*(7), 1143-1158.

Phillips, C., Kottke, A. R., Hashash, Y. M., & Rathje, E. M. (2012). Significance of ground motion time step in one dimensional site response analysis. *Soil Dynamics and Earthquake Engineering*, *43*, 202-217.

Stewart, J. P., & Kwok, A. O. (2008). Nonlinear seismic ground response analysis: Code usage protocols and verification against vertical array data. In *Geotechnical earthquake engineering and soil dynamics IV* (pp. 1-24).

Stewart, J. P., & Yee, E. (2012). Nonlinear Site Response and Seismic Compression at Vertical Array Strongly Shaken by 2007 Niigata-ken Chuetsu-oki Earthquake. *Report to National Earthquake Hazards Reduction Program, Reston, VA.*

Suzuki, H., Tokimatsu, K., Sato, M., & Tabata, K. (2008, October). Soil-pile-structure interaction in liquefiable ground through multi-dimensional shaking table tests using E-Defense facility. In *14th World Conference on Earthquake Engineering, Beijing, China* (No. 0177).

Tokimatsu, K., Suzuki, H., & Sato, M. (2005). Effects of inertial and kinematic interaction on seismic behavior of pile with embedded foundation. *Soil Dynamics and Earthquake Engineering*, *25*(7), 753-762.

Turan, A., Hinchberger, S. D., & El Naggar, H. (2009). Design and commissioning of a laminar soil container for use on small shaking tables. *Soil Dynamics and Earthquake Engineering*, *29*(2), 404-414.

Ueng, T. S., Wang, M. H., Chen, M. H., Chen, C. H., & Peng, L. H. (2005). A large biaxial shear box for shaking table test on saturated sand.

Wilson, P., & Elgamal, A. (2015). Shake table lateral earth pressure testing with dense c-ϕ backfill. *Soil Dynamics and Earthquake Engineering*, *71*, 13-26.

Yee, E., Stewart, J. P., & Tokimatsu, K. (2013). Elastic and large-strain nonlinear seismic site response from analysis of vertical array recordings. *Journal of Geotechnical and Geoenvironmental Engineering*, *139*(10), 1789-1801.